Journal of Drug Delivery

Nanoparticles for Targeted Delivery of Active Agents against Tumor Cells

Guest Editors: Rassoul Dinarvand, Paulo Cesar de Morais, and Antony D'Emanuele

Nanoparticles for Targeted Delivery of Active Agents against Tumor Cells

Journal of Drug Delivery

Nanoparticles for Targeted Delivery of Active Agents against Tumor Cells

Guest Editors: Rassoul Dinarvand, Paulo Cesar de Morais, and Antony D'Emanuele

Editorial Board

Contents

Hindawi Publishing Corporation
Journal of Drug Delivery
Volume 2012, Article ID 528123, 2 pages
doi:10.1155/2012/528123

Editorial

Nanoparticles for Targeted Delivery of Active Agents against Tumor Cells

Rassoul Dinarvand,[1] Paulo Cesar de Morais,[2] and Antony D'Emanuele[3]

[1] *Nanotechnology Research Centre, Faculty of Pharmacy, Tehran University of Medical Sciences, Tehran 1417614411, Iran*
[2] *Núcleo de Física Aplicada, Instituto de Física, Universidade de Brasília, 70910-900 Brasília, DF, Brazil*
[3] *School of Pharmacy and Pharmaceutical Sciences, University of Central Lancashire, Preston PR1 2HE, UK*

Correspondence should be addressed to Rassoul Dinarvand, dinarvand@tums.ac.ir

Received 14 June 2012; Accepted 14 June 2012

Cancer therapy may still be considered as one of the most challenging issues in pharmaceutical sciences. Various new technologies and molecules have been developed to meet the needs of this devastating disease, but there is a long way to go. One of the most important challenges is finding a drug molecule or drug delivery system which only influences the cancer cells. This has not been achieved so far even though a great deal of research has focused on this goal. Most of the cytotoxic agents used for cancer treatment are toxic in nature and not only have an effect on tumor cells, but also normal cells are damaged when exposed with them. As a result, patients may experience intensive side effects which may lead to an early termination in chemotherapy due to their severity.

Targeting the cancer cells specifically and selectively seems to be the best solution for this obstacle. Targeting the cancer cells occurs via two different strategies: passive targeting and active targeting. The conventional approach used for cancer therapy may be considered a sort of passive targeting. Cytotoxic agents used for cancer treatment select the cancer cells due to their faster growth rate. Inevitably, normal fast growing cells and normal fast dividing cells may damage following conventional chemotherapy. In 1986, Matsumura and Maeda brought up a new concept in passive targeting called enhanced permeation and retention (EPR) effect which was widely used in many researches as an approach for targeting tumor cells. In this strategy, the drug delivery system benefits from defective vasculature, fenestrations, and poor lymphatic drainage in tumor tissues. Utilizing molecular targeting moieties is another strategy which is widely used in new researches for targeting tumor cells actively and diminishing chemotherapy side effects.

This special issue will primarily address new approaches for passive and active targeted cancer therapy with a focus on nanoparticle formulations specially those ones that specifically and selectively target tumors.

There is a peper which describes using a natural protein, atelocollagen for oligonucleotide delivery, and evaluating its biological function. The researchers found that when oligonucleotides were used concomitantly with atelocollagen, paracellular flux was enhanced, but when each of these two constituents of the formulation was used separately, no effect was observed. Another paper reviews poly(lactic-co-glycolic acid)- (PLGA-) based nanoparticles especially echogenic ones to enhance gene delivery. Ultrasound may be used to enhance localized gene delivery in tumors. On the other hand, nanoparticles themselves may utilize targeting mechanisms to enhance the targeting potential of the current system. Another paper describes microemulsions in the form of nanocarriers for passive tumor targeting. In this study, an experimental design layout was used to optimize the excipients selection for microemulsion nanocarriers. These nanocarriers possess the ability of solubilizing hydrophobic drugs and physical stability alongside with their capability of passive targeting. In another paper human serum albumin was used as a naturally occurring protein to create nanoparticles for enhanced drug delivery in breast cancer. Albumin-based nanoparticles were further cationized by polyethylenimine. It was shown that delivery efficacy was improved by passive EPR strategy.

One of the papers also reviews carbon nanotubes for cancer therapy and designing drug delivery systems. Carbon nanotubes present a great canvas for surface engineering and creating novel targeted nanoparticles. Another paper presents glucan particles which actively target cancer cells. Glucan particles which benefit from β-glucan derived from the cell wall of *Saccharomyces cerevisiae* provide receptor-mediated uptake by phagocytic macrophage cells who express β-glucan receptors. Different types of nanoparticles were incorporated or surface bounded to these glucan particles to deliver doxorubicin to macrophages. Macrophages further migrate into solid tumors carrying the cytotoxic agent to the target tissues like a Trojan horse, while they are resistant to the effects of doxorubicin due to their nondividing differentiated nature.

Another paper reviews noble metal nanoparticles with a wide variety of biomedical applications which are used for both therapeutic and diagnostic purposes. They also present facile surface chemistry and the possibility of functionalizing on their surfaces.

Finally, in one of the papers, a lipoplatin formulation consisting of liposomal encapsulated cisplatin is reviewed. The purpose of this formulation is to become a substitute for the original cisplatin and has gained positive results in clinical trials. Lipoplatin gives 200-fold higher concentrations in tumor tissues in comparison with cisplatin once more because of the compromised endothelium of tumor tissues.

To sum up, this special issue tries to provide the readers some insight about the targeted nanoparticles which are designed for cancer therapy both for small molecular drugs and gene delivery systems.

Rassoul Dinarvand
Paulo Cesar de Morais
Antony D'Emanuele

Hindawi Publishing Corporation
Journal of Drug Delivery
Volume 2012, Article ID 245835, 9 pages
doi:10.1155/2012/245835

Research Article

Effects of Atelocollagen Formulation Containing Oligonucleotide on Endothelial Permeability

Koji Hanai,[1] Takashi Kojima,[2] Mika Ota,[3] Jun Onodera,[4] and Norimasa Sawada[2]

[1] *Formulation Research and Development Laboratories, Dainippon Sumitomo Pharma Co., Ltd., 1-3-45 Kurakakiuchi, Ibaraki-shi, Osaka 567-0878, Japan*
[2] *Department of Pathology, Sapporo Medical University School of Medicine, S1, W17, Sapporo 060-8556, Japan*
[3] *Environmental Health Science Laboratory, Sumitomo Chemical Co., Ltd., Osaka 554-0022, Japan*
[4] *Research Institute, Koken Co., Ltd., 2-13-10, Ukima, Kita-ku, Tokyo 115-0051, Japan*

Correspondence should be addressed to Koji Hanai, koji-hanai@ds-pharma.co.jp

Received 29 August 2011; Revised 11 December 2011; Accepted 12 December 2011

Academic Editor: Rassoul Dinarvand

Atelocollagen is a major animal protein that is used as a highly biocompatible biomaterial. To date, atelocollagen has been used as an effective drug delivery technology to sustain the release of antitumor proteins and to enhance the antitumor activity of oligonucleotides in *in vivo* models. However, the biological effects of this technology are not fully understood. In the present study, we investigated the effects of atelocollagen on endothelial paracellular barrier function. An atelocollagen formulation containing oligonucleotides specifically increased the permeability of two types of endothelial cells, and the change was dependent on the molecular size, structure of the oligonucleotides used and the concentrations of the oligonucleotide and atelocollagen in the formulation. An immunohistochemical examination revealed that the formulation had effects on the cellular skeleton and intercellular structure although it did not affect the expression of adherens junction or tight junction proteins. These changes were induced through p38 MAP kinase signaling. It is important to elucidate the biological functions of atelocollagen in order to be able to exploit its drug delivery properties.

1. Introduction

Collagen is a major connective tissue protein that plays an important role in the extracellular matrix in animals. As such, collagen possesses good biocompatibility with animal body tissues [1]. Atelocollagen is a type of soluble collagen produced from tropocollagen, the collagen molecule that makes up collagen fibrils, via the elimination of the telopeptide moieties, which are considered to account for most of collagen's antigenicity [1, 2]. Thus, atelocollagen is considered to have little immunogenicity, which makes it a safe biomaterial [1]. In fact, it is widely used for implantable medical and plastic surgical products [1].

Atelocollagen is also used as a drug delivery carrier. For example, a minipellet atelocollagen formulation has been demonstrated to sustain the release and maintain stable blood concentrations of protein drugs for more than 1 week [2]. Many kinds of protein drugs such as interferon-α [3], interleukin-2 [4], nerve growth factor [5], and bone morphogenetic protein [6], and so forth, have been administered using this drug delivery system, and interferon-α and interleukin-2 showed strong antitumor activities in animal models when administered in this manner [3, 4]. In the past decade, as well as being used as a solid substrate, dissolved atelocollagen has been used as a drug delivery vehicle for nucleic acid-based medicines for gene conversion [7], inflammatory disease [8, 9], and tumor therapy. Atelocollagen can be used to deliver most kinds of nucleic acid-based medicines including plasmid DNA [10], antisense oligodeoxynucleotides (ODN) [11–13], short interference RNA (siRNA) [14–20], and micro RNA (miRNA) [21–23]. It is also capable of delivering oligonucleotides to subcutaneous xenografts and metastatic tumors after its local and/or systemic administration.

Many studies, including some involving *in vivo* tumor models, have evidenced the contribution of atelocollagen to the enhancement of drugs' antitumor activities, and some of them described the mechanisms. For example, nucleic acids delivered by atelocollagen are protected against degradation by host nucleases [8, 14, 24], and it has also been shown to improve the delivery efficiency of oligonucleotides to tumors [15, 16]. However, the biological functions of atelocollagen and the mechanism by which it enhances delivery efficiency are still not fully understood. It is essential to reveal the biological characteristics of atelocollagen in order to be able to fully exploit its drug delivery potential. While we were studying the basic properties of atelocollagen, we discovered another of its functions: it increases endothelial permeability. Here, we describe the results of a study of the effects of atelocollagen on intercellular sealing function. We measured transendothelial electrical residence (TER) in order to estimate intercellular barrier function and performed an immunohistochemical examination to see whether any cellular morphological changes were induced.

2. Materials and Methods

2.1. Atelocollagen, Oligonucleotides, and Formulations. Atelocollagen was supplied in aqueous form by Koken (Tokyo, Japan). Rhodamine red-conjugated atelocollagen was prepared in accordance with the manufacturer's instructions (FluoReporter Rhodamine Red-X Protein Labeling Kit; Life technologies Japan, Tokyo, Japan).

The oligodeoxynucleotides (ODN) and double stranded RNA (dsRNA) were synthesized by Eurogentec (Seraing, Belgium). The sequences of the oligonucleotides are listed in Table 1 [20, 25, 26].

Each atelocollagen-oligonucleotide formulation (AC formulation) was prepared by gently mixing aqueous atelocollagen with a solution containing a defined concentration of oligonucleotides. The final oligonucleotide concentration was usually 5 μM and that of atelocollagen was 0.1% w/v unless otherwise stated in the text, tables, and/or figures.

2.2. Transendothelial Electrical Resistance (TER) Measurement. Normal human dermal microvascular endothelial cells (HMVEC) were purchased from EIDIA (Tokyo, Japan). These cells were cultured in EGM (Endothelial Growth Media; EIDIA, Tokyo, Japan) until they reached confluence on 12 mm transwell filters with a 0.4 μm pore size (Corning Glass Works; Corning Japan, Tokyo, Japan) coated with rat tail collagen. Porcine brain microvascular endothelial cells (BMVEC) were purified and maintained according to the method described in a previous study [27].

TER was determined using an EVOM voltohmmeter and an ENDOHM-12 chamber (World Precision Instruments, Sarasota, FL) at 37°C [28]. Cell growth was monitored by measuring TER. Once stable intercellular seals had formed; that is, at confluence, the medium in the inner chamber was exchanged for 400 microliters of culture medium containing 30% v/v of AC formulation. TER was subsequently measured in duplicate every 30 min.

2.3. Measurement of Paracellular Flux. HMVEC cells were also used for the determination of paracellular flux. One hour after treatment with the AC formulation, which was performed as described in Section 2.2, 100 μL of 0.36% w/v Texas red-conjugated dextran (MW: 40 kDa; Life Technologies Japan, Tokyo, Japan) were added to the inner chamber. One hour later, the dextran concentration of the medium in the outer chamber was analyzed by measuring its fluorescence.

To investigate the enhancement of paracellular transport by atelocollagen, solute transportation was compared among the AC formulation, bovine serum albumin, and dextran. Once stable intercellular seals had formed, the medium in the inner chamber was exchanged for 400 microliters of culture medium containing 30% v/v of the AC formulation, which had been produced using 0.1 or 0.3% w/v rhodamine red-conjugated atelocollagen (i.e., approximately 0.03 or 0.1% w/v atelocollagen was added; molecular weight (MW): 300 kDa); 0.1% w/v of fluorescein conjugated dextran (MW: 70 kDa; Life Technologies Japan, Tokyo, Japan); 0.1% w/v of Alexa Fluor 594 conjugated bovine serum albumin (BSA; MW: 66 kDa; Life Technologies Japan, Tokyo, Japan). The solute concentrations of the outer chambers were analyzed by measuring their fluorescence at 1 and 2 hours after the medium exchange.

2.4. Immunohistochemistry. After treatment for 1 hr with the AC formulation, oligonucleotide alone, atelocollagen alone, or phosphate-buffered saline (PBS) as a control, HMVEC cells were fixed with 1% paraformaldehyde for 10 min and then treated with 0.2% Triton X-100 for 10 min. After preincubation with 5% skimmed milk, they were incubated for 1 hr at room temperature with rabbit or mouse antibodies against vascular endothelial (VE)-cadherin (BD Biosciences, San Diego, CA), zonula occludens-1 (ZO-1) (Zymed Laboratories, San Francisco, CA), claudin-5 (Zymed Laboratories, San Francisco, CA), and α-tubulin (Amersham, Poole, UK). Then, the samples were incubated for 1 hr with appropriate secondary antibodies labeled with Alexa Fluor-488 or Alexa Fluor-596 (Life Technologies Japan, Tokyo, Japan). Actin filaments were labeled with Alexa Fluor-546 phalloidin (Life Technologies Japan, Tokyo, Japan). The cells were thoroughly rinsed with PBS between each procedure. The expression of each protein was examined using a laser scanning confocal microscope (MRC 1024; Bio-Rad, Hercules, CA).

2.5. Western Immunoblotting. Western blotting was performed according to the method described in a previous report [29]. For Western blotting of the total cell lysates, the dishes were washed with PBS, and then 300 μL of sample buffer (1 mM $NaHCO_3$ and 2 mM phenylmethylsulfonyl fluoride) was added to 60 mm culture dishes. The cells were scraped and collected in microcentrifuge tubes and then sonicated for 10 sec. The protein concentrations of the samples were determined using a BCA (bicinchoninic acid) protein assay reagent kit (Pierce Chemical, Rockford, IL). For each sample, aliquots of protein (15 μg per lane) were separated by electrophoresis in 4/20% sodium dodecyl

Table 1: Effects of formulation composition on relative TER (%).

(a) Effects of oligonucleotide type.

Oligonucleotides				Atelocollagen	TER (%)
Type, sequences		Reference	Concentration	concentration	
Blank control					100.0
Phosphorothioate Oligodeoxynucleotide	5′-TGCATCCCCCAGGCCACCAT-3′	25	5 μM		92.7
Atelocollagen alone				0.1%	88.1
Phosphorothioate Oligodeoxynucleotide	5′-TGCATCCCCCAGGCCACCAT-3′	25	5 μM	0.1%	45.7
Phosphodiester Oligodeoxynucleotide	5′-TGCATCCCCCAGGCCACCAT-3′		5 μM	0.1%	81.4
Double stranded small RNA	5′-UGCAUCCCCCAGGCCACCAUdTdT-3′ and complemental sequence	20	5 μM	0.1%	57.9

(b) Effects of ODN sequence on TER (%).

Oligonucleotides				Atelocollagen	
Name	Sequence	Reference	Concentration	0%	0.1%
				TER (%)	
Blank control				100	—
ODN-(1)	5′-TGCATCCCCCAGGCCACCAT-3′	25	5 μM	100	58
ODN-(2)	5′-TCGCATCGACCCGCCCACTA-3′	25	5 μM	100	54
ODN-(3)	5′-GCTGATTAGAGAGAGGTCCC-3′	26	5 μM	100	50
ODN-(4)	5′-CCCTGGAGAGAGATTAGTCG-3′		5 μM	96	65

(c) Effects of ODN length on TER (%).

Oligonucleotides		Atelocollagen	
Sequence	Concentration	0%	0.1%
Examination (1)		TER (%)	
Blank control	—	94.6	—
Atelocollagen alone	—	—	94.6
ODN 10-mer (5′-TGCATCCCCC-3′)	5 μM	106.3	102.8
ODN 15-mer (5′-TGCATCCCCCAGGCC-3′)	5 μM	94.1	47.1
ODN 20-mer (5′-TGCATCCCCCAGGCCACCAT-3′; Ref. [25])	5 μM	107.1	50.0
ODN 30-mer (20-mer ODN + 10-mer ODN)	5 μM	102.9	43.8
Examination (2)		TER (%)	
Blank control	—	87.4	—
Atelocollagen alone	—	—	83.3
ODN 20-mer (5′-TGCATCCCCCAGGCCACCAT-3′; Ref. [25])	5 μM	91.7	51.4
ODN 30-mer (20-mer ODN + 10-mer ODN)	5 μM	83.3	26.5
ODN 50-mer (20-mer ODN $\times$ 2 + 10-mer ODN)	5 μM	85.7	35.3
ODN 100-mer (20-mer ODN $\times$ 5)	5 μM	82.4	50.0

(d) Effects of the concentrations of ODN and atelocollagen on TER (%).

ODN concentration	Atelocollagen			
	0%	0.003%	0.03%	0.1%
		TER (%)		
Blank control	94.6			
0.5 μM	100.0			77.8
5 μM	102.8			43.7
50 μM	102.9			50.8
500 μM	91.7			28.5
		TER (%)		
Atelocollagen alone				100.0
5 μM	94.9	98.1	54.9	52.0

ODN sequence: 5′-TGCATCCCCCAGGCCACCAT-3′.
TER(%): relative value at 1.5 hrs compared to the value observed at the start of the experiment.

sulfate polyacrylamide gels (Cosmo Bio, Tokyo, Japan) (SDS PAGE). After being electrophoretically transferred to nitrocellulose membranes (Immobilon; Millipore, Billerica, MA), the membranes were saturated with blocking buffer (trisbuffered saline [TBS] supplemented with 0.1% tween 20 and 4% skimmed milk) for 30 min at room temperature and incubated with antiactin, anti-ZO-1, anti-VE-cadherin (BD Biosciences, San Diego, CA), anticlaudin-5 (Zymed Laboratories, San Francisco, CA), anti-p38 mitogen-activated protein kinase (MAP Kinase or MAPK) (Santa Cruz Biotechnology, Santa Cruz, CA), antiphospho-p38 MAPK (Cell Signaling, Beverly, MA), anti-p42/44 MAPK (Promega, Madison, WI), antiphospho-p42/44 MAPK (Cell Signaling, Beverly, MA), anti-Rho-A, and anti-cdc42 (Santa Cruz Biotechnology, Santa Cruz, CA) antibodies (1:1000) for 1 h at room temperature. The membranes were then incubated with horseradish peroxidase-conjugated anti-rabbit or mouse IgG (Dako A/S, Copenhagen, Denmark) at room temperature for 1 h. The immunoreactive bands were detected using an ECL Western blotting analysis system (GE Healthcare, Little Chalfont, UK).

3. Results

3.1. Modification of Endothelial Sealing Function. Paracellular flux is dependent on the function of tight junctions [30, 31]. We assessed the effects of an AC formulation on the TER of HMVEC to evaluate their tight junction function. As shown in Figure 1 and Table 1(a), the ODN containing AC formulation caused a time-dependent reduction in TER, while TER was hardly affected by treatment with ODN or atelocollagen alone. As for the type of oligonucleotide in the formulation, phosphorothioate ODN produced a more significant reduction in TER than phosphodiester ODN, which only produced slight alterations. A change in the TER value was also induced by treatment with small dsRNA.

Various formulations containing different ratios of ODN and atelocollagen were examined in order to understand which parameters have the greatest effect on the change in TER. As a result, we found that the TER change was dependent on the size of the ODN and the composition of the formulation, but not the ODN sequence, as shown in Tables 1(b), 1(c), and 1(d). Specifically, ODN composed of 15 or more bases were effective and those containing around 30 bases were the most effective, but 10-base-long ODN were not effective. The change in tight junction function was also dependent on the concentrations of ODN and atelocollagen in the formulation.

To verify that the AC formulation increased paracellular flux, the amount of Texas red-labeled dextran (molecular weight: 40 kD) transported across an endothelial cell layer was examined. As shown in Figure 2(a), dextran transport was increased approximately twofold in the cell cultures incubated with the AC formulation.

Next, the paracellular transport of atelocollagen was analyzed and compared with those of BSA and dextran. Neither BSA nor dextran affected the TER value of the cells. Only very small amounts of BSA and dextran penetrated the cell sheet during the 2-hour study period; on the other hand, much more atelocollagen passed through, even though the molecular weight of atelocollagen is 4-5 times higher than those of BSA and dextran (Figure 2(b)).

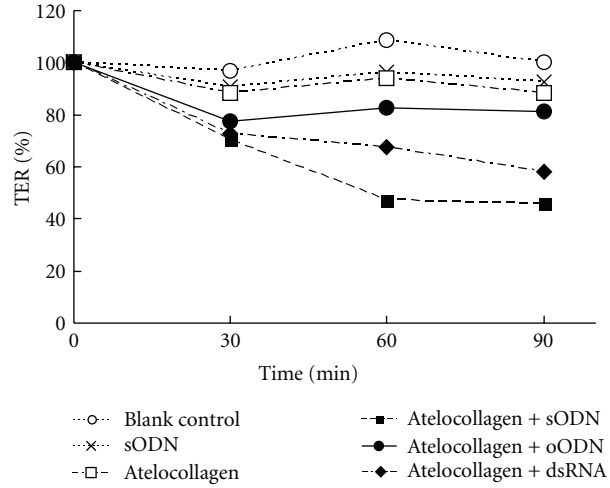

Figure 1: Time-dependent reduction of TER after treatment with different types of oligonucleic acids in combination with atelocollagen. HMVEC cells were treated with 5 μM of oligonucleic acids with or without 0.1% atelocollagen. sODN: phosphorothioate oligodeoxynucleotide, oODN: phosphodiester oligodeoxynucleotide, dsRNA: small double stranded RNA. The sequences of the ODN are described in Table 1(a).

An examination using BMVEC [27] was performed to determine whether the effect of the AC formulation was specific to HMVEC. As a result, we found that the TER value of the BMVEC was also reduced by the AC formulation (and only the AC formulation), as shown in Figure 3. BMVEC forms the blood-brain barrier (BBB), where intercellular sealing function is strictly maintained. These results showed that the AC formulation is able to affect the paracellular flux of endothelial barriers.

3.2. Effects on Cell Morphology. It is well known that increased endothelial permeability is associated with impaired intercellular contact [32–35]. We carried out an immunohistochemical analysis of the cells treated with the AC formulation to clarify how their intercellular sealing was affected. As shown in Figure 4(a), treatment with the AC formulation markedly reduced the degree of intercellular contact, as shown by intercellular gap formation, actin stress fiber formation, cellular contraction, and a lack of VE-cadherin. Adequate expression of claudin-5, one of the key components of the endothelial barrier, was noted at the cell periphery. However, ZO-1 protein expression was absent from the intercellular gaps. On the contrary, Western blotting revealed that treatment with the AC formulation did not affect the expression of these proteins (Figure 4(b)). Although the TER value remained low as long as the AC formulation was present in the culture medium, the treatment did not cause toxicity. The cells survived well for at least 24 hrs, and both the TER and morphology of the cells could be recovered by removing the formulation (data not shown).

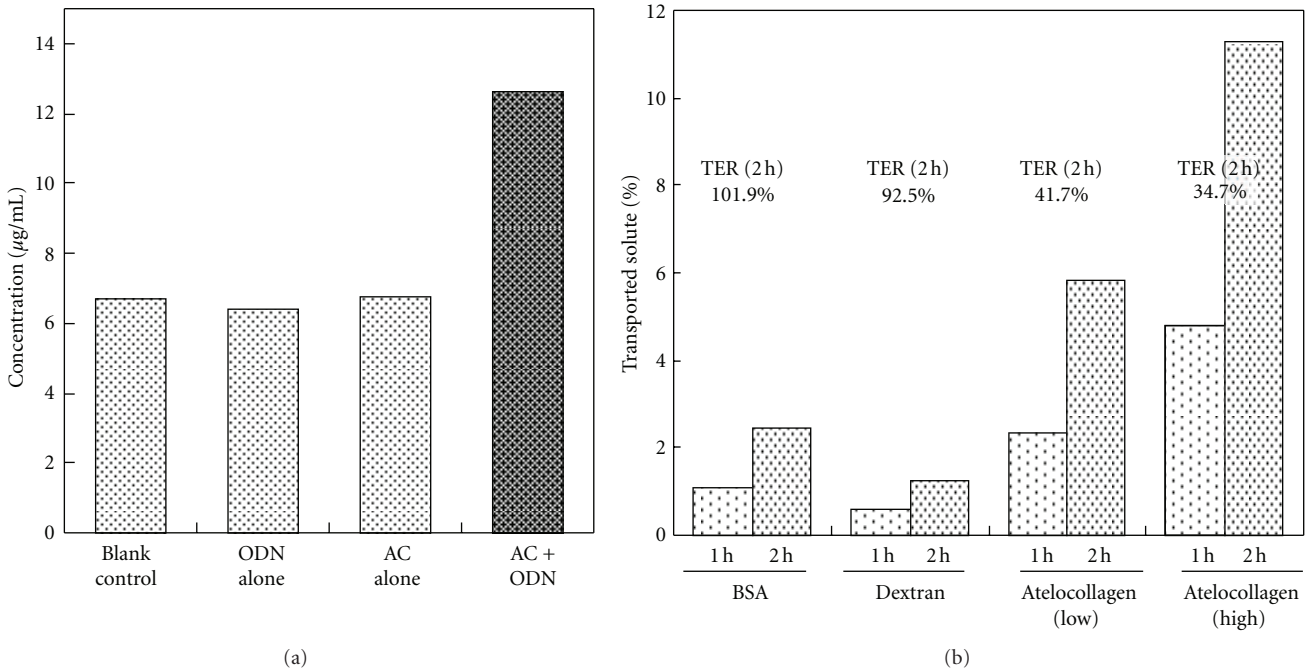

Figure 2: Effects of the AC formulation on endothelial paracellular flux. (a) Increase in dextran permeation induced by the AC formulation. One hour after the addition of oligodeoxynucleotides (ODN), atelocollagen (AC), or the AC formulation (AC + ODN) to the inner chambers, Texas red-conjugated dextran (MW: 40,000) was added to the inner chambers. One hour later, the dextran concentration of the medium in the outer chambers was determined. (b) Enhanced paracellular transport of atelocollagen. 0.1% w/v of Alexa Fluor 594 conjugated bovine serum albumin (BSA; MW: 66 kDa), 0.1% w/v of fluorescein conjugated dextran (dextran; MW: 70 kDa), or rhodamine red-conjugated atelocollagen (0.03% w/v: atelocollagen (Low); 0.1 % w/v: atelocollagen (High); MW of atelocollagen: 300 kDa) with 5 μM of ODN was added to the inner chambers. The solute concentrations of the outer chambers were analyzed by measuring their fluorescence at 1 and 2 hours after the start of the experiment. TER at 2 hours is represented as a percentage value compared to that observed at the start of the experiment.

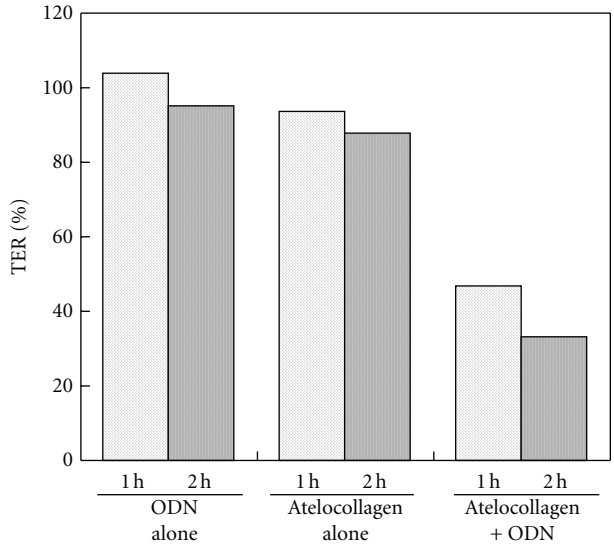

Figure 3: Effects of the AC formulation on the TER of BMVEC. The bar represents TER as a percentage compared to the value observed at the start of the experiment. TER was determined at 1 and 2 hours after treatment with ODN alone (ODN), atelocollagen alone (atelocollagen), the AC formulation (atelocollagen + ODN).

No such morphological changes were induced by treatment with ODN or atelocollagen alone (Figure 4(a)).

Microtubules play an important role in regulating actin formation and hence, endothelial barrier function [36, 37]. We also histopathologically examined the shape of the microtubules. As shown in Figure 5, α-tubulin formed a fine network in the blank control. However, treatment with the AC formulation caused the peripheral fine structure of the α-tubulin network to be lost.

3.3. Activation of Signal Transduction-Related Molecules. Many studies have shown that increased endothelial permeability and impaired intercellular contact can be induced by signal transduction, mainly that of Rho A [32, 38] and p38 MAP kinase [36, 39–42]. Thus, we investigated the effects of the AC formulation on signal transduction. As a result, no differences were found in the expression levels of Rho-A, Cdc42, or P42/44 MAP kinases or their phosphorylated forms. Regarding p38 MAP kinase, although no changes were noted among the control, oligonucleotide alone, or atelocollagen alone groups, the levels of phosphorylated p38 MAP kinase were markedly increased in the cells treated with the AC formulation (Figure 6), which indicates that

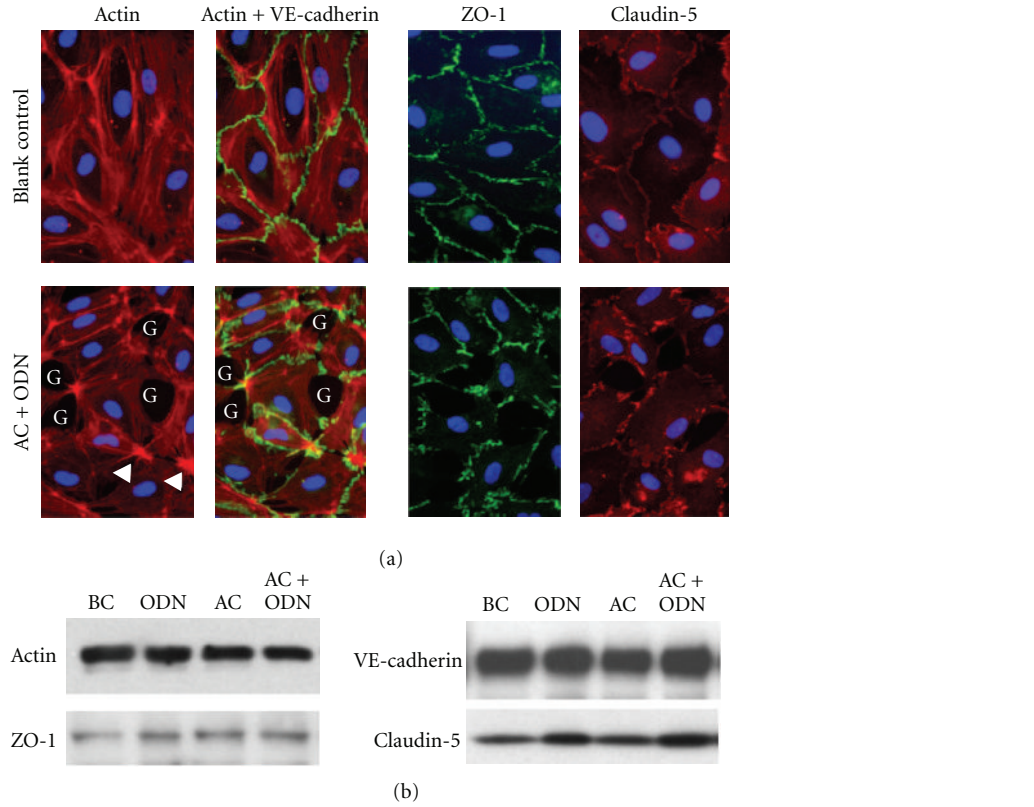

Figure 4: Effects of atelocollagen combined with ODN on intercellular formation. (a) Images of actin, VE-cadherin with actin, ZO-1, and claudin-5 in the endothelial cells of the blank control (upper panels) and the cells treated with the AC formulation (lower panels). Treatment with the AC formulation (AC + ODN) induced changes in cell morphology associated with stress fiber formation (arrowhead), intercellular gap formation (G), and the loss of VE-cadherin and ZO-1. (b) Western blot analysis of actin, VE-cadherin, ZO-1, and claudin-5. The whole cell extract obtained from the cells was separated by SDS-PAGE and immunoblotted with the corresponding antibodies. BC: blank control, ODN: treated with ODN alone, AC: treated with atelocollagen alone, AC + ODN: treated with the AC formulation.

the impact of the AC formulation on tissue permeability is associated with the activation of p38 MAP kinase.

4. Discussion

Collagen plays an important role in the extracellular matrix by supporting cells so that they can form tissues and organs. Atelocollagen is produced from type I collagen and is widely used in its solid state as a biomaterial for medical and surgical products because of its biocompatibility and workability [1]. However, the kinetics, dynamics, and biological functions of atelocollagen after its injection into the living body are still poorly understood, and it is essential to elucidate the characteristics of atelocollagen in order to fully exploit its potential.

Here, we demonstrated a novel biological function of atelocollagen. When endothelial cell sheets were treated with atelocollagen or oligonucleotides alone, the intercellular structure of the sheet was not changed. However, when the atelocollagen and oligonucleotides were administered together, intercellular gaps formed and consequently the paracellular flux of the sheet was elevated. The AC formulation itself was also able to penetrate the sheet. This function might explain the ability of atelocollagen to effectively deliver oligonucleotides. The abovementioned changes were elicited via the activation of p38 MAP kinase, a signal-transduction-related molecule. In addition, the changes observed in this study are similar to those triggered by thrombin [32], histamine [33], TNF-α [34, 36], and VEGF (vascular endothelial growth factor) [43], and so forth. As shown in Section 3.1, the degree to which endothelial function was affected was dependent on the molecular structure of the oligonucleotides including their size and chemical modifications, suggesting that the three-dimensional structure of the oligonucleotide and atelocollagen complex stimulates a signal transduction pathway that acts as a permeability modulator, although the specific pathway that it stimulates remains unknown.

To date, no severe systemic edema or side effects of the AC formulation have been noted, even after the intravenous administration of atelocollagen as an oligonucleotide drug carrier. These findings indicate that atelocollagen could be used as a permeability enhancer at local treatment sites without the adverse systemic effects that cytokines and chemokines sometimes provoke. Since tight junction modulators are regarded as practical drug delivery enhancer candidates [44–46], the function of atelocollagen demonstrated in the present study should be thoroughly investigated.

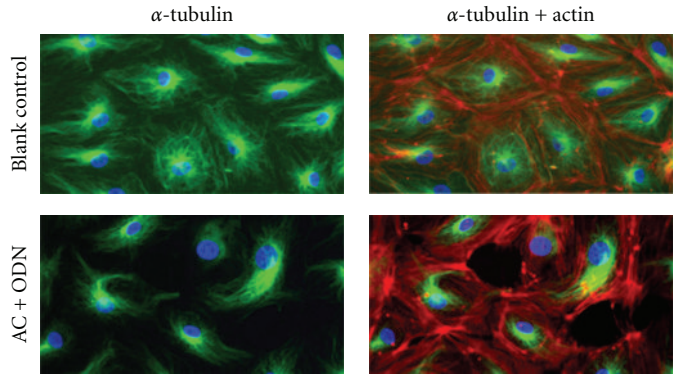

Figure 5: Effects of the AC formulation on the microtubule networks in the endothelial cells. Images of α-tubulin (left panels) and α-tubulin (green) with actin (red) (right panels). In the blank control (upper), the microtubule network was composed of extended fine microtubule structures. After treatment with the AC formulation (AC + ODN), the fine microtubules had been disassembled, and the network had disintegrated (lower).

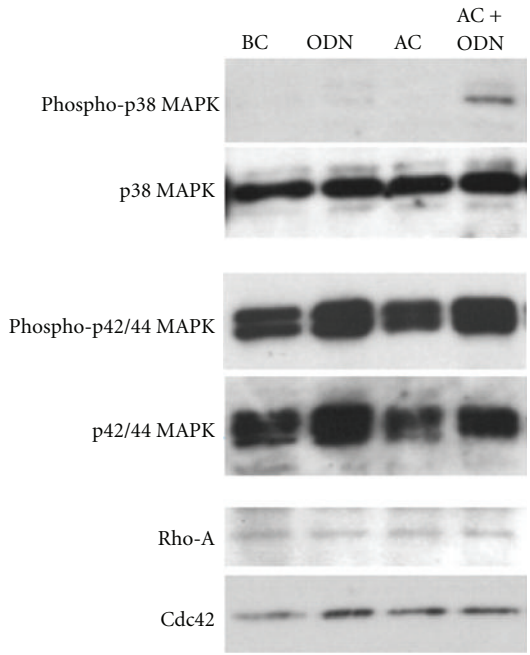

Figure 6: Effects of the AC formulation on the expression of signal transduction-related molecules. Western blot analysis of the expression levels of p38 MAP-kinase, the p42/44 MAP-kinases, and their phosphorylated forms, RhoA and Cdc42 was performed after each treatment. BC: blank control, ODN: treated with ODN alone, AC: treated with atelocollagen alone, AC + ODN: treated with AC formulation. p38 MAP-kinase activation was only enhanced by the AC formulation.

The unique biological functions of atelocollagen have led to the development of unique antitumor therapies and products, such as surgical products; formulations that sustain the release of antitumor proteins [2–4]; treatments that enhance the antitumor activities of various molecules including antisense ODN [11–13], siRNA [14–20, 24], and miRNA [21–23]. Obtaining more information about atelocollagen would allow us to develop the next generation of atelocollagen-mediated drug delivery systems.

Acknowledgments

The authors thank Yoshiko Minakuchi, Taichi Tsujimoto, and Yumi Kotoda for providing technical assistance.

References

[1] T. Miyata, T. Taira, and Y. Noishiki, "Collagen engineering for biomaterial use," *Clinical Materials*, vol. 9, no. 3-4, pp. 139–148, 1992.

[2] K. Fujioka, M. Maeda, T. Hojo, and A. Sano, "Protein release from collagen matrices," *Advanced Drug Delivery Reviews*, vol. 31, no. 3, pp. 247–266, 1998.

[3] K. Marumo, M. Oya, M. Murai, and H. Tazaki, "Application of cytokine drug delivery systems to the immunotherapy of renal cell carcinoma in mice," *International Journal of Urology*, vol. 3, supplement 1, pp. S24–S27, 1996.

[4] T. Fujiwara, K. Sakagami, and K. Orita, "Antitumor effects of a new interleukin-2 slow delivery system on methylcholanthreneinduced fibrosarcoma in mice," *Journal of Cancer Research and Clinical Oncology*, vol. 116, no. 2, pp. 141–148, 1990.

[5] O. Takemoto, T. Yoshimine, A. K. M. G. Muhammad et al., "Distribution of nerve growth factor in cat brains following topical application of solution or Minipellet," *Neurological Research*, vol. 20, no. 2, pp. 116–120, 1998.

[6] H. Maeda, A. Sano, and K. Fujioka, "Controlled release of rhBMP-2 from collagen minipellet and the relationship between release profile and ectopic bone formation," *International Journal of Pharmaceutics*, vol. 275, no. 1-2, pp. 109–122, 2004.

[7] M. Nakamura, Y. Ando, S. Nagahara et al., "Targeted conversion of the transthyretin gene *in vitro* and *in vivo*," *Gene Therapy*, vol. 11, no. 10, pp. 838–846, 2004.

[8] K. Hanai, T. Kurokawa, Y. Minakuchi et al., "Potential of atelocollagen-mediated systemic antisense therapeutics for inflammatory disease," *Human Gene Therapy*, vol. 15, no. 3, pp. 263–272, 2004.

[9] T. Ishimoto, Y. Takei, Y. Yuzawa et al., "Downregulation of monocyte chemoattractant protein-1 involving short interfering RNA attenuates hapten-induced contact hypersensitivity," *Molecular Therapy*, vol. 16, no. 2, pp. 387–395, 2008.

[10] T. Ochiya, Y. Takahama, S. Nagahara et al., "New delivery system for plasmid DNA *in vivo* using atelocollagen as a carrier material: the Minipellet," *Nature Medicine*, vol. 5, no. 6, pp. 707–710, 1999.

[11] K. Hirai, H. Sasaki, H. Sakamoto et al., "Antisense oligodeoxynucleotide against HST-1/FGF-4 suppresses tumorigenicity of an orthotopic model for human germ cell tumor in nude mice," *Journal of Gene Medicine*, vol. 5, no. 11, pp. 951–957, 2003.

[12] Y. Takei, K. Kadomatsu, K. Yuasa, W. Sato, and T. Muramatsu, "Morpholino antisense oligomer targeting human midkine: its application for cancer therapy," *International Journal of Cancer*, vol. 114, no. 3, pp. 490–497, 2005.

[13] K. Nakazawa, T. Nemoto, T. Hata et al., "Single-injection ornithine decarboxylase-directed antisense therapy using atelocollagen to suppress human cancer growth," *Cancer*, vol. 109, no. 5, pp. 993–1002, 2007.

[14] Y. Minakuchi, F. Takeshita, N. Kosaka et al., "Atelocollagen-mediated synthetic small interfering RNA delivery for effective gene silencing *in vitro* and *in vivo*," *Nucleic acids research*, vol. 32, no. 13, p. e109, 2004.

[15] F. Takeshita, Y. Minakuchi, S. Nagahara et al., "Efficient delivery of small interfering RNA to bone-metastatic tumors by using atelocollagen *in vivo*," *Proceedings of the National Academy of Sciences of the United States of America*, vol. 102, no. 34, pp. 12177–12182, 2005.

[16] P. Mu, S. Nagahara, N. Makita, Y. Tarumi, K. Kadomatsu, and Y. Takei, "Systemic delivery of siRNA specific to tumor mediated by atelocollagen: combined therapy using siRNA targeting Bcl-xL and cisplatin against prostate cancer," *International Journal of Cancer*, vol. 125, no. 12, pp. 2978–2990, 2009.

[17] E. Ashihara, E. Kawata, Y. Nakagawa et al., "β-catenin small interfering RNA successfully suppressed progression of multiple myeloma in a mouse model," *Clinical Cancer Research*, vol. 15, no. 8, pp. 2731–2738, 2009.

[18] T. Sasaki, K. Nakashiro, H. Tanaka et al., "Knockdown of Akt isoforms by RNA silencing suppresses the growth of human prostate cancer cells *in vitro* and *in vivo*," *Biochemical and Biophysical Research Communications*, vol. 399, no. 1, pp. 79–83, 2010.

[19] I. Takigami, T. Ohno, Y. Kitade et al., "Synthetic siRNA targeting the breakpoint of EWS/Fli-1 inhibits growth of Ewing sarcoma xenografts in a mouse model," *International Journal of Cancer*, vol. 128, no. 1, pp. 216–226, 2011.

[20] E. Kawata, E. Ashihara, S. Kimura et al., "Administration of PLK-1 small interfering RNA with atelocollagen prevents the growth of liver metastases of lung cancer," *Molecular Cancer Therapeutics*, vol. 7, no. 9, pp. 2904–2912, 2008.

[21] H. Tazawa, N. Tsuchiya, M. Izumiya, and H. Nakagama, "Tumor-suppressive miR-34a induces senescence-like growth arrest through modulation of the E2F pathway in human colon cancer cells," *Proceedings of the National Academy of Sciences of the United States of America*, vol. 104, no. 39, pp. 15472–15477, 2007.

[22] F. Takeshita, L. Patrawala, M. Osaki et al., "Systemic delivery of synthetic microRNA-16 inhibits the growth of metastatic prostate tumors via downregulation of multiple cell-cycle genes," *Molecular Therapy*, vol. 18, no. 1, pp. 181–187, 2010.

[23] Y. Takei, M. Takigahira, K. Mihara, Y. Tarumi, and K. Yanagihara, "The metastasis-associated microRNA miR-516a-3p is a novel therapeutic target for inhibiting peritoneal dissemination of human scirrhous gastric cancer," *Cancer Research*, vol. 71, no. 4, pp. 1442–1453, 2011.

[24] Y. Takei, K. Kadomatsu, Y. Yuzawa, S. Matsuo, and T. Muramatsu, "A small interfering RNA targeting vascular endothelial growth factor as cancer therapeutics," *Cancer Research*, vol. 64, no. 10, pp. 3365–3370, 2004.

[25] S. K. Klimuk, S. C. Semple, P. N. Nahirney et al., "Enhanced anti-inflammatory activity of a liposomal intercellular adhesion molecule-1 antisense oligodeoxynucleotide in an acute model of contact hypersensitivity," *Journal of Pharmacology and Experimental Therapeutics*, vol. 292, no. 2, pp. 480–488, 2000.

[26] K. L. Sewell, R. S. Geary, B. F. Baker et al., "Phase I trial of ISIS 104838, a 2′-methoxyethyl modified antisense oligonucleotide targeting tumor necrosis factor-α," *Journal of Pharmacology and Experimental Therapeutics*, vol. 303, no. 3, pp. 1334–1343, 2002.

[27] K. Nagasawa, H. Chiba, H. Fujita et al., "Possible involvement of gap junctions in the barrier function of tight junctions of brain and lung endothelial cells," *Journal of Cellular Physiology*, vol. 208, no. 1, pp. 123–132, 2006.

[28] T. Soma, H. Chiba, Y. Kato-Mori et al., "Thr^{207} of claudin-5 is involved in size-selective loosening of the endothelial barrier by cyclic AMP," *Experimental Cell Research*, vol. 300, no. 1, pp. 202–212, 2004.

[29] T. Kojima, J. Fuchimoto, H. Yamaguchi et al., "c-Jun N-terminal kinase is largely involved in the regulation of tricellular tight junctions via tricellulin in human pancreatic duct epithelial cells," *Journal of Cellular Physiology*, vol. 225, no. 3, pp. 720–733, 2010.

[30] N. Salamat-Miller and T. P. Johnston, "Current strategies used to enhance the paracellular transport of therapeutic polypeptides across the intestinal epithelium," *International Journal of Pharmaceutics*, vol. 294, no. 1-2, pp. 201–216, 2005.

[31] C. M. Van Itallie and J. M. Anderson, "Claudins and epithelial paracellular transport," *Annual Review of Physiology*, vol. 68, pp. 403–429, 2006.

[32] V. Vouret-Craviari, P. Boquet, J. Pouysségur, and E. Van Obberghen-Schilling, "Regulation of the actin cytoskeleton by thrombin in human endothelial cells: role of Rho proteins in endothelial barrier function," *Molecular Biology of the Cell*, vol. 9, no. 9, pp. 2639–2653, 1998.

[33] Y. Yuan, H. J. Granger, D. C. Zawieja, D. V. DeFily, and W. M. Chilian, "Histamine increases venular permeability via a phospholipase C-NO synthase-guanylate cyclase cascade," *American Journal of Physiology*, vol. 264, no. 5, pp. H1734–H1739, 1993.

[34] B. Wójciak-Stothard, A. Entwistle, R. Garg, and A. J. Ridley, "Regulation of TNF-α-induced reorganization of the actin cytoskeleton and cell-cell junctions by Rho, Rac, and Cdc42 in human endothelial cells," *Journal of Cellular Physiology*, vol. 176, no. 1, pp. 150–165, 1998.

[35] M. Puhlmann, D. M. Weinreich, J. M. Farma, N. M. Carroll, E. M. Turner, and H. R. Alexander, "Interleukin-1β induced vascular permeability is dependent on induction of endothelial tissue factor (TF) activity," *Journal of Translational Medicine*, vol. 3, article 37, 2005.

[36] I. Petrache, A. Birukova, S. I. Ramirez, J. G. N. Garcia, and A. D. Verin, "The role of the microtubules in tumor necrosis factor-α-induced endothelial cell permeability," *American Journal of Respiratory Cell and Molecular Biology*, vol. 28, no. 5, pp. 574–581, 2003.

[37] K. M. Smurova, A. A. Birukova, A. D. Verin, and I. B. Alieva, "Microtubule system in endothelial barrier dysfunction: disassembly of peripheral microtubules and microtubule

reorganization in internal cytoplasm," *Cell and Tissue Biology*, vol. 2, no. 1, pp. 45–52, 2008.

[38] B. Wójciak-Stothard, S. Potempa, T. Eichholtz, and A. J. Ridley, "Rho and Rac but not Cdc42 regulate endothelial cell permeability," *Journal of Cell Science*, vol. 114, no. 7, pp. 1343–1355, 2001.

[39] A. Blois, B. Srebro, M. Mandalà, A. Corti, K. B. Helle, and G. Serck-Hanssen, "The chromogranin A peptide vasostatin-I inhibits gap formation and signal transduction mediated by inflammatory agents in cultured bovine pulmonary and coronary arterial endothelial cells," *Regulatory Peptides*, vol. 135, no. 1-2, pp. 78–84, 2006.

[40] Z. G. Chu, J. P. Zhang, H. P. Song et al., "P38 map kinase mediates burn serum-induced endothelial barrier dysfunction: involvement of F-actin rearrangement and L-caldesmon phosphorylation," *Shock*, vol. 34, no. 3, pp. 222–228, 2010.

[41] D. Yang, P. Xie, S. Guo, and H. Li, "Induction of MAPK phosphatase-1 by hypothermia inhibits TNF-induced endothelial barrier dysfunction and apoptosis," *Cardiovascular Research*, vol. 85, no. 3, pp. 520–529, 2010.

[42] C. G. Kevil, T. Oshima, and S. Alexander, "The role of p38 MAP kinase in hydrogen peroxide mediated endothelial solute permeability," *Endothelium*, vol. 8, no. 2, pp. 107–116, 2001.

[43] B. K. Lal, S. Varma, P. J. Pappas, R. W. Hobson, and W. N. Durán, "VEGF increases permeability of the endothelial cell monolayer by activation of PKB/akt, endothelial nitric-oxide synthase, and MAP kinase pathways," *Microvascular Research*, vol. 62, no. 3, pp. 252–262, 2001.

[44] N. N. Salama, N. D. Eddington, and A. Fasano, "Tight junction modulation and its relationship to drug delivery," *Advanced Drug Delivery Reviews*, vol. 58, no. 1, pp. 15–28, 2006.

[45] L. González-Mariscal, P. Nava, and S. Hernández, "Critical role of tight junctions in drug delivery across epithelial and endothelial cell layers," *Journal of Membrane Biology*, vol. 207, no. 2, pp. 55–68, 2005.

[46] K. Matsuhisa, M. Kondoh, A. Takahashi, and K. Yagi, "Tight junction modulator and drug delivery," *Expert Opinion on Drug Delivery*, vol. 6, no. 5, pp. 509–515, 2009.

Hindawi Publishing Corporation
Journal of Drug Delivery
Volume 2012, Article ID 767839, 20 pages
doi:10.1155/2012/767839

Review Article

PLGA Nanoparticles for Ultrasound-Mediated Gene Delivery to Solid Tumors

Marxa Figueiredo[1] and Rinat Esenaliev[2]

[1] *Department of Pharmacology and Toxicology, University of Texas Medical Branch, 301 University Boulevard, Galveston, TX 77555, USA*
[2] *Department of Neuroscience and Cell Biology, Department of Anesthesiology, and Center for Biomedical Engineering, University of Texas Medical Branch, 301 University Boulevard, Galveston, TX 77555, USA*

Correspondence should be addressed to Marxa Figueiredo, mlfiguei@utmb.edu and Rinat Esenaliev, riesenal@utmb.edu

Received 8 October 2011; Accepted 26 November 2011

Academic Editor: Rassoul Dinarvand

This paper focuses on novel approaches in the field of nanotechnology-based carriers utilizing ultrasound stimuli as a means to spatially target gene delivery *in vivo*, using nanoparticles made with either poly(lactic-co-glycolic acid) (PLGA) or other polymers. We specifically discuss the potential for gene delivery by particles that are echogenic (amenable to destruction by ultrasound) composed either of polymers (PLGA, polystyrene) or other contrast agent materials (Optison, SonoVue microbubbles). The use of ultrasound is an efficient tool to further enhance gene delivery by PLGA or other echogenic particles *in vivo*. Echogenic PLGA nanoparticles are an attractive strategy for ultrasound-mediated gene delivery since this polymer is currently approved by the US Food and Drug Administration for drug delivery and diagnostics in cancer, cardiovascular disease, and also other applications such as vaccines and tissue engineering. This paper will review recent successes and the potential of applying PLGA nanoparticles for gene delivery, which include (a) echogenic PLGA used with ultrasound to enhance local gene delivery in tumors or muscle and (b) PLGA nanoparticles currently under development, which could benefit in the future from ultrasound-enhanced tumor targeted gene delivery.

1. Introduction

To achieve successful gene therapy in a clinical setting, it is critical that gene delivery systems be safe and easy to apply and provide therapeutic transgene expression. Over the past decades, many studies using viral vectors have established the gold standard for successful gene transfer and high-level expression in target cells. However, the upcoming trend is in the development of improved methods for nonviral gene transfer, due to the considerable immunogenicity related to the use of viruses. Nonviral vectors are particularly suitable since they allow ease of large-scale production and are relatively less immunogenic. Recently, several novel nonviral vectors have been developed that approach viruses with respect to transfection efficiency. A variety of nonviral delivery systems that can be used in different clinical settings are also available and one promising direction is the development of biodegradable, echogenic nanoparticle systems that can deliver DNA (or drugs) efficiently by the use of ultrasound-mediated delivery. We will focus our discussion on PLGA nanoparticles and their promise for nucleic acid delivery *in vivo* using ultrasound-mediated gene delivery methods.

2. Current Sonoporation Principles

A relatively novel strategy for gene and drug delivery enhancement is application of echogenic nanoparticles made of poly(d,l-lactic-co-glycolide) (PLGA) or derivatives in combination with relatively low-intensity ultrasound (US). This method (referred to as "sonoporation") can induce cavitation of or near cellular membranes to enhance delivery of drugs and nucleic acids *in vitro* and *in vivo*. In general, low-intensity US can induce beneficial and reversible cellular effects, in contrast to high US intensities, which are more

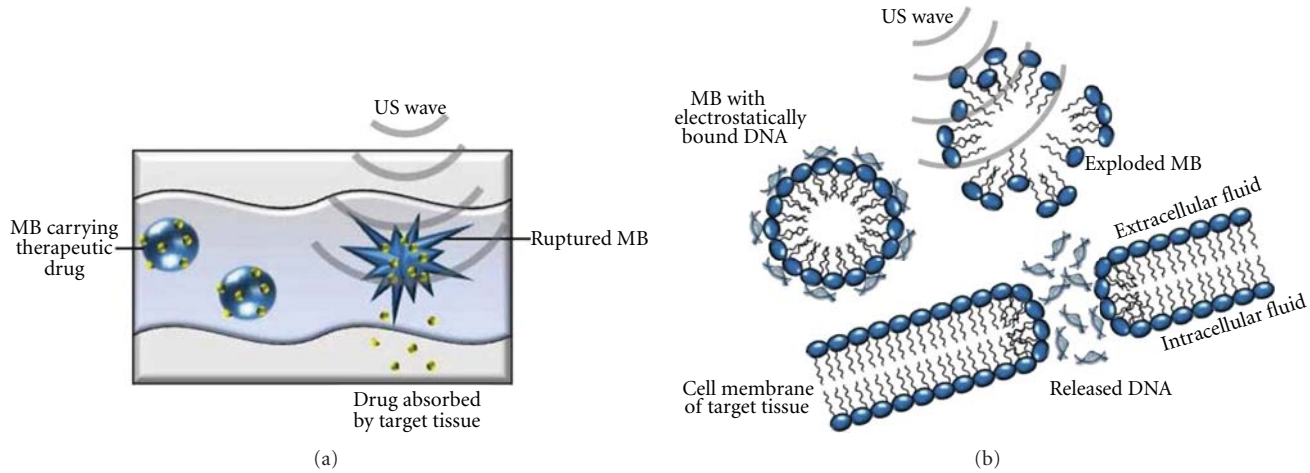

Figure 1: Sonoporation mechanisms for therapeutic delivery. (a) Sonoporation for drug delivery. Drugs can be delivered by sonoporation. Microbubbles with drug attached to the surface or enclosed within the particle travel in capillaries. Upon US exposure MBs rupture, releasing the drug contents. Drugs are absorbed by the target tissue. (b) Sonoporation for gene delivery. When plasmid-DNA-(pDNA-) containing MBs are passed through blood vessels adjacent to tumor cells, US waves rupture MB and release pDNA. Released pDNA penetrates into cells through their membranes by sonoporation. Reproduced with permission from [5].

likely to induce cellular death. Sonoporation is an emerging and promising physical method for drug and gene delivery enhancement *in vitro* and *in vivo* [1–4]. In fact, sonoporation has several advantages over other nonphysical techniques of nucleic acid (DNA, siRNA) delivery including the ability to also deliver viruses and small molecules (reviewed in [5]). Sonoporation, however, has some limitations including penetration depth, some deep (internal) tumors may not be easily accessible by US, and tissues such as bone might interfere with the US penetration. Also, the influence of air within the lung might also impair the ability of US waves to penetrate and deliver genes in the lung. Typically, sonoporation agents (also useful as US contrast agents) can be composed of micro- or nanoparticles filled with either air or gases, which give echogenic properties, surrounded by a shell of lipids or polymeric formulations. Gas-filled lipid particles are called microbubbles (MBs), while echogenic polymeric particles can be defined as either nanoparticles (NPs) or microparticles (MPs) depending on their size. Different types of MB have been synthesized by combining different shell compositions such as albumin, galactose, lipids, or polymers, with different gaseous cores such as air, or high-molecular-weight gases (perfluorocarbon, sulphur hexafluoride, or nitrogen) and several types are available commercially (reviewed in [5]). This paper will focus on echogenic NP use in combination with US-mediated sonoporation to induce gene delivery.

The mechanism of sonoporation involves the motion of MB or NP and disruption induced by low-intensity US sonication (Figure 1). US increases the permeability of cell membranes and the endothelium, thus enhancing therapeutic uptake, and can locally increase drug/nucleic acid transport. Formation of short-lived nanopores (~100 nm) in the plasma membrane lasts a few seconds and is implicated as the dominant mechanism associated with acoustic cavitation [6]. Sonoporation mediates delivery of drugs and/or nucleic acids that have been incorporated into or on the surface of nano/microparticles via covalent or electrostatic interactions, which allow these complexes to circulate in the blood and retain their cargo until activation by US. US application results in localized and spatially controlled particle disruption that enhances gene/drug delivery. Sonoporation-mediated gene delivery has been applied to date in heart, blood vessels, lung, kidney, muscle, brain, and tumors with high efficiency [7]. However, in order to provide high transfection efficiency, ultrasonic parameters (such as acoustic pressure, pulse length, duty cycle, repetition rate, and exposure duration) and nano- or microparticle properties (such as size and echogenic characteristics of air- or gas-filled preparations) should be optimized [7]. The efficiency of drug/gene delivery typically correlates to the cell location relative to the US (transducer and its proximity to acoustically active nano- or microparticles). At ~1 MHz US, echogenic nano/microparticles or microbubbles oscillate steadily. It has been shown that lipid-shelled MB can expand from 2 μm to ~20–55 μm [8]. When MBs expand and collapse near a cell wall, a fluid jet/shock wave is formed followed by an increase in vascular permeability [9]. In this manner, drug or nucleic acid transport may occur by convection through a membrane pore [8], and this US-induced effect may represent the main mechanism for sonoporation-mediated gene or drug delivery. This is supported by correlation of the uptake of a dye with cellular deformation and membrane changes as assessed by scanning electron microscopy, membrane electrophysiology and atomic force microscopy [10–12]. Following pore formation, nonspecific uptake of extracellular molecules can occur, the membrane is repaired, and molecules are, therefore, retained within cells. Mammalian cells have been shown to repair pores of up to ~1000 μm^2 within a short period [13], in a manner

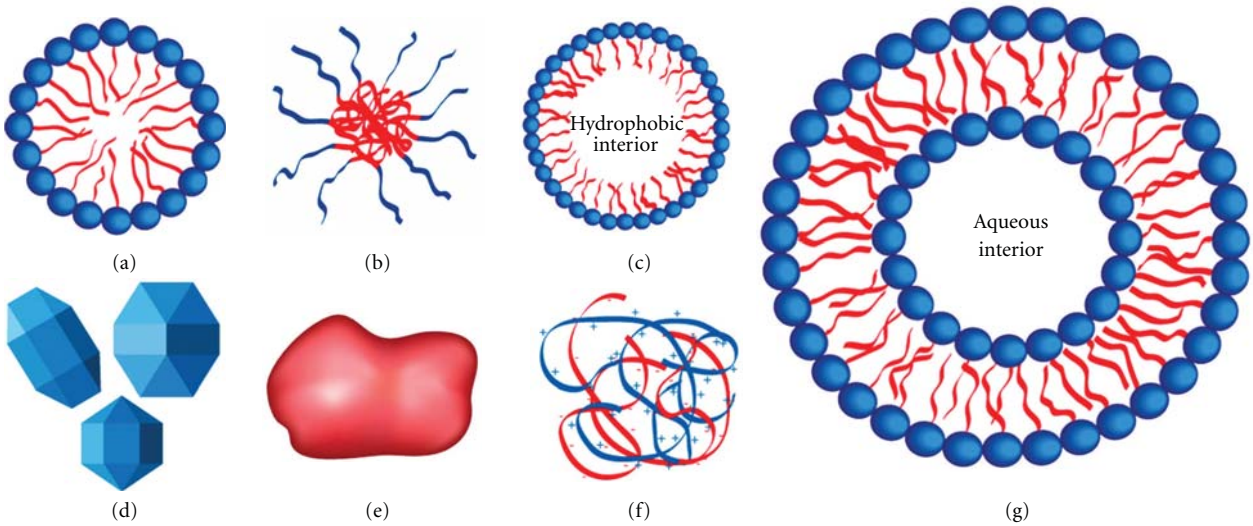

Figure 2: Various nanoparticles (not to scale) that may be used in ultrasound-enhanced drug and gene delivery. (a) Micelle (nonpolymeric) composed of amphiphilic surfactants. (b) Polymeric micelle composed of amphiphilic block copolymers. (c) Nanoemulsion consisting of a hydrophobic liquid core stabilized by surfactant. (d) Crystalline nanoparticles. (e) Amorphous polymeric nanoparticle. (f) Condensed ionic oligomers, such as DNA condensed with PEI or cationic lipids. (g) Single-walled liposome consisting of an amphiphilic bilayer surrounding an aqueous core. Reprinted with permission from [71].

resembling the kinetics of membrane repair after mechanical wounding, and Ca^{2+} levels are thought to promote this response [14, 15].

3. Echogenic Nanoparticles

In this paper, nanoparticles (NPs) are defined as molecules ranging in size from 1 nm to 1 μm and that are able to form a separate phase in aqueous suspension. Echogenic NPs are defined as NPs containing either atmospheric air or gas to form "nanobubbles" that can be used for drug and gene delivery when US is applied. In most medical applications, NPs typically are in suspension and can be classified into micelles, nanoemulsions, and suspensions of solid nanoparticles (Figure 2). Most of them have been tested for US-mediated gene delivery.

3.1. Nanoparticles Used for Gene Delivery

3.1.1. Lipid-Based Nanoparticles. Complexing of cationic lipids and DNA plasmids (lipofection) is efficient at transfection of various cell lines and several lipid combinations are available commercially. However, there has been little combination of US with lipofection, possibly because early studies using ultrasound and gas bubbles showed that the addition of the contrast agents enhanced transfection of naked DNA much more than traditional transfection by lipofection, which is mediated through endocytosis and pinocytosis mechanisms [16]. The incubation time of lipofection from transfection to gene expression is also slower compared to that with naked DNA and contrast agents [17]. Of the few studies that combined US and lipofection, one example highlights the challenges of this method. For example, brain tumor cell transfection using 2 MHz pulsed US for 1 min and Lipofectamine condensed with plasmids coding for green fluorescent protein (GFP) produced no change in transfection efficiency compared to conventional lipofection alone [18]. Therefore, it appears that lipofection is not enhanced by US unless gas bubbles are introduced in the liposome or present as a separate agent. If gas bubbles are present, the transfection by naked DNA + US then appears to be effcient *in vitro*. However, there are several advantages with respect to enhanced durability when plasmids are complexed with cationic lipids.

3.1.2. Polymeric Nanoparticles. Polymers used for drug and gene delivery typically include polystyrene (PS), poly(lactic acid) (PLA), poly(lactic-co-glycolic acid) (PLGA), and polyplexes of plasmids and cationic polymers. Application of US to solid polymeric nanoparticles appears to be effective in reducing cavitation threshold in water, even in the absence of preformed gas bubbles [19]. For example, we have shown that PS nanoparticles can reduce the threshold of US-induced cavitation activity in pure water from about 7.3 bar to <5 bar, depending upon the size and concentration used [1, 20]. We observed that the threshold decreased with increasing particle concentration and particle sizes [1, 20]. Thus, even without the use of gas bubble contrast agents, there was sufficient cavitational activity to produce significant bioeffects. Although other investigators have used other polymer and polyplex nanoparticles, they did not report whether these particles lowered thresholds or enhanced US activity. For potential translational applications, it would be very beneficial to know whether other types of solid nanoparticles can lower the cavitation threshold in blood or in intracellular liquids.

One important reason for selecting NP over commercially available MBs as sonoporation enhancers is the ability of NPs

to extravasate in capillaries and beyond, whereas MBs cannot due to their larger dimensions. In fact, this capability of NPs enables their efficient delivery to tumor cells, where US can then induce spatially confined cavitational activity (sonoporation) to enhance gene delivery. For example, we have shown that approach allowed for vasculature disruption only in US-irradiated tumors of nude mice, while no disruption was observed in nonirradiated controls [21]. In another study, we investigated the influence of polystyrene nanoparticles (100 and 280 nm in diameter and concentration up to 0.2% w/w) on cavitation threshold in water at the frequency of 20 kHz. Then, we studied efficacy of cancer chemotherapy with this technique *in vivo*. The experiments were performed in athymic nude mice bearing human colon KM20 tumors, which are highly resistant to chemotherapy. Ultrasound with the frequency of 20 kHz in combination with i.v. injected polystyrene nanoparticles was applied to enhance delivery of chemotherapeutic agent 5-fluorouracil [1]. Our studies demonstrated that US irradiation in combination with the NP and drug injections significantly decreased tumor volume and resulted in complete tumor regression at optimal irradiation conditions, while the volume of control (nonirradiated) tumors increased despite drug injections. These data suggest that US-induced drug delivery may improve efficacy of current cancer treatment regimens, suggesting PS + US do not cause significant tumor cell toxicity and can be used safely to deliver drugs or nucleic acids. For instance, when PS + US were used to deliver 5-FU, the antitumor effect was augmented dramatically for this drug, with a 60% growth rate reduction and enhanced necrosis throughout the tumors as observed by histology. Another *in vivo* study showed that polystyrene nanoparticles decrease cavitation threshold in water, and application of this drug delivery technique substantially improved the efficacy of cancer therapy in nude mice with colon tumors when US was used in combination with polymer NP injections [20].

Gene Delivery by Polymeric PLGA Nanoparticles. Several studies have shown efficient US-enhanced gene delivery using polyplexes of DNA and cationic-derivatized natural polymers, such as cationized dextran [22] and gelatin [23]. In these experiments, 3 MHz US (2 W/cm^2, 10% duty cycle) typically was applied for 1 to 2 minutes transdermally to various tissues *in vivo* such as tumors or muscle. Insonation always enhanced gene expression for a few days. The authors speculated that cavitation-induced cell membrane damage and permeation were responsible for the enhanced gene expression.

Arguably, superior polymeric nanoparticle formulations for gene delivery using US may be composed of PLGA, a polymer approved by the FDA for its excellent profile of biodegradability, drug biocompatibility, suitable biodegradation kinetics, mechanical properties, and ease of processing (reviewed in [24]). PLGA and its derivatives have been the center focus for developing nano/microparticles encapsulating therapeutic drugs in a biodegradable format. Many macromolecular drugs including proteins, peptides, genes, vaccines, antigens, and human growth factors can be incorporated successfully into PLGA- or PLGA/PLA-based nano/microparticles. And several microparticle formulations already are available in the market (reviewed in [25]). However, intense research is ongoing to refine and enhance PLGA-based NP over other delivery systems, including developing blends of PLGA with other polymers, for example, chitosan, pectin, poly(propylene fumarate), poloxamers and poloxamines, polypyrroles, gelatin, poly(vinyl alcohol) (PVA), PVA-chitosan-PEG, and poly(ortho-esters) (reviewed in [25]). These novel technologies can produce PLGA- and PLGA-based nano/microparticles for drug delivery and can dramatically expand the new field for efficient drug/gene delivery if the nanoparticles can be rendered echogenic or acoustically active.

Biodegradable PLGA NPs can sustain delivery of drugs, proteins, peptides, and plasmid DNA, owing to their ability to protect macromolecules from degradation in endolysosomes (reviewed in [26]). NPs have distinct advantages for drug delivery since they can penetrate deep into tissues through fine capillaries, across fenestrations present in the epithelial lining and, generally, are taken up efficiently by the cells, allowing efficient delivery of therapeutic agents. NPs also have the advantage of sustaining the release of the encapsulated therapeutic agent over a period of days to several weeks compared with natural polymers that have a relatively short duration of drug release [27]. The safety of PLGA-based NPs in the clinic has been well established [28] and polyethylene-glycol- (PEG-) conjugated PLGA NPs are currently emerging as molecules with reduced systemic clearance compared with similar NPs lacking PEG [29]. Therefore, the field of gene delivery will continue to refine and expand into PLGA NP for *in vivo* use, particularly with US-mediated enhancements in efficiency.

Defining Sonoporation Parameters for Successful Gene Delivery Using NP. Efficacy and safety of cancer chemo- and biotherapy are limited by poor penetration of anticancer drugs from blood into tumor cells. Tumor blood vessel wall, slow diffusion in the interstitium, and cancer cell membrane create significant physiological barriers for macromolecular agents. We have used nano- and microparticles in tumors followed by ultrasound-induced cavitation for safe and efficient drug and gene delivery. In several studies, sonoporation has effectively enhanced anticancer drug or gene delivery in tumor cells and tissues. In our experience, sonoporation does not appear to negatively impact cellular viability of insonated tumor cells or normal surrounding tissues after treatment with either chemotherapeutic drugs [2] or plasmid DNA *in vitro* [30] or *in vivo* [4] when MBs are utilized as the gene carrier (Optison or SonoVue). SonoVue is an ultrasound contrast agent made of MB stabilized by phospholipids and containing sulphur hexafluoride (SF6), an innocuous gas [31] and manufactured by Bracco Diagnostics Inc, USA. Optison is an ultrasound contrast agent, consisting of gas-filled MBs surrounded by a solid shell of heat-denatured human albumin [32] resulting in a size range of 2.0 to 4.5 μm and manufactured by GE Healthcare, USA. For example, we have shown minor damage to MCF-7 breast cancer cells following exposure to low-intensity US in the presence of either Optison MB or a chemotherapeutic drug,

5-fluorouracil (5-FU) as assessed by low lactate dehydrogenase (LDH) release (a measure of cytotoxicity) and MTT cell viability assays. However, depending on the US parameters chosen, temperature changes can be observed *in vitro*. For example, increases in US duty cycle enhanced cell death associated with either Optison or 5-FU, using 3 MHz and 2 W/cm^2 for 1 min, while temperature changes were negligible at low US duty cycles (5%). When a duty cycle of 20% was used, heating occurred from 18°C to 36°C, while, at a duty cycle of 50%, heating rose up to 40°C. Optison at 10% appeared to protect cells from the US heating bioeffects. Cell viability was decreased by Optison dramatically when a 50% duty cycle was used and augmented by 5-FU delivery. Therefore, careful selection of US parameters is required to avoid any heating and cell toxicity. Interestingly, immediately after treatment, cell death was most dependent on Optison; however, 24 h after treatment, cell death was more dependent on 5-FU, and the best minimal effective dose for cell killing was 10 μg/mL. Furthermore, treatment with 5-FU and US increased the levels of Bax and p27^{kip1} proapoptotic proteins, but the addition of Optison appeared to suppress apoptotic protein expression. This study clearly illustrates the need for experimental design aimed at dissociating specific from nonspecific toxicity effects of a gene or drug delivered by sonoporation in order to better refine the conditions for delivery *in vivo*. Another detailed study that illustrated the importance of examining the best parameters for delivering macromolecules used a macromolecule that modeled the M_w of drugs or plasmid DNA and delivery with Optison [1, 30], whereby transfection was obtained up to ~37% with minimal cell death, identifying optimal parameters of US exposure able to produce efficient delivery of macromolecules.

Like MBs, in our experience, echogenic nanoparticles made from polystyrene (PS) or PLGA also do not appear to produce any toxic effects in the presence of US. For example, in an *in vivo* DU145 prostate cancer model, no alterations are seen histologically to indicate cell death in tissues for PLGA NP plus US, even in the presence of pDNA:PEI complexes [3]. The next section will cover in detail strategies for US-mediated DNA delivery with PLGA and PEI:pDNA NP *in vivo*.

3.1.3. Ultrasound Enhances Gene Delivery by PLGA When pDNA Is Complexed with Polycationic Polymers. Over the years, a significant number of cationic polymers have been explored as carriers for gene delivery (reviewed in [33]) since they condense DNA into small particles and facilitate uptake by endocytosis. One of these cationic polymers is poly(ethylene imine) or PEI (reviewed in [34]). The potential of PEI was first described for gene delivery applications in 1995 [35]. Several molecular weights of PEI have been investigated with the most suitable forms ranging in 5–25 kDa [36, 37]. Higher-molecular-weight PEI increases cytotoxicity due to polymer aggregation at the cell surface [38]. Low-molecular-weight PEI is less toxic yet is usually less effective for gene delivery, since the lower amount of positive charges per molecule makes it difficult for small PEIs to appropriately condense negatively charged DNA molecules. Gene delivery research has used either hyperbranched or linear PEI, and branched PEI has shown stronger complexation with DNA since it typically forms smaller complexes DNA:linear PEI [39]. The condensation behavior of branched PEI:DNA is less dependent on buffering than high-molecular-weight PEI, yet the transfection efficiency of linear PEI (22 kD):DNA complexes is typically higher than that of branched PEI (25 kD) when prepared in a salt-containing buffer [39]. *in vivo*, linear PEI:DNA complexes prepared in high salt conditions are 100-fold less active than complexes prepared in low salt conditions, suggesting efficient transgene expression depends greatly on the size of DNA complexes.

Recently, we have shown that linear PEI (*in vivo* JetPEI) can enhance echogenic PLGA NP plasmid DNA (pDNA) delivery *in vivo* with US. Several ways exist to produce PLGA:PEI:pDNA particles from the original PLGA structure and branched or linear PEI molecules and these are depicted. The order in which PLGA particles are formulated with polycation PEI appears to affect gene expression magnitude. For example, Zhang et al. (Figure 3(a)) have compared three formulation methods for preparing microparticles containing PLGA PEI and pDNA and evaluated the methods for buffering capacity, cellular uptake, transfection efficiency, and toxicity. In the first method, PLGA PEI pDNA microparticles are prepared by entrapping pDNA in blended PLGA/PEI using the double emulsion water-in-oil-in-water solvent evaporation technique (PA) [40]. In a second approach, PEI-pDNA polyplexes are prepared and then entrapped in PLGA microparticles using a double emulsion solvent evaporation method (PB). Microparticles prepared using formulation methods PA and PB are then compared against PLGA microparticles with PEI conjugated to the surface using carbodiimide chemistry (PC); 0.5% PVA is identified as the optimum concentration of surfactant for generating the strongest transfection efficiencies. N : P ratios of 5 and 10 are selected for preparation of each group. Gel electrophoresis demonstrated that all PLGA formulations had strong pDNA binding capacity with significantly lower *in vitro* cytotoxicity for PLGA PEI microparticles than for PEI alone. PLGA PEI pDNA microparticles mediate higher cellular uptake efficiency and consequently higher transgene expression than unmodified PLGA microparticles in COS7 and HEK293 cells.

Preparing PEI-pDNA polyplexes prior to entrapment in PLGA microparticles (PB) results in a higher pDNA loading capacity than pDNA loaded onto unmodified PLGA microparticles. PLGA PEI pDNA microparticles prepared in this manner and with a N:P ratio of 5 provide the strongest transfection efficiency, which is ~500-fold and ~1800-fold higher than that obtained with unmodified PLGA pDNA microparticles in HEK293 cells and in COS-7 cells, respectively, (Figure 3(a)) [40]. One downside of this formulation strategy is that the particles generated are in the micron range, limiting systemic *in vivo* use. This study, however, guided our rationale for developing improved PLGA:PEI:pDNA particles, whereby strategy refinement was achieved by producing instead echogenic nanoparticles of PLGA. For our studies, we selected linear PEI (LPEI) (Figure 3(b)) [3] since it is reportedly less toxic to cells than

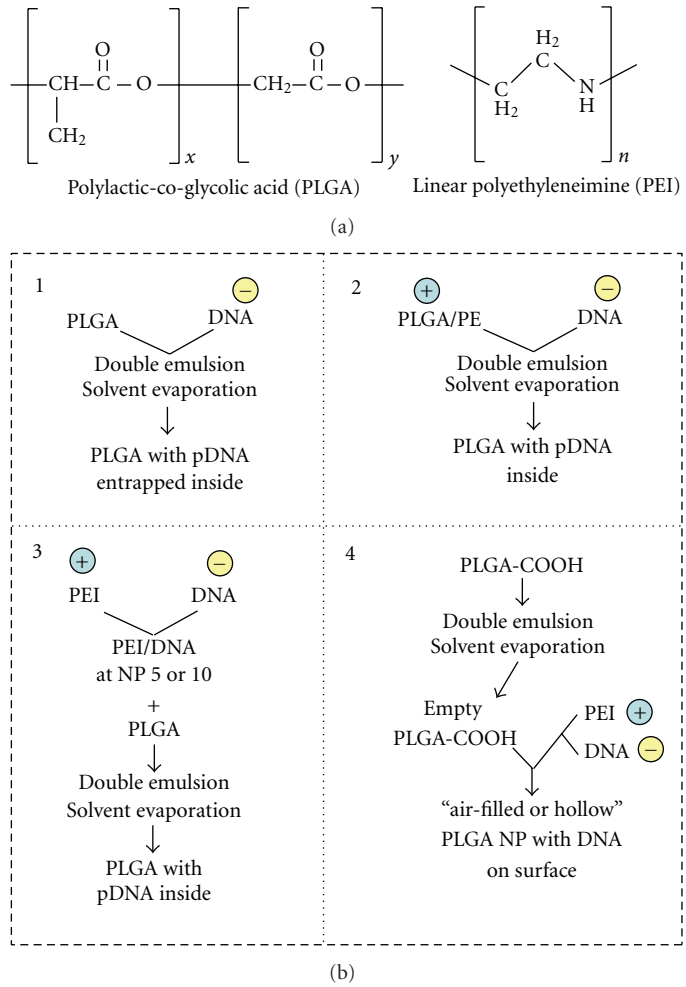

Figure 3: Different strategies to complex DNA with PLGA-based nanoparticles. (a) Structure of polylactic-co-glycolic acid (PLGA) and linear polyethylenimine (PEI). A branched PEI can also be utilized to form complexes. (b) Schematic of the preparation methods of PLGA formulations using methods that result in plasmid DNA incorporation on the inside or the surface of PLGA particles as reported in [3, 40].

its branched counterparts, perhaps due to mediating a lower condensation of LPEI:DNA complexes and a more efficient intracellular dissociation following uptake. LPEI:DNA complexes have been shown to enter the nucleus more readily than branched PEI:DNA [39].

The PLGA:PEI:pDNA complexes shown in Figure 3(b)-(4) are effective in delivering genes to the lung (Figure 4(a)) and prostate tumors when ultrasound is applied (Figure 4(b)). Pulmonary gene delivery can be an excellent route for gene therapy of lung-related genetic diseases and may induce immunity towards pathogens entering the body via the airways. For example, PLGA NPs prepared bearing polyethyleneimine (PEI) on their surface were characterized for their potential to transfect the pulmonary epithelium [41]. These particles were synthesized at different PLGA-PEI ratios and loaded with DNA in several PEI-DNA ratios, exhibiting narrow size distributions, with mean particle sizes ranging from 207 to 231 nm. Zeta potential was strongly positive (>30 mV) and loading efficiency high (>99%). Internalization of the pDNA-loaded PLGA-PEI NP was examined in the human airway submucosal epithelial cell line, Calu-3, and gene expression was detected in the endo-lysosomal compartment as soon as 6 h following application of particles (Figure 4(a)). NP cytotoxicity was dependent on the PEI-DNA ratio and the best cell viability was achieved by PEI-DNA ratios of 1 : 1 and 0.5 : 1. Although this example did not use US to mediate gene delivery, it illustrated the potential of PLGA-PEI NP for achieving lung epithelium transfection as well as the importance of carefully titrating the ratio of PEI to pDNA in order to not exacerbate this cationic polymer toxicity effects.

In our *in vivo* studies with similar PLGA:PEI:pDNA NP, we have shown that polyplexes of β-gal reporter gene plasmid DNA and linear polyethyleneimine derivative (*in vivo* JetPEI) can be formed and complexed with ~200 nm echogenic PLGA NP [3]. PLGA:PEI:pDNA complexes were administered into DU145 prostate tumor-bearing nude mice and, immediately after, a low-intensity US was applied to the tumor site. Pulsed insonation for 5 minutes at 1 MHz and −7 bars produced a significantly greater expression of the

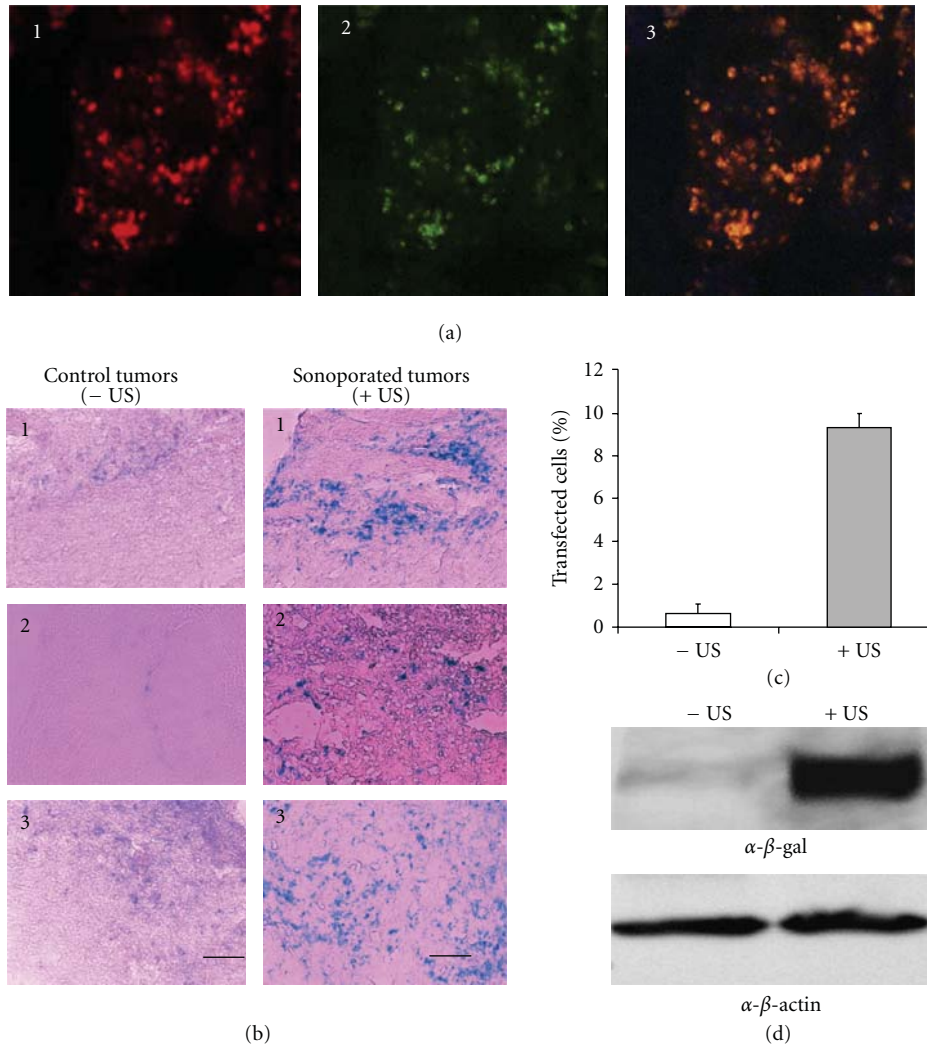

Figure 4: PLGA nanoparticles deliver plasmid DNA efficiently *in vitro* and *in vivo*. (a) *In vitro delivery*: cellular internalization in calu-3 cells 6 h after application of PLGA-PEI nanoparticles loaded with rhodamine-labeled GFP encoding plasmid DNA. (1) Immunofluorescence of anti-lysosomal-associated-membrane-protein-1 (LAMP-1) (red), (2) intracellular distribution of rhodamine-labeled DNA (green), and (3) superimposition of the confocal micrographs indicating colocalization of the DNA in the lysosomal compartments (orange-yellow). Reproduced with permission from [41]. (b) *In vivo delivery*: a special formulation, PLGA:PEI:DNA is excellent for I.V. gene delivery *in vivo*. (a) Bgal expression in control (left) and ultrasonicated (right) tumors with PLGA/PEI/DNA complex nanoparticles injected intravenously. Light scattering microscopy images taken at 20x; bar represents 100 μm. ~10% of tumor cells are transfected in ultrasonicated tumors compared to controls ($^*P < 0.01$). Reproduced from [3] with permission from Elsevier. (c) Percentage of B-galactosidase-positive (Bgal+) cells in DU145 tumors in the absence of ultrasound (−US) and presence of US (+US). $^*P < 0.05$. (d) Western blot showing the levels of B-gal protein are higher in tumors that received US (+US) compared to those without US treatment (−US). Levels of B-gal are shown relative to those of a control housekeeping protein, beta-actin.

reporter gene in the tumor (~10% cells are positive for the reporter gene LacZ) compared to the noninsonated bilateral control tumor (~1% cells positive for LacZ gene) (Figure 4). Therefore, US augmented gene delivery *in vivo*. One important component of these studies was the echogenic property of the PLGA nanoparticles. These particles were prepared in a manner that resulted in "air-filled" particles that were able to oscillate in the acoustic field, which likely stimulated their or DNA uptake by endocytosis. The particles zeta potential was 13.4 ± 2.6 mV, and echogenicity properties were tested using ultrasound imaging, which revealed a similar acoustic activity as standard Definity microbubble particles. Definity particles are lipid-encapsulated microbubbles containing perfluoropropane gas ranging in size from 1.1 to 3.3 μm [42] and manufactured by Bristol-Myers Squibb Medical Imaging, US. The overexpression of the β-gal reporter gene delivered was examined by X-gal staining and Western blot, and at least an 8-fold increase was observed in cell transfection efficiency in irradiated tumors compared to nonirradiated control. Negligible cell death was produced by ultrasonication and we determined the pDNA condensed by PEI was protected from degradation even under US

conditions. These results indicated that this formulation is promising for *in vivo* gene delivery of plasmid DNA using sonoporation. PLGA and PEI each are formulation choices that have certain advantageous chemical and structural characteristics that can enhance pDNA delivery in tumor cells. The advantage of PLGA, as discussed earlier, is the biodegradability profile and echogenicity of the prepared NP. The advantage of the *in vivo* jetPEI, as shown by our data, was its ability to protect pDNA from any potential US-induced damage. Also, PEI could further enhance NP translation potential as this polymer already has been utilized in clinical trials for bladder cancer [43]. Moreover, an important rationale for using PEI to condense pDNA and complex it to the surface of echogenic PLGA NP is to enable delivery of a large amount of pDNA ($\geq 50\,\mu$g) [3], which is usually necessary to achieve efficacy in *in vivo* gene therapy settings [4], while still preserving the nanoscale dimensions of the chimeric NP (~ 200 nm). In some cases, pDNA can be loaded inside the PLGA NP, but usually this results in minimal encapsulation (5%) for this NP type, requiring a microparticle production. For example, IL-10 is an anti-inflammatory molecule that has achieved interest as a therapeutic for neuropathic pain. In one recent study, encapsulation of plasmid was low (only $\sim 8\,\mu$g pIL-10) when PLGA microparticles of $\sim 4.6\,\mu$m were utilized to deliver IL-10 [44]. And although this PLGA:pIL-10 therapy was able to relieve neuropathic pain for greater than 74 days in an animal model following direct intrathecal administration, a micron-sized particle such as this may be less desirable for tumor therapy and targeting, for example, as penetration and retention into tumor vasculature is desired with or without using sonoporation for gene delivery. However, refinements are possible that will allow incorporation of other choices of cationic polymers for DNA condensation and loading onto echogenic PLGA NP for further reductions in any potential PEI *in vivo* toxicity [38, 45], and potential approaches will be discussed as follows.

Another polycation that would potentially be useful for condensing pDNA while enhancing US-mediated gene delivery is poly(L-lysine) or PLL, which has been used widely in gene therapy studies. One interesting recent study has shown that improvements can be made to PLL to reduce cytotoxicity and enhance transfection efficiency. This more efficient polymer is composed of short oligolysine grafts strung from a hydrophobic polymer backbone [46] and gives transfection efficiency greatly superior to PLL. The oligolysine graft length was altered to improve DNA-polymer interactions and overall transfection efficiency. Additionally, when PKKKRKV heptapeptides (the Simian virus SV40 large T-antigen nuclear localization sequence) were added onto the oligolysine polymer backbone, transfection efficiency was further enhanced and reporter gene expression levels reached levels higher than, or comparable to, JetPEI, FuGENE 6, and Lipofectamine 2000, the latter being notorious for cytotoxicity accompanying high transfection efficiency. Using heparin decomplexation assays, the mechanism for the enhanced gene delivery was determined to involve the relative strength of the polymer-DNA complex, contributing to the therapeutic promise of these novel oligolysine reagents since they are able to better release DNA during the transfection process following nuclear uptake.

Another potential DNA condensation agent for high-level gene delivery would involve the use of dendrimers of poly(amidoamine) or PAMAM. These have several advantages over PEI *in vitro* and *in vivo*, including a lower toxicity profile and reduced nonspecific lung transfection. An interesting recent study has shown that pDNA condensed with PAMAM starburst dendrimers (generation 4 and 5) can efficiently transfect tumor cells *in vitro* and *in vivo* [47]. Following intravenous injection of polyplexes into immunecompetent mice bearing subcutaneous, well-vascularized murine neuroblastoma (Neuro2A), luciferase reporter gene expression was detected predominantly in the tumor, while negligible transgene expression levels were detected in other organs as determined by bioluminescent *in vivo* imaging (BLI) (Figure 5(a)). Compared to linear PEI (LPEI), Luc expression was relatively higher and lung signals were greatly reduced for PAMAM-G5:pLuc, indicating this is a promising polyplex for *in vivo* gene delivery to tumors. Additionally, repeated applications of this polyplex type were well tolerated and resulted in prolonged average transgene expression in tumors as determined by BLI (Figure 5(b)). Fluorescence *in vivo* imaging using these polyplexes labeled with near-infrared emitting semiconductor quantum dots revealed that, although lung accumulation was similar for both PAMAM and LPEI polyplexes, only LPEI polyplexes induced high luciferase expression in lung. The mechanism proposed may involve aggregation of LPEI:pDNA with blood components that can induce backpressure in the blood flow, pushing plasmid through the lung endothelium into the vicinity of alveolar cells. Alveolar type II pneumocytes, beside endothelial cells, comprise the major fraction of transfected cells following of LPEI:pDNA i.v. injection. Therefore the authors concluded that although PAMAM polyplexes were trapped within the lung due to charge interactions, the occlusion of capillaries might not be effective enough to induce effects similar to LPEI in lung, and transfection signals are not detectable. At any rate, the PAMAM-G5 dendrimer could be a potential candidate for loading pDNA onto echogenic PLGA NP since, as PEI, it promises to have highly desirable characteristics of enhanced gene delivery that is restricted to tumors and a reduced off-target (lung) reporter gene expression *in vivo*. Finally, another promising new cationic polymer that could be a great candidate for complexing with PLGA is one containing a branched oligoethyleneimine (OEI, 800 Da) core, diacrylate esters as linkers, and oligoamines as surface modifications [48]. Although complex in structure, these are also promising since they exhibit low cytotoxicity *in vivo* and were shown to transfect tumor tissue at levels comparable to those with PEI but were better tolerated with no change in liver histology or liver enzymes, while LPEI and BPEI resulted in an increase in liver enzyme levels, suggesting early necrotic stages in liver 24 h after treatment. OEI also exhibited a more tumor-specific gene expression profile than when PEI was used, with lower lung transgene expression. Finally, dendrimers also can be used to target nucleic acid delivery to particular cells or tissues using cell-penetrating peptides.

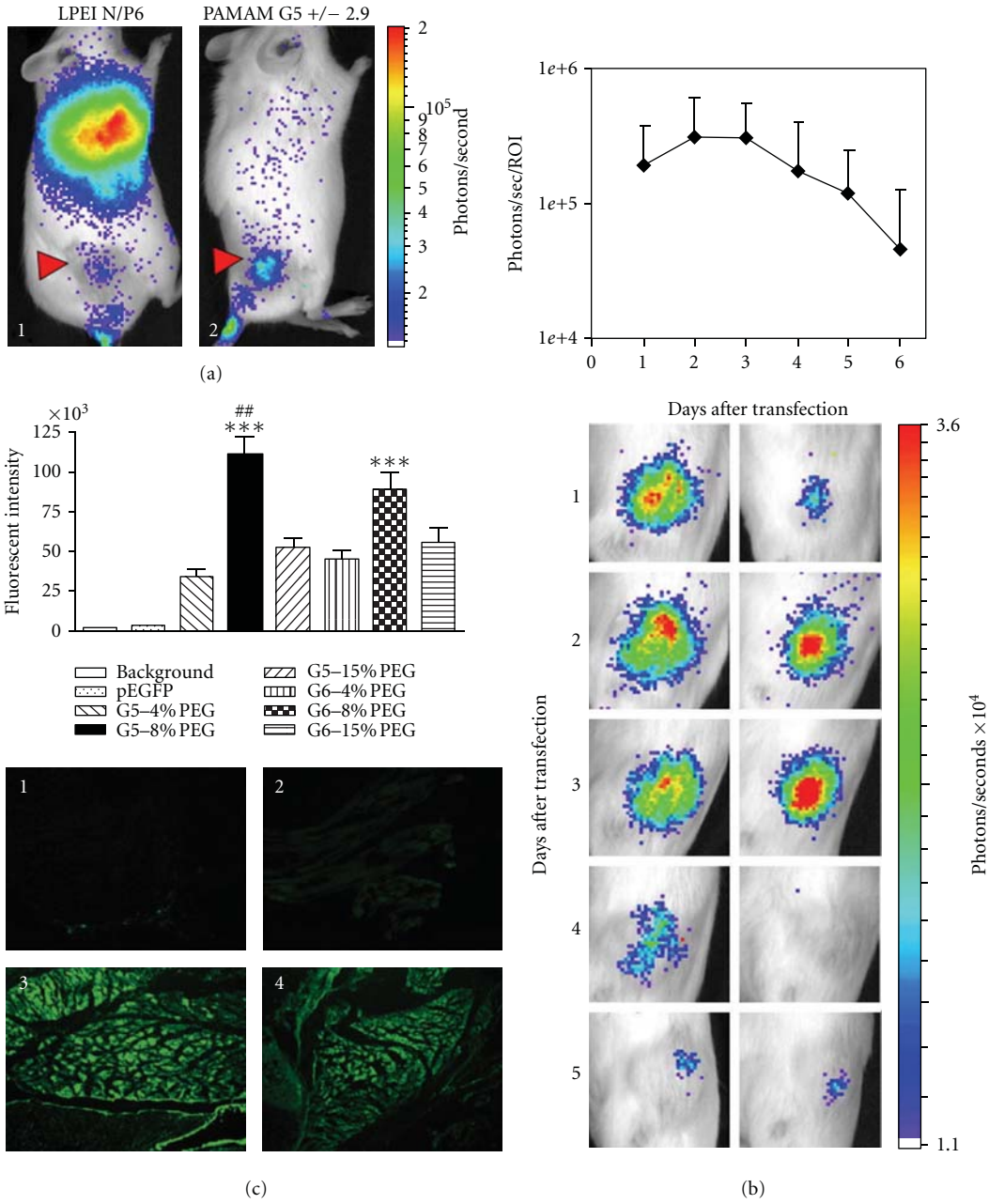

Figure 5: PAMAM-dendrimer-based complexes may be an alternative to PEI for pDNA delivery *in vivo* using NP. (a) PLGA:PAMAM-G5 gives higher tumor expression of reporter pDNA and lower nonspecific lung transfection for a more favorable biocompatible profile *in vivo*. In this example, A/J mice with subcutaneous Neuro2A tumors received a single intravenous injection of LPEI polyplexes N/P 6 (1) or PAMAM-EDA G5 polyplexes charge ratio 2.9/1 (2) containing plasmid pCpG-hCMV-Luc (2.5 mg/kg based on pDNA) and BLI was carried out 24 h later. Reprinted with permission from [47]. (b) Prolonged reporter gene expression in Neuro2a following intravenous administration of pCpG-hCMV-Luc/PAMAM-EDA G5 polyplexes (±2.9). Reprinted with permission from [47]. (c) PLGA:PAMAM G5-PEG nanoparticles deliver plasmid DNA more effectively (muscle) than G5. Reprinted with permission from [54].

For example, PAMAM-G5 dendrimers displaying cyclic RGD targeting peptides (PAMAM-RGD) improved transport [49] and also could deliver siRNA in polyplex complexes of ~200 nm, mediating more efficient nucleic acid delivery through multicellular 3D U87 glioma spheroids than that of native PAMAM dendrimers, presumably by interfering with integrin-ECM contacts present in a three-dimensional tumor model [50].

Although highly efficient nonviral gene carriers, one common drawback of LPEI, PLL, and PAMAM dendrimer cationic polymers is that these may present a high toxicity *in vivo*, even if a relatively low cytotoxicity is initially observed *in vitro*. Therefore, some solutions have included surface modification to significantly help reduce their toxicity [51–53]. For example, to help expand the *in vivo* applications of PAMAM, one study attempted to improve characteristics

of this polymer as a gene delivery carrier by incorporation of polyethylene glycol (PEG, molecular weight 5,000). PEG is known to convey water solubility and biocompatibility to conjugated copolymers and usually does not adversely affect self-assembly of copolymer with pDNA, still allowing nanosized complex formation with a narrow particle size distribution. When PEG was conjugated to G5 and G6 PAMAM dendrimers (PEG-PAMAM) at three different molar ratios of 4%, 8%, and 15% (PEG to surface amine per PAMAM dendrimer molecule) [54], *in vitro* and *in vivo* cytotoxicities were reduced significantly. Also, hemolysis was reduced, especially at higher PEG molar ratios. Among all of the PEG-PAMAM dendrimers, 8% PEG-conjugated G5 and G6 dendrimers (G5-8% PEG, G6-8% PEG) were the most efficient in delivering genes to muscle following direct administration to neonatal mouse quadriceps (Figure 5(c)). Consistent with the *in vivo* results, these two 8% PEG-conjugated PAMAM dendrimers could also mediate the highest *in vitro* transfection in 293A cells. Therefore, G5-8% PEG and G6-8% PEG possess a great potential for gene delivery and could conceivably be adapted to condense nucleic acids and be loaded atop echogenic PLGA NP for US-mediated enhancements in intramuscular gene delivery.

Other preparations successful in intramuscular gene delivery have been described, of interest since they enhance US-mediated gene delivery. These include efficient gene transfer in muscle to deliver basic fibroblast growth factor (bFGF) angiogenic gene therapy in limb ischemia. Bubble liposomes (DSPE-PEG_{2000}-OMe with perfluoropropane) were used to transfect muscle in the presence of US [55]. In this example, bFGF was delivered and capillary vessels were enhanced and blood flow improved in the bFGF + MB + US-treated groups compared to other treatment groups (non-treated, bFGF alone, or bFGF + US). Skeletal muscle is a target of interest for gene delivery since it can mediate gene therapy of both muscle (e.g., Duchenne Muscular dystrophy) and nonmuscle disorders (e.g., cancer, ischemia, or arthritis). Its usefulness is due mainly to the long-term gene expression profile following gene transfer, which makes it an excellent target tissue for the high-level production of therapeutic proteins such as cytoskeletal proteins, trophic factors, hormones, or antitumor cytokines. Refining the conditions for sonoporation as well as the optimal formulation for achieving high-level transgene expression in skeletal muscle will continue to be an important focus of gene therapy delivery efforts for treating tumors, and in particular the delivery of antitumor cytokines.

3.1.4. MB Can Enhance NP Gene Delivery by Sonoporation in Muscle Tissue. An interesting concept to aid NP gene delivery by sonoporation has employed combination with microbubbles *in vivo*. In one example, the hypothesis was tested that combination of a low concentration of MB could help reduce any US bioeffects and allow similar levels of transfection to occur when using PLGA NP at a lower US intensity and with a shorter duration in time. One interesting study examined the potential of improving siRNA delivery of retinal cells (RPE-J) in the presence of PLGA NP and a small amount of SonoVue MB [56]. Low-intensity US or 15–20% SonoVue MB also increased the siRNA delivery efficiency when a lower concentration of PEG and Poly-lysine-conjugated PLGA particles were used. The combination of US with MB was used to select the optimal enhancement of NP delivery but did not furhter increase the cellular uptake of NP, but it achieved significantly higher PDGF-BB gene silencing compared to NP alone.

Another example of combining NP with MB to enhance gene delivery is shown in Figure 6. This study showed that gene delivery of recombinant growth factors to stimulate arteriogenesis is possible through a combination of NP, an albumin-based MB contrast-agent, and US *in vivo* (Figure 6(a)) [57]. After verifying that ultrasonic MB destruction effectively deposited intravascular polystyrene nanoparticles into mouse adductor skeletal muscle, FGF-2-bearing biodegradable PLGA NPs (FGF-2-NP) were generated and coadministered intraarterially with MB, and delivery was spatially targeted to ischemic mouse hind limbs using 1 MHz US. The delivery of FGF2-NP stimulated appreciable arteriogenic remodeling in ischemic mouse hind-limb adductor muscles. This response included an increase in the total number of large and moderate diameter arterioles (i.e., $>15\,\mu$m in diameter), as well as a marked luminal expansion of both collateral and transverse arterioles (Figure 6(b)) two weeks after treatment. This system efficiently delivered PLGA FGF2-NP to mouse muscle in a model of hind-limb arterial insufficiency. This method has several features that may enhance its potential for successful clinical translation, including minimally invasive targeting, sustained growth-factor delivery, and retention of growth factor bioactivity. Ultimately, these results indicate that ultrasonic MB destruction has potential as a platform for therapeutic delivery of NP *in vivo* for vascular remodeling, and depending on antitumor therapeutics chosen, this may have important implications also for tumor therapy using cytokine gene delivery, for example.

3.1.5. Future Formulations: Promise for Echogenic PEGylated or Dendrimer PLGA Formulations. As we have shown, PLGA NP can be echogenic and serve as a contrast agent in addition to as a gene delivery vehicle. For example, *in vivo* ultrasound imaging can be accomplished with a high-resolution small animal imaging system and is illustrated in Figure 7. We show an example of US imaging for examining the kinetics of PLGA NP *in vivo* (prostate tumors) by using novel, high-resolution ultrasound imaging system Vevo 770 developed by VisualSonics (Toronto, Canada). The system has the ability to visualize and quantify tumors, hemodynamics, and therapeutic interventions with resolution down to 30 microns noninvasively and in real time. Figure 7(a) shows an image of a DU145 prostate tumor in a nude mouse obtained with the system following intravenous administration of PLGA NP (same NP as described in Figure 4(b)). The system was capable of detecting the distribution of an unlabeled ultrasound contrast agent (UCA, VisualSonics) and allowed its visualization in the tumor (the areas with high concentration are represented in green). A specially developed computer code allowed to quantify kinetics of

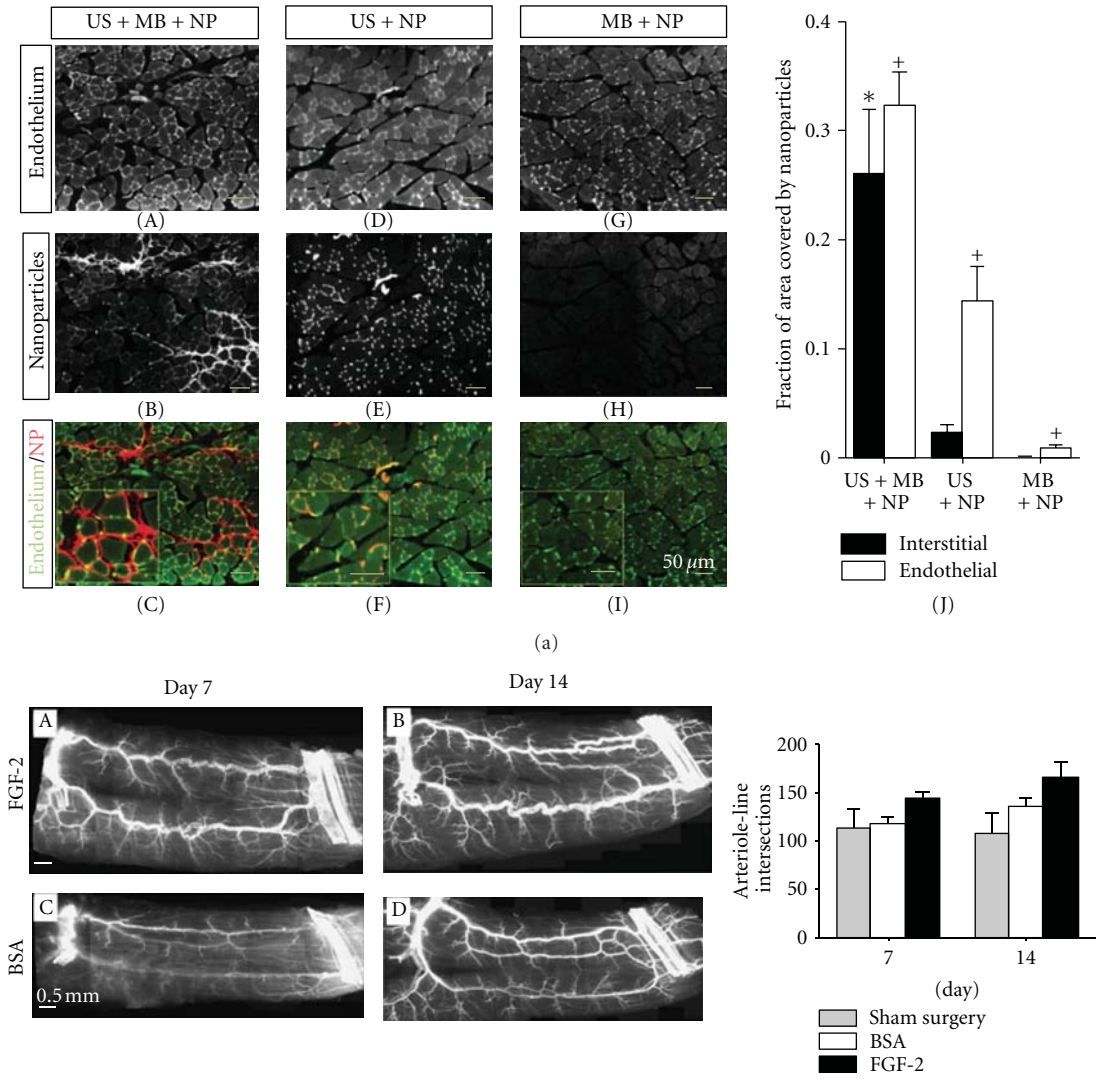

Figure 6: Nanoparticle uptake can be enhanced by ultrasonication in the presence of microbubbles in skeletal muscle *in vivo*. (a) Gracilis skeletal muscle cross-sections illustrating fluorescent polystyrene nanoparticle (NP) delivery for each treatment. (A)–(I) Muscle treated with ultrasound (US) + microbubbles (MB) + nanoparticles (NP) combinations. For the conditions of US + MB + NP, NPs (red) accumulate in vessel walls and muscle interstitium (BS-1 lectin staining, green). For muscle treated with US + NP, NPs colocalized with endothelium but minimal interstitial deposition was observed. Muscle treated with MB + NP was almost void of NP. (J) Bar graph representing the fraction of interstitial area (regions outside of muscle fibers and vascular structures) or endothelial cell area (cells comprising the walls of blood vessels) occupied by NP. Values are means with standard deviations. *indicates significantly different ($P < 0.05$) than interstitial area of all other groups. +indicates significantly different ($P < 0.05$) than endothelial cell area of all other groups. (b) The delivery of FGF-2 bearing nanoparticles by ultrasonic microbubble destruction elicits arteriogenic remodeling in gracilis adductor muscle. (A)–(D) Representative whole-mount images of fluorescently labeled SM α-actin+ vessels in gracilis adductor muscles 7 and 14 days after FGF-2 (A) and (B) and BSA (C) and (D) treatment. Note the significant increase in arteriolar caliber and density in FGF-2-treated muscles. (E) Bar graph of arteriole line intersections at both time points for FGF-2, BSA, and sham surgery treatment. Values are means with standard errors. *indicates significantly different ($P < 0.05$) than BSA and sham surgery at day 14. Reprinted from [57] with permission from Wiley.

this UCA in the tumor (Figure 7(a), right panel). There was a sharp increase of the concentration in the whole tumor within first 2 to 3 seconds after the injection that was followed by a wash-out process (decrease of the contrast intensity). The necrotic areas at the center of the tumor had similar kinetics but less concentration of the UCA due to lower vascularization (Figure 7(b), left panel). In contrast, injection of the PLGA nanoparticles into the same mouse (after clearance from the UCA) demonstrated almost constant concentration of the PLGA nanoparticles 15 seconds after the injection (Figure 7(b), right part). This effect resulted from competition of two processes: (1) the decrease of nanoparticles concentration in blood and (2) the increase of their concentration in the tumor blood vessels due to

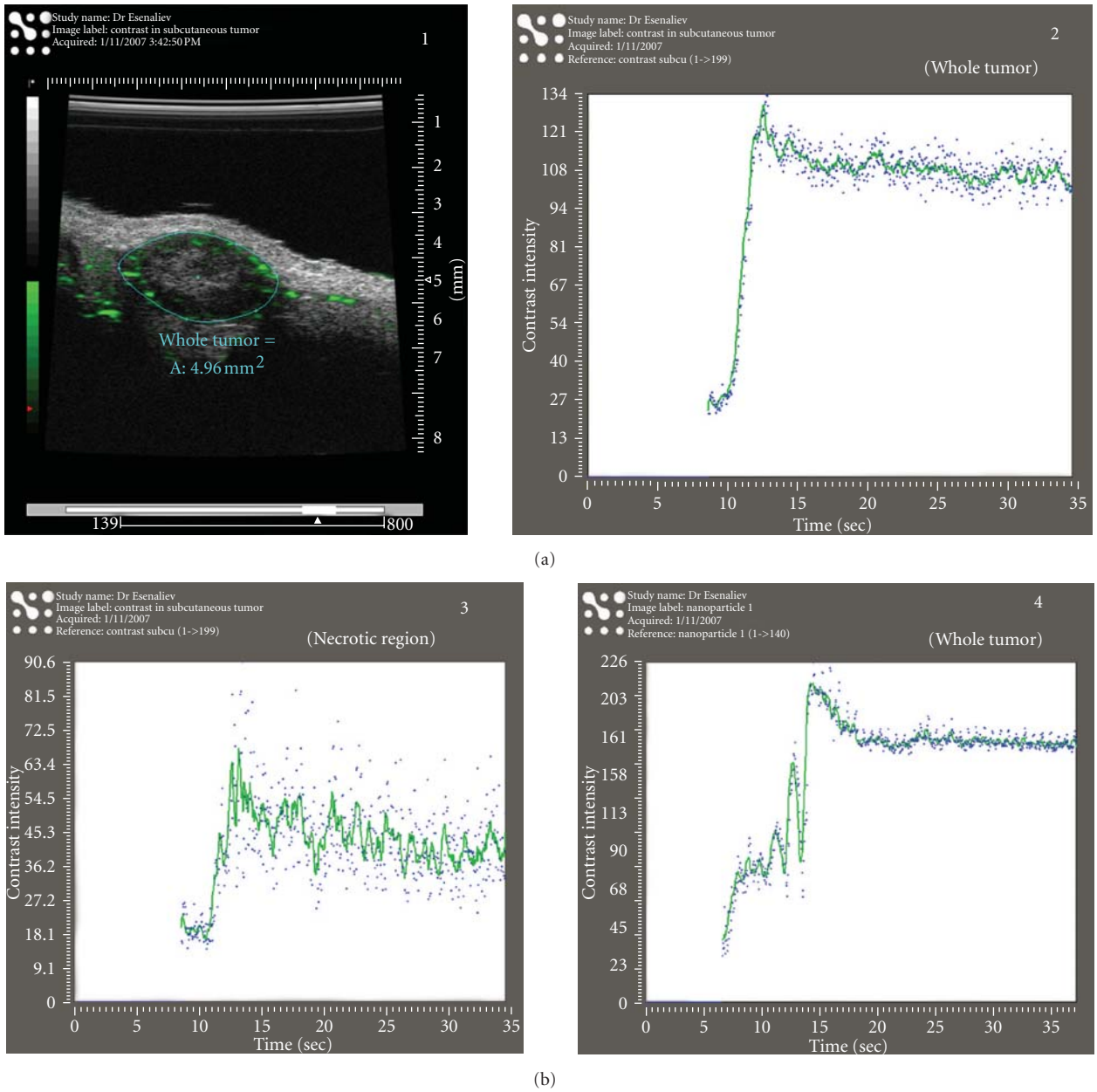

Figure 7: . Echogenic PLGA nanoparticles can be utilized also as ultrasound contrast agents *in vivo*. (a) (1) A tumor image obtained with the high-resolution ultrasound system VEVO770 (VisualSonics). (2) Kinetics of the contrast agent in the whole tumor shown in (1). (b) (3) Kinetics of the contrast agent in the central area of the tumor shown in (1). (4) Kinetics of the PLGA nanoparticles in the whole tumor shown in (1).

the EPR effect. Moreover, the contrast intensity produced by the PLGA nanoparticles (~175) was much higher compared to that of the UCA (~100). These data indicate that high-resolution ultrasound small animals imaging systems are able to detect the PLGA nanoparticles in tumors *in vivo* and that these nanoparticles are highly echogenic.

Further modifications can be made to echogenic PLGA NP to enhance their potential for longer circulation half-life and for enabling tumor-specific targeting. For example, surface modifications can be made to polymeric nanoparticles to add PEGylated phospholipids in order to escape recognition and clearance by the mononuclear phagocyte system and achieve passive tumor targeting. Nanoparticles consisting of a shell of PLGA encapsulating a liquid core of perfluorooctyl bromide (PFOB) can be decorated with poly(ethylene glycol-2000)-grafted distearoylphosphatidylethanolamine (DSPE-PEG) and resulting particles still are echogenic and can allow visualization of MIA-PaCa-2 pancreatic tumors *in vivo*, following intratumoral or intravenous injection (Figure 8(a)). In this example, the tumor was visualized only following intratumoral UCA injection. Despite the absence of echogenic

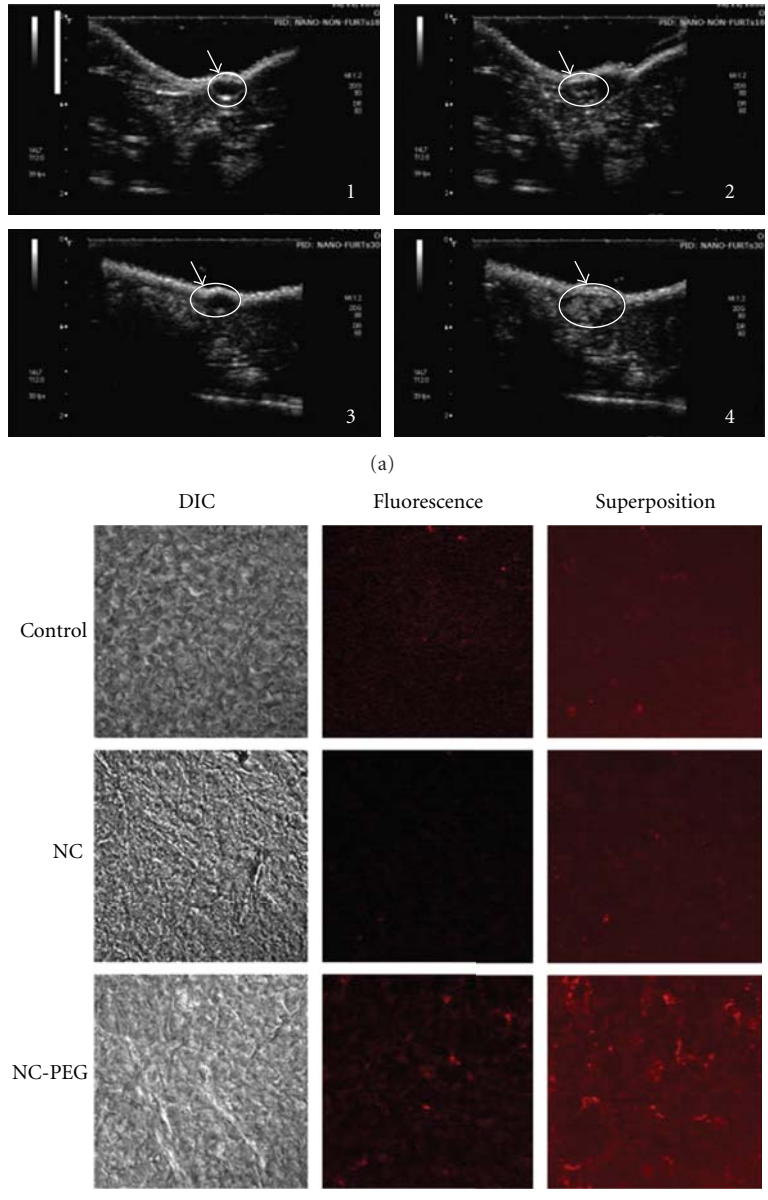

Figure 8: PEG-PLGA particles as ultrasound contrast agents *in vivo*. (a) Ultrasound images of mouse pancreatic tumors obtained in a nonlinear imaging mode before injection (1)–(3) and after intratumoral injection of plain nanocapsules (2) or PEGylated nanocapsules (4). The tumor is indicated as the region of interest (ROI) represented by a circle. (b) Confocal microscopy images of tumor slices from a control mouse (control) and mice after 24 h of an intravenous injection of non-PEGylated nanocapsules (NC) and PEGylated nanocapsules (NCL-PEG). DIC corresponds to differential interference Nomarski contrast. Red fluorescence corresponds to PLGA dyed with Nil Red. Reprinted from [58] with permission from Elsevier.

signal in the tumor after intravenous injection of NP, histological analysis revealed their accumulation within the tumor [58], and this accumulation can be explained by their increased circulation time due to their PEGylated surface (Figure 8(b)). PEG coating protects NC-PEG against plasma protein adsorption and therefore against recognition by phagocytic cells. The increased circulation time favors their passive targeting in tumor tissue by the enhanced permeation and retention effect [59]. A quantitative biodistribution of NC-PEG likely would have been helpful to assessing their actual concentration in tumors and determining the concentration threshold necessary for ultrasonography with these new UCAs.

4. Novel Directions

4.1. PLGA as an Ultrasound Contrast Agent. Other UCAs recently developed by Nestor et al. include air-filled nanocapsules made of PLGA. These have a critical advantage over current commercial UCAs, which are not capable of

penetrating the irregular tumor vasculature due to their larger dimensions. These new nanoscale UCAs based on PLGA can therefore be used to enhance tumor detection since they display enhanced stability compared to commercially available UCAs when in the presence of US. Air-filled nanocapsules with a mean diameter of ~370 nm have been shown to maintain a spherical shape and thickness <50 nm and remain echogenic [60], providing an enhancement of up to 15 dB at a concentration of 0.045 mg/mL at a frequency of 10 MHz. Loss of signal for air-filled nanocapsules was 2 dB after 30 min, suggesting high stability. This UCA therefore has the potential to be applied to ultrasound imaging. Other NPs that are in development as UCAs include polymer-based multifunctional nanoparticles that exhibit a near-infrared absorption and can be used as a novel photoacoustic contrast system [61, 62]. Photoacoustics is a new imaging modality in which laser light is shined into tissue and adsorbed by inherent or synthetic molecules or particles and generates ultrasound. Submicron-sized NPs with a high encapsulation efficiency have been created by the incorporation of near-infrared (NIR) dyes in PLGA via a spray-drying process. Subsequent centrifugation yielded two size fractions ranging from ~445–550 nm to ~253–305 nm in diameter [61, 62]. These NIR PLGA NP exhibited photoacoustic properties using an Nd:YAG laser-based system but did not show any detrimental effects on cell viability or mitochondrial activity. Photoacoustics properties persisted in cell culture for up to 2 days, suggesting the excellent photoacoustic properties plus the low cytotoxicity profile renders these dye-loaded PLGA particles promising candidates for a resorbable photoacoustic contrast system *in vivo*.

4.2. The Future for Biodegradable PLGA for Gene Delivery

4.2.1. Developing Better PLGA Nanoparticles. One improvement that might impact PLGA NP effectiveness as a gene delivery agent *in vivo* is to improve the acidic microclimate developed during polymer degradation which can potentially damage the nucleic acid that may be encapsulated or complexed to the NP. Buffering agents have been used that incorporate antacid (0, 3% $MgOH_2$) [63], whereby PLGA microspheres maintained a more homogeneous surface, resulting in a significant reduction of the commonly seen "burst effect." For example, PLGA microspheres of ~47 micron have been shown to completely release pDNA over the course of two months, addressing some of the major problems associated with DNA encapsulation and release. We envision that these same buffering principles might be applicable to smaller PLGA particles to help reduce any pDNA degradation that might occur secondary to polymer degradation prior to or following US-mediated gene delivery *in vivo*.

4.2.2. Current New Technology: Nonechogenic PLGA NP Have Been Used with Success for Targeted Drug Delivery. Several studies have reported the use of PLGA NP or MP for targeting drug delivery to tumor cells. These PLGA NPs are still under development and are not echogenic. Thus, these new approaches will be useful when adapted for the field of ultrasound-mediated gene delivery. We envision that the same targeting moieties can be conjugated or complexed onto PLGA particles with acoustic activity for future applications to gene delivery by sonoporation. We describe here examples of targeting using PLGA NP, including the studies described in Figure 8. In Figure 9(a), PLGA-based MPs were produced that were able to target prostate tumor cells expressing the prostate-specific membrane antigen or PSMA [64]. A set of air-filled MBs of various biocompatible polymer compositions were prepared and characterized in terms of morphology and echogenic properties after exposure to US. MBs derived from PLG-poly(ethylene glycol) (PEG) copolymer resulted in being the most effective in terms of reflectivity. PLGA-PEG was therefore preconjugated before MB preparation with an urea-based PSMA inhibitor [65]. Using this copolymer as a starting material, the MBs were examined *in vitro* for their targeting efficacy toward PSMA-positive cells. Fluorescence microscopy showed a specific and efficient adhesion of targeted MBs to LNCaP cells. This model for targeting PSMA might be further optimized for smaller particle use (echogenic nanoparticles) and used for prostate cancer diagnosis and drug or gene delivery.

Additional targeting moieties for PLGA NP have utilized aptamers, which are single-stranded RNA or DNA oligonucleotides ~15–60 bp in length that can bind with high affinity to specific molecular targets. Most aptamers to proteins bind with a Kd of ~1 pM to 1 nM, which is an affinity level similar to that of monoclonal antibodies. Moreover, aptamers are able to bind to nucleic acid, proteins, and small organic compounds and enable targeting to specific cells, in a manner similar to the concept of high-affinity antibodies. For example, a targeting nanoparticle was developed that had a mucin-1- (MUC-1-) specific Aptamer (Apt-NP) conjugated to the surface (Figure 9(b)). MUC1 protein is an attractive target for anticancer drug delivery owing to its overexpression in most adenocarcinomas. In this study, a reported MUC1 protein aptamer was exploited to target Paclitaxel- (PTX-) loaded PLGA NPs of ~225.3 nm in size. Using MCF-7 breast cancer cells as a MUC1-overexpressing model, the aptamer increased the uptake of nanoparticles into the target cells as measured by flow cytometry. Moreover, the PTX-loaded Apt-NPs enhanced *in vitro* drug delivery and cytotoxicity to MUC1+ cancer cells, as compared with nontargeted NP lacking the MUC1 aptamer. The behavior of this novel aptamer-NP bioconjugate suggests that MUC1 aptamers may have a wider application potential in targeted gene delivery towards MUC1-overexpressing tumors [66]. Other aptamers used for targeted delivery of NP have included PLGA conjugated to polyethylene glycol (PEG), which have been used to deliver encapsulated prodrugs. PLGA NP are targeted using aptamers with affinity for the extracellular domain of PSMA [67, 68]. Such NP are highly efficacious compared to prodrugs *in vivo,* and pharmacokinetic studies showed improvements in tolerability and efficacy compared to standard chemotherapy (Figure 10). We envision that such a NP design might greatly enhance gene delivery targeted specifically to prostate cancer cells expressing PSMA.

Other uses of aptamers have included a PLGA NP of ~156 nm decorated with aptamer AS1411 (Apt-NP)

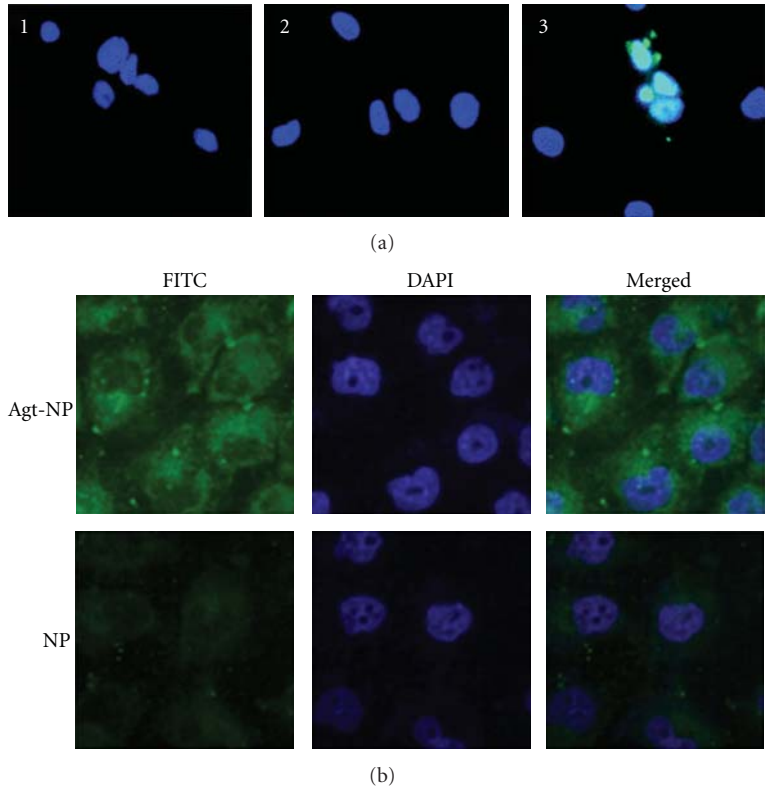

Figure 9: Targeted nanoparticles are promising for future *in vivo* gene delivery approaches. (a) PSMA-targeted PLGA-based microparticles enter LNCaP (PSMA+) PCa cells. Untreated control (1), after 30 min of exposure to nontargeted FITC-loaded (2), and targeted FITC-loaded (3) MBs. Cell nuclei were stained with Hoechst (blue). The number of green-positive cells per field was significantly different from that of nontargeted MBs. Reprinted from [64] with permission from American Chemical Society. (b) Confocal fluorescent scanning microscopy images detecting cellular uptake of MUC-1 targeted Aptamer conjugated NPs (top row) or NPs (bottom row) in MCF-7 cells. Green fluorescent FITC was encapsulated in Apt-NPs and NPs. The nuclei were stained blue with DAPI. The right column showed the merged images of the FITC and the DAPI channels. MCF-7 cells were exposed to FITC-encapsulated Apt-NPs or NPs at 100 μg/mL for 2 hours. Reprinted from [66] under the terms of the Creative Commons Attribution License.

[69]. AS1411 is a DNA aptamer that specifically binds to nucleolin, a protein upregulated in the plasmsa membrane of both cancer cells and angiogenic blood vessels. Apt-NP was used to facilitate antiglioma delivery of paclitaxel (PTX). The Ap-nucleolin interaction significantly enhanced cellular association of nanoparticles in C6 glioma cells and increased the cytotoxicity of its payload. Prolonged circulation and enhanced PTX accumulation at the tumor site were achieved by Ap-PTX-NP, which also yielded higher tumor inhibition on C6 glioma xenografts and prolonged survival when comapred to PTX-NP (untargeted) and Taxol. Therefore, aptamer-functionalized PLGA NP can be an efficient therapeutic and this design might be adapted as well for successful potential gene delivery to glioma.

Antibodies. Other PLGA NP that have been used for effective cellular targeting have included PLGA nanobubbles (NB) for cancer targeting and imaging using optical and US modalities. For example, PLGA NBs have been conjugated with cancer-targeting ligands such as a humanized antibody to target the overexpressed TAG-72 antigen [70]. NB-assisted dual-mode imaging was demonstrated on a gelatin phantom with multiple embedded tumor simulators at different NB concentrations, demonstrating the feasibility of using dual-mode contrast agents for cancer targeting and simultaneous fluorescence/US imaging. Another PLGA-PEG NP recently described coupled the J591 monoclonal antibody to its surface in order to direct targeting towards PSMA-expressing prostate cancer cells. A pDNA encoding β-gal was complexed to this NP via a salicyl-hydroxamic-acid- (SHA-) derivatized PEI. After encapsulation, an 8- to 10-fold enhancement in gene expression was attained due to enhanced specific internalization and uptake of the complex in PSMA-expressing cells. The release of pDNA from NP showed a small initial burst release followed by a 5% release over 48 h. The release accelerated thereafter and ~60% was released within a month. Also, the PEG-PLGA composition (triblock polymer) was found to enhance the polyplex/microparticle localization to the cell nucleus and this enhanced the endocytic process of J591-mediated targeting in prostate cancer cells.

RGD. Another class of polymeric contrast agents with targeting potential was described in which the Arg-Gly-Asp (RGD) peptide sequence was conjugated to either PLA or PLGA microcapsules [72, 73]. These hollow, biodegradable

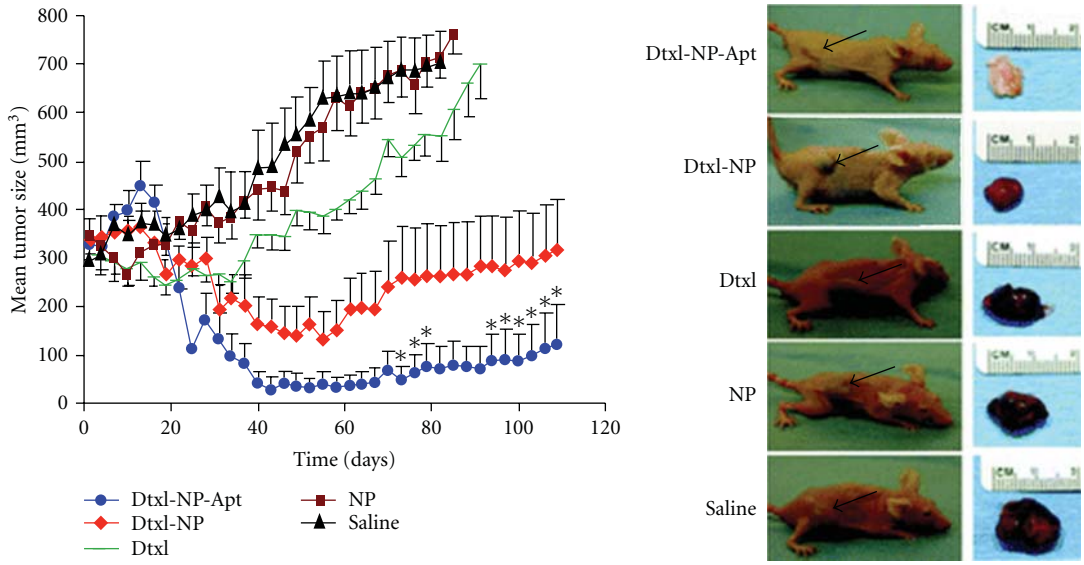

Figure 10: Future Potential of PLGA-based nanoparticles for realizing efficient *in vivo* drug delivery. (a) PLGA formulations for drug delivery. The antitumor efficacy of single intratumoral injections of drugs or controls was compared for several NP groups. Groups examined included saline, pegylated PLGA NP (NP), Docatexel- (Dtxl-) encapsulated NP (Dtxl-NP) at 40 mg/kg, or Dtxl-NP-PSMA targeted Aptamer conjugates at 40 mg/kg (Dtxl-NP-Apt). Aptamer-targeted NPs were more efficacious in tumor reduction compared to control groups. Data points labeled with "*" were statistically significant compared with all other groups by analysis of variance (ANOVA) at a 95% confidence interval. (b) Representative mice at the end point for each group are shown (left) alongside images of excised tumors (right). For the Dtxl-NP-Apt group, which achieved complete tumor regression, the scar tissue and underlying skin at the site of injection are shown. Black arrows point to the position of the implanted tumor on each mouse. Reprinted from [68] with permission from PNAS.

microcapsules targeted $\alpha v\beta 3$ and $\alpha v\beta 5$ integrins, typically expressed during angiogenesis. *In vitro* results indicated that the modified capsules remained echogenic and adhered specifically to the breast cancer cell line MDA-MB-231. An interesting modification of this approach has been utilization of a cyclic RGD targeting moiety conjugated via a micelle-type PLGA-4 arm-PEG branched polymer for detecting and treating pancreatic cancer [74]. These NPs contained the 4-arm PEG as a corona and PLGA as a core, while the particle surface was conjugated with cRGD for *in vivo* tumor targeting. The hydrodynamic size of NP was ~150–180 nm and NIR microscopy and flow cytometry studies showed that the cRGD-conjugated NPs were taken up more efficiently by U87MG glioma cells overexpressing integrins. Whole-body imaging showed that the cRGD NP had the highest accumulation in pancreatic tumors at 48 h after-injection with low *in vivo* toxicity. We would predict additional receptor targeting will be attempted in the near future and this will likely extend targeting of PLGA nanoparticles to the VEGFR and EGFR family of receptors to achieve enhanced drug and gene delivery, as already has been shown to work for microbubbles targeting the VEGFR2 receptor in tumor-associated endothelial cells [75, 76].

Proapoptotic. PLGA NPs coated with a proapoptotic monoclonal antibody have been efficient in delivering drugs in a targeted manner. For example, use of NP coated with Conatumumab or AMG 655 death-receptor 5 antibodies (DR5-NP) has preferentially targeted DR5-expressing cells and has induced apoptosis in a specific manner while also delivering encapsulated drugs such as camptothecin [77]. This is an interesting example of antibody conjugation to NP surface that can be exploited for the dual functions of targeted drug delivery and cell killing. Another example used gene delivery to achieve apoptosis in prostate tumors by delivering pDNA expressing an shRNA against annexin A2 [78]. In prostate cancer progression, annexin A2 is upregulated cancer. These PLGA NP sustained intracellular delivery of shRNA and achieved long-term downregulation of annexin A2. Intratumoral administration of pDNA-shAnxA2-loaded NP to xenograft prostate tumors in nude mice inhibited tumor growth through reductions in annexin A2 and VEGF levels. This interesting study suggests that the use of sustained-release polymeric NP for delivering shRNA constructs might serve as an effective adjuvant treatment option for cancer.

One important final consideration for practical use of PLGA or any NP for receptor and other tumor-targeted genes delivery is the size range required for therapeutically effective drug concentrations at tumor sites while reducing undesirable side effects. For example, targeted drug delivery using long-circulating particulate drug carriers of controlled size (<100 nm diameter) (reviewed in [79]) holds great potential to improve the treatment of cancer by selectively providing enhanced permeability and retention (EPR) and optimal tumor distribution of NP.

4.3. Future Uses: Targeted Echogenic PLGA Nanoparticles for Theranostic Applications. For future applications, echogenic

PLGA NP will be important to achieving theranostic applications (diagnostic and therapeutic) for cancer. For example, for early cancer diagnosis and therapy, new systems will be continually designed and developed with key components uniquely structured at nanoscale according to medical requirements. For imaging, it is envisioned that quantum dots with emissions in the near-infrared (NIR) range will continue to be utilized for delivering drugs and/or nucleic acids. For example, quantum dots have been successfully conjugated onto a surface of a nanocomposite material consisting of a spherical polystyrene matrix (<150 nm). Internally embedded supraparamagnetic Fe_3O_4 nanoparticles (<10 nm) could be successfully loaded with PTX onto this nanocomposite material by using a layer of PLGA [80]. Variations of such a nanocarrier were then successfully conjugated to antibodies or aptamers to achieve cell-specific targeting. For example, these PTX-loaded PLGA nanocarriers were conjugated to an anti-PSMA antibody for targeting of LNCaP prostate tumors with high specificity *in vivo*. For diagnostic applications, we envision that nanoparticle contrast agents will become of increasing interest for high-resolution imaging in medicine. For example, a novel dual-modal contrast agent has been developed for structural and functional imaging of cancer [81]. This contrast agent was fabricated by encapsulating indocyanine green (ICG) in PLGA MB. The technical feasibility of concurrent structural and functional imaging was demonstrated through a series of tests in which an aqueous suspension of ICG-PLGA MB was injected into a transparent tube embedded in an Intralipid phantom at different flow rates and concentrations. Concurrent fluorescence imaging and B-mode ultrasound imaging successfully captured the changes of microbubble flow rate and concentration with high linearity and accuracy. One potential application of the proposed ICG-PLGA MB would be for the identification and characterization of peritumoral neovasculature. Enhanced coregistration between tumor structural and functional boundaries could be achieved using US-guided near-infrared diffuse optical tomography. In a similar manner, photoacoustic imaging applications also will be implemented, for example, NP exhibiting a near-infrared (NIR) absorption can be prepared by incorporation of ICG into PLGA [61, 62]. These NPs were biocompatible *in vitro* and had a high NIR dye encapsulation efficiency (>98%) and two different size fractions were obtained of ~640 nm and ~390 nm. Cytotoxicity studies indicated no changes in metabolic activity, proliferation, or membrane integrity. Their high optical absorption at ~800 nm in combination with absence of cytotoxicity qualifies the ICG-PLGA particles as promising candidates for degradable photoacoustic contrast agents in future studies.

Other nanoparticles in development include composite PLGA-magnetic particles for simultaneous drug delivery and imaging [82], and these might also be applied to gene delivery in future applications. These magnetic nanoparticles were embedded in PLGA matrices (PLGA-MNP) to achieve a dual-drug delivery and imaging system and were capable of encapsulating both hydrophobic and hydrophilic drugs in a 2 : 1 ratio while retaining favorable biocompatibility and cellular uptake properties. For targeted delivery of drugs, targeting ligands such as Herceptin were tested, demonstrating enhanced cellular uptake. Also, magnetic resonance imaging was used to show improved contrast by PLGA-MNP compared to commercial contrast agents due to higher T2 relaxivity with a blood circulation half-life of ~47 min in a rat model. These PLGA-based matrices may be applied to both imaging and adapted to achieve successful gene delivery.

5. Conclusions

PLGA and other nanoparticle delivery systems in general have distinct advantages for gene delivery, such as protecting DNA from degradation and enhancing complex stability. PLGA-based NPs can penetrate deeply into tissues through fine capillaries and are generally taken up efficiently by cells. This allows efficient delivery and accumulation of therapeutic agents, such as conventional medicines, vaccine antigens, proteins, and genes, to target sites (tissues or organs) in the body. PLGA NPs also have the advantage of sustained and controlled release of the encapsulated therapeutic agent over a period of days to several weeks compared with natural polymers, which have a relatively short duration of drug release. PLGA and other NP, if synthesized in a manner to render acoustic activity, can strongly promote not only therapy delivery but also serve as contrast agents for standard US-mediated imaging or photoacoustic imaging. PLGA NP will continue to be refined and improved also to target gene and drug delivery to certain cells and tissues via conjugation of highly specific antibodies, aptamers, or other molecules to their surface. For gene delivery, other nucleic acid types will be expanded either loaded onto or into PLGA NP, including promising directions using siRNA/miRNA technology to silence multiple tumor-promoting genes, for example.

Overall, the promise of these technologies and approaches using PLGA NPs represents a novel and potentially more effective means to manage cancer and other diseases. However, thorough evaluation for pharmacokinetics, biodistribution, toxicity, and efficacy of particular therapeutic agents (gene or drugs) is still required before widespread use will be achieved for PLGA NP in clinical trials. Nevertheless, gene delivery using PLGA- or PLGA-based polymers is an attractive area with vast opportunities for biomedical research. During the past few years, research on PLGA NP has increased in the field of drug delivery and targeting of NP to cancer cells or blood vessels within tumors. We predict these improvements also may promote advances in the gene delivery applications of PLGA NP. These polymers are increasingly becoming feasible candidates for delivering nucleic acids as anticancer agents and for vaccine immunotherapy. We also believe that PLGA-based NP will be developed further to enable treatment and diagnosis of a variety of other diseases besides cancer. Therefore, our predictions are that PLGA-related NP technology should play increasingly more important and mainstream roles in tissue engineering and in other emerging areas such as stem cell research.

Acknowledgments

The authors acknowledge the Department of Pharmacology and Toxicology and the Center for Biomedical Engineering at UTMB for continued support of their research in gene delivery by sonoporation and molecular imaging research.

References

[1] I. V. Larina, B. M. Evers, T. V. Ashitkov, C. Bartels, K. V. Larin, and R. O. Esenaliev, "Enhancement of drug delivery in tumors by using interaction of nanoparticles with ultrasound radiation," *Technology in Cancer Research and Treatment*, vol. 4, no. 2, pp. 217–226, 2005.

[2] O. V. Chumakova, A. V. Liopo, B. M. Evers, and R. O. Esenaliev, "Effect of 5-fluorouracil, optison and ultrasound on MCF-7 cell viability," *Ultrasound in Medicine and Biology*, vol. 32, no. 5, pp. 751–758, 2006.

[3] O. V. Chumakova, A. V. Liopo, V. G. Andreev et al., "Composition of PLGA and PEI/DNA nanoparticles improves ultrasound-mediated gene delivery in solid tumors in vivo," *Cancer Letters*, vol. 261, no. 2, pp. 215–225, 2008.

[4] O. Zolochevska, X. Xia, B. J. Williams, A. Ramsay, S. Li, and M. L. Figueiredo, "Sonoporation delivery of interleukin-27 gene therapy efficiently reduces prostate tumor cell growth in vivo," *Human Gene Therapy*, vol. 22, no. 12, pp. 1537–1550, 2011.

[5] O. Zolochevska and M. L. Figueiredo, "Advances in sonoporation strategies for cancer," *Frontiers of Bioscience*, vol. 4, pp. 988–1006, 2012.

[6] C. M. H. Newman and T. Bettinger, "Gene therapy progress and prospects: ultrasound for gene transfer," *Gene Therapy*, vol. 14, no. 6, pp. 465–475, 2007.

[7] H. D. Liang, J. Tang, and M. Halliwell, "Sonoporation, drug delivery, and gene therapy," *Proceedings of the Institution of Mechanical Engineers, Part H*, vol. 224, no. 2, pp. 343–361, 2010.

[8] S. M. Stieger, C. F. Caskey, R. H. Adamson et al., "Enhancement of vascular permeability with low-frequency contrast-enhanced ultrasound in the chorioallantoic membrane model," *Radiology*, vol. 243, no. 1, pp. 112–121, 2007.

[9] P. Zhong, Y. Zhou, and S. Zhu, "Dynamics of bubble oscillation in constrained media and mechanisms of vessel rupture in SWL," *Ultrasound in Medicine and Biology*, vol. 27, no. 1, pp. 119–134, 2001.

[10] C. X. Deng, F. Sieling, H. Pan, and J. Cui, "Ultrasound-induced cell membrane porosity," *Ultrasound in Medicine and Biology*, vol. 30, no. 4, pp. 519–526, 2004.

[11] M. Duvshani-Eshet, L. Baruch, E. Kesselman, E. Shimoni, and M. Machluf, "Therapeutic ultrasound-mediated DNA to cell and nucleus: bioeffects revealed by confocal and atomic force microscopy," *Gene Therapy*, vol. 13, no. 2, pp. 163–172, 2006.

[12] T. A. Tran, S. Roger, J. Y. le Guennec, F. Tranquart, and A. Bouakaz, "Effect of ultrasound-activated microbubbles on the cell electrophysiological properties," *Ultrasound in Medicine and Biology*, vol. 33, no. 1, pp. 158–163, 2007.

[13] P. L. McNeil, "Repairing a torn cell surface: make way, lysosomes to the rescue," *Journal of Cell Science*, vol. 115, part 5, pp. 873–879, 2002.

[14] P. L. McNeil and R. A. Steinhardt, "Loss, restoration, and maintenance of plasma membrane integrity," *Journal of Cell Biology*, vol. 137, no. 1, pp. 1–4, 1997.

[15] R. K. Schlicher, H. Radhakrishna, T. P. Tolentino, R. P. Apkarian, V. Zarnitsyn, and M. R. Prausnitz, "Mechanism of intracellular delivery by acoustic cavitation," *Ultrasound in Medicine and Biology*, vol. 32, no. 6, pp. 915–924, 2006.

[16] A. Lawrie, A. F. Brisken, S. E. Francis, D. C. Cumberland, D. C. Crossman, and C. M. Newman, "Microbubble-enhanced ultrasound for vascular gene delivery," *Gene Therapy*, vol. 7, no. 23, pp. 2023–2027, 2000.

[17] S. Mehier-Humbert, T. Bettinger, F. Yan, and R. H. Guy, "Ultrasound-mediated gene delivery: kinetics of plasmid internalization and gene expression," *Journal of Controlled Release*, vol. 104, no. 1, pp. 203–211, 2005.

[18] S. Koch, P. Pohl, U. Cobet, and N. G. Rainov, "Ultrasound enhancement of liposome-mediated cell transfection is caused by cavitation effects," *Ultrasound in Medicine and Biology*, vol. 26, no. 5, pp. 897–903, 2000.

[19] C. K. Holland and R. E. Apfel, "Thresholds for transient cavitation produced by pulsed ultrasound in a controlled nuclei environment," *Journal of the Acoustical Society of America*, vol. 88, no. 5, pp. 2059–2069, 1990.

[20] I. V. Larina, B. M. Evers, C. Bartels, T. V. Ashitkov, K. V. Larin, and R. O. Esenaliev, "Ultrasound-enhanced drug delivery for efficient cancer therapy," in *Proceedings of the 24th Annual International Conference of the IEEE Engineering in Medicine and Biology and the Annual Fall Meeting of the Biomedical Engineering Society EMBS/BMES Conference*, Houston, Tex, USA, 2002.

[21] Y. Ivanova, B. M. Evers, R. Thomas, T. V. Ashitkov, and R. O. Esenaliev, "Nanoparticles and ultrasound for delivery of model macromolecular anti-cancer drugs in tumors," in *Proceedings of the 24th Annual International Conference of the IEEE Engineering in Medicine and Biology and the Annual Fall Meeting of the Biomedical Engineering Society EMBS/BMES Conference*, Houston, Tex, USA, 2002.

[22] H. Hosseinkhani, T. Kushibiki, K. Matsumoto, T. Nakamura, and Y. Tabata, "Enhanced suppression of tumor growth using a combination of NK4 plasmid DNA-PEG engrafted cationized dextran complex and ultrasound irradiation," *Cancer Gene Therapy*, vol. 13, no. 5, pp. 479–489, 2006.

[23] H. Hosseinkhani, T. Aoyama, O. Ogawa, and Y. Tabata, "Ultrasound enhancement of in vitro transfection of plasmid DNA by a cationized gelatin," *Journal of Drug Targeting*, vol. 10, no. 3, pp. 193–204, 2002.

[24] J. M. Lü, X. Wang, C. Marin-Muller et al., "Current advances in research and clinical applications of PLGA-based nanotechnology," *Expert Review of Molecular Diagnostics*, vol. 9, no. 4, pp. 325–341, 2009.

[25] R. C. Mundargi, V. R. Babu, V. Rangaswamy, P. Patel, and T. M. Aminabhavi, "Nano/micro technologies for delivering macromolecular therapeutics using poly(d,l-lactide-co-glycolide) and its derivatives," *Journal of Controlled Release*, vol. 125, no. 3, pp. 193–209, 2008.

[26] J. Panyam and V. Labhasetwar, "Biodegradable nanoparticles for drug and gene delivery to cells and tissue," *Advanced Drug Delivery Reviews*, vol. 55, no. 3, pp. 329–347, 2003.

[27] J. Panyam, M. M. Dali, S. K. Sahoo et al., "Polymer degradation and in vitro release of a model protein from poly(D,L-lactide-co-glycolide) nano-and microparticles," *Journal of Controlled Release*, vol. 92, no. 1-2, pp. 173–187, 2003.

[28] R. Langer, "Drug delivery and targeting," *Nature*, vol. 392, no. 6679, pp. 5–10, 1998.

[29] C. S. Fishburn, "The pharmacology of PEGylation: balancing PD with PK to generate novel therapeutics," *Journal of Pharmaceutical Sciences*, vol. 97, no. 10, pp. 4167–4183, 2008.

[30] I. V. Larina, B. M. Evers, and R. O. Esenaliev, "Optimal drug and gene delivery in cancer cells by ultrasound-induced

cavitation," *Anticancer Research*, vol. 25, no. 1, pp. 149–156, 2005.

[31] M. Schneider, "Characteristics of SonoVuetrade mark," *Echocardiography*, vol. 16, no. 7, part 2, pp. 743–746, 1999.

[32] S. Podell, C. Burrascano, M. Gaal, B. Golec, J. Maniquis, and P. Mehlhaff, "Physical and biochemical stability of Optison, an injectable ultrasound contrast agent," *Biotechnology and Applied Biochemistry*, vol. 30, part 3, pp. 213–223, 1999.

[33] X. Gao, K. S. Kim, and D. Liu, "Nonviral gene delivery: what we know and what is next," *AAPS Journal*, vol. 9, no. 1, pp. E92–E104, 2007.

[34] W. F. Lai, "In vivo nucleic acid delivery with PEI and its derivatives: current status and perspectives," *Expert Review of Medical Devices*, vol. 8, no. 2, pp. 173–185, 2011.

[35] O. Boussif, F. LezoualC'H, M. A. Zanta et al., "A versatile vector for gene and oligonucleotide transfer into cells in culture and in vivo: polyethylenimine," *Proceedings of the National Academy of Sciences of the United States of America*, vol. 92, no. 16, pp. 7297–7301, 1995.

[36] A. Baker, M. Saltik, H. Lehrmann et al., "Polyethylenimine (PEI) is a simple, inexpensive and effective reagent for condensing and linking plasmid DNA to adenovirus for gene delivery," *Gene Therapy*, vol. 4, no. 8, pp. 773–782, 1997.

[37] C. Meunier-Durmort, H. Grimai, L. M. Sachs, B. A. Demeneix, and C. Forest, "Adenovirus enhancement of polyethylenimine-mediated transfer of regulated genes in differentiated cells," *Gene Therapy*, vol. 4, no. 8, pp. 808–814, 1997.

[38] D. Fischer, T. Bieber, Y. Li, H. P. Elsässer, and T. Kissel, "A novel non-viral vector for DNA delivery based on low molecular weight, branched polyethylenimine: effect of molecular weight on transfection efficiency and cytotoxicity," *Pharmaceutical Research*, vol. 16, no. 8, pp. 1273–1279, 1999.

[39] L. Wightman, R. Kircheis, V. Rössler et al., "Different behavior of branched and linear polyethylenimine for gene delivery in vitro and in vivo," *Journal of Gene Medicine*, vol. 3, no. 4, pp. 362–372, 2001.

[40] X. Q. Zhang, J. Intra, and A. K. Salem, "Comparative study of poly (lactic-co-glycolic acid)-poly ethyleneimine-plasmid DNA microparticles prepared using double emulsion methods," *Journal of Microencapsulation*, vol. 25, no. 1, pp. 1–12, 2008.

[41] M. Bivas-Benita, S. Romeijn, H. E. Junginger, and G. Borchard, "PLGA-PEI nanoparticles for gene delivery to pulmonary epithelium," *European Journal of Pharmaceutics and Biopharmaceutics*, vol. 58, no. 1, pp. 1–6, 2004.

[42] C. Sonne, F. Xie, J. Lof et al., "Differences in definity and optison microbubble destruction rates at a similar mechanical index with different real-time perfusion systems," *Journal of the American Society of Echocardiography*, vol. 16, no. 11, pp. 1178–1185, 2003.

[43] O. N. Gofrit, A. Shapiro, D. Pode et al., "Combined local bladder hyperthermia and intravesical chemotherapy for the treatment of high-grade superficial bladder cancer," *Urology*, vol. 63, no. 3, pp. 466–471, 2004.

[44] R. G. Soderquist, E. M. Sloane, L. C. Loram et al., "Release of plasmid DNA-encoding IL-10 from PLGA microparticles facilitates long-term reversal of neuropathic pain following a single intrathecal administration," *Pharmaceutical Research*, vol. 27, no. 5, pp. 841–854, 2010.

[45] D. Fischer, A. von Harpe, K. Kunath, H. Petersen, Y. Li, and T. Kissel, "Copolymers of ethylene imine and N-(2-hydroxyethyl)-ethylene imine as tools to study effects of polymer structure on physicochemical and biological properties of DNA complexes," *Bioconjugate Chemistry*, vol. 13, no. 5, pp. 1124–1133, 2002.

[46] S. S. Parelkar, D. Chan-Seng, and T. Emrick, "Reconfiguring polylysine architectures for controlling polyplex binding and non-viral transfection," *Biomaterials*, vol. 32, no. 9, pp. 2432–2444, 2011.

[47] G. Navarro, G. Maiwald, R. Haase et al., "Low generation PAMAM dendrimer and CpG free plasmids allow targeted and extended transgene expression in tumors after systemic delivery," *Journal of Controlled Release*, vol. 146, no. 1, pp. 99–105, 2010.

[48] V. Russ, H. Elfberg, C. Thoma, J. Kloeckner, M. Ogris, and E. Wagner, "Novel degradable oligoethylenimine acrylate ester-based pseudodendrimers for in vitro and in vivo gene transfer," *Gene Therapy*, vol. 15, no. 1, pp. 18–29, 2008.

[49] C. L. Waite and C. M. Roth, "Binding and transport of PAMAM-RGD in a tumor spheroid model: the effect of RGD targeting ligand density," *Biotechnology and Bioengineering*, vol. 108, no. 12, pp. 2999–3008, 2011.

[50] C. L. Waite and C. M. Roth, "PAMAM-RGD conjugates enhance siRNA delivery through a multicellular spheroid model of malignant glioma," *Bioconjugate Chemistry*, vol. 20, no. 10, pp. 1908–1916, 2009.

[51] T. I. Kim, H. J. Seo, J. S. Choi et al., "PAMAM-PEG-PAMAM: novel triblock copolymer as a biocompatible and efficient gene delivery carrier," *Biomacromolecules*, vol. 5, no. 6, pp. 2487–2492, 2004.

[52] K. C. Wood, S. R. Little, R. Langer, and P. T. Hammond, "A family of hierarchically self-assembling linear-dendritic hybrid polymers for highly efficient targeted gene delivery," *Angewandte Chemie International Edition*, vol. 44, no. 41, pp. 6704–6708, 2005.

[53] J. S. Choi, K. S. Ko, J. S. Park, Y. H. Kim, S. W. Kim, and M. Lee, "Dexamethasone conjugated poly(amidoamine) dendrimer as a gene carrier for efficient nuclear translocation," *International Journal of Pharmaceutics*, vol. 320, no. 1-2, pp. 171–178, 2006.

[54] R. Qi, Y. Gao, Y. Tang et al., "PEG-conjugated PAMAM dendrimers mediate efficient intramuscular gene expression," *AAPS Journal*, vol. 11, no. 3, pp. 395–405, 2009.

[55] K. Negishi, M. Kobayashi, I. Ochiai et al., "Association between fibroblast growth factor 23 and left ventricular hypertrophy in maintenance hemodialysis patients. Comparison with B-type natriuretic peptide and cardiac troponin T," *Circulation Journal*, vol. 74, no. 12, pp. 2734–2740, 2010.

[56] J. Du, Q. S. Shi, Y. Sun et al., "Enhanced delivery of monomethoxypoly(ethylene glycol)-poly(lactic-co-glycolic acid)-poly l-lysine nanoparticles loading platelet-derived growth factor BB small interfering RNA by ultrasound and/or microbubbles to rat retinal pigment epithelium cells," *Journal of Gene Medicine*, vol. 13, no. 6, pp. 312–323, 2011.

[57] J. C. Chappell, J. Song, C. W. Burke, A. L. Klibanov, and R. J. Price, "Targeted delivery of nanopartides bearing fibroblast growth factor-2 by ultrasonic microbubble destruction for therapeutic arteriogenesis," *Small*, vol. 4, no. 10, pp. 1769–1777, 2008.

[58] R. Díaz-López, N. Tsapis, M. Santin et al., "The performance of PEGylated nanocapsules of perfluorooctyl bromide as an ultrasound contrast agent," *Biomaterials*, vol. 31, no. 7, pp. 1723–1731, 2010.

[59] H. Maeda, "The enhanced permeability and retention (EPR) effect in tumor vasculature: the key role of tumor-selective macromolecular drug targeting," *Advances in Enzyme Regulation*, vol. 41, pp. 189–207, 2001.

[60] M. M. Néstor, N. P. E. Kei, N. A. M. Guadalupe, M. E. S. Elisa, G. Q. Adriana, and Q. G. David, "Preparation and in vitro evaluation of poly(D,L-lactide-co-glycolide) air-filled nanocapsules as a contrast agent for ultrasound imaging," *Ultrasonics*, vol. 51, no. 7, pp. 839–845, 2011.

[61] Y. Kohl, C. Kaiser, W. Bost et al., "Preparation and biological evaluation of multifunctional PLGA-nanoparticles designed for photoacoustic imaging," *Nanomedicine*, vol. 7, no. 2, pp. 228–237, 2011.

[62] Y. Kohl, C. Kaiser, W. Bost et al., "Near-infrared dye-loaded PLGA nanoparticles prepared by spray drying for photoacoustic applications," *International Journal of Artificial Organs*, vol. 34, no. 2, pp. 249–252, 2011.

[63] N. K. Varde and D. W. Pack, "Influence of particle size and antacid on release and stability of plasmid DNA from uniform PLGA microspheres," *Journal of Controlled Release*, vol. 124, no. 3, pp. 172–180, 2007.

[64] V. Sanna, G. Pintus, P. Bandiera et al., "Development of polymeric microbubbles targeted to prostate-specific membrane antigen as prototype of novel ultrasound contrast agents," *Molecular Pharmaceutics*, vol. 8, no. 3, pp. 748–757, 2011.

[65] K. P. Maresca, S. M. Hillier, F. J. Femia et al., "A series of halogenated heterodimeric inhibitors of prostate specific membrane antigen (PSMA) as radiolabeled probes for targeting prostate cancer," *Journal of Medicinal Chemistry*, vol. 52, no. 2, pp. 347–357, 2009.

[66] C. Yu, Y. Hu, J. Duan et al., "Novel aptamer-nanoparticle bioconjugates enhances delivery of anticancer drug to MUC1-positive cancer cells in vitro," *PLoS ONE*, vol. 6, no. 9, Article ID e24077, 2011.

[67] S. Dhar, N. Kolishetti, S. J. Lippard, and O. C. Farokhzad, "Targeted delivery of a cisplatin prodrug for safer and more effective prostate cancer therapy in vivo," *Proceedings of the National Academy of Sciences of the United States of America*, vol. 108, no. 5, pp. 1850–1855, 2011.

[68] O. C. Farokhzad, J. Cheng, B. A. Teply et al., "Targeted nanoparticle-aptamer bioconjugates for cancer chemotherapy in vivo," *Proceedings of the National Academy of Sciences of the United States of America*, vol. 103, no. 16, pp. 6315–6320, 2006.

[69] J. Guo, X. Gao, L. Su et al., "Aptamer-functionalized PEG-PLGA nanoparticles for enhanced anti-glioma drug delivery," *Biomaterials*, vol. 32, no. 31, pp. 8010–8020, 2011.

[70] J. S. Xu, J. Huang, R. Qin et al., "Synthesizing and binding dual-mode poly (lactic-co-glycolic acid) (PLGA) nanobubbles for cancer targeting and imaging," *Biomaterials*, vol. 31, no. 7, pp. 1716–1722, 2010.

[71] G. A. Husseini and W. G. Pitt, "Micelles and nanoparticles for ultrasonic drug and gene delivery," *Advanced Drug Delivery Reviews*, vol. 60, no. 10, pp. 1137–1152, 2008.

[72] J. D. Lathia, L. Leodore, and M. A. Wheatley, "Polymeric contrast agent with targeting potential," *Ultrasonics*, vol. 42, no. 1–9, pp. 763–768, 2004.

[73] M. A. Wheatley, J. D. Lathia, and K. L. Oum, "Polymeric ultrasound contrast agents targeted to integrins: importance of process methods and surface density of ligands," *Biomacromolecules*, vol. 8, no. 2, pp. 516–522, 2007.

[74] H. Ding, K. T. Yong, I. Roy et al., "Bioconjugated PLGA-4-arm-PEG branched polymeric nanoparticles as novel tumor targeting carriers," *Nanotechnology*, vol. 22, no. 16, Article ID 165101, 2011.

[75] J. K. Willmann, R. Paulmurugan, K. Chen et al., "US imaging of tumor angiogenesis with microbubbles targeted to vascular endothelial growth factor receptor type 2 in mice," *Radiology*, vol. 246, no. 2, pp. 508–518, 2008.

[76] S. Pochon, I. Tardy, P. Bussat et al., "BR55: a lipopeptide-based VEGFR2-targeted ultrasound contrast agent for molecular imaging of angiogenesis," *Investigative Radiology*, vol. 45, no. 2, pp. 89–95, 2010.

[77] F. Fay, K. M. McLaughlin, D. M. Small et al., "Conatumumab (AMG 655) coated nanoparticles for targeted pro-apoptotic drug delivery," *Biomaterials*, vol. 32, no. 33, pp. 8645–8653, 2011.

[78] A. R. Braden, M. T. Kafka, L. Cunningham, H. Jones, and J. K. Vishwanatha, "Polymeric nanoparticles for sustained down-regulation of annexin A2 inhibit prostate tumor growth," *Journal of Nanoscience and Nanotechnology*, vol. 9, no. 5, pp. 2856–2865, 2009.

[79] S. Bisht and A. Maitra, "Dextran-doxorubicin/chitosan nanoparticles for solid tumor therapy," *Wiley Interdisciplinary Reviews. Nanomedicine and Nanobiotechnology*, vol. 1, no. 4, pp. 415–425, 2009.

[80] H. S. Cho, Z. Dong, G. M. Pauletti et al., "Fluorescent, superparamagnetic nanospheres for drug storage, targeting, and imaging: a multifunctional nanocarrier system for cancer diagnosis and treatment," *ACS Nano*, vol. 4, no. 9, pp. 5398–5404, 2010.

[81] R. X. Xu, J. Huang, J. S. Xu et al., "Fabrication of indocyanine green encapsulated biodegradable microbubbles for structural and functional imaging of cancer," *Journal of Biomedical Optics*, vol. 14, no. 3, Article ID 034020, 2009.

[82] A. Singh, F. Dilnawaz, S. Mewar, U. Sharma, N. R. Jagannathan, and S. K. Sahoo, "Composite polymeric magnetic nanoparticles for co-delivery of hydrophobic and hydrophilic anticancer drugs and MRI imaging for cancer therapy," *ACS Applied Materials & Interfaces*, vol. 3, no. 3, pp. 842–856, 2011.

Hindawi Publishing Corporation
Journal of Drug Delivery
Volume 2012, Article ID 236713, 11 pages
doi:10.1155/2012/236713

Research Article

Development, Characterization, and In Vitro Evaluation of Tamoxifen Microemulsions

E. Monteagudo,[1] Y. Gándola,[2] L. González,[2] C. Bregni,[1] and A. M. Carlucci[1]

[1] *Department of Pharmaceutical Technology, Faculty of Pharmacy and Biochemistry, University of Buenos Aires, Junín 956, 1113 Buenos Aires, Argentina*
[2] *Institute of Biochemistry and Biophysics, (IQUIFIB), National Science Research Council (CONICET), Junín 956, 1113 Buenos Aires, Argentina*

Correspondence should be addressed to A. M. Carlucci, adrianac@ffyb.uba.ar

Received 31 August 2011; Accepted 2 October 2011

Academic Editor: Rassoul Dinarvand

Microemulsions (MEs) were designed by an innovative rational development, characterized, and used to load up to 20 mM of Tamoxifen citrate (TMX). They were made with acceptable and well-characterized excipients for all the routes of administration. Some of their properties, such as nanometric mean size and long stability shelf life, make them interesting drug delivery systems. The results obtained after the in vitro inhibition of estradiol-induced proliferation in MCF-7 breast cancer cells demonstrated a significant effect in cell growth. A decreasing of at least 90% in viable cells was shown after the incubation with MEs containing 20 mM of TMX. Besides, two compositions which loaded 10 mM of drug showed a cytotoxic effect higher than 70%. These results encourage the evaluation of alternative protocols for this drug administration, not only for estrogen receptor (ER) positive tumors, but also for ER negative.

1. Introduction

One of the major problems facing cancer therapy is administering the required therapeutic concentration of the drug at the tumor site for the desired period of time. Targeted drug delivery to solid tumors is necessary in order to achieve optimum therapeutic outcomes. It would, therefore, be desirable to develop chemotherapeutics that can either passively or actively target cancerous cells. Passive targeting exploits the characteristic features of tumor biology that allow nanocarriers to accumulate in the tumor by the enhanced permeability and retention (EPR) effect [1]. Whereas free drugs may diffuse nonspecifically, a nanocarrier can extravasate into the tumor tissues via the leaky vessels by the EPR effect. The dysfunctional lymphatic drainage in tumors retains the accumulated nanocarriers. Particles with diameter <200 nm resulted in the most effective ones [2, 3].

Microemulsions (MEs) are extensively studied nanocarriers; they are defined as a system of water, oil, and amphiphile which is a single optically isotropic and thermodynamically stable liquid solution. Their structure consists in microdomains of lipids or water stabilized by an interfacial film of surfactant and cosurfactant molecules. They can be classified as oil in water (o/w) or water in oil (w/o) and the droplet size is lower than 150 nanometers. They present a number of advantages as drug delivery system, such as the ability to solubilize hydrophobic drugs, spontaneous assemble, long-term physical stability, and ease of manufacturing [4]. They presented successful results for all administration routes. There have also been of an increasing interest for their administration via the parenteral route [5, 6], due to the number of acceptable excipients available nowadays [7, 8].

Tamoxifen citrate (TMX) (Figure 1), is an antiestrogen, nonsteroidal derivative of triphenylethylene with poor water solubility [9], that is widely used in hormone therapy and breast cancer prevention even in an advanced stage. Its use is especially indicated for postmenopausal women who have estrogen-receptor- (ER-) positive breast cancer. It is an estradiol competitive inhibitor for the estrogen receptor. It inhibits proliferation by arresting the cell cycle

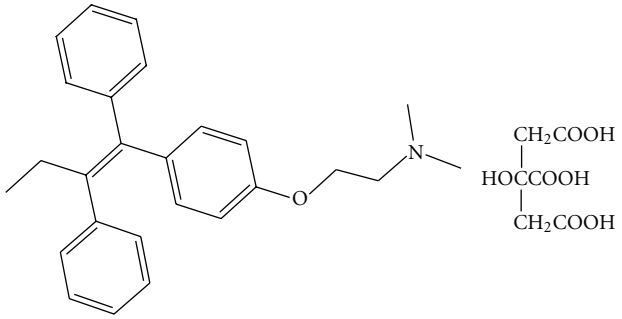

Figure 1: Chemical structure of tamoxifen citrate.

and induces breast cancer cells apoptosis [6, 10, 11]. It is also thought to induce a tumoricidal effect on estrogen receptor-negative cells by increasing the secretion of inhibitory growth factors. Recent reports have shown that TMX may possess antiangiogenic activity through its antiestrogenic effects [1].

TMX is administered by oral route in dose ranges from 20 to 40 mg a day, but up to 200 mg a day has been reported [12]. Regarding pharmacokinetics, its oral bioavailability is affected by the first pass effect and is a substrate for some protein families that mediate toxic compounds efflux outside the organism [13]; it also presents vulnerability to enzymatic degradation in both intestine and liver. Following long-term therapy, TMX has some major side effects, including higher incidence of endometrial cancer, liver cancer, thromboembolic disorders, and development of drug resistance [1].

To address the challenges of targeting tumors with nanotechnology, it is necessary to combine the rational design of nanocarriers with the fundamental understanding of tumor biology. It is to remark that an increasing number of nanovectors are currently being tested for breast cancer treatment, including liposomes and albumin-bound paclitaxel as examples [14].

Because of the above-mentioned reasons, TMX represents a promising lipophilic model drug either for oral or parenteral administration using MEs as passive targeting drug delivery system. Therefore, an alternative protocol for oral, IM, or IV administration in breast cancer or in ER-negative tumors would be evaluated taking advantage of ME properties [15].

The aim of the present work was to design and characterize o/w MEs composed by pharmaceutically accepted excipients for TMX delivery. They would be further proposed for alternative protocols of oral or parenteral administration. The biological behavior of the selected compositions for passive targeting drug delivery was also evaluated in MCF-7 human breast cancer cell line.

2. Materials and Methods

2.1. Material. Phosphatidylcholine (PC, Phospholipon 90 NG) was purchased from Phospholipid, Germany; Polyoxyethylene Sorbitan Monooleate (Polysorbate 80, PS 80) was from Fisher Chemicals, NJ, USA; Tamoxifen citrate was from Saporiti S.A., Buenos Aires, Argentina; ethanol was bought at J. T. Baker, USA; Capmul MCM L (glycerol monocaprylocaprate) and Captex 355 (caprylic/capric Triglyceride) were purchased from Abitec, Columbus, USA. Estradiol was from Sigma Aldrich. St. Louis, MO, USA. Imwitor 408 (propylene glycol caprylate) and Myiglyol 840 (propylene glycol dicaprylate/dicaprate) were from Sasol, Witten, Germany. Oleic acid and Isopropyl mirystate were from Merck, Germany. Propylene-glycol and polyethylene glycol 400 were bought at BASF, NJ, USA. Labrafil M 1944 CS (oleoyl macrogolglycerides (polyoxylglycerides) and Transcutol P (diethylene glycol monoethyl ether) were purchased from Gatefossé, France. All reagents were of analytical grade. Distilled water was obtained from a Milli-Q equipment.

2.2. Preliminary Solubility Evaluation for the Screening of Components. PS 80 was selected as surfactant model because it is listed as a generally recognized as safe (GRAS) excipient. In addition, it is extensively used for different ways of administration, including the parenteral route [16], and for microemulsions' preparation [8].

The solubility of TMX in a number of excipients was estimated. They were Isopropyl myristate (IPM), Mygliol 840, Captex 355, Oleic acid, Imwitor 408, phosphatidylcholine (PC) and Capmul MCM L. PC is solid at room temperature, so a suspension was prepared (being 16% m/v the maximum concentration tested). These oils are widely used as no polar phases for ME formulation [17, 18]. PC has also been used for the formulation of parenteral MEs [19].

Regarding cosurfactants, five compounds were tested: Ethanol, Polyethilenglycol 400 (PEG 400), Transcutol P, Labrafil 1944 CS, and Propylenglycol (PG). All of them are included in the FDA inactive ingredients guide.

To determine the drug solubility of TMX in excipients, drug in excess was added until turbidity was reached. Then, the samples were left to equilibrate using a Rotating Bottle apparatus (Varian, USA) at 5 RPM. If the solution was clear after rotation for a short time, a more active compound was added. Otherwise, the sample was left to equilibrate for 72 hours and it was, then, filtered using 0.45 μm PVDF membranes (Pall life sciences, USA). The filtered sample was analyzed by HPLC.

Quantitative determinations of TMX were performed using a Shimadzu Class VP HPLC. The chromatographic conditions were: column Zorbax Eclipse XDB Phenyl with detection at 254 nm; temperature was fixed at 35°C. The mobile phase was constituted by methanol (1000 mL), water (320 mL), acetic acid glacial (2 mL), octansulphonate (1.08 g), and triethylamine (1 mL).

These same conditions were also used for the determination of solubilizing capacity shown by formulations. All experiments with TMX were carried out using amber glass material due to drug photosensitivity.

2.3. Preliminary Cytotoxicity Assay. Although nonionic surfactants are considered less toxic than ionic surfactants, they are often reported as responsible for a number of adverse effects [20]. This is the main issue that pharmaceutical design has to overcome when formulating MEs, because high levels of surfactants are sometimes needed.

To assess the extent in which PS 80 could affect cell viability, a cytotoxicity assay using different concentrations was performed (5, 10, 20, and 25% m/v). The five co-surfactants in solutions of 35% m/v and the seven lipids in suspensions of 4% and 16% m/v were also evaluated.

For cytotoxicity studies, cells were seeded in clear 96-well plates (Corning Costar, Fisher Scientific, USA) at a density of 10,000 cells/well. After 24 hours, 5 μL of the samples were added in 200 μL of medium. Cells were incubated at 37°C for 48 hours in a 5% CO_2 atmosphere. Finally, the amount of viable cells was determined using CellTiter 96 AQueous Nonradioactive Cell Proliferation Assay (MTS), Promega.

2.4. Pseudoternary Phase Diagram Construction. Based on solubility and preliminary cytotoxicity results, excipients were selected to perform ME region screening. Different amounts of PS 80 and each one of the selected co-surfactants and oil phases were mixed using magnetic stirrer during 10 minutes. Then, water was added and samples were left to equilibrate using a thermal bath at 37°C (Varian, USA) for 1 hour. The adopted criteria used for considering a formulation as an ME was based on the visual analysis of the compositions searching for clear, single-phase, isotropic and low-viscous systems.

2.5. Screening and Optimization of MEs. Once the screening was finished, a number of compositions were selected on basis of noncytotoxic effect of their components and also on a high TMX solubilizing capacity. After that they were evaluated for MCF-7 cells' survival as described above.

2.6. Preparation of TMX-Loaded MEs. TMX-loaded MEs were prepared by weighing appropriate amounts of PS 80, the co-surfactant, and oil phase selected according with previous adopted criteria; gentle magnetic stirring during 10 minutes at room temperature was applied so as to obtain homogenous samples, which were left to equilibrate using a thermal bath at 37°C (Varian, USA) for 1 hour. Next, three different amounts of TMX were added and dissolved with magnetic stirring. Finally, the corresponding amount of water for each one of the selected compositions was added under agitation at room temperature.

2.7. Physicochemical Characterization of TMX-Loaded MEs. Density was measured using a Mettler Toledo 30 px. Formulation of pH was determined with a pHmeter Mettler Toledo seven easy. Conductivity was assessed using an Accumet research AR20 at 25°C; for rheological measurements a Brookfield DV-III Ultra at 25°C was used. Polarization microscopy was performed using an Olympus BH microscope [21].

Droplet size was analyzed with a Nanozetasizer ZS, Malvern Instruments, UK. Samples were not diluted to carry out the measurements and assays were performed at 25°C. The polydispersity index indicates the size distribution within a ME population. The z potential of the formulations was determined using the same equipment (Nanozetasizer ZS, Malvern Instruments, UK). Samples of the formulation were placed in the electrophoretic cell, where an electric field of about 15 V/cm was applied. The electrophoretic mobility measured was converted into z potential using the Smoluchowski equation.

The morphology of MEs was studied using transmission electron microscopy (TEM). The MEs were first diluted in water (1 : 40), a sample drop was placed onto a grid covered with Formvar film and the excess was drawn off with a filter paper. Samples were subsequently stained with uranyl acetate solution for 30 s. Samples were finally dried in a closed container with silica gel and analyzed. The droplet diameter was estimated using a calibrated scale.

Chemical stability was performed using the HPLC equipment described for solubility assays (Shimadzu Class VP HPLC), and the chromatographic conditions were also the same. For short time stability studies, samples were left on the bench at room temperature for a month and, then, were reanalyzed. Direct observation of the formulations was used to evaluate drug precipitation or other physical change during the evaluation period.

The objective of thermodynamic stability is to evaluate the phase separation and effect of temperature variation on MEs formulation. All the MEs prepared were centrifuged (Eppendorf Centrifuge 5810) at 15,000 rpm for 15 min, and then they were observed visually for phase separation. Formulations that did not show any sign of phase separation after centrifugation were subjected to freeze thaw cycle. In a freeze thaw study, TMX MEs were evaluated for two freeze thaw cycles between (−20°C and +25°C) with storage at each temperature for not less than 4 h [22].

2.8. Cell Culture Conditions. MCF-7 human breast cancer cell line was obtained from the American Type Culture Collection (ATCC) (Rockville, MD, USA). Cells were maintained in Dulbecco's minimum essential medium (DMEM) supplemented with 10% fetal bovine serum (FBS), 50 μg/mL gentamycine (Invitrogen Argentina), and 2 mM L-glutamine (Invitrogen Argentina). Cells were cultured in 75 cm^2 culture flasks at 37°C in a humidified atmosphere of 5% CO_2.

2.9. Cytotoxicity and In Vitro Performance of the Selected TMX-Loaded MEs. For in vitro performance studies, cells were seeded in 96-well plates at a density of 5,000 cells/well. After 24 hours, medium was replaced by phenol-red-free media containing 2 mM L-glutamine for 24 hours. To analyze effects of selected TMX-loaded formulations, cells were subsequently incubated with estradiol 10 nM and the TMX-loaded MEs; in parallel, a TMX suspension containing 10 mM of drug in presence and in absence of estradiol was also evaluated. Cells were incubated further for 48 hours and then cell viability was assessed by the cell proliferation assay (MTS).

2.10. Statistical Analysis. Statistical calculations were performed with the GraphPad InStat statistical package for Windows. Data shown in tables and figures of in vitro properties evaluation represent mean of three determinations ± standard deviation (SD). Statistical significance of the

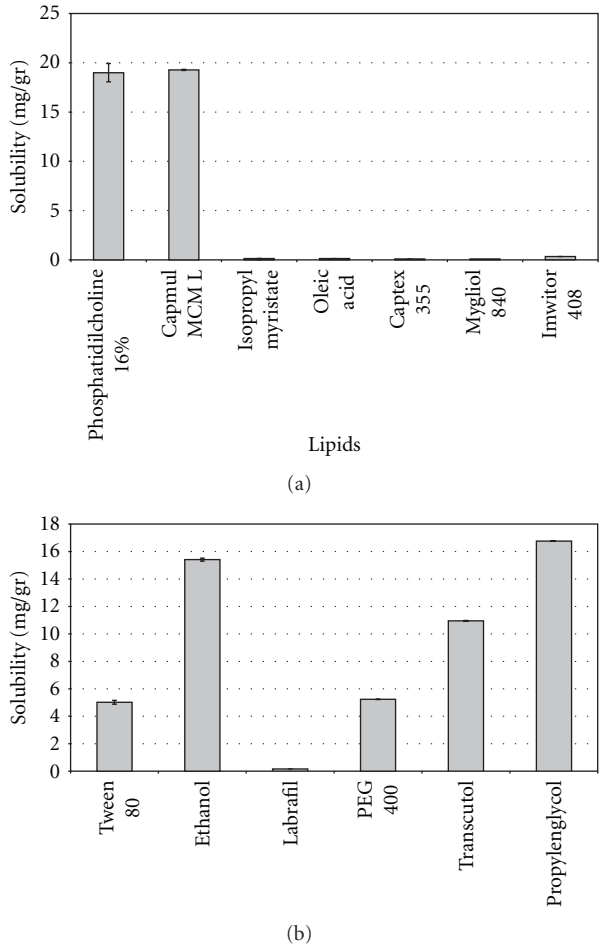

FIGURE 2: (a) Solubility of Tamoxifen citrate in oil phases (expressed in mg/g). Each bar represents the mean of three samples ± SD. (b) Solubility of Tamoxifen Citrate in Polysorbate 80 and cosurfactants (expressed in mg/g). Each bar represents the mean of three samples ± SD.

differences between the groups was calculated by the Tukey-Kramer multiple comparison test and probability value of P smaller than 0.05 indicated a statistically significant difference.

3. Results and Discussion

3.1. Preliminary Solubility Evaluation. TMX resulted almost insoluble in IPM, Mygliol 840, Captex 355, Oleic acid, and Imwitor 408 and showed solubility near 20 mg/g in the PC suspension and in Capmul MCM L (Figure 2(a)). Therefore, only PC and Capmul MCM L were selected for the forthcoming screening. The selection of the oily phase is very important because the drug solubility in the formulation depends mainly on it [23, 24]. So, this property results, fundamental in the search for high solubilizing capacity systems.

Lipid solubility values found in this work are in accordance with previous studies and significantly higher compared to other lipids not considered in this study [25]. They also were significantly higher than TMX solubility in water (≈20 mg/mL and ≈0.4 μg/mL, resp.). Furthermore, the high solubility in PC is in accordance with previous works [26], which stated that active compounds with an intermediate lipophilicity (Log P of 4.0 and above, being 7.9 the value of the Tamoxifen) have a high tendency to be solubilized by phospholipids.

Solubility of TMX in the five co-surfactants and in PS 80 is depicted in Figure 2(b). The highest solubilizing capacity was achieved with PG and ethanol; therefore, both compounds were selected to act as coemulsifiers in the forthcoming ME screening. However, TMX showed a considerable solubility in PEG 400 and Transcutol P, but it resulted significantly lower than the selected compounds ($P < 0.05$). Finally, Labrafil 1944 CS was discarded because it was the co-surfactant with the lowest drug solubilizing capacity.

Solubility of TMX in PS 80 was around 5 mg/g; however, it is expected that these results slightly impact on the final therapeutic agent solubilization. The most important factor that contributes to the final ME solubilizing capacity in poorly water soluble drugs is the solubility in the lipid internal phase [26].

3.2. Preliminary Cytotoxicity Study. In order to avoid interference when testing selected vehicles for in vitro performance, a preliminary cytotoxicity experiment on the MCF-7 cancer cell line was performed.

As it can be observed in Figure 3(a), only samples containing 5% m/v of PS 80 exhibited low cytotoxicity; higher concentrations than 5% m/v showed a percentage of cell viability after treatment lower than 50%. Therefore, it can be concluded that formulations containing PS 80 at concentrations above 5% would be toxic to the cells. Because of it, false-positive results could be addressed when evaluating their in vitro performance. As a result of the preliminary surfactant cytotoxicity experiments and in order to avoid excipient related effects on the cells, final formulations have been diluted prior to their in vitro performance evaluation. Oleic acid was the only no polar phase associated with cytotoxicity effect at both assayed concentrations (Figure 3(b)). Labrafil CS was the only cosurfactant which showed that inconvenience.

3.3. Screening and Optimization of MEs. Based on solubility and cytotoxicity results, the following excipients were selected to perform the preliminary microemulsion screening: PS 80 as surfactant, ethanol, and PG as co-surfactants and PC and Capmul MCM L as the oil phases.

Once the screening was finished, a number of compositions which resulted to be isotropic were selected and are shown in Table 1. The selection included compositions with a relative proportion of PS 80 lower than 20%, relative concentrations of each one of the oil phases between 8 and 16%; the level of the co-surfactants was fixed in 25%. None of these compositions containing PG as cosurfactant, matched the adopted criterion for considering ME system and they were discarded for the next step of selection.

In relation to Capmul MCM L, promising results were observed in agreement with other authors; as it has been

Table 1: Composition of the selected microemulsions after the screening of excipients.

Formula	Polysorbate 80 (%)	PC (%)	Capmul MCM L	Propylene glycol (%)	Ethanol (%)	Water (%)
1	20	8			25	47
2	20	12			25	43
3	20	16			25	39
4	15	8			25	52
5	15	12			25	48
6	20		8		25	47
7	20		12		25	43
8	20		16		25	39
9	15		8		25	52
10	15		12		25	48
11	20		8	25		47
12	20		12	25		43
13	20		16	25		39
14	15		8	25		52
15	15		12	25		48

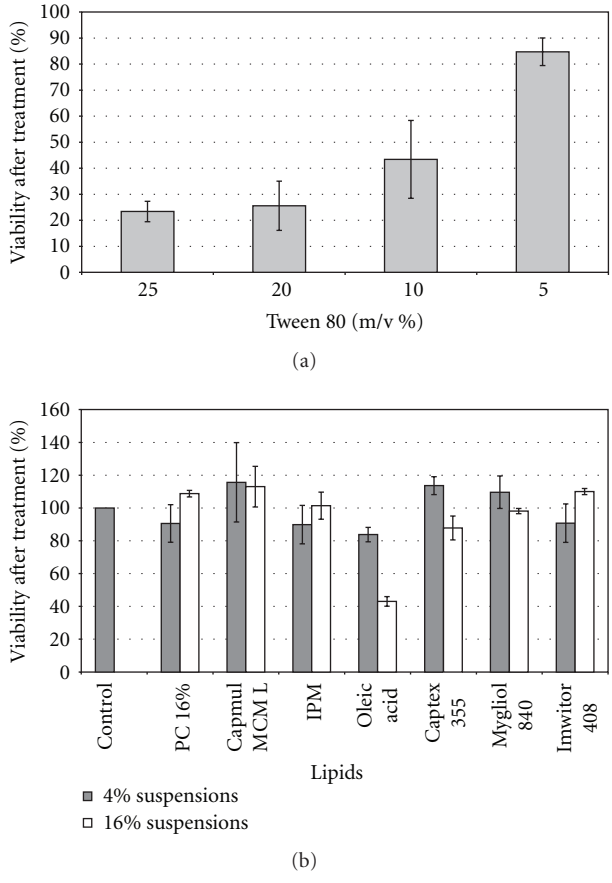

Figure 3: (a) Cell viability of MCF-7 breast cancer cells incubated at 37°C for 48 hrs with Polysorbate 80 at 25, 20, 10, and 5% m/v, respectively. Each bar represents the mean of three samples ± SD. (b) Cell viability of MCF-7 breast cancer cells incubated at 37°C for 48 hrs with suspensions of 4% and 16% of each one of the selected lipids. Each bar represents the mean of three samples ± SD.

recorded medium chain monoglycerides are known for their ease of emulsification when compared to fixed oils or long-chain fatty acids [5, 18]. They also exhibit good solubilizing capacity. However, this oil phase could not be forthcoming evaluated in MEs' selection because of the high cytotoxicity exhibited in cell cultures. Formulations containing Capmul MCM L as oil phase were highly cytotoxic even though they were diluted to avoid surfactant toxicity and that the lipid alone did not show that property (Figures 4(a) and 4(b)). In this case, cytotoxicity may be due to the effect of the lipid on cells when delivered by ME. For this reason, MEs containing Capmul MCM L were discarded for the in vitro inhibition of proliferation experiments and their pseudoternary phase diagrams are not shown.

At this stage of the work, only MEs containing PC, ethanol, and PS 80 were selected. For their pseudoternary phase diagrams construction, two different surfactant/co surfactant ratios: 0.8 and 0.6 were considered (Figures 5(a) and 5(b)). Outside the isotropic systems areas, coarse emulsions or gel-like structures were found for both studied surfactant/cosurfactant ratios. MEs were found down to a water concentration of 5% in both cases and up to 75% for the systems containing a higher surfactant level (0.8 ratio) and 65% for the one with lower surfactant level (0.6 ratio). Therefore, the higher level of surfactant did not significantly affect the total area covered by isotropic systems in the pseudoternary diagrams. After this, the study of ME region was carried out again with the formulations containing 4 mM of drug, so as to evaluate if there were significant changes in ME regions. No significant changes in ME regions were observed in both Pseudoternary phase diagram using MEs containing 4 mM of TMX.

This way of research, in which cytotoxicity evaluation is done during the pharmaceutical development process, may result at last, in biological findings more representative; and

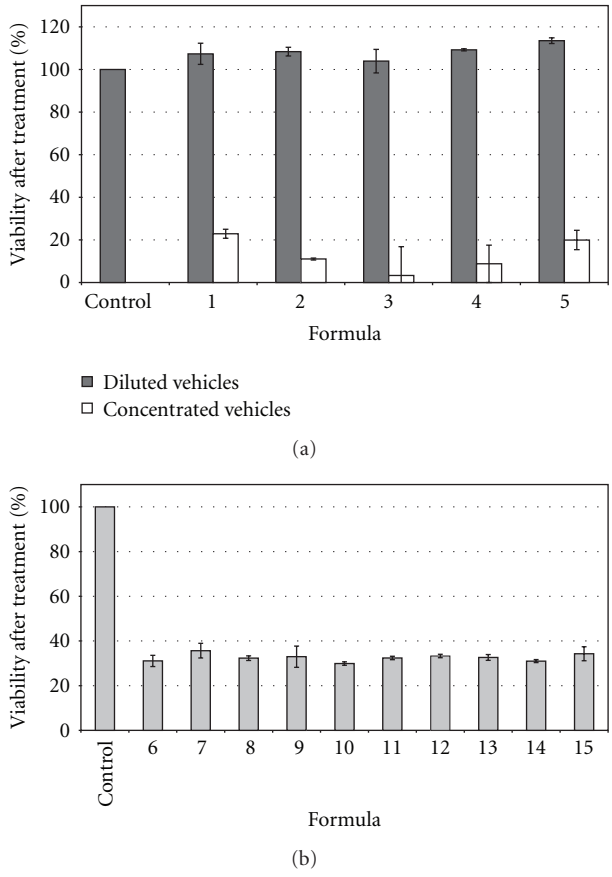

Figure 4: (a) Cell viability of MCF-7 breast cancer cells incubated at 37°C for 48 hrs with selected microemulsions N° 1 to N° 5, after a dilution (1 : 5) and without dilution. Each bar represents the mean of three samples ± SD. (b) Cell viability of MCF-7 breast cancer cells incubated at 37°C for 48 hrs with selected microemulsions N° 6 to N° 15 after 1 : 5 dilution. Each bar represents the mean of three samples ± SD.

additionally in a shorter period of time. It is remarkable that Cavalli et al. have recently reported that sometimes the results are partially affected by the conditions of culture medium, as the use of Dimethyl sulfoxide (DMSO) in cytotoxicity assays, for example [27].

3.4. Preparation and Solubility Evaluation of Selected MEs Containing TMX. Results are shown in Figure 6 and as it can be observed, there is a synergic effect regarding drug solubility in the MEs compared to the solubility in the isolated excipients. This means that, in some cases, the difference observed for solubilizing capacity is tenfold higher.

Taking into account the composition of the MEs, the solubility seems to increase with the raise in the lipid phase content. Thus, the higher the surfactant percentage for the same lipid level, the higher the solubility in the ME. Considering TMX water solubility (≈0.4 μg/mL) [28–30], these systems represent an improvement of around 150000 fold for vehicle 4, which exhibited a solubility of 60 mg/g.

3.5. Physicochemical Characterization. A significant lowering effect of approximately 1.5 points in pH values was observed when TMX was added. Conductivity values obtained for the selected compositions correspond to those of o/w MEs [31, 32].

The low viscosity values are representative for MEs (Table 2). The differences observed for viscosity values might be the result of the interaction between ME droplets in oil/water systems. It is expected that PS 80 hydrophilic chains are strongly hydrated and connected with hydrogen bonds; this allows the interaction between the droplets, thus raising the viscosity values [33]. It is also to remark that the higher PC concentrations in the compositions, the higher viscosity was observed.

All selected formulations were nonbirefringent when analyzed with the polarized microscope, confirming their isotropy. It was concluded that MEs were not electrically charged (z potential equal to 0 mV) due to their ionic characteristics and dipolar attributes.

Since ME formation process is generally a random stirring process; the resulting delivery system may result in a polydispersed system in which different droplet sizes can coexist. This information is extremely valuable in practice because both stability and viscosity depend on the drop size distribution [34]. The later in vivo or in vitro behavior depends on this property as well [35]. Results shown in Table 3 are in the typical range for a ME composition with a narrow range of polydispersion as the polydispersity index (PDI) shown [7]. TEM images also confirmed this size distribution (Figure 7) for blank ME N° 2. The addition of TMX did not significantly change droplet size of formulations comparing with empty ones, even at the highest TMX (20 mM). This is an interesting advantage for the selected compositions, because the loading of a lipophilic active compound could result in an increase in the droplet size and, eventually, could compromise the system physical stability [35].

A short stability testing was carried out with selected formulations. For this purpose, TMX 10 mM was loaded in order to achieve a final concentration of approximately 5.10–4 M in the culture media as the higher dose, according to literature data [36]. Results demonstrated that all formulations showed a 100 ± 2% of the initial content after a month of observation. Obtained values confirm the total solubilization of the drug and absence of rapid degradation (data not shown). Regarding physicochemical values, no significant changes in the values measured at the beginning of the study were obtained after the studied period. No precipitation or change in appearance was observed by direct visual observation. None of the fifteen ME formulations has shown any sign of in-stabilization during the thermodynamic stability tests carried out.

3.6. In Vitro Performance of Selected MEs. As a preliminary experiment, the five empty MEs were cultured to assess if they have any effect on cell proliferation in presence of 10 nM of estradiol. Two controls were also included: one adding estradiol (10 nM) to the cells in order to determine its proliferation effect and the other containing only the cells. As

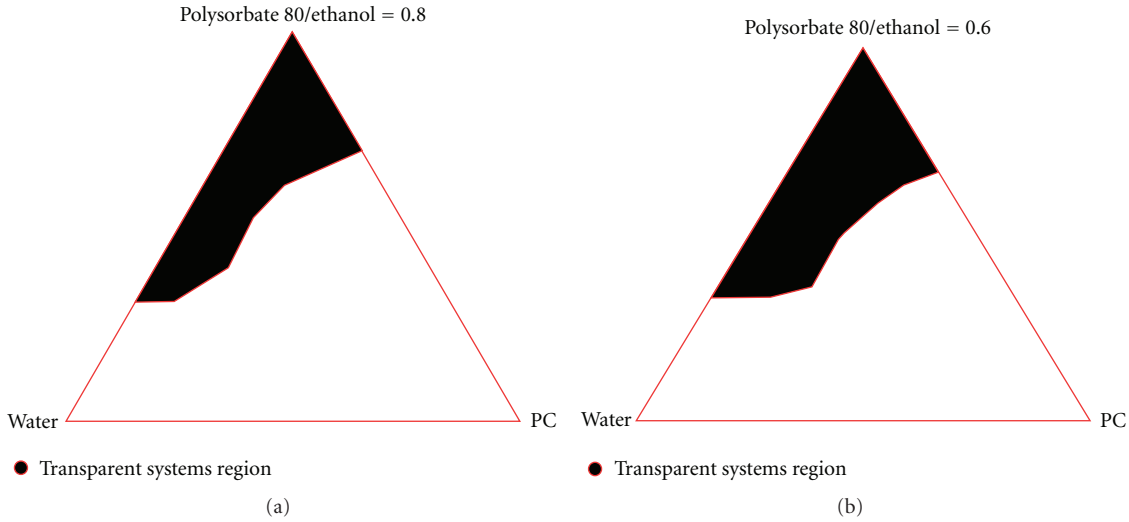

Figure 5: Pseudoternary phase diagrams of the selected formulations (Ratios Polysorbate 80: ethanol 0.8 and 0.6, resp.).

Table 2: Physicochemical parameters measured in the selected microemulsions. Data are expressed as mean ± SD ($n = 3$).

Formula	Viscosity (mPa·s) Empty ME	pH (Empty ME)	pH (Loaded ME)	Conductivity (uS/cm) Empty ME	Density (g/mL) Empty ME
1	45.7 ± 1.8	6.11 ± 0.02	4.62 ± 0.02	71.1 ± 0.9	1.00 ± 0.01
2	59.4 ± 4.3	6.09 ± 0.01	4.62 ± 0.02	40.7 ± 1.1	0.98 ± 0.01
3	79.3 ± 7.7	5.96 ± 0.02	4.67 ± 0.01	65.2 ± 1.6	0.99 ± 0.01
4	21.2 ± 2.3	6.15 ± 0.02	4.54 ± 0.01	42.6 ± 0.8	0.99 ± 0.01
5	29.9 ± 2.2	6.00 ± 0.05	4.61 ± 0.02	40.2 ± 1.1	0.97 ± 0.01

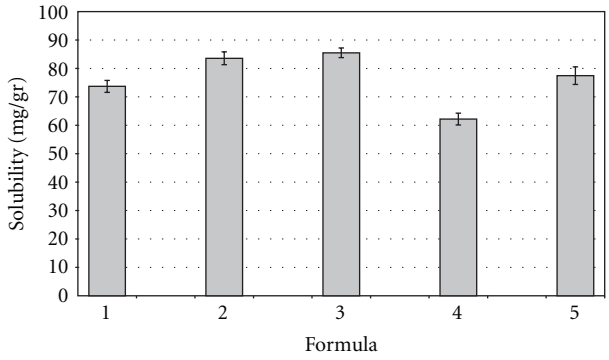

Figure 6: Solubility of Tamoxifen citrate in the selected vehicles. Each bar represents the mean of three samples ± SD (standard deviation for $n = 3$).

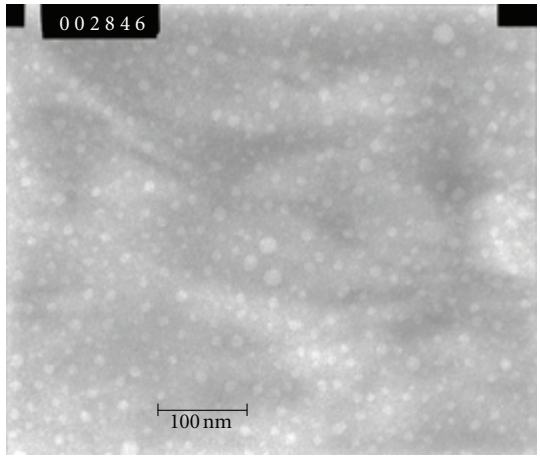

Figure 7: TEM photograph of Formulation 2 (×100000; dilution 1 : 40).

it is shown in Figure 8, none of the empty ME showed effects *per se* over the MCF-7 cell line; it can be observed, instead, the proliferative effect of estradiol on MCF-7 cell line. Results confirmed that the dilution adopted was not cytotoxic.

The five selected formulations were loaded with the following TMX concentrations, 11 mg/g (20 mM), 5.5 mg/g (10 mM) and 2.2 mg/g (4 mM); it is important to remark that the in vitro performance of selected MEs was carried out in a culture media containing estradiol 10 nM.

The percentage of cellular viability of MCF-7 cells following inoculation of the above-mentioned TMX concentrations is illustrated in Figure 8. There was a significant decrease in cell growth for all formulations containing the

Table 3: Mean droplet size for selected empty and loaded microemulsions. PdI: polydispersity index.

Formula	Droplet size (nm) Empty ME	pdI	Droplet size (nm) Loaded ME	pdI
1	5.72	0.344	6.04	0.407
2	5.37	0.237	6.04	0.297
3	5.41	0.256	4.97	0.174
4	9.54	0.365	9.62	0.368
5	8.43	0.389	8.33	0.210

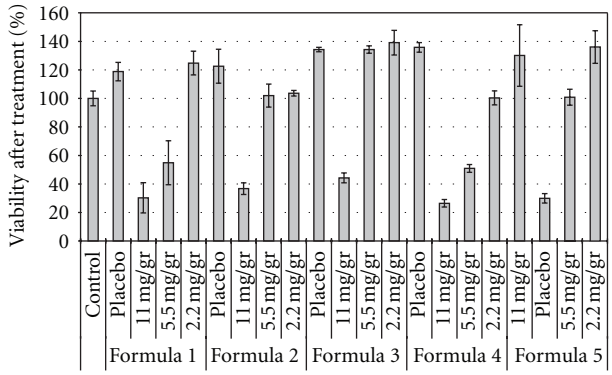

Figure 8: Cell viability of MCF-7 breast cancer cells incubated with empty microemulsions and formulations containing Tamoxifen citrate in the following concentrations: 11 mg/g (20 mM), 5.5 mg/g (10 mM), 2.2 mg/g (4 mM). Each bar represents the mean of three samples ± SD.

highest concentration of TMX. The viable cell percentages after treatment were around 30 to 40% in all cases, that is, at least 90% less of viable cells than the empty compositions; ME N° 4 was the one which shown the highest cytotoxic effect. The same behavior was shown by the formulations 1 and 4 with the intermediate concentration of drug; in these cases the differences shown were 75% and 90%, respectively.

This cytotoxic effect was not observed when formulations N° 1, 3, and 5 were loaded with 4 mM of TMX. But it is to remark that both ME N° 2 and ME N° 4 showed a significant lower number in viable cells when loading this drug concentration. Additionally, it is worth noting that formulas 1, 4, and 5 showed a dose dependent effect. Formulations 2 and 3 did not show significant differences between the effect exerted by 10 mM and the 4 mM TMX concentrations. The TMX suspension was not able to significantly decrease the number of viable cells in any cell culture condition (data not shown).

Even though TMX mechanism of action has not been completely elicited, it was reported that it acts primarily through estrogen receptors (ERs) by modulation of gene expression that finally leads to cell cycle arrest. However, it has been informed that at higher concentrations could induce breast cancer cell apoptosis [36]. This is an ER independent and nongenomic effect; it was found in ER negative breast cancer cells and other cell types such as malignant gliomas, pancreatic carcinomas, and melanomas. On the other hand, estradiol has an antiapoptotic influence in both, ER positive and negative cells, in addition to its proliferative effect on ER positive cells; the antiapoptotic effect has also been reported in MCF-7 breast cancer cell line [37].

From the results obtained in cell cultures, it might conclude that all the compositions containing 20 mM of TMX showed an important cytotoxic effect. This phenomenon would be related with the induction of cellular apoptosis described above; the effect was also observed in ME N° 1 and 4 containing 10 mM TMX.

The % of viable cells observed would indicate that seven of the fifteen assayed compositions were able to solubilize an enough amount of TMX capable to show a modification in the apoptosis cellular induction. It is also interesting to remark that this phenomenon is observed in presence of the above demonstrated proliferative effect of estradiol.

It can be concluded that formulations 1 and 4 had the best in vitro performance because they were able to show an important antiproliferative effect even when they were loading the intermediate dose.

Another interesting observation to point out is that formulation 3 showed the highest percentage of cell viability at any TMX concentration; this formula is the one which has the highest PC (16%) concentration. Previous reports showed that PC content is increased in cancer cells and have an important role in their proliferation [38, 39]. So, it is expected that this stimulation on cell proliferation can be attributed to the levels of PC. This observation and the mechanism described above suggest that the proposed MEs would present a high cellular uptake; anyway, PC proliferation effect has to be considered in further pharmacotherapeutic evaluation.

The obtained MEs are promising in the current state of increasing interest for nanocarriers that can be used for TMX delivery. For example, Chawla and Amiji, examined biodegradable polymeric nanoparticles uptake and distribution in MCF-7 breast cancer cell line. They compared TMX intracellular concentration when delivered by the nanoparticles and in solution, and they found that the drug uptake from the nanoparticles followed a saturable transport. Therefore, above certain concentration, TMX intracellular concentration was much higher when delivered by the solution [1]. On the contrary, MEs designed in this work did not show signs of limited transport in none of the selected drug concentrations. Besides, it is expected that MEs can improve drug cellular uptake not even for a better

drug solubilizing capacity but also for the improvement in biopharmaceutical parameters that have been extensively described for them [4, 7, 8, 13, 15, 17, 18].

Al Haj et al. evaluated TMX-loaded solid lipid nanoparticles for parenteral administration, and, though promising, these systems required a sophisticated preparation method because they were elaborated by high pressure homogenization technique [40]. Instead of this, the ease of preparation is a common ME characteristic.

Tagne et al. evaluated a nanoemulsion containing TMX that has a significantly better in vitro performance reducing cell proliferation when compared to a TMX-loaded suspension. However, they have used a concentration of TMX equal to 3×10^{-5} M for all the cell culture treatments, while our MEs were able to solubilize more than 100-fold higher of TMX [6]. These authors claimed for an important cellular uptake because of the nanometric sizes of the nanoemulsions. Similar results could be expected with our formulations but the in vivo therapeutic parameters would be improved because of the drug concentration achieved.

Another important difference between both works is the technique of preparation. They used a microfluidizer processor which provides a resultant high shear rate by accelerating the product through microchannels to a high velocity for size reduction to the nanoscale range. They previously prepared a suspension of TMX and then the mixture was homogenized. On the contrary, MEs involve a spontaneous process of formation for a defined composition and the selection of the composition is searched through a screening of components. As a result of these two different techniques they found a negative z potential while we observed no charges on the droplets' layers. Another consequence was that they obtained a bimodal distribution of mean droplet sizes; on the contrary, we observed a more uniform distribution. In conclusion, the above-mentioned differences are in relation with the fact that Tagne et al. have prepared nanoemulsions, while our work deals on MEs; it is very clear in literature the differences between them independently that they could have similar compositions and mean droplet size [4, 8, 41].

More recently, the electrospray technique was proposed to produce TMX-loaded poly(amidoamine)-cholesterol conjugate nanoparticles in powder form without any excipient in a single step. Spite of this, the nanoparticles showed sizes higher than 200 nm and a drug loading of about 40% [27].

It is also necessary to remark that the cell culture experiments were carried out with no reagent addition; this is a very important issue because previous report [27, 42] found that MCF7 cells are highly sensitive towards DMSO. Indeed, volumes equal to or higher than 2 μL (2% v/v) result in a cytotoxic effect that partially overlaps the one observed in cells treated with free TMX diluted in DMSO. Therefore, this "background" cytotoxicity leads to an overestimation of the free TMX activity. On the contrary, every step done in this work during the development of the experimental design was adjusted so as to strictly evaluate the in vitro behavior showed by each one of the selected compositions.

4. Conclusion

The present work describes a novel interdisciplinary rational screening for a ME composition, its optimization, and the corresponding in vitro performance evaluation on MCF-7 breast cancer cell line. The development included physicochemical properties evaluation and drug solubility in selected formulations. The experimental design began with the proposal of extensively studied excipients for the screening, after that, the first criterion adopted for excipient selection was based on solubilizing capacity; then cytotoxic was evaluated. The final criterion of selection was the ability to form MEs shown by each one of the excipients.

It is our opinion that this design layout allows a faster optimization of MEs composition. The drug-loading capacity was investigated using TMX, a poorly water soluble antineoplastic drug, as an active compound model. Nonadherence to oral medication is an increasingly recognized concern in the care of cancer patients and considering that every year, hundreds of thousands of women worldwide are recommended to take TMX for 5 years; a different protocol of treatment would be evaluated. Not only other oral administration protocol but also an IM or IV formulation can finally be proposed after the in vivo experiments. In addition, some other ER-negative cancers, which have also shown to be sensitive to TMX may be further evaluated with MEs' containing different pharmacological doses. Thus, a more efficient drug release profile would potentially prevent the development of cancer cell resistance.

Consequently, these MEs result in a promising alternative for further in vivo evaluation. Finally, Peer et al. mentioned that for rapid and effective clinical translation, the nanocarriers should present some characteristics that these ones do exhibit [2]. They are made with biocompatible, well-characterized, and easily functionalized excipients; they are both soluble and colloidal dosage forms under aqueous conditions which are related to increased effectiveness. And they have a low rate of aggregation and a long shelf life. They would also exhibit differential uptake efficiency in the target cells over normal cells because they show passive targeting.

Acknowledgment

Support for these studies was provided by the National Agency of Scientific and Technological Promotion (ANPCyT); Ministry of Science, Technology and Productive Innovation, Argentina, the University of Buenos Aires; the National Science Research Council (CONICET).

References

[1] J. S. Chawla and M. M. Amiji, "Cellular uptake and concentrations of tamoxifen upon administration in poly(E-caprolactone) nanoparticles," *AAPS PharmSci*, vol. 5, no. 1, article E3, 2003.

[2] D. Peer, J. M. Karp, S. Hong, O. C. Farokhzad, R. Margalit, and R. Langer, "Nanocarriers as an emerging platform for cancer therapy," *Nature Nanotechnology*, vol. 2, no. 12, pp. 751–760, 2007.

[3] E. Cukierman and D. R. Khan, "The benefits and challenges associated with the use of drug delivery systems in cancer therapy," *Biochemical Pharmacology*, vol. 80, no. 5, pp. 762–770, 2010.

[4] M. J. Lawrence and G. D. Rees, "Microemulsion-based media as novel drug delivery systems," *Advanced Drug Delivery Reviews*, vol. 45, no. 1, pp. 89–121, 2000.

[5] R. G. Strickley, "Solubilizing excipients in oral and injectable formulations," *Pharmaceutical Research*, vol. 21, no. 2, pp. 201–230, 2004.

[6] J. B. Tagne, S. Kakumanu, D. Ortiz, T. Shea, and R. J. Nicolosi, "A nanoemulsion formulation of tamoxifen increases its efficacy in a breast cancer cell line," *Molecular Pharmaceutics*, vol. 5, no. 2, pp. 280–286, 2008.

[7] A. A. Date and M. S. Nagarsenker, "Parenteral microemulsions: an overview," *International Journal of Pharmaceutics*, vol. 355, no. 1-2, pp. 19–30, 2008.

[8] S. Gupta and S. P. Moulik, "Biocompatible microemulsions and their prospective uses in drug delivery," *Journal of Pharmaceutical Sciences*, vol. 97, no. 1, pp. 22–45, 2008.

[9] S. Gao and J. Singh, "In vitro percutaneous absorption enhancement of a lipophilic drug tamoxifen by terpenes," *Journal of Controlled Release*, vol. 51, no. 2-3, pp. 193–199, 1998.

[10] J. L. Jones, B. J. Daley, B. L. Enderson, J. R. Zhou, and M. D. Karlstad, "Genistein inhibits tamoxifen effects on cell proliferation and cell cycle arrest in T47D breast cancer cells," *American Surgeon*, vol. 68, no. 6, pp. 575–577, 2002.

[11] R. L. Sutherland, R. E. Hall, and I. W. Taylor, "Cell proliferation kinetics of MCF-7 human mammary carcinoma cells in culture and effects of tamoxifen on exponentially growing and plateau-phase cells," *Cancer Research*, vol. 43, no. 9, pp. 3998–4006, 1983.

[12] J. G. Hardman, L. E. Limbird, and A. G. Gilman, *The Pharmacological Basis of Therapeutics*, McGraw-Hill, New York, NY, USA, 10th edition, 2006.

[13] S. C. Shin, J. S. Choi, and X. Li, "Enhanced bioavailability of tamoxifen after oral administration of tamoxifen with quercetin in rats," *International Journal of Pharmaceutics*, vol. 313, no. 1-2, pp. 144–149, 2006.

[14] T. Tanaka, P. Decuzzi, M. Cristofanilli et al., "Nanotechnology for breast cancer therapy," *Biomedical Microdevices*, vol. 11, no. 1, pp. 49–63, 2009.

[15] S. Kakumanu, J. B. Tagne, T. A. Wilson, and R. J. Nicolosi, "A nanoemulsion formulation of dacarbazine reduces tumor size in a xenograft mouse epidermoid carcinoma model compared to dacarbazine suspension," *Nanomedicine*, vol. 7, no. 3, pp. 277–283, 2011.

[16] R. Rowe, P. Sheskey, and M. Quinn, *Handbook of Pharmaceutical Excipients*, Pharmaceutical Press, London, UK, 6th edition, 2010.

[17] C. W. Pouton, "Formulation of poorly water-soluble drugs for oral administration: physicochemical and physiological issues and the lipid formulation classification system," *European Journal of Pharmaceutical Sciences*, vol. 29, no. 3-4, pp. 278–287, 2006.

[18] A. A. Kale and V. B. Patravale, "Development and evaluation of lorazepam microemulsions for parenteral delivery," *AAPS PharmSciTech*, vol. 9, no. 3, pp. 966–971, 2008.

[19] A. Spernath, A. Aserin, and N. Garti, "Fully dilutable microemulsions embedded with phospholipids and stabilized by short-chain organic acids and polyols," *Journal of Colloid and Interface Science*, vol. 299, no. 2, pp. 900–909, 2006.

[20] N. Gursoy, J. S. Garrigue, A. Razafindratsita, G. Lambert, and S. Benita, "Excipient effects on in vitro cytotoxicity of a novel paclitaxel self-emulsifying drug delivery system," *Journal of Pharmaceutical Sciences*, vol. 92, no. 12, pp. 2411–2418, 2003.

[21] F. Nielloud and G. Marti-Mestres, *Pharmaceutical Emulsions and Suspensions*, Marcel Dekker, New York, NY, USA, 2000.

[22] A. K. Singh, A. Chaurasiya, A. Awasthi et al., "Oral bioavailability enhancement of exemestane from self-microemulsifying drug delivery system (SMEDDS)," *AAPS PharmSciTech*, vol. 10, no. 3, pp. 906–916, 2009.

[23] A. Palamakula and M. A. Khan, "Evaluation of cytotoxicity of oils used in coenzyme Q10 Self-Emulsifying Drug Delivery Systems (SEDDS)," *International Journal of Pharmaceutics*, vol. 273, no. 1-2, pp. 63–73, 2004.

[24] C. J. H. Porter, C. W. Pouton, J. F. Cuine, and W. N. Charman, "Enhancing intestinal drug solubilisation using lipid-based delivery systems," *Advanced Drug Delivery Reviews*, vol. 60, no. 6, pp. 673–691, 2008.

[25] Y. S. R. Elnaggar, M. A. El-Massik, and O. Y. Abdallah, "Self-nanoemulsifying drug delivery systems of tamoxifen citrate: design and optimization," *International Journal of Pharmaceutics*, vol. 380, no. 1-2, pp. 133–141, 2009.

[26] M. Sznitowska, E. A. Dabrowska, and S. Janicki, "Solubilizing potential of submicron emulsions and aqueous dispersions of lecithin," *International Journal of Pharmaceutics*, vol. 246, no. 1-2, pp. 203–206, 2002.

[27] R. Cavalli, A. Bisazza, R. Bussano et al., "Poly(amidoamine)-cholesterol conjugate nanoparticles obtained by electrospraying as novel tamoxifen delivery system," *Journal of Drug Delivery*, vol. 2011, Article ID 587604, 9 pages, 2011.

[28] G. R. De Lima, G. Facina, J. Y. Shida et al., "Effects of low dose tamoxifen on normal breast tissue from premenopausal women," *European Journal of Cancer*, vol. 39, no. 7, pp. 891–898, 2003.

[29] G. Cavallaro, L. Maniscalco, M. Licciardi, and G. Giammona, "Tamoxifen-loaded polymeric micelles: preparation, physicochemical characterization and in vitro evaluation studies," *Macromolecular Bioscience*, vol. 4, no. 11, pp. 1028–1038, 2004.

[30] F. X. Hu, K. G. Neoh, and E. T. Kang, "Synthesis and in vitro anti-cancer evaluation of tamoxifen-loaded magnetite/PLLA composite nanoparticles," *Biomaterials*, vol. 27, no. 33, pp. 5725–5733, 2006.

[31] P. Boonme, K. Krauel, A. Graf, T. Rades, and V. B. Junyaprasert, "Characterization of microemulsion structures in the pseudoternary phase diagram of isopropyl palmitate/water/Brij 97:1-butanol," *AAPS PharmSciTech*, vol. 7, no. 2, article 45, pp. E1–E6, 2006.

[32] W. Zhu, A. Yu, W. Wang, R. Dong, J. Wu, and G. Zhai, "Formulation design of microemulsion for dermal delivery of penciclovir," *International Journal of Pharmaceutics*, vol. 360, no. 1-2, pp. 184–190, 2008.

[33] F. Podlogar, M. Gašperlin, M. Tomšič, A. Jamnik, and M. B. Rogač, "Structural characterisation of water-Tween 40/Imwitor 308-isopropyl myristate microemulsions using different experimental methods," *International Journal of Pharmaceutics*, vol. 276, no. 1-2, pp. 115–128, 2004.

[34] S. A. Charman, W. N. Charman, M. C. Rogge, T. D. Wilson, F. J. Dutko, and C. W. Pouton, "Self-emulsifying drug delivery systems: formulation and biopharmaceutic evaluation of an investigational lipophilic compound," *Pharmaceutical Research*, vol. 9, no. 1, pp. 87–93, 1992.

[35] B. D. Tarr and S. H. Yalkowsky, "Enhanced intestinal absorption of cyclosporin in rats through the reduction of emulsion droplet size," *Pharmaceutical Research*, vol. 6, no. 1, pp. 40–43, 1989.

[36] H. K. Dhiman, A. R. Ray, and A. K. Panda, "Three-dimensional chitosan scaffold-based MCF-7 cell culture for the determination of the cytotoxicity of tamoxifen," *Biomaterials*, vol. 26, no. 9, pp. 979–986, 2005.

[37] A. Zheng, A. Kallio, and P. Härkönen, "Tamoxifen-induced rapid death of MCF-7 breast cancer cells is mediated via extracellularly signal-regulated kinase signaling and can be abrogated by estrogen," *Endocrinology*, vol. 148, no. 6, pp. 2764–2777, 2007.

[38] M. Bañez-Coronel, A. Ramírez de Molina, A. Rodríguez-González et al., "Choline kinase alpha depletion selectively kills tumoral cells," *Current Cancer Drug Targets*, vol. 8, no. 8, pp. 709–719, 2008.

[39] S. Sinha Roy, S. Mukhopadhyay, S. Mukherjee, and S. K. Das, "Breast cancer is associated with an increase in the activity and expression of cholinephosphotransferase in rats," *Life Sciences*, vol. 83, no. 19-20, pp. 661–665, 2008.

[40] N. A. Al Haj, R. Abdullah, S. Ibrahim, and A. Bustamam, "Tamoxifen drug loading solid lipid nanoparticles prepared by hot high pressure homogenization techniques," *American Journal of Pharmacology and Toxicology*, vol. 3, no. 3, pp. 219–224, 2008.

[41] P. Shah, D. Bhalodia, and P. Shelat, "Nanoemulsion: a pharmaceutical review," *Systematic Reviews in Pharmacy*, vol. 1, no. 1, pp. 24–32, 2010.

[42] M. Licciardi, G. Cavallaro, M. Di Stefano, G. Pitarresi, C. Fiorica, and G. Giammona, "New self-assembling polyaspartylhydrazide copolymer micelles for anticancer drug delivery," *International Journal of Pharmaceutics*, vol. 396, no. 1-2, pp. 219–228, 2010.

Hindawi Publishing Corporation
Journal of Drug Delivery
Volume 2012, Article ID 686108, 8 pages
doi:10.1155/2012/686108

Research Article

Cationic Albumin Nanoparticles for Enhanced Drug Delivery to Treat Breast Cancer: Preparation and *In Vitro* Assessment

Sana Abbasi,[1] Arghya Paul,[1] Wei Shao,[1] and Satya Prakash[1,2]

[1] *Biomedical Technology and Cell Therapy Research Laboratory, Department of Biomedical Engineering, Faculty of Medicine, McGill University, 3775 University Street, Montreal, QC, Canada H3A 2B4*
[2] *Artificial Cells and Organs Research Centre, Faculty of Medicine, McGill University, 3775 University Street, Montreal, QC, Canada H3A 2B4*

Correspondence should be addressed to Satya Prakash, satya.prakash@mcgill.ca

Received 13 July 2011; Accepted 10 September 2011

Academic Editor: Rassoul Dinarvand

Most anticancer drugs are greatly limited by the serious side effects that they cause. Doxorubicin (DOX) is an antineoplastic agent, commonly used against breast cancer. However, it may lead to irreversible cardiotoxicity, which could even result in congestive heart failure. In order to avoid these harmful side effects to the patients and to improve the therapeutic efficacy of doxorubicin, we developed DOX-loaded polyethylenimine- (PEI-) enhanced human serum albumin (HSA) nanoparticles. The formed nanoparticles were ~137 nm in size with a surface zeta potential of ~+15 mV, prepared using 20 μg of PEI added per mg of HSA. Cytotoxicity was not observed with empty PEI-enhanced HSA nanoparticles, formed with low-molecular weight (25 kDa) PEI, indicating biocompatibility and safety of the nanoparticle formulation. Under optimized transfection conditions, approximately 80% of cells were transfected with HSA nanoparticles containing tetramethylrhodamine-conjugated bovine serum albumin. Conclusively, PEI-enhanced HSA nanoparticles show potential for developing into an effective carrier for anticancer drugs.

1. Introduction

Doxorubicin (Adriamycin) is a commonly used anti-cancer drug. It is most often used against breast and esophageal carcinomas, osteosarcoma and soft-tissue sarcomas, and Hodgkin's and non-Hodgkin's lymphomas [1]. The effectiveness of doxorubicin (DOX) in treating various types of cancers is greatly limited by the serious side effects caused by the drug. The initial side effects caused as a result of DOX administration include less serious symptoms, such as nausea, vomiting, myelosuppression, and arrhythmia, which are usually reversible [1]. However, DOX-associated cardiomyopathy and congestive heart failure have raised grave concern among health practitioners [2]. A widely researched approach of increasing the efficacy, while lowering the deleterious side effects caused by anti-cancer agents such as doxorubicin, is of developing nanoparticle-based drug delivery systems [3–5].

Various kinds of nanoparticles have been studied for the delivery of DOX, which include poly(butylcyanoacrylate) [6], poly(isohexylcyanoacrylate) [7], poly(lactic-co-glycolic acid [8], chitosan [9], gelatine [10], and liposomes [11]). In addition, Dreis et al. employed human serum albumin (HSA) nanoparticles of a size range between 150 and 500 nm to deliver DOX to a neuroblastoma cell line [3]. These nanoparticles showed a loading efficiency of 70–95% and an increased anti-cancer effect as compared to free DOX. The endogenous HSA serves as a suitable material for nanoparticle formation as albumin is naturally found in the blood and is thus easily degraded, nontoxic, and nonimmunogenic [12]. Albumin is an acidic protein and remains stable between pH range 4–9 and temperatures up to 60°C. In addition, clinical studies carried out with HSA particle formulations, Albunex [13] and Abraxane [14], have shown that albumin-based nanoparticles do not have any adverse effects on the body.

Furthermore, albumin-based nanoparticle delivery systems are easily accumulated in tumor tissue due to the enhanced permeability and retention (EPR) effect [15–17]. The vasculature in an active tumor is different from the vessels found in normal tissue. The distinctive tumor vasculature

has the following properties: hypervasculature, poorly developed vascular architecture, a defective lymphatic drainage, and slow venous blood return [15, 16]. These characteristics lead to the preferential accumulation and retention of macromolecules and nanoparticles in the tumor tissue. Therefore, using a nanoparticle delivery system to deliver low-molecular-weight anti-cancer drugs will be passively targeted to the tumour tissue through the EPR effect [17]. In addition, studies have also suggested that accumulation of albumin-based nanoparticles within the tumor tissue is also because of transcytosis, which occurs by the binding of albumin to 60-kDa glycoprotein (gp60) receptor, which then results in the binding of gp60 with caveolin-1 and the consequent formation of transcytotic vesicles [12, 18]. Taking into consideration the factors mentioned above, HSA seems to be a suitable material to use for nanoparticle synthe-sis.

The surface properties of nanoparticles play a vital role in the cellular internalization of the particles. A neutrally charged surface does not show tendency of interacting with cell membranes, while charged groups found on nanoparticles are actively involved in nanomaterial-cell interaction [19]. Cho and Caruso found in their study of cellular internalization of gold nanoparticles that positively charged particles demonstrate greater adherence to the cell membrane and are thus taken up by the cells more than negatively and neutrally charged nanoparticles [20]. Cationic nanoparticles are shown to bind the negatively charged functional groups, such as sialic acid, found on cell surfaces and initiate translocation [19]. Due to the highly efficient transfection property of positively charged nanoparticles, many nanoparticle-based drug and gene delivery systems are positively charged. In this study, poly(ethylenimine) (PEI), a cationic polymer, has been used to coat the HSA nanoparticles in order to add stability and a positive surface charge to the nanoparticles. PEI may possess a linear or branched structure, with molecular weight ranging between 1 and 1000 kDa [21]. Typically, branched low-molecular-weight PEI (<25 kDa) has been observed to result in higher cellular uptake. As shown in our previous study, higher-molecular-weight PEI (70 kDa) leads to more cytotoxicity than lower-molecular-weight PEI (25 kDa) [22]. The most commonly used stabilizing agent for the preparation of HSA nanoparticles, glutaraldehyde, has been reported to interfere with the release of the encapsulated material [10, 23]. Thus, PEI is being employed as an alternative to glutaraldehyde in the current study.

PEI has been previously used to stabilize HSA nanoparticles. Initially, HSA nanoparticles stabilized using PEI were studied as vectors for protein delivery [24]. The osteoinductive growth factor, bone morphogenetic protein-2 (BMP-2), was encapsulated using PEI-coated albumin nanoparticles, and results showed that the bioactivity of the BMP-2 was retained, suggesting that the developed nanoparticles, are promising vectors for systemic protein administration [24]. In addition, Zhang et al. showed that the encapsulation efficiency of BMP-2 using PEI-coated albumin nanoparticles was >90% [25]. Furthermore, the efficacy of PEI-coated albumin nanoparticles for the delivery of BMP-2 was also confirmed *in vivo* with rats [26]. More recently, we showed that PEI-coated HSA nanoparticles were promising vectors for siRNA delivery [22].

In the current research study, the effectiveness of DOX-loaded polyethylenimine- (PEI-) enhanced HSA nanoparticles used against MCF-7 breast cancer cells was investigated. We prepared the nanoparticles using an ethanol desolvation method and characterized by measuring particle size, surface zeta potential, and cellular uptake [22, 27, 28]. The cytotoxicity of the developed DOX-loaded nanoparticles was assessed in comparison to free DOX at varying drug concentrations over different time points. Results were promising and suggest that the study needs to be followed up with an *in vivo* investigation of the DOX-loaded PEI-enhanced HSA nanoparticles (Figure 1).

2. Materials and Methods

2.1. Materials. Human serum albumin (HSA fraction V, purity 96–99%), 8% glutaraldehyde, and branched polyethylenimine (PEI) (M_W ~ 25,000) were purchased from Sigma Aldrich (ON, Canada). Doxorubicin hydrochloride was purchased from Calbiochem (Gibbstown, USA). All other reagents were purchased from Fischer (ON, Canada). Tetramethylrhodamine-conjugated bovine serum albumin (BSA) was purchased from Invitrogen (ON, Canada). To maintain the cell culture, the reagents such as fetal bovine serum, trypsin, Dulbecco's modified Eagle's Medium (DMEM), and Opti-MEM I Reduced Serum Medium were obtained from Invitrogen (ON, Canada). The breast cancer cell line, MCF-7, was purchased from ATCC (ON, Canada). Promega Cell-Titer 96 AQueous Non-Radioactive Cell Proliferation MTS Assay kit was purchased from Promega (Wis, USA).

2.2. Cell Culture. MCF-7 cells were cultured on tissue culture plates as per the manufacturer's instructions. MCF-7 cells were grown in Dulbecco's modified Eagle's Medium (Invitrogen) supplemented with 10% (v/v) fetal bovine serum (FBS) and placed in an incubator with 5% CO_2 at 37°C. The cells used in the experiments were obtained from passages 5-6.

2.3. Preparation of DOX-Loaded PEI-Enhanced HSA Nanoparticles. PEI-coated HSA nanoparticles were prepared at room temperature using an ethanol desolvation technique [22, 27–29]. In brief, 20 mg of HSA was added to 1 mL of 10 mM NaCl (aq) under constant stirring (800 rpm) at room temperature. The solution was stirred for 10 min. After total dissolution, the solution was titrated to pH 8.5 with 1 N NaOH (aq) and stirred for 5 min. This aqueous phase was desolvated by the dropwise addition of ethanol to aqueous HSA solution under constant stirring. Ethanol was added until the HSA solution became turbid (~1-2 mL). Cross-linking agent, 8% glutaraldehyde, was added to form stable HSA particles. The obtained nanoparticles were centrifuged three times and washed with deionized water (dH_20), followed by resuspension in an equal volume of PBS. PEI dissolved in dH_20 was added to the nanoparticle

preparation to allow PEI to form an outer coating due to electrostatic binding. For the preparation of drug-loaded HSA nanoparticles, doxorubicin was added to 1 mL HSA solution after pH adjustment and allowed to stir for 4 hrs, followed by ethanol addition. To determine the drug encapsulation efficiency, an indirect method was employed as shown by Sebak et al. [27]. The unloaded drug was quantified by measuring the free drug found in the supernatant of the prepared drug-loaded nanoparticles, using a UV spectrophotometer. Using the amount of unloaded drug, the drug-loaded quantity was determined (Total drug added (μg)—free drug). The encapsulation efficiency was then calculated using the amount of drug loaded into the nanoparticles: amount of drug loaded (μg)/theoretical maximum drug loading (μg) [8].

2.4. Purification of PEI-Enhanced HSA Nanoparticles. PEI-coated HSA nanoparticles were ultracentrifuged (16500 g) for 12 min and added to 10 mM NaCl (aq) by vortexing and ultrasonication (Branson 2510). This method was repeated thrice to ensure complete removal of impurities.

2.5. Determining Particle Size and Surface Zeta Potential. The particle size and zeta potential were measured by electrophoretic laser Doppler anemometry, using a zeta potential analyzer (Brookhaven Instruments Corporation, USA). The nanoparticles were diluted 1 : 15 with distilled water prior to measurement [27].

2.6. Surface Characterization of PEI-Enhanced HSA Nanoparticles. The size and shape of the HSA nanoparticles were observed by transmission electron microscopy (TEM), using Philips CM200 200 kV TEM (Markham, Canada). The samples for TEM were prepared by ultracentrifuging the nanoparticles and washing with distilled water, followed by air drying the samples overnight to allow removal of moisture [22, 27, 29].

2.7. Transfection of MCF-7 Breast Cancer Cells with PEI-Enhanced HSA Nanoparticles. Prior to transfecting cells with nanoparticles, cells were washed with PBS and replenished with fresh serum-free DMEM. The PEI-coated HSA nanoparticles were prepared using 5% of Rhodamine-tagged HSA. The nanoparticles were purified and added to the cells. After 8 hrs of incubation of cells at 37°C with the nanoparticles, the culture medium was replaced with fresh DMEM, containing 10% FBS. Under the fluorescence microscope (TE2000-U, Nikon; USA), pictures were taken to assess the levels of transfection. The percentage of transfected cells was calculated by using the average of the number of cells exhibiting fluorescence under five different fields of view.

2.8. Cell Viability Assay. The number of surviving cells was assessed using the Promega Cell-Titer 96 AQueous Non-Radioactive Cell Proliferation MTS Assay kit. 3-(4,5-dimethylthiazol-2-yl)-5-(3-carboxymethoxyphenyl)-2-(4-sulfophenyl)-2H-tetrazolium, (MTS), and phenazine methosulfate reagents were used. Live cells reduce MTS to form formazan, a compound soluble in tissue-culture media. The amount of formazan is proportional to the number of living cells and can be quantified by measuring the absorbance of formazan, using 1420-040 Victor3 Multilabel Counter (Perkin Elmer, USA) at 490 nm. The intensity of the color produced by formazan indicates the viability of cells. MCF-7 cells were seeded onto a 96-well plate (10^4 cells per well) 24 hrs before treatment. Cytotoxicity was measured at the predetermined time for each experiment using the MTS assay which was performed as per the manufacturer's protocol.

2.9. TUNEL Assay. The DeadEnd Colorimetric TUNEL System detects DNA fragmentation (an indicator of apoptosis) of each cell undergoing apoptosis. The fragmented ends of DNA are labelled by a modified TUNEL (TdT-mediated dUTP Nick-End Labeling) assay. The terminal deoxynucleotidyl transferase (TdT) enzyme adds a biotinylated nucleotide at the 3′-OH ends of DNA; the biotinylated nucleotides are conjugated with horseradish-peroxidase-labelled streptavidin. The peroxidase is then detected using its substrate, hydrogen peroxide, and the chromogen, diaminobenzidine (DAB). Following the manufacturer's protocol, the nuclei of apoptotic cells are stained brown.

3. Results and Discussion

3.1. Optimizing Coating of Cationic DOX-Loaded PEI-Enhanced HSA Nanoparticles. The desolvation technique used to prepare the HSA nanoparticles [22, 27, 30] is simple to perform; the synthesized particles were consistent in size, surface zeta potential, and morphology. The desolvation technique involves a liquid-liquid phase separation of an aqueous homogenous albumin solution, leading to the formation of a colloidal (or coacervate) phase that contains the nanoparticles [31]. In addition, the size of the nanoparticles formed by this technique can be altered based upon the various parameters of the technique, such as concentration and pH of HSA solution, volume and rate of ethanol addition [22, 29, 32]. In our previous research paper, we presented that the smallest nanoparticle size was achieved with 20 mg/mL HSA at pH 8.5 and ~1-2 mL of 100% ethanol [22]. These parameters were kept unchanged in this study as well. Glutaraldehyde cross-linking was carried out to stabilize the formed HSA nanoparticles before PEI surface coating; this also increases the drug entrapment ability of the HSA nanoparticles [3]. The encapsulation efficiency of DOX within PEI-enhanced HSA nanoparticles was calculated to be ~88.24 + 2.13%.

In the current study, PEI-enhanced HSA nanoparticles were prepared by coating the HSA nanoparticles that have a negative surface charge with electrostatic binding to the positively charged PEI. As HSA is an acidic protein, it carries a negative zeta potential in ~pH 8.5 and thus allows the positive PEI to bind to HSA nanoparticles [12, 33, 34]. The amount of PEI used for surface coating of the nanoparticles was optimized. Table 1 shows that as the amount of PEI was increased, an increase in the particle size

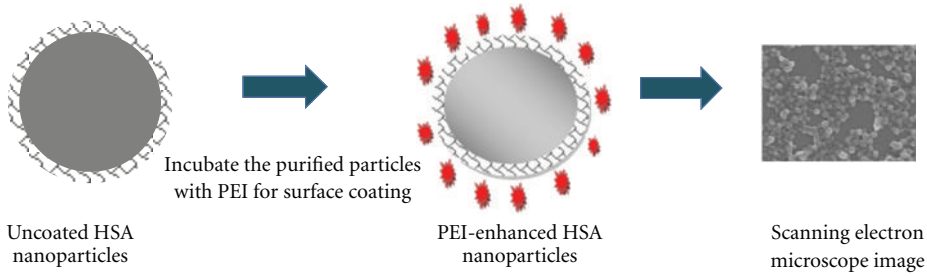

Figure 1: Formation of polyethylenimine- (PEI-) enhanced HSA nanoparticles.

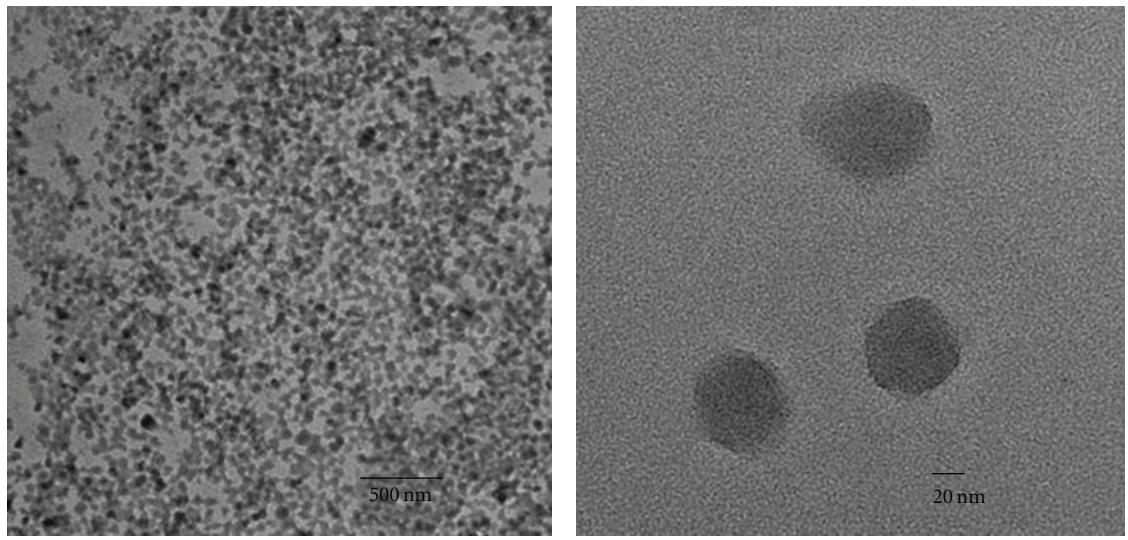

Figure 2: (a) Transmission electron microscope images of drug-loaded PEI-enhanced HSA nanoparticles. (b) Higher magnification image of the nanoparticles.

Table 1: Effect of the amount of PEI added (μg per mg of HSA) on the physical characteristics of drug-loaded PEI-enhanced HSA nanoparticles prepared at pH 8.5, 20 mg/mL HSA (mean ± S.D., $n = 3$).

Amount of PEI (μg) added per mg of HSA	Particle size (nm)	Zeta potential (mV)
0	99.63 ± 6.01	−46.9 ± 5.06
10	105.6 ± 8.07	+6.14 ± 1.11
20	121.7 ± 2.78	+12.3 ± 0.18
30	137.2 ± 8.20	+17.92 ± 1.04
40	135.5 ± 4.27	+18.38 ± 3.7

was observed, and the surface zeta potential became positive. This increase in size was gradual and could be attributed to the addition of the PEI surface coating or slight aggregation of the particles. The surface zeta potential increased from approximately −47 to +18 mV, clearly indicating that the PEI was successfully adsorbed to the nanoparticle surface. Furthermore, results presented in Table 2 show that 8 hrs of incubation at a stirring speed of 1000 rpm resulted in the smallest particle size and maximum zeta potential.

Table 2: Effect of incubation time for PEI coating and stirring speed during the desolvation step on the physical characteristics of drug-loaded PEI-enhanced HSA nanoparticles, prepared with 20 mg/mL HSA and 30 μg of PEI added per mg of HSA (mean ± S.D., $n = 3$).

Time of incubation with PEI (hrs)	Stirring speed (rpm)	Particle size (nm)	Zeta potential (mV)
4	250	412.76 ± 12.7	8.94 ± 0.12
	500	248.43 ± 1.7	7.20 ± 0.19
	1000	130.47 ± 11.3	4.24 ± 0.08
8	250	362.77 ± 0.65	17.4 ± 0.36
	500	218.57 ± 15.9	19.14 ± 0.51
	1000	100.73 ± 3.93	18.39 ± 0.27
12	250	332.67 ± 16.2	16.13 ± 0.91
	500	205.17 ± 8.16	10.99 ± 0.71
	1000	111.53 ± 4.72	13.73 ± 0.36

Conditions were optimized to attain the smallest particle size and maximum zeta potential in order to achieve the highest cellular uptake [19]. Size dependence of cellular uptake has

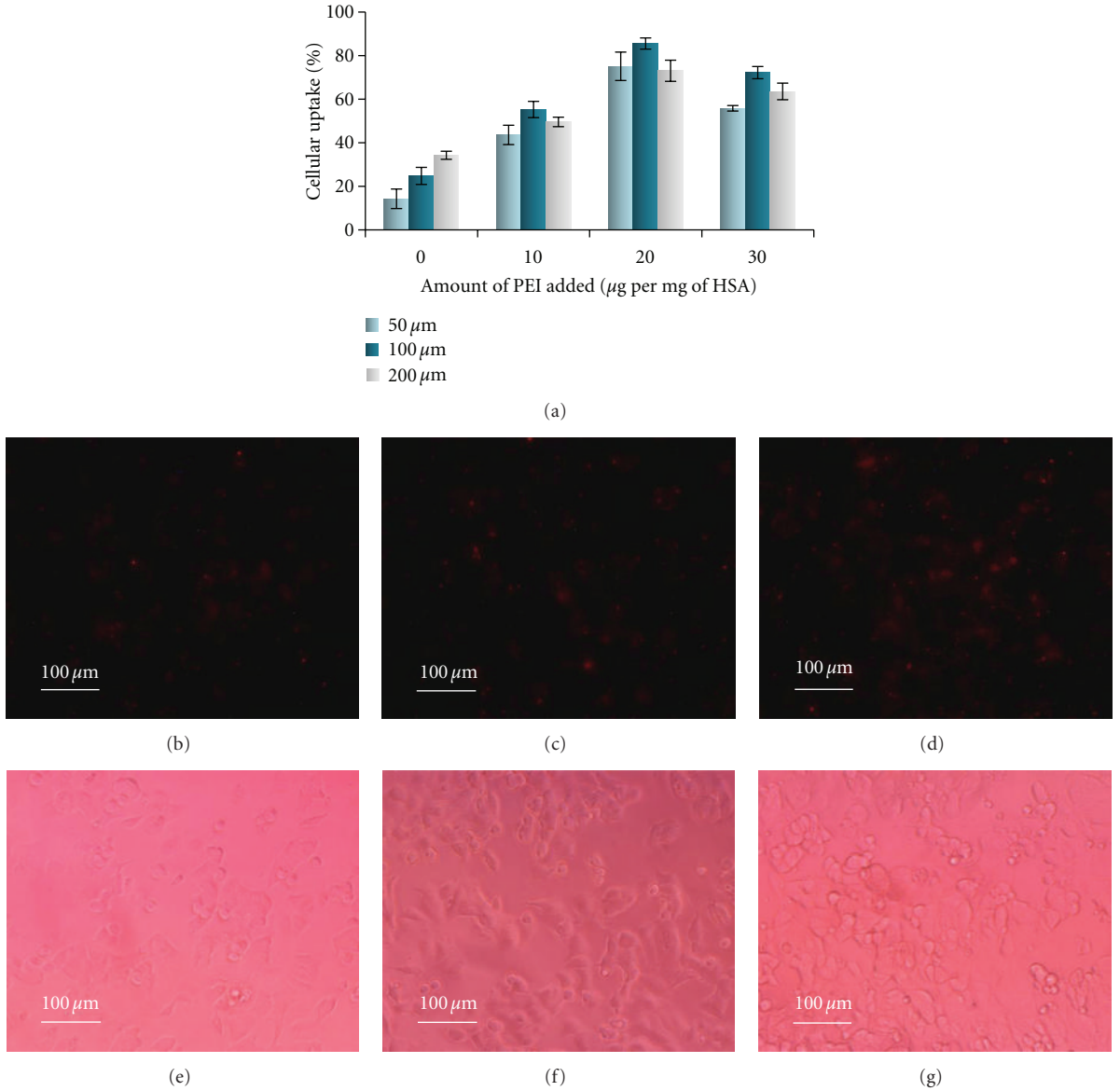

Figure 3: Cellular uptake of PEI-enhanced nanoparticles was assessed with respect to different amounts of PEI used for coating (mean ± S.D., $n = 3$). PEI-enhanced HSA nanoparticles were prepared using an ethanol desolvation technique with 20 mg/mL HSA. The nanoparticles were composed of 5% tetramethylrhodamine-conjugated BSA, and the cellular uptake was observed under a fluorescence microscope (TE2000-U, Nikon; USA). (a) Percentage of cellular uptake with nanoparticles prepared using 0, 10, 20, and 30 μg of PEI per mg of HSA. Varying quantities of nanoparticle preparations were added to the cells: 50, 100, and 200 μL. Fluorescence images of cellular uptake of different HSA nanoparticle preparations, consisting of tetramethylrhodamine-conjugated BSA, are shown; (b) uncoated HSA nanoparticles, (c) 10 μg and (d) 30 μg of PEI added per mg of HSA to form PEI-enhanced HSA nanoparticles. Corresponding bright field images are illustrated below (e, f, and g).

been studied previously [35]. For instance, Prabha et al. showed that smaller nanoparticles (~70 nm) experienced a 27-fold greater transfection than larger nanoparticles in COS-7 cell line, with all other parameters kept constant [35]. Similarly, surface charge of nanoparticles plays an important role in determining their transfection efficiency [19]. Harush-Frenkel et al. found that cationic nanoparticles resulted in rapid internalization through a clathrin-mediated pathway, while nanoparticles with a negative surface charge showed less efficient cellular uptake [36]. The TEM images shown in Figure 2 illustrate roughly spherical shape of the formed HSA nanoparticles of approximately 100 nm of size.

3.2. Increased Cellular Uptake of PEI-Enhanced HSA Nanoparticles. The cellular internalization of PEI-enhanced HSA nanoparticles was assessed by transfecting MCF-7 breast cancer cells with nanoparticles prepared with Rhodamine-tagged HSA. As shown in Figure 3, images were taken using

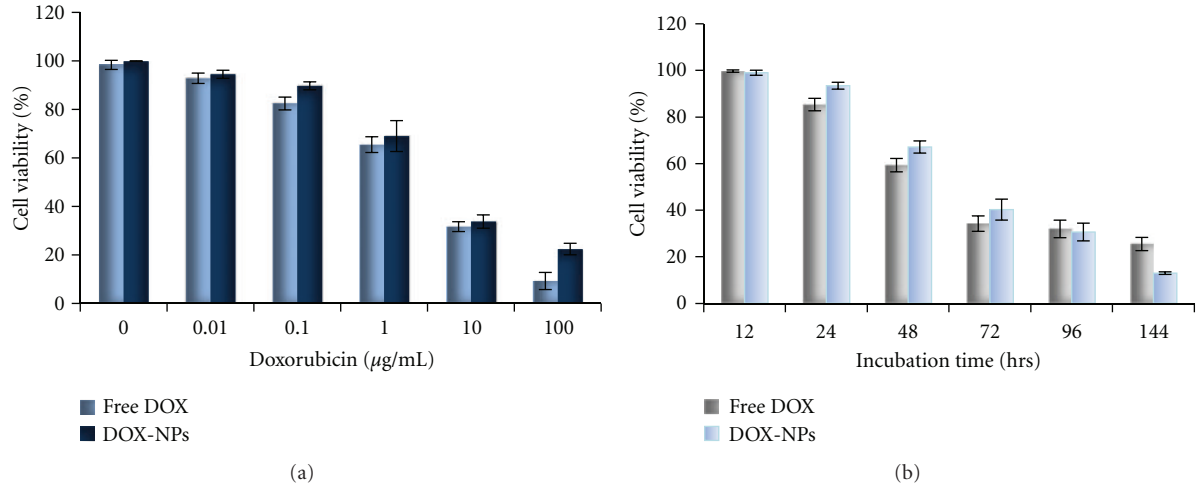

Figure 4: : (a) Dose-response cytotoxicity of DOX-loaded PEI-enhanced HSA nanoparticles as compared to free DOX administered to MCF-7 breast cancer cells in log-phase culture after 48 hrs of treatment with different concentrations of DOX. (b) Time of exposure: cytotoxicity resulting from DOX-loaded PEI-enhanced HSA nanoparticles versus free DOX over 96 hrs was measured. The concentration of DOX administered was 1 μg/mL to MCF-7 breast cancer cells. Percentage of viable cells was assessed by an MTS assay and then compared to untreated cells in the control wells (mean ± S.D., $n = 3$).

a fluorescence microscope (TE2000-U, Nikon; USA). Cell transfection was measured with respect to the amount of PEI added to coat the nanoparticles. It is essential to optimize the amount of PEI used for coating the nanoparticles as this helps determine how much of the polymer is required to reach the maximum adsorption capacity of the surface of the nanoparticles and their corresponding surface zeta potential. Firstly, the lowest percentage of cell transfection was observed with uncoated nanoparticles, which can be attributed to the negative surface zeta potential of the uncoated HSA nanoparticles. Based on Figure 3(a), it can be concluded that increasing the amount of PEI, up to 20 μg of PEI per mg of HSA, used for coating the nanoparticles leads to an increase in cell transfection. Further increasing the amount of PEI used for coating the nanoparticles did not translate into higher transfection efficiency. This observation could be explained by reaching the maximum capacity of PEI binding with the surface of HSA nanoparticles. Figures 3(b), 3(c), and 3(d) show corresponding fluorescence images of cellular uptake of PEI-enhanced HSA nanoparticles. The increase in cell transfection due to coating the nanoparticles with PEI is in agreement with previously published results. Cationic nanoparticles are shown to bind the negatively charged functional groups, such as sialic acid, found on cell surfaces and initiate transcytosis [19]. PEI-based nanoparticles have shown increased cellular uptake of siRNA. *In vivo* administration of siRNA delivered using PEI-based nanoparticles resulted in 80% decrease in the target gene expression; however, cytotoxicity was a concern [37, 38]. Therefore, a reasonable conclusion to draw from the results of the cell transfection experiment would be that the PEI adsorbed to the surface of the nanoparticles aids in the internalization of the particles.

3.3. DOX Delivery with PEI-Enhanced HSA Nanoparticles to Kill Breast Cancer Cells. The efficacy of anti-cancer chemotherapy is limited by the cytotoxic effect on healthy cells due to a lack of selectivity of the drugs and poor uptake of the therapeutics by the tumor cells [19, 39, 40]. Doxorubicin, a strong antineoplastic agent, has been shown to cause irreversible cardiomyopathy, which could also lead to congestive heart failure [1, 19, 40]. In order to overcome this issue, many researchers have tried delivering DOX by nanoparticles that reduce the amount of drug reaching cardiac tissue while increasing the accumulation of the drug-loaded nanoparticles in the tumor tissue [7, 9, 32, 41–43]. Furthermore, by incorporating a layer of PEI on the surface of the HSA nanoparticles, we aimed to increase their cellular uptake in the tumor tissue. Previously, uncoated HSA nanoparticles were studied for the delivery of DOX to neuroblastoma cell lines. Results suggested that DOX delivered using nanoparticles was more cytotoxic against cancer cells as compared to free DOX. In our study, we observed that the cytotoxicity of DOX-loaded nanoparticle and free DOX against MCF-7 breast cancer cells was about the same after 48 hrs as the DOX concentration was increased, shown in Figure 4(a). However, assessing the cytotoxicity at different time points in Figure 4(b) showed that DOX-loaded nanoparticles led to a greater decrease in cell viability as compared to free DOX after 144 hrs. This observation can be explained by the slow release of DOX from the nanoparticles. These results would be more effective *in vivo* as the free drug would diffuse out of the tumor tissue, while the nanoparticles would accumulate within the tumor tissue due to the EPR effect and release the drug over time. Images of treated cells after TUNEL staining in Figures 5(a), 5(b), and 5(c) confirm that the cytotoxic effect of DOX-loaded nanoparticles was comparable to free DOX. Figure 5(c) shows that the cells remained healthy and viable after the addition of PEI-enhanced HSA nanoparticles, suggesting that the nanoparticle formulation does not have cytotoxic effects.

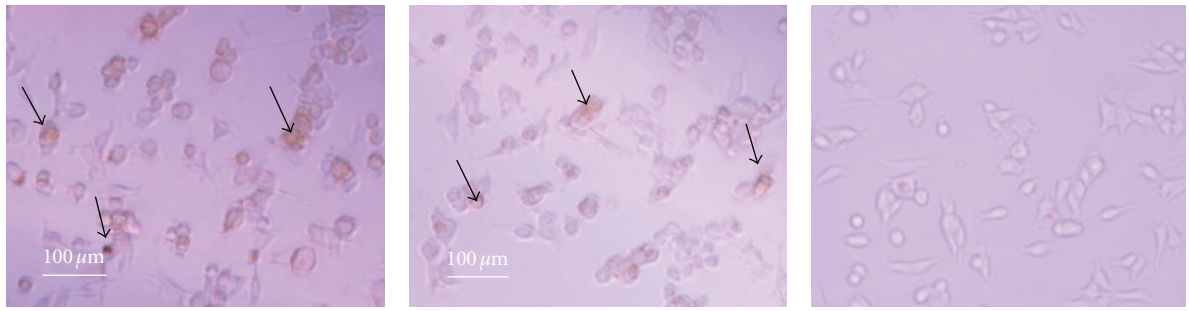

(a) DOX-NPs (b) Free DOX (c) Empty NPs

Figure 5: TUNEL assay to confirm cell death after DOX administration (24 hrs): (a) DOX-loaded PEI-enhanced HSA nanoparticles, (b) free DOX, and (c) empty PEI-enhanced HSA nanoparticles. The concentration of DOX administered was 1 μg/mL to MCF-7 breast cancer cells grown in a 96-well plate. The black arrows point towards cells showing TUNEL staining.

4. Conclusion

In our current study, we used modified HSA nanoparticles by adding an outer coating of the polyethylenimine (PEI) to improve the therapeutic index of doxorubicin against MCF-7 breast cancer cells. The nanoparticles prepared were characterized based upon size and surface charge with respect to the amount of PEI used for coating. A rise in the surface zeta potential of the nanoparticles confirms the electrostatic binding of PEI with the surface of HSA nanoparticles. Different microscopic techniques were employed to observe the shape, dispersion, and morphology of the nanoparticles. PEI-enhanced HSA nanoparticles resulted in a higher cell transfection percentage, indicating that the addition of the layer of cationic polymer did improve cell penetration of the particles. PEI-enhanced HSA nanoparticles illustrated a more potent cytotoxic effect on MCF-7 breast cancer cells over longer time duration. The results shown in this study are promising and set a platform for further examining the suitability of this PEI-enhanced delivery system *in vivo*.

Acknowledgments

This work is supported by a research Grant to S. Prakash from Canadian Institutes of Health Research (CIHR) (MOP 93641). S. Abbasi is supported by the McGill Faculty of Medicine Internal Studentship—G. G. Harris Fellowship and the Ontario-Quebec Exchange Fellowship. A. Paul acknowledges the financial support from NSERC Alexander Graham Bell Canada Graduate Scholarship**.** The authors are grateful for the assistance provided for TEM imaging by Dr. Xue-Dong Liu, McGill, Department of Physics.

References

[1] P. K. Singal and N. Iliskovic, "Doxorubicin-induced cardiomyopathy," *The New England Journal of Medicine*, vol. 339, no. 13, pp. 900–905, 1998.

[2] P. K. Singal, T. Li, D. Kumar, I. Danelisen, and N. Iliskovic, "Adriamycin-induced heart failure: mechanism and modulation," *Molecular and Cellular Biochemistry*, vol. 207, no. 1-2, pp. 77–85, 2000.

[3] S. Dreis, F. Rothweiler, M. Michaelis, J. Cinatl, J. Kreuter, and K. Langer, "Preparation, characterisation and maintenance of drug efficacy of doxorubicin-loaded human serum albumin (HSA) nanoparticles," *International Journal of Pharmaceutics*, vol. 341, no. 1-2, pp. 207–214, 2007.

[4] M. L. Hans and A. M. Lowman, "Biodegradable nanoparticles for drug delivery and targeting," *Current Opinion in Solid State and Materials Science*, vol. 6, no. 4, pp. 319–327, 2002.

[5] R. Seigneuric, L. Markey, D. S. A. Nuyten et al., "From nanotechnology to nanomedicine: applications to cancer research," *Current Molecular Medicine*, vol. 10, no. 7, pp. 640–652, 2010.

[6] A. E. Gulyaev, S. E. Gelperina, I. N. Skidan, A. S. Antropov, G. Y. Kivman, and J. Kreuter, "Significant transport of doxorubicin into the brain with polysorbate 80-coated nanoparticles," *Pharmaceutical Research*, vol. 16, no. 10, pp. 1564–1569, 1999.

[7] C. Cuvier, L. Roblot-Treupel, J. M. Millot et al., "Doxorubicin-loaded nanospheres bypass tumor cell multidrug resistance," *Biochemical Pharmacology*, vol. 44, no. 3, pp. 509–517, 1992.

[8] J. Park, P. M. Fong, J. Lu et al., "PEGylated PLGA nanoparticles for the improved delivery of doxorubicin," *Nanomedicine: Nanotechnology, Biology, and Medicine*, vol. 5, no. 4, pp. 410–418, 2009.

[9] K. A. Janes, M. P. Fresneau, A. Marazuela, A. Fabra, and M. J. Alonso, "Chitosan nanoparticles as delivery systems for doxorubicin," *Journal of Controlled Release*, vol. 73, no. 2-3, pp. 255–267, 2001.

[10] E. Leo, M. A. Vandelli, R. Cameroni, and F. Forni, "Doxorubicin-loaded gelatin nanoparticles stabilized by glutaraldehyde: involvement of the drug in the cross-linking process," *International Journal of Pharmaceutics*, vol. 155, no. 1, pp. 75–82, 1997.

[11] A. N. Lukyanov, T. A. Elbayoumi, A. R. Chakilam, and V. P. Torchilin, "Tumor-targeted liposomes: doxorubicin-loaded long-circulating liposomes modified with anti-cancer antibody," *Journal of Controlled Release*, vol. 100, no. 1, pp. 135–144, 2004.

[12] F. Kratz, "Albumin as a drug carrier: design of prodrugs, drug conjugates and nanoparticles," *Journal of Controlled Release*, vol. 132, no. 3, pp. 171–183, 2008.

[13] S. B. Feinstein, J. Cheirif, F. J. Ten Cate et al., "Safety and efficacy of a new transpulmonary ultrasound contrast agent: initial multicenter clinical results," *Journal of the American College of Cardiology*, vol. 16, no. 2, pp. 316–324, 1990.

[14] N. K. Ibrahim, N. Desai, S. Legha et al., "Phase I and pharmacokinetic study of ABI-007, a Cremophor-free, protein-stabilized, nanoparticle formulation of paclitaxel," *Clinical Cancer Research*, vol. 8, no. 5, pp. 1038–1044, 2002.

[15] H. Maeda, J. Wu, T. Sawa, Y. Matsumura, and K. Hori, "Tumor vascular permeability and the EPR effect in macromolecular therapeutics: a review," *Journal of Controlled Release*, vol. 65, no. 1-2, pp. 271–284, 2000.

[16] H. Maeda, "Tumor-selective delivery of macromolecular drugs via the EPR effect: background and future prospects," *Bioconjugate Chemistry*, vol. 21, no. 5, pp. 797–802, 2010.

[17] Y. J. Son, J. S. Jang, Y. W. Cho et al., "Biodistribution and anti-tumor efficacy of doxorubicin loaded glycol-chitosan nanoaggregates by EPR effect," *Journal of Controlled Release*, vol. 91, no. 1-2, pp. 135–145, 2003.

[18] N. Desai, V. Trieu, Z. Yao et al., "Increased antitumor activity, intratumor paclitaxel concentrations, and endothelial cell transport of cremophor-free, albumin-bound paclitaxel, ABI-007, compared with cremophor-based paclitaxel," *Clinical Cancer Research*, vol. 12, no. 4, pp. 1317–1324, 2006.

[19] A. Verma and F. Stellacci, "Effect of surface properties on nanoparticle-cell interactions," *Small*, vol. 6, no. 1, pp. 12–21, 2010.

[20] J. Cho and F. Caruso, "Investigation of the interactions between ligand-stabilized gold nanoparticles and polyelectrolyte multilayer films," *Chemistry of Materials*, vol. 17, no. 17, pp. 4547–4553, 2005.

[21] A. Kichler, "Gene transfer with modified polyethylenimines," *Journal of Gene Medicine*, vol. 6, no. 1, pp. S3–S10, 2004.

[22] S. Abbasi, A. Paul, and S. Prakash, "Investigation of siRNA-loaded polyethylenimine-coated human serum albumin nanoparticle complexes for the treatment of breast cancer," *Cell Biochemistry and Biophysics*. In press.

[23] S. Segura, S. Espuelas, M. J. Renedo, and J. M. Irache, "Potential of albumin nanoparticles as carriers for interferon gamma," *Drug Development and Industrial Pharmacy*, vol. 31, no. 3, pp. 271–280, 2005.

[24] G. Wang, K. Siggers, S. Zhang et al., "Preparation of BMP-2 containing bovine serum albumin (BSA) nanoparticles stabilized by polymer coating," *Pharmaceutical Research*, vol. 25, no. 12, pp. 2896–2909, 2008.

[25] S. Zhang, G. Wang, X. Lin et al., "Polyethylenimine-coated albumin nanoparticles for BMP-2 delivery," *Biotechnology Progress*, vol. 24, no. 4, pp. 945–956, 2008.

[26] S. Zhang, M. R. Doschak, and H. Uludağ, "Pharmacokinetics and bone formation by BMP-2 entrapped in polyethylenimine-coated albumin nanoparticles," *Biomaterials*, vol. 30, no. 28, pp. 5143–5155, 2009.

[27] S. Sebak, M. Mirzaei, M. Malhotra, A. Kulamarva, and S. Prakash, "Human serum albumin nanoparticles as an efficient noscapine drug delivery system for potential use in breast cancer: preparation and in vitro analysis," *International Journal of Nanomedicine*, vol. 5, no. 1, pp. 525–532, 2010.

[28] C. Weber, J. Kreuter, and K. Langer, "Desolvation process and surface characteristics of HSA-nanoparticles," *International Journal of Pharmaceutics*, vol. 196, no. 2, pp. 197–200, 2000.

[29] K. Langer, S. Balthasar, V. Vogel, N. Dinauer, H. Von Briesen, and D. Schubert, "Optimization of the preparation process for human serum albumin (HSA) nanoparticles," *International Journal of Pharmaceutics*, vol. 257, no. 1-2, pp. 169–180, 2003.

[30] A. Khan, A. Paul, S. Abbasi, and S. Prakash, "Mitotic and antiapoptotic effects of nanoparticles coencapsulating human VEGF and human angiopoietin 1 on vascular endothelial cells," *International Jounral of Nanomedicine*, vol. 6, no. 1, pp. 1069–1081, 2011.

[31] F. M. Menger and B. M. Sykes, "Anatomy of a coacervate," *Langmuir*, vol. 14, no. 15, pp. 4131–4137, 1998.

[32] W. Lin, A. G. Coombes, M. C. Davies, S. S. Davis, and L. Illum, "Preparation of sub-100 nm human serum albumin nanospheres using a pH-coacervation method," *Journal of Drug Targeting*, vol. 1, no. 3, pp. 237–243, 1993.

[33] H. D. Singh, G. Wang, H. Uludağ, and L. D. Unsworth, "Poly-L-lysine-coated albumin nanoparticles: stability, mechanism for increasing in vitro enzymatic resilience, and siRNA release characteristics," *Acta Biomaterialia*, vol. 6, no. 11, pp. 4277–4284, 2010.

[34] V. P. Torchilin, R. Rammohan, V. Weissig, and T. S. Levchenko, "TAT peptide on the surface of liposomes affords their efficient intracellular delivery even at low temperature and in the presence of metabolic inhibitors," *Proceedings of the National Academy of Sciences of the United States of America*, vol. 98, no. 15, pp. 8786–8791, 2001.

[35] S. Prabha, W. Z. Zhou, J. Panyam, and V. Labhasetwar, "Size-dependency of nanoparticle-mediated gene transfection: studies with fractionated nanoparticles," *International Journal of Pharmaceutics*, vol. 244, no. 1-2, pp. 105–115, 2002.

[36] O. Harush-Frenkel, E. Rozentur, S. Benita, and Y. Altschuler, "Surface charge of nanoparticles determines their endocytic and transcytotic pathway in polarized MDCK cells," *Biomacromolecules*, vol. 9, no. 2, pp. 435–443, 2008.

[37] A. C. Hunter, "Molecular hurdles in polyfectin design and mechanistic background to polycation induced cytotoxicity," *Advanced Drug Delivery Reviews*, vol. 58, no. 14, pp. 1523–1531, 2006.

[38] N. Tietze, J. Pelisek, A. Philipp et al., "Induction of apoptosis in murine neuroblastoma by systemic delivery of transferrin-shielded siRNA polyplexes for downregulation of Ran," *Oligonucleotides*, vol. 18, no. 2, pp. 161–174, 2008.

[39] K. L. Maughan, M. A. Lutterbie, and P. S. Ham, "Treatment of breast cancer," *American Family Physician*, vol. 81, no. 11, pp. 1339–1346, 2010.

[40] A. H. Partridge, H. J. Burstein, and E. P. Winer, "Side effects of chemotherapy and combined chemohormonal therapy in women with early-stage breast cancer," *Journal of the National Cancer Institute. Monographs*, no. 30, pp. 135–142, 2001.

[41] S. Bennis, C. Chapey, P. Couvreur, and J. Robert, "Enhanced cytotoxicity of doxorubicin encapsulated in polyisohexylcyanoacrylate nanospheres against multidrug-resistant tumour cells in culture," *European Journal of Cancer Part A*, vol. 30, no. 1, pp. 89–93, 1994.

[42] L. Brannon-Peppas and J. O. Blanchette, "Nanoparticle and targeted systems for cancer therapy," *Advanced Drug Delivery Reviews*, vol. 56, no. 11, pp. 1649–1659, 2004.

[43] R. Dhankhar, S. P. Vyas, A. K. Jain, S. Arora, G. Rath, and A. K. Goyal, "Advances in novel drug delivery strategies for breast cancer therapy," *Artificial Cells, Blood Substitutes, and Biotechnology*, vol. 38, no. 5, pp. 230–249, 2010.

Hindawi Publishing Corporation
Journal of Drug Delivery
Volume 2012, Article ID 837327, 10 pages
doi:10.1155/2012/837327

Review Article

Carbon Nanotubes in Cancer Therapy and Drug Delivery

Abdelbary M. A. Elhissi,[1] Waqar Ahmed,[2] Israr Ul Hassan,[3] Vinod. R. Dhanak,[4] and Antony D'Emanuele[1]

[1] *Institute of Nanotechnology and Bioengineering, School of Pharmacy and Biomedical Sciences, University of Central Lancashire, Preston PR1 2HE, UK*
[2] *Institute of Nanotechnology and Bioengineering, School of Computing, Engineering and Physical Sciences, University of Central Lancashire, Preston PR1 2HE, UK*
[3] *Mathematics and Sciences Unit, College of Art and Applied Sciences, Dhofar University, P.O. Box 2509, 211 Salalah, Oman*
[4] *Department of Physics, University of Liverpool, Liverpool L69 3BX, UK*

Correspondence should be addressed to Abdelbary M. A. Elhissi, aelhissi@uclan.ac.uk

Received 13 June 2011; Accepted 9 August 2011

Academic Editor: Rassoul Dinarvand

Carbon nanotubes (CNTs) have been introduced recently as a novel carrier system for both small and large therapeutic molecules. CNTs can be functionalized (i.e., surface engineered) with certain functional groups in order to manipulate their physical or biological properties. In addition to the ability of CNTs to act as carriers for a wide range of therapeutic molecules, their large surface area and possibility to manipulate their surfaces and physical dimensions have been exploited for use in the photothermal destruction of cancer cells. This paper paper will discuss the therapeutic applications of CNTs with a major focus on their applications for the treatment of cancer.

1. Introduction

The major aim of developing nanocarrier drug delivery systems is to enhance the therapeutic effect or reduce toxicity of therapeutically active materials. This is conventionally achieved using spherically shaped vesicle nanocarriers such as liposomes. Alternatively, carbon nanotubes (CNTs) are essentially cylindrical molecules made of carbon atoms. CNTs are graphene sheets rolled into a seamless cylinder that can be open ended or capped, having a high aspect ratio with diameters as small as 1 nm and a length of several micrometers. CNTs made from a single graphene sheet results in a single-walled nanotubes (SWNT) while several graphene sheets make up multiwalled carbon nanotubes (MWNTs) [1, 2] (Figure 1). Ever since their discovery in 1991 by Iijima [1], there has been intense interest in these allotropes of carbon due to their unique physical and chemical properties and potential applications in a wide range of fields, from electronic devices and sensors to nanocomposite materials of high strength and low weight. Pristine CNTs are not soluble. It was only after the development of strategies to functionalize these molecules with organic groups and render them soluble that opened the way to bioapplications of CNTs. Due to their high surface area, they are capable of adsorbing or conjugating with a wide variety of therapeutic molecules. Thus, CNTs can be surface engineered (i.e., functionalized) in order to enhance their dispersability in the aqueous phase or to provide the appropriate functional groups that can bind to the desired therapeutic material or the target tissue to elicit a therapeutic effect. CNTs might help the attached therapeutic molecule to penetrate through the target cell to treat diseases [3–6] and a recent example of CNTs with a variety of functional groups relevant to cancer therapy [7] is shown in Figure 2. Here, we provide an overview of the therapeutic applications of CNTs with a major focus on their use in the treatment of cancer.

2. Cellular Uptake of CNTs

The cellular uptake of CNTs has been confirmed in a range of studies but the mechanism of CNT penetration into cells is still not well understood. Because of their needle-like shapes,

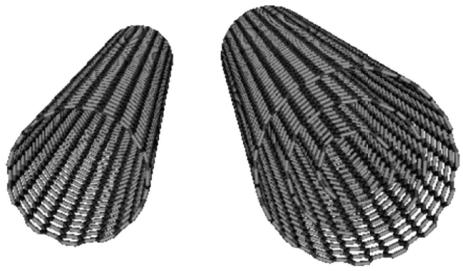

Figure 1: Carbon nanotubes (CNTs) are graphene sheets rolled into a cylindrical shape. Several sheets may roll into MWNTs whilst a single sheet rolls into a SWNT [2].

CNTs might be able to perforate cellular membrane and pass into the cellular components without causing apparent cell damage [3, 4, 8–11]. An *in vitro* CNTs nanoinjector system has been developed by Chen and coworkers [6]. The nanoinjector was designed using an atomic force microscope (AFM) tip and functionalized MWNTs attached to a model cargo compound via a disulfide linker. The MWNTs nanoinjector successfully transported into the cell where the disulfide bond was broken, resulting in the release of the cargo compound within the cytosol (Figure 3).

The perpendicular positioning of the nanotubes to the cell membranes suggests that uptake of CNTs was similar to that of nanoneedles which diffuse through cell membrane without causing cell death [5] (Figure 4). In a study conducted by Kam and coworkers [12], fluoreceinated protein attached to SWNTs-biotin was detected in the endosomes, suggesting that uptake of the nanotubes occurred via endocytosis. By contrast, no protein was internalized in the absence of the nanotubes. Using epifluorescence and confocal microscopy, functionalized CNTs labeled with a fluorescent agent have been shown to penetrate through the cell to the cytoplasm or the nucleus of fibroblasts [3]. In another study, it has been reported that the uptake mechanism of MWNTs is highly dependent on the length of nanotubes since those which are shorter than 1 μm were easier to internalize into cells and the process of cellular uptake was reported not to be via endocytosis [13].

3. CNTs as Carriers for Drugs, Genes, and Proteins

CNTs have been investigated as potential nanocarriers for the delivery of drugs, genes, and proteins. Most of the research on CNTs has focused on their potential for delivery of anticancer agents. This might be attributed to their unique needle-like shapes which enable them to be functionalized in order to adsorb or covalently link to a wide variety of therapeutic materials and internalize them into the target cell. Moreover, the well-established safety of vesicle-based carriers particularly liposomes has discouraged many researchers from investigating CNTs in the treatment of many diseases other than cancer.

3.1. CNTs as Carriers of Anticancer Molecules. It is well known that cancer cells overexpress folic acid (FA) receptors, and several research groups have designed nanocarriers with engineered surfaces to which FA derivatives can be attached. Moreover, nonspherical nanocarriers (e.g., CNTs) have been reported to be retained in the lymph nodes for longer periods of time compared to spherical nanocarriers [14] (e.g., liposomes). Thus, CNTs might be used for targeting lymph node cancers as shown by various investigators [15–17]. In these studies, magnetic nanoparticles containing the anticancer cisplatin were entrapped into folic-acid-functionalized MWNTs. An external magnet was employed to drag the nanotubes to the lymph nodes where the drug was shown to be released over several days and the tumor to be selectively inhibited. In a recent study, Yang et al. [18] have loaded the anticancer molecule gemcitabine into magnetic MWNTs and, using mice, they reported high activity against lymph node metastasis when the formulation was injected subcutaneously [18]. In another study, the poorly water-soluble anticancer camptothecin has been loaded into polyvinyl alcohol-functionalized MWNTs and reported to be potentially effective in treatment of breast and skin cancers [19].

Dhar and coworkers [20] have developed what they called the "longboat delivery system" (Figure 5). A complex of cisplatin and FA derivative was attached to a functionalized SWNT via a number of amide bonds to comprise the "longboat" which has been reported to be taken up by cancer cells via endocytosis, followed by the release of the drug and its subsequent interaction with the nuclear DNA. Another platinum anticancer, namely, carboplatin, after being incorporated into CNTs has been shown to inhibit the proliferation of urinary bladder cancer cells *in vitro*. In another study, anticancer effects have been shown to be dependent on the method used to entrap the drug in the CNTs, which highlighted the possible effects of preparation conditions on the therapeutic activity of therapeutic molecules associated with CNTs [21].

Paclitaxel is a poorly water-soluble anticancer molecule. In the commercialized paclitaxel product (Taxol), Cremophor EL is used to solubilise the drug. Unfortunately, Cremophor EL itself is toxic, which makes finding a suitable alternative a high priority. Moreover, the circulation time of Taxol is very short. Coating the nanocarriers (e.g., liposomes) with hydrophilic polymers such as polyethylene glycol (PEG) has been established as a strategy to prolong circulation of the nanocarrier-entrapped molecules in the blood by making the carrier highly evasive to uptake by the blood macrophages [22, 23]. PEGylation of paclitaxel increases the circulation time in the blood over Taxol [24]. Functionalized SWNTs were conjugated with paclitaxel through branched PEG chains via a cleavable ester bond. The resultant formulation was more effective in suppressing tumour growth *in vivo* than Taxol or paclitaxel-PEG conjugate in a 4T1 breast cancer animal model. The PEGylated nanotubes were able to prolong the circulation and greatly enhance cellular uptake of the drug by the cancer cells [25]. Similar findings of anticancer activity have been recently shown when paclitaxel was loaded into PEGylated SWNTs or MWNTs using HeLa cells

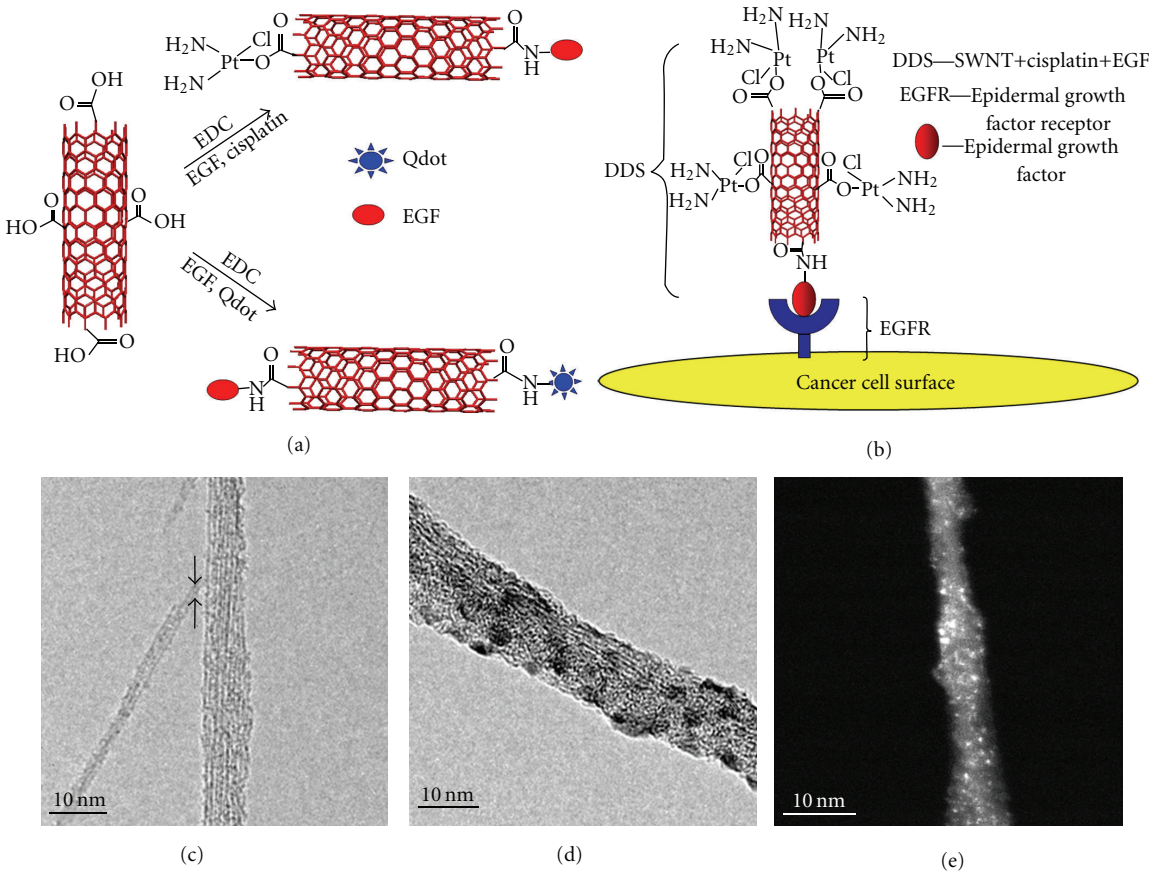

Figure 2: (a) Schematic representation of functionalization of SWNTs with quantum dots, EDC, and cisplatin; (b) SWNT bioconjugated with cisplatin and EGF, targeting cancer cell surface receptor EGFR; (c)–(e) TEM images showing the various functional groups, with cisplatin shown as bright spots [7].

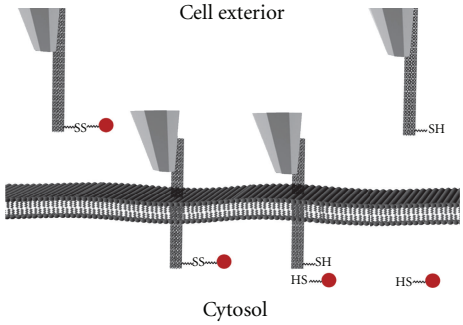

Figure 3: A schematic diagram showing that an AFM-controlled MWNT-based nanoinjector was able to penetrate into a cell and release the attached cargo compound after the breakage of the disulfide bond. This was followed by successful retraction of the nanoinjector with no apparent cell damage being produced [6].

and MCF-7 cancer cell lines [26]. Multidrug resistance is a significant obstacle to successful anticancer drug therapy since the P-glycoprotein efflux transporter can interfere with the accumulation of anticancer drugs in the target cells, resulting in reduced effectiveness of therapy [27, 28]. Recently, using hepatoma cell lines, PEGylated MWNTs have been

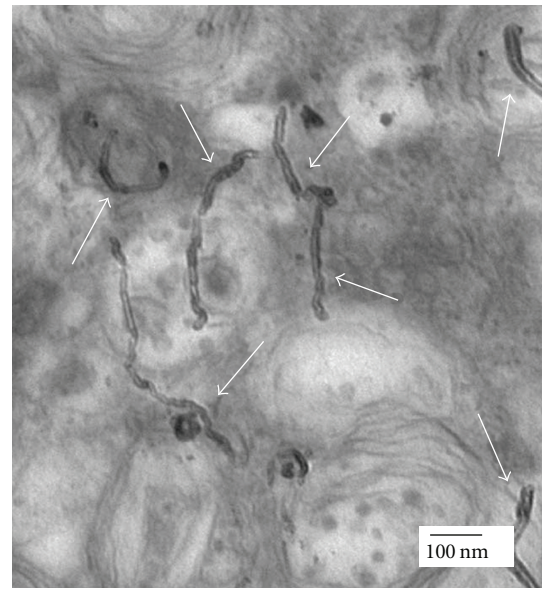

Figure 4: The perpendicular positioning of MWNTs (pointed at by the white arrows) during internalization into HeLa cells suggests that cellular uptake of CNTs by the cells was similar to that of nanoneedles [5].

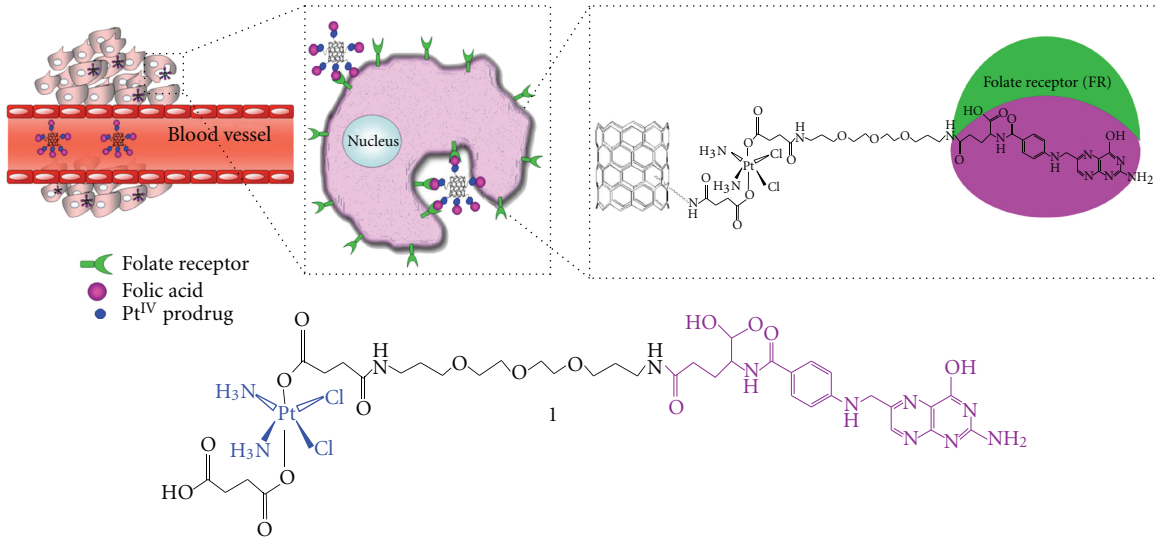

Figure 5: The "longboat" anticancer system in which the chemotherapeutic agent cisplatin is attached from one end to the FA derivative and from the opposite end to a SWNT via an amide link [20].

shown to accumulate in multidrug resistant cells as efficient as in nonresistant cells, as observed by confocal microscopy [29]. Interestingly, Liu and coworkers reported that although PEGylation of SWNTs can prolong blood circulation time of the associated anticancer molecule, it may cause an accumulation of the nanotubes in the dermal tissues of mice, suggesting that the degree of coating with PEG requires optimisation [30].

Similar to FA receptors, biotin receptors may be overexpressed on the surfaces of certain cancer cells. Therefore, biotin-functionalized SWNTs conjugated with the anticancer agent taxoid using a cleavable linker have been designed [31]. The drug was transported via endocytosis, released in the cell and interacted with microtubules as evaluated by flow cytometry. This resulted in the formation of a stable microtubule-taxoid complex and finally caused apoptosis and cell death (Figure 6).

A targeted delivery system of FA-tethered SWNTs-doxorubicin (DOX) has been designed. Bioadhesive polymers such as chitosan (CHI) and sodium alginate (ALG) were included to enhance the aqueous dispersability of the nanotubes while FA was used to improve the targeting properties of the nanotubes (Figure 7). Transmission electron microscopy (TEM) indicated that the drug was released after being transported into the tumor cell (HeLa cell) at the low pH of the lysosome [32] but not at the normal physiological pH of 7.4 (Figure 8). Recently, a novel approach has been introduced by covalently attaching PAMAM dendrimers to FA-treated MWNTs. Using this approach to deliver nanotubes, flow cytometry and confocal microscopy indicated possible targeting of cancer cells that overexpress FA receptors [33]. Li and coworkers (2011) have designed a novel system which was referred to as "dual-targeted drug nanocarrier" by conjugating MWNTs with iron nanoparticles and folate molecules. This system was efficiently loaded with doxorubicin and demonstrated superior delivery to HeLa cells when compared to free doxorubicin [34].

3.2. CNTs as Carriers of Immunoactive Compounds, Proteins, and Genetic Materials. The ability of macromolecules (e.g., genes) to cross the biological barriers and be expressed within a target cell is particularly challenging, owing to their hydrophilicity and large molecular size. Gene therapy aims to use genetic material to treat diseased cells by repairing the cause of the disease. Since genetic materials are poorly able to cross the biological membranes, the use of viral or nonviral vectors to carry the gene and internalize it into the cell is necessary. Nonviral vectors are less efficient than viral vectors [35] and short lived [36]; however, they are far safer [37, 38]. Pantarotto and coworkers have developed novel functionalized SWNT-DNA complexes and reported high DNA expression compared with naked DNA [4]. Generally, functionalized SWNTs have been suggested as suitable nonviral carriers of macromolecules and internalization of such macromolecules into living cells by CNTs has been reported to take place via energy-dependent endocytosis [39]. Confocal microscopy and flow cytometry have shown much greater fluorescent activity of protein and DNA when conjugated to SWNTs as compared to the naked macromolecules [40] indicating that CNTs are promising vectors for gene and protein. Cai and coworkers have introduced an approach to gene delivery named "carbon nanotube spearing" [10]. Plasmid DNA with a fluorescent protein were immobilized onto nickel-embedded CNTs. The formulation was "speared" into Bal 17 B lymphoma cells using a magnetic field, which produced high transfection in the target cells [10]. In another study, exposure of HeLa cells to DNA attached to SWNTs at 37°C resulted in gene internalization. However, at lower temperature (e.g., 4°C), no internalization took place (Figure 9), possibly because gene transport occurs by energy-dependent endocytosis [39].

A more recent strategy in gene therapy, namely, gene silencing, involves the use of small interfering RNA (siRNA). This approach has been shown efficient in the treatment of many diseases including various cancers. In cancer,

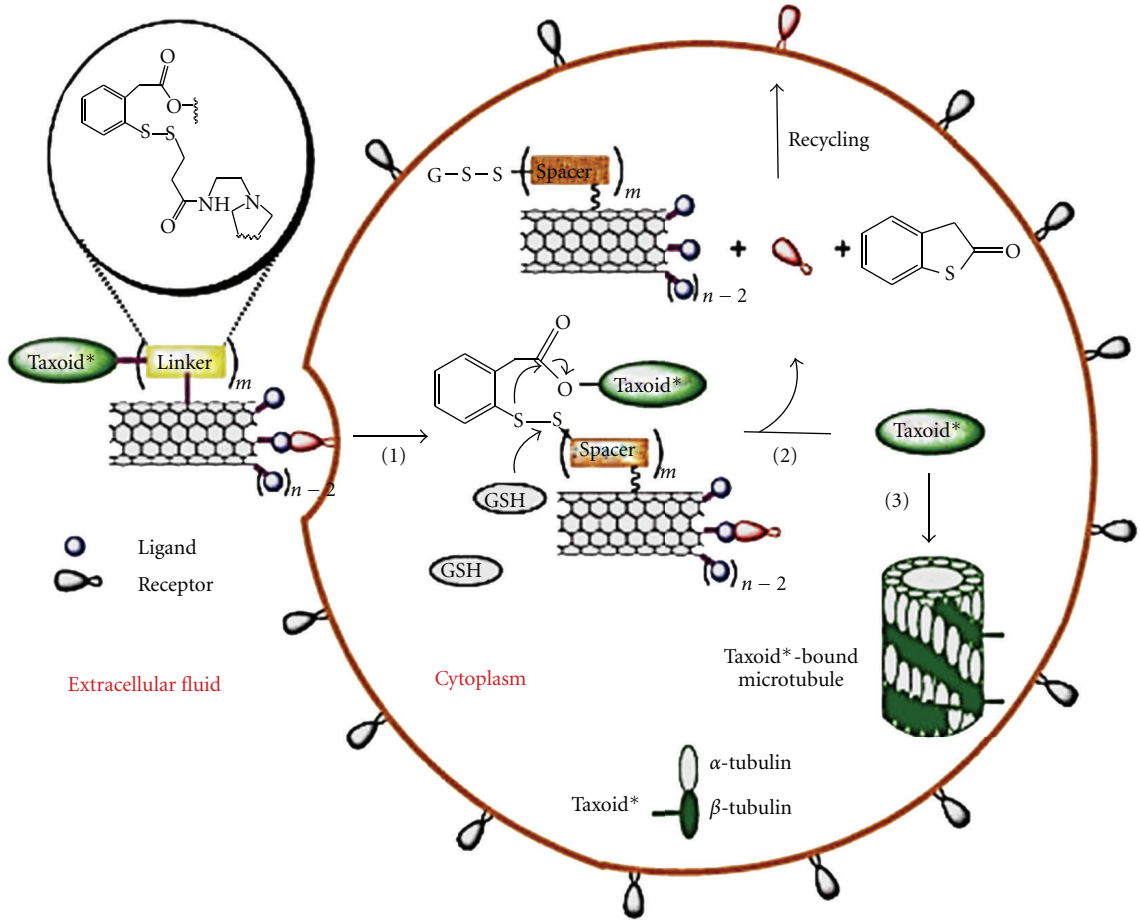

Figure 6: (1) Internalization of the CNTs carried conjugate into the tumour cell via receptor-mediated endocytosis. (2) Taxoid was released by the cleavage of the chemical linker. (3) The free taxoid molecules were bound to microtubules to form stabilized microtubules, resulting in arrest of cell mitosis and induction of apoptosis [31].

antitumor immunity might be inhibited by suppressors of cytokine signaling 1 (SOCS1). siRNA can be conjugated to phospholipid-functionalized SWNTs using a cleavable disulfide linker, resulting in efficient gene silencing and subsequent death of the targeted cell [9]. In a recent study, amino-functionalized MWNTs-siRNA complexes have shown successful suppression of tumor and prolonged survival in lung tumor of an animal model [41]. Many types of cancer (e.g., leukemia) can overexpress cyclinA(2), and suppression of this material is expected to prevent tumor growth. Functionalized SWNTs have been designed as carrier for siRNA for internalization into K562 cells and subsequent inhibition of the production of cyclinA(2) and treatment of chronic myelogenous leukemia. It has been found that suppression of cyclinA(2) expression using siRNA-CNTs can promote apoptosis in the targeted tumor [42]. Similar findings have been reported, for instance, functionalized SWNTs have been conjugated to telomerase reverse transcriptase (TERT) siRNA. The target gene was successfully silenced, and tumor growth was inhibited *in vitro* using murine tumor cell lines and *in vivo* using a mouse model [43]. In another study, CNTs cationically functionalized with polyethylene imines have been shown capable of complexing with siRNA and generating a silencing activity of up to 30% and cytotoxicity of up to 60% [44].

Streptavidin is a protein that has anticancer activity [45]; however, due to its very large molecular weight (approximately 60,000 Da), it does not penetrate through cells. Kam and coworkers [12] have used a conjugate of streptavidin with SWNTs-biotin, which resulted in internalization of the protein into model cancer cells by adsorption-mediated endocytosis. Transmission electron and confocal microscopy have shown that MWNTs can act as transporters of the recombinant ricin A chain protein, resulting in high death rates of cancer cells (e.g., up to 75% of HeLa cells were killed) [46].

Immunotherapy may be an alternative to gene therapy in the treatment of cancer. Antitumor immunotherapy using CNTs has been recently researched. Tumor-specific monoclonal antibodies, radiometal ion chelates, and fluorescent probe have been attached to SWNTs. Targeting the tumor (lymphoma) using a range of techniques has been reported to be successful [47]. MWNTs have been conjugated to tumour lysate protein as an antigen. This specifically increased the antitumor immune response [48].

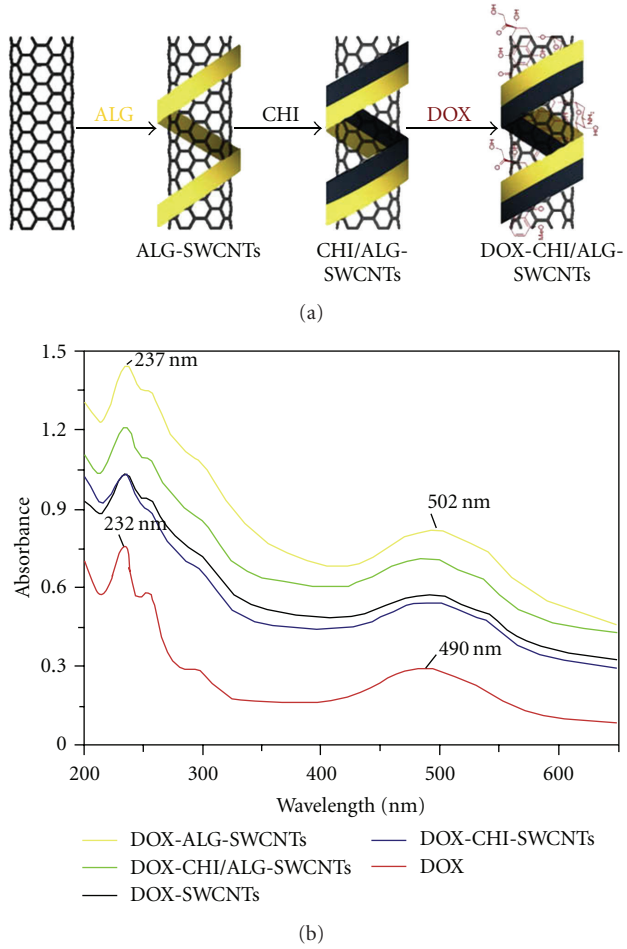

Figure 7: (a) Preparation of SWNTs-DOX after inclusion of bioadhesive polymers to enhance nanotubes dispersability in aqueous phase. (b) UV absorption spectra of DOX formulations [32].

Glioma is a brain tumor that is able to evade the host immune system, resulting in lack of benefit from conventional chemotherapy. This is because glioma cells secrete the immunosuppressive cytokines such as prostaglandins E and TGF-Beta and IL-10 [17, 49]. Macrophages have a preferential affinity towards CNTs when compared to glioma cells [50]. Using a GL261 murine intracranial glioma cancer model, VanHandel and coworkers [51] have developed an immunotherapy approach using MWNTs based on the fact that macrophages prefer to engulf CNTs compared with glioma cells. MWNTs caused an increase in the influx of macrophages into the glioma cells. This was reported to be accompanied by an increase in the levels of IL-10 expression, suggesting that immunomodulation using CNTs is a possible strategy to treat cancer.

Angiogenesis targeting antibodies E4G10 were attached to SWNTs via radiometal ion chelates. This formulation has been reported to reduce the volume of the tumor and prolong survival in animal models [52]. Moreover, oxidized MWNTs can be injected subcutaneously to a hepatocarcinoma-bearing animal to induce an immune response, which has been reported to retard tumor growth [53]. This suggests that CNTs themselves could possibly be surface-engineered to have anticancer activity by inducing an immune response against tumor.

A major obstacle to effective anticancer therapy is the multidrug resistance caused by enhanced efflux of anticancer drugs by the overexpressed p-glycoprotein, resulting in poor anticancer effect. Li and coworkers (2010) have shown that SWNTs can be functionalized with p-glycoprotein antibodies and loaded with the anticancer agent doxorubicin. Compared with free doxorubicin, this formulation demonstrated higher cytotoxicity by 2.4-fold against K562R leukemia cells [54].

3.3. Photothermal Therapy of Cancer Using CNTs. CNTs are able to absorb light in the near infrared (NIR) region, resulting in heating of the nanotubes [55]. This unique property of CNTs has been exploited as a method to kill cancer cells via thermal effects [39, 56–68].

Optical coupling of light with CNTs is predicted to be at highest when the length of the nanotubes is more than half the wave length of the incident light beam as determined by the antenna theory [66]. Engineering the structure of MWNTs by creating intentional surface defects might enhance the antenna properties of the nanotubes. Such engineered "defects" or dopants will cause scattering in the travelling currents and also increase the heating of the nanotube. This physicoelectronic characteristic of the engineered MWNTs can be employed to thermally destruct the tumor cells by using MWNTs that have good heat conducting properties. Examples of dopants include boron [67] and nitrogen [57] (N-doping). N-doped MWNTs have been shown to produce photoablative kill of model kidney cancer cells when NIR light was used. Moreover, the length of nanotubes has been found to be a major determinant of nanotube ability to transfer heat and kill the tumor with lengths between 700 and 1,100 nm being most desirable to kill the tumor [57] (Figure 10).

In a study conducted by Gannon and coworkers [56], SWNTs were functionalized using Kentera (a polyphenylene ethynylene-based polymer). The incubation of the nanotubes with hepatic tumor cells followed by application of radiofrequency field caused a concentration-dependent thermal destruction of the tumor cells which was demonstrated by development of apoptotic cells that caused complete necrosis of the tumor cells. By contrast, tumor cells that were injected with the Kentera alone (without CNTs) were viable after the application of the radiofrequency field. In the same study, it has been reported that *in vivo* injection of the Kentera-functionalized SWNTs was tolerated by rabbits [56]. Unfortunately, the resultant thermal destruction is not selective towards cancer cells and the access to deep tumor areas is generally poor, necessitating the inclusion of targeting moieties such as FA on the surfaces of CNTs [37]. Folate-bearing nanotubes having the size of 0.81 nm and a maximum absorbance at 980 nm were used for photothermal therapy of cancer [58]. The tumor cells were exposed to 980 nm laser radiations, resulting in photothermal destruction of cancer cells both *in vitro* and *in vivo*.

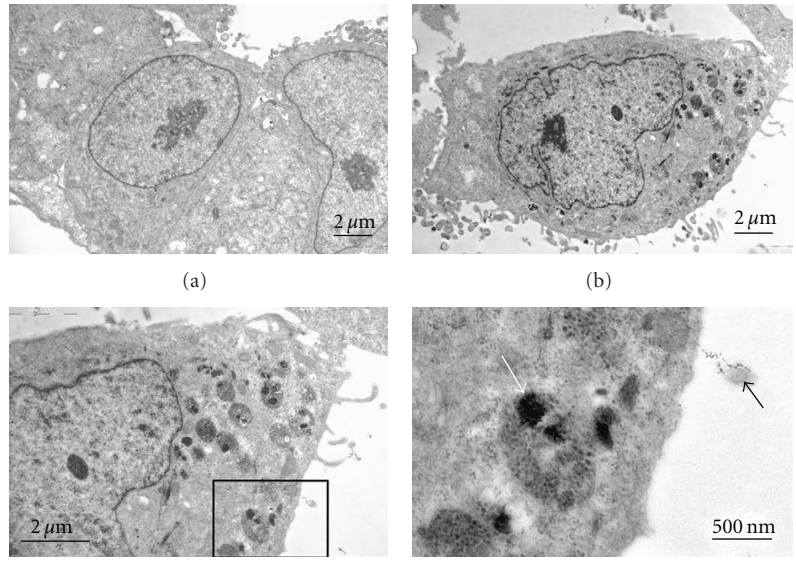

Figure 8: TEM showing the difference between HeLa cancer cells before treatment and after treatment with carbon nanotube formulations and the fate of the nanotubes: (a) HeLa cells before treatment, (b) HeLa cells treated with DOX-FA-CHI-ALG-SWNTs, (c) a magnified image of (b), and (d) magnified image of the boxed region in (c). The black arrow points at a SWNT-containing vesicle, and the white arrow points at some aggregated nanotubes inside a lysosome [32].

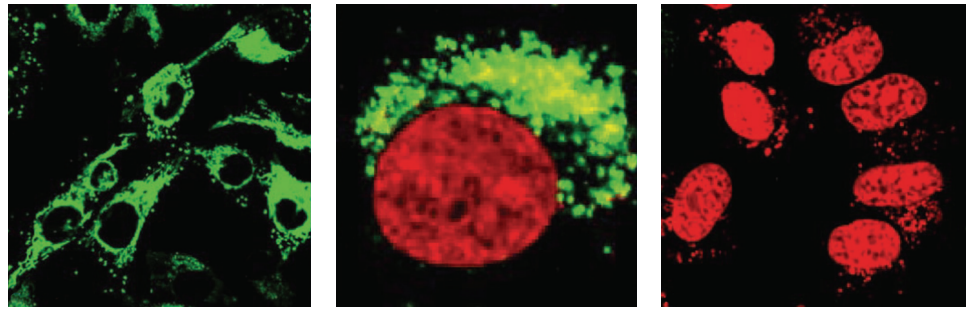

Figure 9: Confocal microscopy showing the internalization of labeled single strand DNA into Hela cell using SWNTs. (a) The labeled DNA (green colour) is surrounding the nucleus (black circles) at 37°C. (b) The nucleus stained using DRAQ5 (red color) is surrounded by the labeled DNA (green colour) after internalization at 37°C. (c) At 4°C, no DNA internalization has occurred [39].

3.4. CNTs for Other Therapeutic Applications. The use of CNTs has been expanding to include therapeutic applications other than cancer. For instance, surface-engineered CNTs may be able to capture pathogenic bacteria in liquid medium [69–71]. Thus, CNTs themselves might have antimicrobial activity since microorganisms may be adsorbed onto the engineered surfaces of CNTs. Moreover, using E. coli as a model microorganism, it has been reported that the electronic properties of SWNTs may regulate their antibacterial activity. The antibacterial effect was attributed to carbon-nanotube-induced oxidation of the intracellular antioxidant glutathione, resulting in increased oxidative stress on the bacterial cells and eventual death [72].

Functionalized CNTs have been demonstrated to be able to act as carriers for antimicrobial agents such as the antifungal amphotericin B [73, 74]. CNTs can attach covalently to amphotericin B and transport it into mammalian cells. This reduced the antifungal toxicity as compared to the toxicity of the free drug since 40% of the cells were killed by the CNTs-free formulation compared to no cell death by the CNTs formulation. It has also been reported that the antifungal activity was increased using the CNTs [73].

4. Conclusions

CNTs are promising needle-like carriers of both small drug molecules as well as macromolecules such as genes and proteins. CNTs can be functionalized so that certain molecules are attached to their surfaces via covalent or noncovalent bonding. The needle-like shape of the CNTs enables them to perforate cellular membranes and transport the carried therapeutic molecules to the cellular components. This process

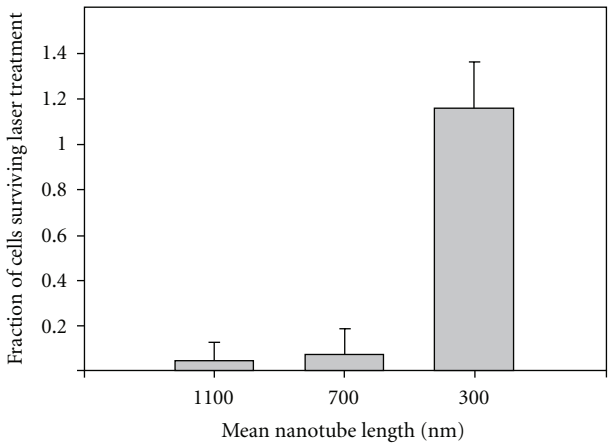

Figure 10: The relationship between cell survival and CNTs length using photothermal therapy. This has shown that nanotube lengths of 700 and 1100 nm are much more desirable in killing tumor cells compared with the length of 300 nm [57].

is thought to take place via endocytosis. CNTs have exclusive properties that would make them appropriate in the medical field such as their ability to adsorb pathogenic microorganisms and conduct heat. CNTs have been introduced to drug delivery research for a limited number of years and therefore extensive amounts of research is expected to be produced in the forthcoming years in order to explore their potential.

References

[1] S. Iijima, "Helical microtubules of graphitic carbon," *Nature*, vol. 354, no. 6348, pp. 56–58, 1991.

[2] http://www-ibmc.u-strasbg.fr/ict/vectorisation/nanotubes_eng.shtml.

[3] D. Pantarotto, J. P. Briand, M. Prato, and A. Bianco, "Translocation of bioactive peptides across cell membranes by carbon nanotubes," *Chemical Communications*, vol. 10, no. 1, pp. 16–17, 2004.

[4] D. Pantarotto, R. Singh, D. McCarthy et al., "Functionalized carbon nanotubes for plasmid DNA gene delivery," *Angewandte Chemie International Edition*, vol. 43, no. 39, pp. 5242–5246, 2004.

[5] A. Bianco, K. Kostarelos, and M. Prato, "Applications of carbon nanotubes in drug delivery," *Current Opinion in Chemical Biology*, vol. 9, no. 6, pp. 674–679, 2005.

[6] X. Chen, A. Kis, A. Zettl, and C. R. Bertozzi, "A cell nanoinjector based on carbon nanotubes," *Proceedings of the National Academy of Sciences of the United States of America*, vol. 104, no. 20, pp. 8218–8222, 2007.

[7] A. A. Bhirde, V. Patel, J. Gavard et al., "Targeted killing of cancer cells in vivo and in vitro with EGF-directed carbon nanotube-based drug delivery," *ACS Nano*, vol. 3, no. 2, pp. 307–316, 2009.

[8] N. W. S. Kam, Z. Liu, and H. Dai, "Carbon nanotubes as intracellular transporters for proteins and DNA: An investigation of the uptake mechanism and pathway," *Angewandte Chemie*, vol. 44, pp. 1–6, 2005.

[9] N. W. S. Kam, Z. Liu, and H. Dai, "Functionalization of carbon nanotubes via cleavable disulfide bonds for efficient intracellular delivery of siRNA and potent gene silencing," *Journal of the American Chemical Society*, vol. 127, no. 36, pp. 12492–12493, 2005.

[10] D. Cai, J. M. Mataraza, Z. H. Qin et al., "Highly efficient molecular delivery into mammalian cells using carbon nanotube spearing," *Nature Methods*, vol. 2, no. 6, pp. 449–454, 2005.

[11] C. Klumpp, K. Kostarelos, M. Prato, and A. Bianco, "Functionalized carbon nanotubes as emerging nanovectors for the delivery of therapeutics," *Biochimica et Biophysica Acta*, vol. 1758, no. 3, pp. 404–412, 2006.

[12] N. W. S. Kam, T. C. Jessop, P. A. Wender, and H. Dai, "Nanotube molecular transporters: internalization of carbon nanotube-protein conjugates into mammalian cells," *Journal of the American Chemical Society*, vol. 126, no. 22, pp. 6850–6851, 2004.

[13] V. Raffa, G. Ciofani, S. Nitodas et al., "Can the properties of carbon nanotubes influence their internalization by living cells?" *Carbon*, vol. 46, no. 12, pp. 1600–1610, 2008.

[14] S. T. Reddy, A. Rehor, H. G. Schmoekel, J. A. Hubbell, and M. A. Swartz, "In vivo targeting of dendritic cells in lymph nodes with poly(propylene sulfide) nanoparticles," *Journal of Controlled Release*, vol. 112, no. 1, pp. 26–34, 2006.

[15] F. Yang, D. L. Fu, J. Long, and Q. X. Ni, "Magnetic lymphatic targeting drug delivery system using carbon nanotubes," *Medical Hypotheses*, vol. 70, no. 4, pp. 765–767, 2008.

[16] F. Yang, J. Hu, D. Yang et al., "Pilot study of targeting magnetic carbon nanotubes to lymph nodes," *Nanomedicine*, vol. 4, no. 3, pp. 317–330, 2009.

[17] Y. Liu, K. Y. Ng, and K. O. Lillehei, "Cell-mediated immunotherapy: a new approach to the treatment of malignant glioma," *Cancer Control*, vol. 10, no. 2, pp. 138–147, 2003.

[18] F. Yang, C. Jin, D. Yang et al., "Magnetic functionalised carbon nanotubes as drug vehicles for cancer lymph node metastasis treatment," *European Journal of Cancer*, vol. 47, no. 12, pp. 1873–1882, 2011.

[19] N. G. Sahoo, H. Bao, Y. Pan et al., "Functionalized carbon nanomaterials as nanocarriers for loading and delivery of a poorly water-soluble anticancer drug: a comparative study," *Chemical Communications*, vol. 47, no. 18, pp. 5235–5237, 2011.

[20] S. Dhar, Z. Liu, J. Thomale, H. Dai, and S. J. Lippard, "Targeted single-wall carbon nanotube-mediated Pt(IV) prodrug delivery using folate as a homing device," *Journal of the American Chemical Society*, vol. 130, no. 34, pp. 11467–11476, 2008.

[21] S. Hampel, D. Kunze, D. Haase et al., "Carbon nanotubes filled with a chemotherapeutic agent: a nanocarrier mediates inhibition of tumor cell growth," *Nanomedicine*, vol. 3, no. 2, pp. 175–182, 2008.

[22] A. L. Klibanov, K. Maruyama, V. P. Torchilin, and L. Huang, "Amphipathic polyethyleneglycols effectively prolong the circulation time of liposomes," *FEBS Letters*, vol. 268, no. 1, pp. 235–237, 1990.

[23] T. M. Allen, T. Mehra, C. Hansen, and Y. C. Chin, "Stealth liposomes: an improved sustained release system for 1-β-D-arabinofuranosylcytosine," *Cancer Research*, vol. 52, no. 9, pp. 2431–2439, 1992.

[24] C. Li, D. Yu, T. Inoue et al., "Synthesis and evaluation of water-soluble polyethylene glycol-paclitaxel conjugate as a paclitaxel prodrug," *Anti-Cancer Drugs*, vol. 7, no. 6, pp. 642–648, 1996.

[25] Z. Liu, K. Chen, C. Davis et al., "Drug delivery with carbon nanotubes for in vivo cancer treatment," *Cancer Research*, vol. 68, no. 16, pp. 6652–6660, 2008.

[26] C. L. Lay, H. Q. Liu, H. R. Tan, and Y. Liu, "Delivery of paclitaxel by physically loading onto poly(ethylene glycol) (PEG)-graftcarbon nanotubes for potent cancer therapeutics," *Nanotechnology*, vol. 21, no. 6, Article ID 065101, 2010.

[27] J. Y.-W. Chan, A. C.-Y. Chu, and K.-P. Fung, "Inhibition of P-glycoprotein expression and reversal of drug resistance of human hepatoma HepG2 cells by multidrug resistance gene (mdr1) antisense RNA," *Life Sciences*, vol. 67, no. 17, pp. 2117–2124, 2000.

[28] S. S. Suri, H. Fenniri, and B. Singh, "Nanotechnology-based drug delivery systems," *Journal of Occupational Medicine and Toxicology*, vol. 2, no. 1, article 16, 2007.

[29] J. Cheng, M. J. Meziani, Y.-P. Sun, and S. H. Cheng, "Poly(ethylene glycol)-conjugated multi-walled carbon nanotubes as an efficient drug carrier for overcoming multidrug resistance," *Toxicology and Applied Pharmacology*, vol. 250, no. 2, pp. 184–193, 2011.

[30] X. Liu, H. Tao, K. Yang, S. Zhang, S.-T. Lee, and Z. Liu, "Optimization of surface chemistry on single-walled carbon nanotubes for in vivo photothermal ablation of tumors," *Biomaterials*, vol. 32, no. 1, pp. 144–151, 2011.

[31] J. Chen, S. Chen, X. Zhao, L. V. Kuznetsova, S. S. Wong, and I. Ojima, "Functionalized single-walled carbon nanotubes as rationally designed vehicles for tumor-targeted drug delivery," *Journal of the American Chemical Society*, vol. 130, no. 49, pp. 16778–16785, 2008.

[32] X. Zhang, L. Meng, Q. Lu, Z. Fei, and P. J. Dyson, "Targeted delivery and controlled release of doxorubicin to cancer cells using modified single wall carbon nanotubes," *Biomaterials*, vol. 30, no. 30, pp. 6041–6047, 2009.

[33] X. Shi, H. W. Su, M. Shen et al., "Multifunctional dendrimer-modified multiwalled carbon nanotubes: synthesis, characterization, and in vitro cancer cell targeting and imaging," *Biomacromolecules*, vol. 10, no. 7, pp. 1744–1750, 2009.

[34] R. Li, R. Wu, L. Zhao et al., "Folate and iron difunctionalized multiwall carbon nanotubes as dual-targeted drug nanocarrier to cancer cells," *Carbon*, vol. 49, no. 5, pp. 1797–1805, 2011.

[35] E. Fortunati, A. Bout, M. A. Zanta, D. Valerio, and M. Scarpa, "In vitro and in vivo gene transfer to pulmonary cells mediated by cationic liposomes," *Biochimica et Biophysica Acta*, vol. 1306, no. 1, pp. 55–62, 1996.

[36] T. Rochat and M. A. Morris, "Gene therapy for cystic fibrosis by means of aerosol," *Journal of Aerosol Medicine*, vol. 15, no. 2, pp. 229–235, 2002.

[37] F. D. Ledley, "Non-viral gene therapy," *Current Opinion in Biotechnology*, vol. 5, no. 6, pp. 626–636, 1994.

[38] C. Coutelle and R. Williamson, "Liposomes and viruses for gene therapy of cystic fibrosis," *Journal of Aerosol Medicine*, vol. 9, no. 1, pp. 79–88, 1996.

[39] N. W. S. Kam, M. O'Connell, J. A. Wisdom, and H. Dai, "Carbon nanotubes as multifunctional biological transporters and near-infrared agents for selective cancer cell destruction," *Proceedings of the National Academy of Sciences of the United States of America*, vol. 102, no. 33, pp. 11600–11605, 2005.

[40] N. W. S. Kam, Z. Liu, and H. Dai, "Carbon nanotubes as intracellular transporters for proteins and DNA: an investigation of the uptake mechanism and pathway," *Angewandte Chemie International Edition*, vol. 45, no. 4, pp. 577–581, 2006.

[41] J. E. Podesta, K. T. Al-Jamal, M. A. Herrero et al., "Antitumor activity and prolonged survival by carbon-nanotube-mediated therapeutic sirna silencing in a human lung xenograft model," *Small*, vol. 5, no. 10, pp. 1176–1185, 2009.

[42] X. Wang, J. Ren, and X. Qu, "Targeted RNA interference of cyclin A2 mediated by functionalized single-walled carbon nanotubes induces proliferation arrest and apoptosis in chronic myelogenous leukemia K562 cells," *ChemMedChem*, vol. 3, no. 6, pp. 940–945, 2008.

[43] Z. Zhang, X. Yang, Y. Zhang et al., "Delivery of telomerase reverse transcriptase small interfering RNA in complex with positively charged single-walled carbon nanotubes suppresses tumor growth," *Clinical Cancer Research*, vol. 12, no. 16, pp. 4933–4939, 2006.

[44] A. K. Varkouhi, S. Foillard, T. Lammers et al., "SiRNA delivery with functionalized carbon nanotubes," *International Journal of Pharmaceutics*, vol. 416, no. 2, pp. 419–425, 2011.

[45] S. L. Hussey and B. R. Peterson, "Efficient delivery of streptavidin to mammalian cells: clathrin-mediated endocytosis regulated by a synthetic ligand," *Journal of the American Chemical Society*, vol. 124, no. 22, pp. 6265–6273, 2002.

[46] X. Weng, M. Wang, J. Ge et al., "Carbon nanotubes as a protein toxin transporter for selective HER2-positive breast cancer cell destruction," *Molecular BioSystems*, vol. 5, no. 10, pp. 1224–1231, 2009.

[47] M. R. McDevitt, D. Chattopadhyay, B. J. Kappel et al., "Tumor targeting with antibody-functionalized, radiolabeled carbon nanotubes," *Journal of Nuclear Medicine*, vol. 48, no. 7, pp. 1180–1189, 2007.

[48] J. Meng, J. Duan, H. Kong et al., "Carbon nanotubes conjugated to tumor lysate protein enhance the efficacy of an antitumor immunotherapy," *Small*, vol. 4, no. 9, pp. 1364–1370, 2008.

[49] I. F. Parney, C. Hao, and K. C. Petruk, "Glioma immunology and immunotherapy," *Neurosurgery*, vol. 46, no. 4, pp. 778–792, 2000.

[50] B. Kateb, M. Van Handel, L. Zhang, M. J. Bronikowski, H. Manohara, and B. Badie, "Internalization of MWCNTs by microglia: possible application in immunotherapy of brain tumors," *NeuroImage*, vol. 37, no. 1, pp. S9–S17, 2007.

[51] M. VanHandel, D. Alizadeh, L. Zhang et al., "Selective uptake of multi-walled carbon nanotubes by tumor macrophages in a murine glioma model," *Journal of Neuroimmunology*, vol. 208, no. 1-2, pp. 3–9, 2009.

[52] A. Ruggiero, C. H. Villa, J. P. Holland et al., "Imaging and treating tumor vasculature with targeted radiolabeled carbon nanotubes," *International Journal of Nanomedicine*, vol. 5, no. 1, pp. 783–802, 2010.

[53] J. Meng, M. Yang, F. Jia et al., "Subcutaneous injection of water-soluble multi-walled carbon nanotubes in tumor-bearing mice boosts the host immune activity," *Nanotechnology*, vol. 21, no. 14, Article ID 145104, 2010.

[54] R. Li, R. Wu, L. Zhao, M. Wu, L. Yang, and H. Zou, "P-glycoprotein antibody functionalized carbon nanotube overcomes the multidrug resistance of human leukemia cells," *ACS Nano*, vol. 4, no. 3, pp. 1399–1408, 2010.

[55] M. E. Brennan, J. N. Coleman, A. Drury, B. Lahr, T. Kobayashi, and W. J. Blau, "Nonlinear photoluminescence from van Hove singularities in multiwalled carbon nanotubes," *Optics Letters*, vol. 28, no. 4, pp. 266–268, 2003.

[56] C. J. Gannon, P. Cherukuri, B. I. Yakobson et al., "Carbon nanotube-enhanced thermal destruction of cancer cells in a noninvasive radiofrequency field," *Cancer*, vol. 110, no. 12, pp. 2654–2665, 2007.

[57] S. V. Torti, F. Byrne, O. Whelan et al., "Photo-dynamic therapeutics based on CNx multi-walled nanotubes," *International Journal of Nanomedicine*, vol. 2, no. 4, pp. 707–714, 2007.

[58] F. Zhou, D. Xing, Z. Ou, B. Wu, D. E. Resasco, and W. R. Chen, "Cancer photothermal therapy in the near-infrared region by using single-walled carbon nanotubes," *Journal of Biomedical Optics*, vol. 14, no. 2, Article ID 021009, 2009.

[59] N. H. Levi-Polyachenko, E. J. Merkel, B. T. Jones, D. L. Carroll, and J. H. Stewart, "Rapid photothermal intracellular drug delivery using multiwalled carbon nanotubes," *Molecular Pharmaceutics*, vol. 6, no. 4, pp. 1092–1099, 2009.

[60] C.-H. Wang, Y.-J. Huang, C.-W. Chang, W.-M. Hsu, and C.-A. Peng, "Invitro photothermal destruction of neuroblastoma cells using carbon nanotubes conjugated with GD2 monoclonal antibody," *Nanotechnology*, vol. 20, no. 31, Article ID 315101, 2009.

[61] A. Burke, X. Ding, R. Singh et al., "Long-term survival following a single treatment of kidney tumors with multiwalled carbon nanotubes and near-infrared radiation," *Proceedings of the National Academy of Sciences of the United States of America*, vol. 106, no. 31, pp. 12897–12902, 2009.

[62] A. Burlaka, S. Lukin, S. Prylutska et al., "Hyperthermic effect of multi-walled carbon nanotubes stimulated with near infrared irradiation for anticancer therapy: in vitro studies," *Experimental Oncology*, vol. 32, no. 1, pp. 48–50, 2010.

[63] S. Ghosh, S. Dutta, E. Gomes et al., "Increased heating efficiency and selective thermal ablation of malignant tissue with DNA-encased multiwalled carbon nanotubes," *ACS Nano*, vol. 3, no. 9, pp. 2667–2673, 2009.

[64] Y. Xiao, X. Gao, O. Taratula et al., "Anti-HER2 IgY antibody-functionalized single-walled carbon nanotubes for detection and selective destruction of breast cancer cells," *BMC Cancer*, vol. 9, article 1471, p. 351, 2009.

[65] H. K. Moon, S. H. Lee, and H. C. Choi, "In vivo near-infrared mediated tumor destruction by photothermal effect of carbon nanotubes," *ACS Nano*, vol. 3, no. 11, pp. 3707–3713, 2009.

[66] N. Huang, H. Wang, J. Zhao, H. Lui, M. Korbelik, and H. Zeng, "Single-wall carbon nanotubes assisted photothermal cancer therapy: animal study with a murine model of squamous cell carcinoma," *Lasers in Surgery and Medicine*, vol. 42, no. 9, pp. 638–648, 2010.

[67] J. D. Jackson, *Classical Electrodynamics*, John Wiley & Sons, New York, NY, USA, 3rd edition, 1999.

[68] J. Xu, M. Xiao, R. Czerw, and D. L. Carroll, "Optical limiting and enhanced optical nonlinearity in boron-doped carbon nanotubes," *Chemical Physics Letters*, vol. 389, no. 4-6, pp. 247–250, 2004.

[69] L. Gu, T. Elkin, X. Jiang et al., "Single-walled carbon nanotubes displaying multivalent ligands for capturing pathogens," *Chemical Communications*, no. 7, pp. 874–876, 2005.

[70] A. S. Brady-Estévez, S. Kang, and M. Elimelech, "A single-walled-carbon-nanotube filter for removal of viral and bacterial pathogens," *Small*, vol. 4, no. 4, pp. 481–484, 2008.

[71] L. R. Arias and L. Yang, "Inactivation of bacterial pathogens by carbon nanotubes in suspensions," *Langmuir*, vol. 25, no. 5, pp. 3003–3012, 2009.

[72] C. D. Vecitis, K. R. Zodrow, S. Kang, and M. Elimelech, "Electronic-structure-dependent bacterial cytotoxicity of single-walled carbon nanotubes," *ACS Nano*, vol. 4, no. 9, pp. 5471–5479, 2010.

[73] W. Wu, S. Wieckowski, G. Pastorin et al., "Targeted delivery of amphotericin B to cells by using functionalized carbon nanotubes," *Angewandte Chemie International Edition*, vol. 44, no. 39, pp. 6358–6362, 2005.

[74] M. Benincasa, S. Pacor, W. Wu, M. Prato, A. Bianco, and R. Gennaro, "Antifungal activity of amphotericin B conjugated to carbon nanotubes," *ACS Nano*, vol. 5, no. 1, pp. 199–208, 2011.

Hindawi Publishing Corporation
Journal of Drug Delivery
Volume 2012, Article ID 143524, 13 pages
doi:10.1155/2012/143524

Research Article

Glucan Particles for Macrophage Targeted Delivery of Nanoparticles

Ernesto R. Soto, Abaigeal C. Caras, Lindsey C. Kut, Melissa K. Castle, and Gary R. Ostroff

Program in Molecular Medicine, University of Massachusetts Medical School, 373 Plantation Street, Worcester, MA 01605, USA

Correspondence should be addressed to Gary R. Ostroff, gary.ostroff@umassmed.edu

Received 1 June 2011; Revised 20 July 2011; Accepted 20 July 2011

Academic Editor: Rassoul Dinarvand

Glucan particles (GPs) are hollow, porous 2–4 μm microspheres derived from the cell walls of Baker's yeast (*Saccharomyces cerevisiae*). The 1,3-β-glucan outer shell provides for receptor-mediated uptake by phagocytic cells expressing β-glucan receptors. GPs have been used for macrophage-targeted delivery of soluble payloads (DNA, siRNA, protein, and small molecules) encapsulated inside the hollow GPs via core polyplex and layer-by-layer (LbL) synthetic strategies. In this communication, we report the incorporation of nanoparticles as cores inside GPs (GP-NP) or electrostatically bound to the surface of chemically derivatized GPs (NP-GP). GP nanoparticle formulations benefit from the drug encapsulation properties of NPs and the macrophage-targeting properties of GPs. GP nanoparticle formulations were synthesized using fluorescent anionic polystyrene nanoparticles allowing visualization and quantitation of NP binding and encapsulation. Mesoporous silica nanoparticles (MSNs) containing the chemotherapeutic doxorubicin (Dox) were bound to cationic GPs. Dox-MSN-GPs efficiently delivered Dox into GP phagocytic cells resulting in enhanced Dox-mediated growth arrest.

1. Introduction

The development of effective drug delivery systems presents multiple challenges, such as issues of drug solubility, targeting, *in vivo* stability and clearance, and toxicity. Nanotechnology-based drug delivery systems are a promising approach to fulfill the need for new delivery systems offering several advantages, such as high drug binding capacity due to their large surface area, improved solubility and bioavailability of hydrophobic drugs, extended drug half-life, improved therapeutic index, reduced immunogenicity, and the possibility for controlled release [1–3]. Nanoparticles can also be synthesized with control over average size, size distribution, and particle shape, all key factors related to cellular uptake mechanisms and improved penetration across biological barriers. Additionally, some nanoparticles offer the possibility for combined use as therapeutic and diagnostic/imaging tools. A new term, theranostics, has been recently proposed to describe these types of nanoparticles [4]. The successful development of nanoparticle-based delivery systems is exemplified by the use of nanomaterials for anticancer drug formulations [5, 6].

A primary challenge to realizing the full promise of nanoparticle-based drug delivery is the lack of optimal strategies to achieve selective and efficient cellular targeting. The mechanism of NP uptake is dependent on particle size and shape [7–9], and several competing uptake mechanisms result in undesired processes including off-target accumulation in other organs tissues and cells, rapid clearance from *in vivo* circulation (especially NPs less than 5 nm) [10, 11], opsonization and macrophage clearance [7, 12], and complement activation by proteins that results in hypersensitivity reactions [13]. NPs can be somewhat targeted by attaching ligands with specificity to receptors that are overexpressed in certain cells (i.e., folate and transferrin receptors in cancer cells [14–18]), or targeting cell populations with high selectivity by grafting specific targeting moieties to cell surface receptors known to be expressed only on target cells (i.e., antibodies to target prostate-specific membrane antigen (PSMA) [19] or galactose to target asialoglycoprotein

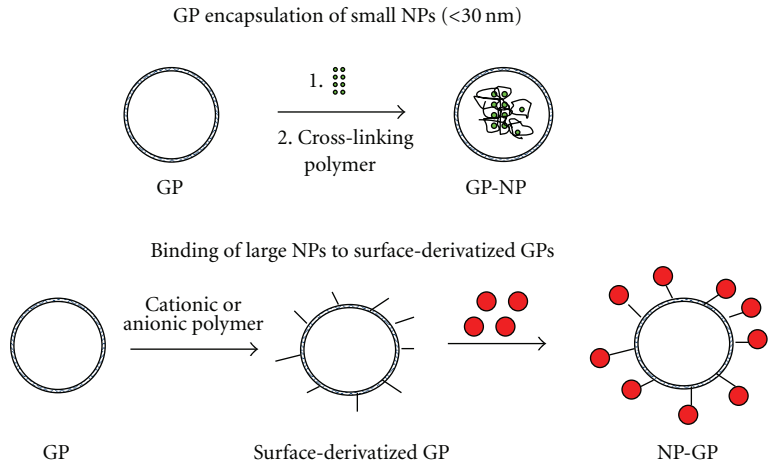

Figure 1: Schematic representation of glucan particle/nanoparticle synthesis strategies.

receptors on hepatocyte cells [20]). Some interfering processes can be reduced by coating of the nanoparticles with a hydrophilic polymer (i.e., PEG polymer brush or stealth nanoparticles). PEG is a nonimmunogenic, nontoxic, and protein-binding resistant polymer. PEG coating of nanoparticles prevents opsonization by shielding surface charges, reducing macrophage clearance, increasing steric repulsion of blood components, and increasing hydrophilicity and *in vivo* circulation of NPs [12, 21].

Glucan particles (GPs) are porous, hollow microspheres that are prepared from *Saccharomyces cerevisiae* (Baker's yeast). The glucan microspheres have an average diameter of 2–4 microns and are composed of 1,3-D-glucan and trace amounts of chitin. The 1,3-D-glucan polysaccharide on the GP surface serves as a ligand for receptor-mediated cell uptake by phagocytic cells bearing β-glucan receptors (dectin-1 (D1) receptor and complement receptor 3 (CR3)) [22], such as macrophages and dendritic cells in the immune system. GP uptake has been demonstrated to be dectin-1 dependent *in vitro* [23]. The ability to selectively target phagocytic cells makes the glucan particle an attractive drug delivery vehicle for this cell population. The hollow and porous material properties of GPs allow for the encapsulation, transport, delivery, and release of electrostatically bound payloads. Previously we have reported the use of GPs for macrophage-targeted delivery of soluble payload macromolecules (i.e., proteins [23], DNA [24], and siRNA [25, 26]), and small drug molecules, such as the antibiotic rifampicin [27]. However, the use of GPs for small drug molecule delivery is limited since the majority of small drug molecules are neutral, monovalent in charge, or insoluble in water, and such payloads are not easily trapped within glucan particles using the polyplex core or LbL encapsulation methods developed for nucleic acids and proteins.

We report here a new targeted-nanoparticle delivery application for glucan particles incorporating insoluble preformed nanoparticles (NPs) of less than 30 nm in diameter as cores inside glucan particles (GP-NP), or nanoparticles electrostatically bound to the surface of derivatized glucan particles (NP-GP) (Figure 1). The advantages of GP nanoparticle encapsulation include: (1) glucan receptor targeted delivery (2) the encapsulation of payload complexes that cannot be prepared *in situ* as the synthetic conditions are not compatible with glucan particles, (3) the loading of nanoparticles that can enhance the ability to load small drug molecules (neutral, hydrophobic drugs) into GPs, and (4) the incorporation of nanoparticles with an intrinsic property, such as magnetic nanoparticles, thus increasing the versatility of the particles, as the same formulation could be used for drug delivery and the magnetic properties employed for cell purification or imaging applications [28].

The development of GP nanoparticle-loaded formulations used two types of model nanoparticles: (1) fluorescent polystyrene nanoparticles of narrow size distribution to allow for the visualization and characterization by fluorescent techniques and (2) mesoporous silica nanoparticles (MSNs) for the encapsulation of the chemotherapeutic drug, doxorubicin to assess biological activity. MSNs are highly porous nanoparticles prepared from tetraethyl orthosilicate polymerized on a template such as a surfactant micelle [29, 30]. Since the discovery of MSNs in 1992, much work has been done to evaluate these materials for absorption, catalysis, chemical devices, and more recently as drug delivery agents (i.e., delivery of the cancer drugs camptothecin, paclitaxel, doxorubicin [31–33]). MSNs were chosen as a model nanoparticle because of their ease of synthesis, binding capacity for small drug molecules, and the possibility of extending the capabilities of GP-targeted drug delivery to hydrophobic drugs. We chose to study the delivery of doxorubicin (Dox) as a first step in the development of GP macrophage-targeted delivery of chemotherapeutics. Macrophages are nondividing differentiated cells and are resistant to the cytotoxic DNA replication inhibitor, doxorubicin. Macrophages are known to migrate into solid tumors, and we hypothesize that they will act as Trojan horses carrying lethal doses of Dox-GPs into tumors for targeted cancer drug delivery to rapidly dividing tumor cells.

2. Materials and Methods

2.1. Materials. Carboxylate-modified red fluorescent nanoparticles and Alamar blue were purchased from Invitrogen (Carlsbad, CA); glucan particles (GP) were prepared from Baker's yeast (Fleishmans Baker's yeast, AB Mauri Food Inc, Chesterfield MO, USA) according to a previously published procedure [24]. Polyethylenimines (PEIs, molecular weight of 1.2, 10, and 100 kDa) were purchased from Polysciences (Warrington, PA, USA). All other PEIs, chemicals for the synthesis of MSNs, and solvents were purchased from Sigma Aldrich (Allentown, PA, USA) and used as received. Materials for cell tissue culture experiments were purchased from Gibco Scientific (Grand Island, NY, USA) or Fisher Scientific (Fairlawn, NJ, USA).

2.2. Preparation of 20 nm Nanoparticle Cores Inside GPs. Fluorescent 20 nm nanoparticles were used at a concentration of 4.5×10^{15} particles/mL. Dry glucan particles were mixed with 5 μL nanoparticle suspension/mg GP to obtain a uniform paste, incubated at room temperature for 1 h, and the GP-NP-loaded formulation was lyophilized. This hydration-loading-lyophilization procedure was repeated using water (5 μL/mg GP) to hydraulically push nanoparticles into GPs by capillary action. The dry GP-NPs were hydrated and washed after the second lyophilization to remove free nanoparticles, sterilized in 70% ethanol at -20°C, aseptically washed three times with 0.9% saline, resuspended in 0.9% saline, counted with a hematocytometer, and GP concentration adjusted to a concentration of 1×10^8 particles/mL. Samples were evaluated by fluorescence microscopy, flow cytometry, zeta potential, and for GP-mediated uptake into phagocytic cells.

2.3. Synthesis of Cationic GPs. GPs (5 mg) were resuspended in 10 mLs of water by homogenization. Potassium periodate (0.4 mL of a 1 mg/mL solution) was added and the mixture stirred in the dark at room temperature for at least six hours. Oxidized GP samples were washed three times with water, and used immediately for reductive amination synthesis. Cationic polymers (PEIs) and water were added to the oxidized GP samples (1 μmol PEI/mg GP), and the particles were resuspended and mixed at room temperature overnight. The aminated samples were reduced with sodium borohydride (0.1 g) and incubated at room temperature for 48 hours. The reduced samples were washed with water. Tris buffer (5 mLs, pH 7.5, 0.05 M) was added and the sample incubated for 30 minutes. The samples were washed with water, resuspended in 70% ethanol, and stored overnight at -20°C for sterilization, then aseptically washed three times with 0.9% saline, resuspended in 0.9% saline, particles counted with a hematocytometer, and the particle suspensions diluted to a concentration of 1×10^8 particles/mL and stored at -20°C.

Periodate oxidized glucan particles ($n = 5$ samples) were evaluated for aldehyde content using a hydroxylamine hydrochloride assay [34]. Oxidized GP samples (5 mg) were incubated in 1 mL of DMSO at 50°C for 2 h to dissolve the particles. The samples were centrifuged to remove insoluble material (chitin). Hydroxylamine hydrochloride solution (0.5 mL, 0.5 N) containing 0.05% w/v methyl orange added to the samples, and the mixture was incubated at room temperature for 4 hours. The samples were titrated with a standardized 0.01 M sodium hydroxide solution until a red-to-yellow endpoint was achieved.

The level of PEI coupling in the PEI-GP samples was measured with a ninhydrin assay. PEI-GP samples (1 mg) were resuspended in 100 μL of water and mixed with 100 μL of 2% w/v ninhydrin in DMSO. The samples were heated at 100°C for 20 min, cooled to room temperature, and 800 μL of ethanol was added. PEI samples of different concentrations were also treated with ninhydrin to prepare calibration curves and determine the linear response range of each of the PEIs used in the chemical modification of GPs. Absorbance was measured at 570 nm for the calibration curve controls, PEI-GP samples, and blank GP controls. A total of three samples of each PEI-GP were analyzed with the ninhydrin assay.

2.4. Binding of Nanoparticles to Surface Derivatized GPs. GP or PEI-GP samples (10 μL 1×10^8 part/mL) and rhodamine labeled carboxylated nanoparticles of different diameter (20, 100 and 200 nm) were mixed at NP/GP ratios of 1/1, 10/1, and 100/1 in a final volume of 100 μL in 0.9% saline. The samples were incubated in the dark for 1 hour and the unbound nanoparticles separated from the GPs containing bound nanoparticles by centrifugation (10000 rpm for 2 min). The samples were then washed with 0.9% saline (100 μL) to remove unbound nanoparticles from the pellet, washed pellet samples resuspended in 0.9% saline (100 μL) and fluorescence of the carboxylate polystyrene nanoparticles (excitation = 580 nm, emission = 605 nm) measured in all fractions to quantify bound and unbound nanoparticles. The average of at least five measurements was collected for each experimental condition. NP-GP samples were also evaluated by zeta potential measurements, flow cytometry, and fluorescence microscopy. The NP-GP samples were tested for nanoparticle-binding stability to GPs by incubation in phosphate buffer saline (PBS, pH 7) containing 10% fetal bovine serum (FBS), or sodium acetate buffer (0.1 M, pH 5) over 48 hours. Samples were processed by centrifugation to remove free nanoparticles, washed and supernatant fractions analyzed for released cPS-NPs, and pelleted fractions evaluated by fluorescence microscopy to assess binding of cPS-NPs to GPs.

2.5. Mesoporous Silica Nanoparticles (MSNs). MSN samples containing phosphate and amine functional groups were prepared by the cocondensation method reported by Lu et al. [32, 33]. A solution containing cetyl trimethylammonium bromide (CTAB, 0.5 g) in water (24 mLs), and NaOH (2 M, 0.2 mL) was heated to 80°C and stirred vigorously until the solutes were dissolved. A solution containing the MSN reagents (tetraethylorthosilicate, TEOS (2.5 mLs) and amino-propyltriethoxysilane, APTS (12 μLs)) were then added and the mixture stirred at 80°C for 15 minutes. 3-Trihydroxysilylpropyl methylphosphonate (0.63 mL) was added and the solution was incubated for 2 hours at 80°C with stirring. The solution was cooled at room temperature and

then centrifuged (3,000 g for 20 minutes), washed with 50 mLs of methanol, and dried at room temperature. The CTAB was extracted from the MSN by refluxing the particles (850 mg) in an acidic methanol mixture (90 mLs of methanol and 5 mLs of 12.1 M HCl) for 24 hours. The particles were then washed three times with 50 mLs of methanol and left to dry overnight. MSN samples were characterized by dynamic light scattering (DLS) particle size measurements, and zeta potential.

2.6. Doxorubicin Binding to MSN. MSN suspensions and doxorubicin (0–2 μmol Dox/mg MSN) were incubated in 1 mL of DMSO overnight at room temperature. The samples were then centrifuged and the supernatant removed. The Dox-MSN pellets were lyophilized and washed three times with 1 mL of water to remove Dox bound on the outside of MSN. A total of five Dox-MSN samples were prepared for each Dox loading concentration. Dox-MSN samples were resuspended in sterile water at a concentration of 1 mg/mL and stored at -20°C. The amount of Dox bound to MSN was quantified by incubating 0.2 mg samples of Dox-MSN in methanol (1 mL) overnight at room temperature to completely extract Dox. Doxorubicin was quantified by fluorescence spectroscopy (excitation = 480 nm, emission = 550 nm).

2.7. Synthesis of Dox-MSN-PEI-GP. 25 k PEI-GPs, unmodified GPs (10 μL, 1×10^8 particles/mL), and Dox-MSN nanoparticles (10 μL, 5×10^{-5} to 5×10^{-2} mg Dox-MSN/mL) were mixed at a final volume of 100 μL in 0.9% saline. The concentration range of Dox-MSN allowed studying binding to PEI-GP at Dox-MSN/PEI-GP ratios from 0.0005 to 5 pg Dox-MSN/GP. The samples were incubated in the dark for 1 hour at room temperature and the unbound Dox-MSN separated from the PEI-GP or GPs-containing bound nanoparticles by centrifugation (10000 rpm for 2 min). Additional control samples containing only Dox-MSN were processed in the purification procedure. The samples were then washed with 0.9% saline (100 μL) to remove unbound nanoparticles from the pellet, washed pellet samples resuspended in 0.9% saline (100 μL), and fluorescence of doxorubicin measured in all fractions to quantify amount of bound and unbound Dox-MSN. The average of at least three measurements was collected for each experimental condition. Dox-MSN-PEI-GP and Dox-MSN-GP samples were also evaluated by zeta potential measurements, and fluorescence microscopy. The samples were evaluated for stability by incubation in phosphate buffer saline (PBS, pH 7) containing 10% fetal bovine serum (FBS), or sodium acetate buffer (0.1 M, pH 5) over 48 hours. At various time points, samples were processed by centrifugation to remove free nanoparticles, washed and supernatant fractions analyzed by fluorescence spectroscopy to quantify released Dox, and pellet fractions were analyzed by fluorescence microscopy to confirm stability of Dox-MSN-PEI-GP samples.

2.8. Dynamic Light Scattering (DLS) and Zeta Potential Measurements. Size and zeta potential of nanoparticle samples and zeta potential of GP/NP samples were determined with a Malvern Zetasizer Nano-ZS (Malvern Instruments, Worcestershire, UK). Solvents and buffers were filtered through 0.22 μm filters before sample preparation. A suspension of particles (1 mg/mL for nanoparticle samples, 2×10^6 particles/mL for GP samples) was diluted in 1 mL of 20 mM Hepes buffer, vortexed, and transferred to a 1 mL clear zeta potential cuvette (DTS1061, Malvern). Zeta potential was collected at 25°C from −150 to +150 mV. The results are the average three samples. For each sample a total of 30 measurements were collected and analyzed with the Dispersion Technology software 4.20 (Malvern) producing diagrams of zeta potential distribution versus total counts. DLS measurements were obtained from samples in the same zeta potential cells at 25°C. The average of 20 measurements/sample was collected in the size range from 1 nm to 10000 nm. The data were analyzed with the Dispersion Technology software producing histograms for particle size versus % intensity.

2.9. Flow Cytometry (FACS). FACS measurements were obtained using a Becton Dickinson FACSCalibur instrument (BD, Franklin Lakes, NJ, USA). Samples were prepared for FACS analysis by binding of 2×10^7 nanoparticles to 2×10^6 GP particles. The bound NP-GP samples were washed from unbound nanoparticles and resuspended at 2×10^6 GP/mL in PBS. Unmodified GPs were used as negative control and rhodamine-labeled GPs as the positive control. The particles were analyzed with an FL4 laser at 605 nm by collecting an average of 15000 measurements. Gating and analysis was performed using FlowJo 6.4.2 software.

2.10. Dox-MSN/GP Cell Delivery. Dox-MSN samples were prepared as described in Section 2.6. Dox-MSN samples were bound to 25 k PEI-GP or unmodified GP particles as described in Section 2.7. The samples were prepared by binding 0–5×10^{-4} mg Dox-MSN/1×10^6 PEI-GP or GPs, equivalent to 0–5 pg Dox-MSN/glucan particle. The amount of PEI-GP or GP particles was chosen to test for cell uptake at a 10 : 1 GP : cell ratio to maximize phagocytic cell uptake. Based on the binding of Dox to Dox-MSN, the Dox-MSN-PEI-GP samples contained 0–0.15 nmol Dox. Dox-MSN-free nanoparticles and soluble Dox (free Dox) were also evaluated in the same concentration range. These samples were evaluated for cellular uptake and Dox delivery using the NIH3T3-D1 cell line. This cell line was derived from the NIH3T3 fibroblast cell line by the integration of the dectin-1 gene to produce cells expressing the β-1,3-D-glucan receptor dectin-1 allowing for efficient GP phagocytosis [35, 36]. Samples were resuspended in complete DMEM medium (250 μL) and added to 24 well plates containing 1×10^5 cells in 0.5 mL complete DMEM medium. After incubation for 3 hours at 37°C under 5% CO_2, the cells were fixed with 1% formalin and observed microscopically for fluorescent Dox-MSN/PEI-GP phagocytosis. To determine the effects of Dox-MSN/PEI-GP, Dox-MSN, or free Dox on cell growth and viability, these samples were incubated for 3 hours with cells as described above, and the cell monolayers were washed in complete DMEM and incubated for an additional 48 hours. Alamar blue (50 μL) was added, the cells

incubated at 37°C for 2 hrs, and fluorescence was measured, excitation wavelength = 530 nm, emission wavelength = 590 nm. Fluorescent response is dependent on the reduction of the Alamar blue indicator by metabolically active cells and is an indicator of cell number and viability. Growth arrest was calculated from the fluorescence response of the sample wells relative to the response of control wells containing cells incubated in the absence of doxorubicin. The results are the average of four samples prepared for each Dox-MSN formulation evaluated for NIH3T3-D1 growth arrest.

3. Results and Discussion

Glucan particles have been used for macrophage-targeted delivery of a wide range of payload macromolecules [23–27]. Soluble payloads can be efficiently encapsulated inside GPs by both polyplex and layer-by-Layer (LbL) synthetic approaches. There is a growing interest to extend the use of the GP delivery technology for small drug molecules (i.e., chemotherapeutics and antibiotics). However, GPs have limitations in the encapsulation of small molecules as most of these molecules are neutral in charge and cannot be trapped by the noncovalent techniques used to assemble macromolecule polyplexes inside GPs. Also, hydrophobic drugs present a challenge for loading inside GPs. The combination of established nanoparticle encapsulation technologies and glucan particles offers an attractive opportunity to extend the use of GPs for macrophage-targeted delivery of small drug molecules. Here we present the results of model systems using polystyrene nanoparticles and mesoporous silica nanoparticles to demonstrate the GP-mediated small drug molecule delivery as GP-nanoparticle-drug formulations.

3.1. Use of Glucan Particles for Encapsulation or Surface Binding of Polystyrene (PS) Nanoparticles. Rhodamine-labeled carboxylate polystyrene nanoparticles (cPS-NPs) were used as a model system because of their uniform narrow size distribution, high fluorescent signal, and the ability to cross-link or bind carboxylate nanoparticles to the surface of cation-modified GPs through electrostatic interactions. cPS-NPs (20 nm in diameter) were used to prepare nanoparticle cores encapsulated within the hollow cavity of GPs. The freeze-thaw cycles during the nanoparticle-loading process caused nanoparticle aggregation trapping the cPS-NPs inside GPs. Additionally, the inclusion of a cationic polymer, like polyethylenimine (PEI) or chitosan, electrostatically cross-linked the aggregated nanoparticles inside GPs and slowed down their release. Figure 2 shows microscopic images of GP nanoparticle cores and receptor-targeted uptake by cells bearing glucan receptors. cPS-NPs were loaded at a concentration of 2.25×10^{13} nanoparticles/mg GP, and measurement of unbound cPS-NPs collected from washing the GP-cPS NP cores demonstrated that nanoparticle encapsulation efficiency was greater than 80%. The high cPS-NP encapsulation capacity in the hollow cavity in GPs results in the loading of >30,000, 20 nm cPS-NPs per glucan particle. However, there is a limit to the size of nanoparticles that can be encapsulated inside GPs because the average pore size in the shell of GPs is less than 40 nm. To overcome this size limitation, an alternative approach was devised to bind nanoparticles to the outer GP shell.

Table 1: PEI surface functionalization results and zeta potential values of GP and PEI-GPs.

GP sample	PEI surface functionalization results μmol PEI/mg GP	Zeta potential peak (±5 mV)
GP	—	2.4
1.2 k PEI-GP	0.012 ± 0.002	22.1
1.8 k PEI-GP	0.031 ± 0.021	21.7
10 k PEI-GP	0.015 ± 0.001	21.1
25 k PEI-GP	0.0136 ± 0.003	30.2
100 k PEI-GP	0.0192 ± 0.001	33.3

Cationic GPs were synthesized by functionalization of the GP surface with branched PEIs varying in molecular weight. The cationic PEI-GP library was prepared by reductive amination of oxidized glucan particles with PEI following similar procedures reported for other polysaccharides [37]. The 1,3-glycosidic bonds are stable to oxidation; thus oxidation of glucan particles takes place only at the reducing terminal glucose monomers (<2%) in the β-glucan structure of the particles. This limits the grafting of PEIs to ~0.12 μmol PEI/mg GP. The yield of periodate oxidation of the terminal glucose in the particles (60 ± 10%) was determined using a hydroxylamine hydrochloride assay. This oxidation step limits the reaction of cationic PEIs by reductive animation to less than 0.07 μmol PEI/mg GP. Binding of the cationic polymers to the glucan particles was confirmed by a ninhydrin test. The results of PEI grafting shown in Table 1 confirmed that the levels of PEI covalently linked to GPs ranged from 0.01 to 0.03 μmol PEI/mg GP (15–40% yield based on a maximum PEI grafting of 0.07 μmol PEI/mg GP). The molecular weight of PEI does not seem to have an effect on grafting; therefore, it is likely that accessibility of the oxidized glucose units on the particle surface is the controlling parameter in the reaction.

Zeta potential results (Table 1) confirmed the synthesis of cationic GPs. Zeta potential has been previously used to follow reaction sequences on nano- and microparticles [38]. Unmodified GPs are neutral and a significant shift to a positive potential demonstrated PEI linkage to GPs. One limitation of zeta potential measurements is the effect of particle aggregation on zeta potential to establish a quantitative relation between the number of surface groups and the zeta potential values. The zeta potential results of PEI-GP samples indicate that enough PEI has been grafted on the GP surface to shift the zeta potential of neutral GPs to ~20 mV (low molecular weight PEI) or ~30 mV (high molecular weight PEI).

Fluorescent anionic carboxylate polystyrene nanoparticles (cPS-NPs) of three diameters (20, 100, and 200 nm) were used to measure the binding capacity of PEI-GPs and control GPs. Larger nanoparticles (0.5, 1, and 2 um) were also evaluated, but quantitative analysis was difficult due to spontaneous aggregation of cPS-NPs with the GPs. cPS-NP-loaded GP samples prepared with nanoparticles of 200 nm or

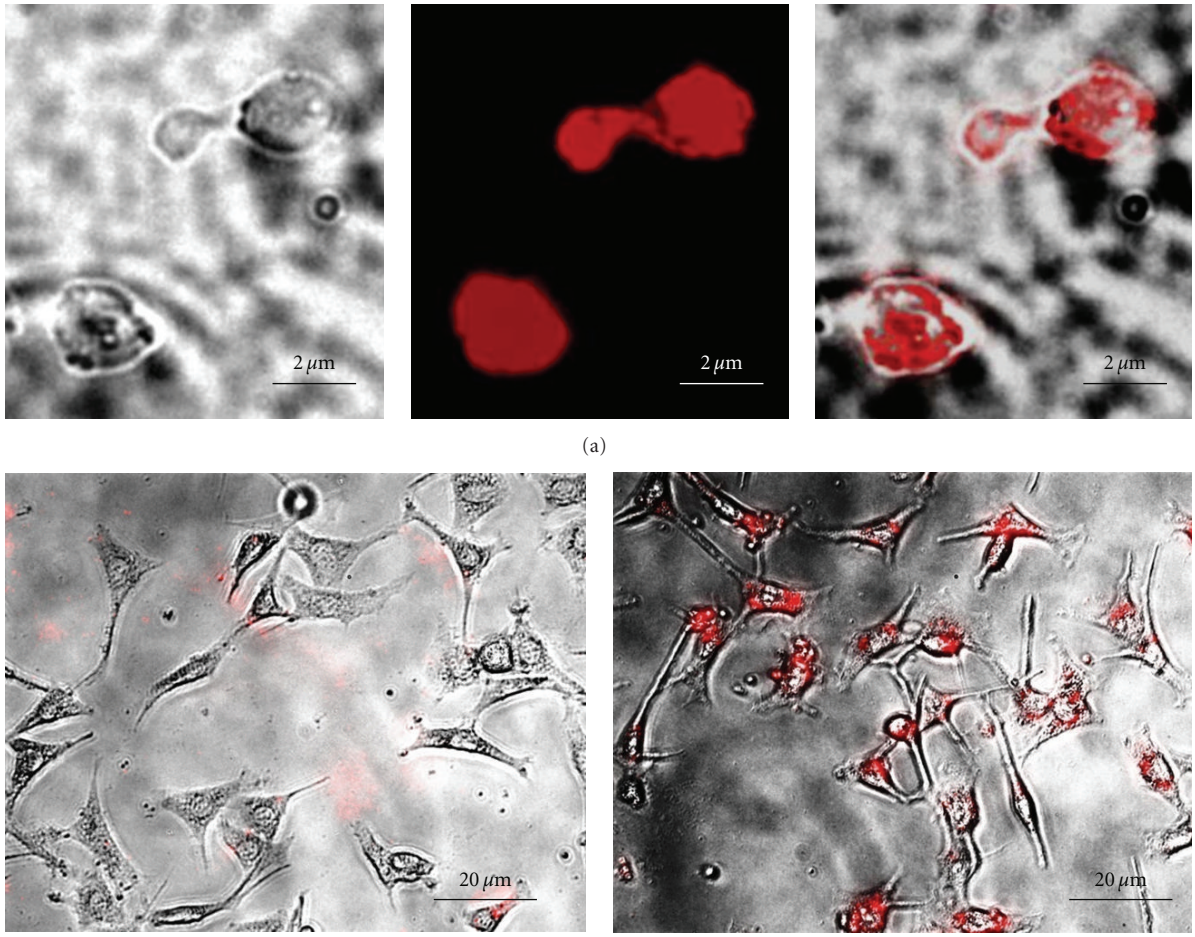

Figure 2: (a) Microscopic images of GPs containing 20 nm anionic fluorescent carboxylate polystyrene nanoparticles. (b) Fluorescent photomicrographs showing uptake of GP-cPS-NPs by control NIH3T3 fibroblast cells (left) and GP phagocytosing proficient NIH3T3-D1 cells (right).

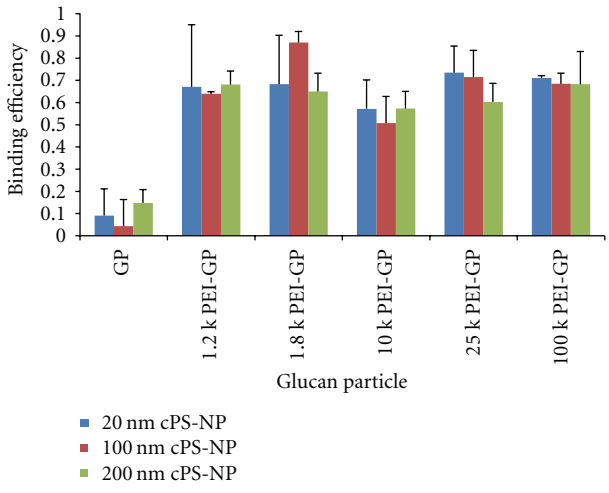

Figure 3: Binding efficiency of GPs derivatized with different molecular weights of PEI for anionic fluorescent polystyrene nanoparticles of 20, 100, and 200 nm in diameter (experimental results were obtained at a cPS-NP/GP ratio of 100 : 1, the values correspond to average of at least five samples).

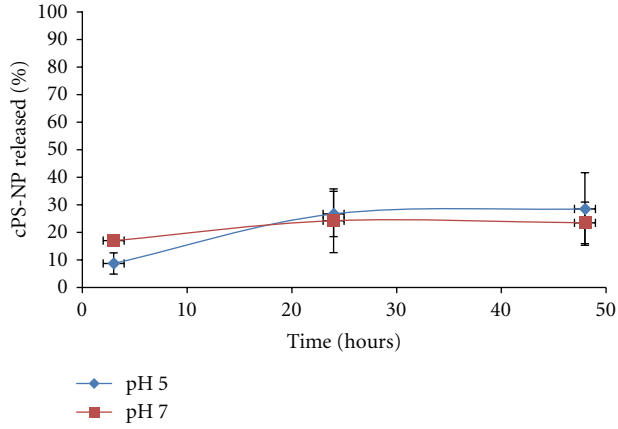

Figure 4: Stability of cPS-NP-GP. cPS-NP released from PEI-GP samples following incubation in PBS + 10% FBS (pH 7) or 0.1 M acetate buffer +10% FBS (pH 5).

less in diameter can be separated from GPs by centrifugation. The amount of cPS-NPs bound to the GPs was measured

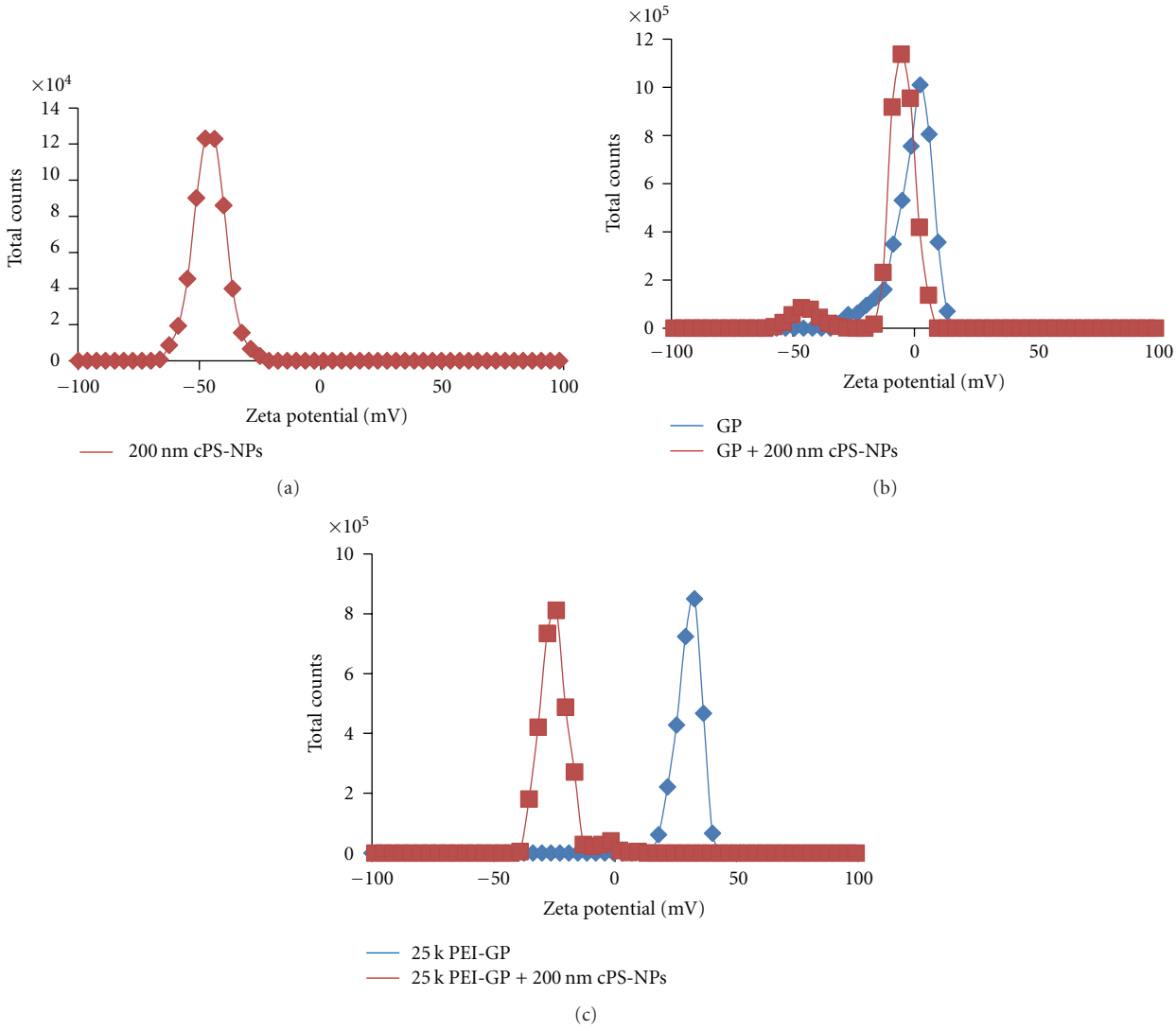

Figure 5: Zeta potential of (a) 200 nm anionic polystyrene NPs alone, (b) glucan particle (GP) control + cPS-NPs, and (c) 25 k PEI-GP + cPS-NPs.

from the fluorescence of unbound cPS-NPs collected in the supernatant and the bound nanoparticles in the NP-GP pellet fractions. The binding efficiency is defined as the ratio of fluorescence emission measurements of cPS-NPs in the pellet fraction divided by the input cPS-NPs.

$$\frac{\text{Measured cPS-NP fluorescence in pellet}}{\text{input}} = \text{binding efficiency} \quad (1)$$

Figure 3 shows that the PEI-GPs readily bind cPS-NPs. The binding efficiency of PEI-GPs for fluorescent anionic polystyrene nanoparticles was carried out at a ratio of 100 : 1 cPS-NPs : glucan particle and ranged from 50 to 90%. The unmodified GP control had minimal cPS-NP binding. The content of amines/GP increases with PEI molecular weight; however, there is no correlation between amine content (surface charge) and binding efficiency indicating that at the cPS-NP/GP ratio used in the data presented in Figure 3 that the binding is limited by the nanoparticle concentration. At lower cPS-NP/GP ratio (10 : 1 or 1 : 1), we measured binding efficiencies higher than 95%. It was not possible to measure binding at cPS-NP/GP ratios higher than 100 : 1 due to inefficient separation of the excess unbound cPS-NPs from the GP pellets.

cPS-NP-PEI-GP samples were evaluated for nanoparticle-binding stability at pH 5 and pH 7 in buffers containing 10% fetal bovine serum (FBS) to simulate cell uptake conditions. Fluorescence measurements of the released nanoparticles into solution and microscopic evaluation of the samples after 48 h incubation showed that more than 60% of the anionic nanoparticles remained bound to the modified PEI-GP particles (Figure 4). The stability of the electrostatic binding of cPS-NP to PEI-GPs provides for efficient glucan-mediated uptake of the cPS-NP-PEI-GPs into cells expressing glucan receptors (Figure 6).

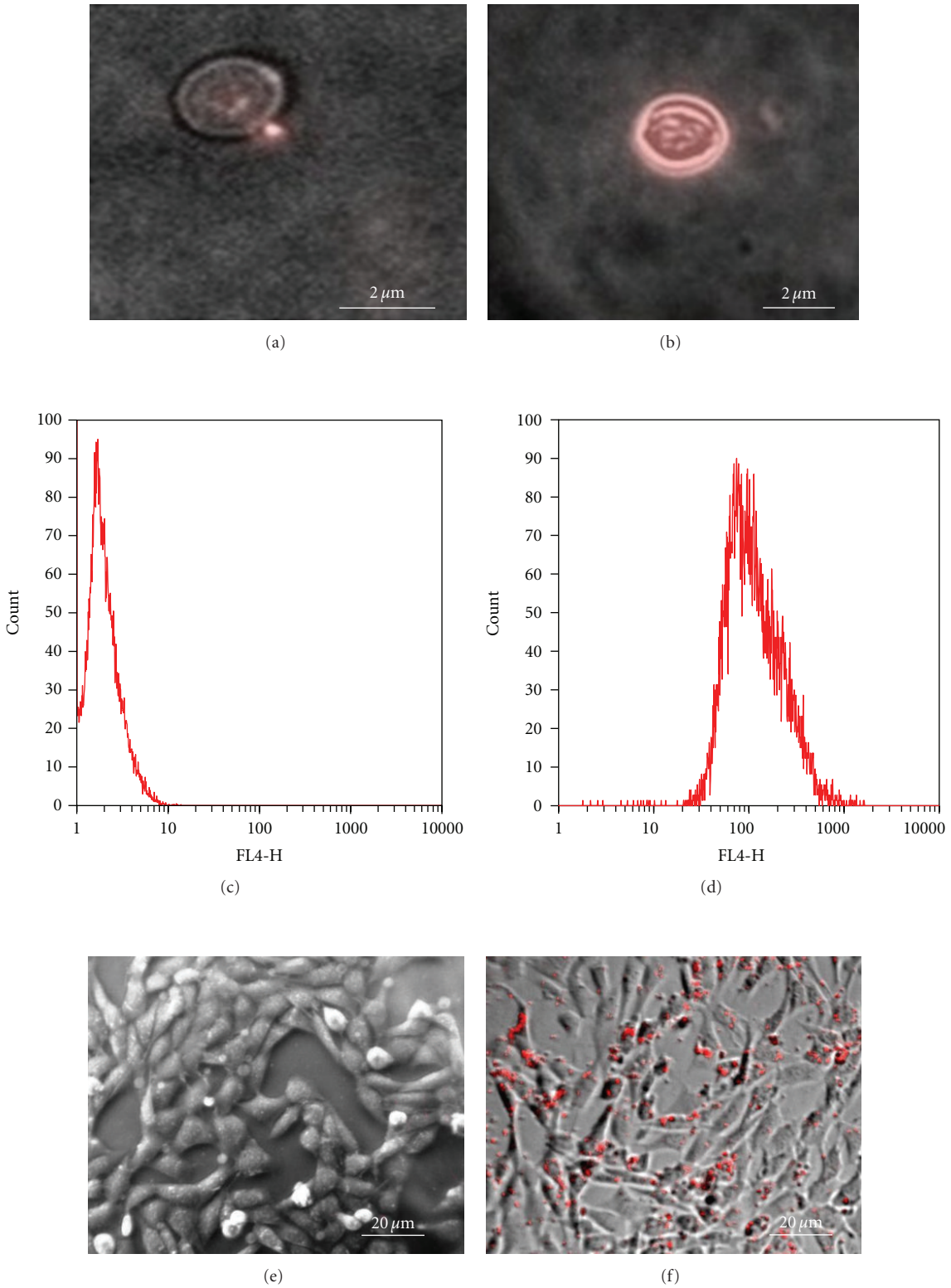

Figure 6: Microscopic images of (a) GP + 200 nm cPS-NPs and (b) 25 k PEI-GP + 200 nm cPS-NPs. FACS results of (c) GP + 200 nm cPS-NPs and (d) 25 k PEI-GP + 200 nm cPS-NPs. Microscopic images showing NIH 3T3-D1 uptake of (e) GP + 200 nm cPS-NPs and (f) 25 k PEI-GP + 200 nm cPS-NPs.

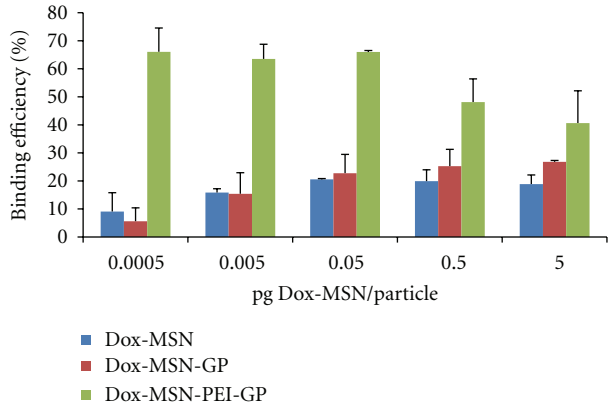

Figure 7: Binding efficiency of Dox-MSN binding to 25 k PEI-GP (the results are the average of three samples).

Zeta potential was also used to demonstrate the binding of the anionic cPS-NPs to cationic PEI-GPs. The zeta potential data in Figure 5 shows the binding of cPS-NPs to cationic GPs as the zeta potential of the cationic GPs shift to an anionic value (−25 mV). Further, the effective separation of unbound cPS-NPs from the cPS-NP-GP sample is clear as there is only one peak (cPS-NP-GP) and no evidence of unbound cPS-NPs at ∼−50 mV. In contrast, the zeta potential of the unmodified control GPs did not significantly shift following incubation with 200 nm cPS-NPs.

Microscopic evaluation (Figures 6(a) and 6(b)) of these samples confirmed the binding of the fluorescent nanoparticles to the surface of PEI-GPs with the cPS-NP fluorescence localized around the perimeter of the GP shells. Unmodified control GPs did not show fluorescent cPS-NPs rosetting the GPs. Flow cytometry was used to quantitate the binding of fluorescent cPS-NPs to unmodified GP and PEI-GPs. The results, shown in Figures 6(c) and 6(d), confirmed the fluorescent cPS-NP binding to the PEI-modified GPs. Although the number of 200 nm nanoparticles that can be bound to the surface of modified GPs (∼70 cPS-NP/GP) is significantly less than the number of 20 nm particles that can be trapped inside GPs (>30,000 20 nm cPS-NP/GP), these two NP formulation strategies allow the use of GPs for the targeted drug delivery of drug-nanoparticle conjugates over a wide range of NP sizes and surface chemistries. Figures 6(e) and 6(f) show NIH3T3-D1 uptake of cPS-NP nanoparticles bound to 25 k PEI-GP. These particle uptake experiments demonstrate that cPS-NP electrostatically bound to PEI-GPs are more efficiently delivered to phagocytic cells than cPS-NP nanoparticles incubated with the control GP particles or free cPS-NPs. Additionally, the cell uptake experiments using cPS-NP-PEI-GP samples confirmed the stability results (Figure 3) of the electrostatically bound samples and that the low level of PEI surface modification of GPs, or the binding of anionic nanoparticles to the PEI-GP surface had no apparent impact on glucan-mediated phagocytosis or cellular toxicity.

3.2. Use of Glucan Particles for the Delivery of Mesoporous Silica Nanoparticles Loaded with Doxorubicin. Many types of nanoparticles have been used for drug delivery and imaging (i.e., silica nanoparticles, carbon nanotubes, gold nanoparticles, polymeric nanogels, magnetic iron oxide nanoparticles, quantum dots, and PLGA nanoparticles [1, 2, 39]). The drug can be physically trapped within nanoparticles, or chemically bound to the surface of the NPs. Methods have also been developed to precisely control particle size. We chose to study mesoporous silica nanoparticles (MSN) as a model system with GPs because of their ease of synthesis and ability to trap chemotherapeutic drugs (i.e., doxorubicin). A MSN sample containing tetraethoxyorthosilicate (TEOS), aminopropyltriethoxysilane (APTS), and 3-trihydroxysilylpropyl methylphosphonate was synthesized following the procedure reported by Lu et al. [32, 33]. The MSN was synthesized by a co-condensation method and the phosphate compound selected to have a larger alkyl chain than APTS to provide a particle with the outermost surface groups corresponding to anionic phosphate. This prevents aggregation of MSNs from interparticle hydrogen bonding between surface silanol groups and amine groups. Successful synthesis of this MSN sample was confirmed by zeta potential (−31.1 ± 5 mV) and DLS particle size measurements (MSN average size of 120 nm, polydispersity index PDI of 0.4). The broad particle size distribution and large particle size prevented the use of MSNs for loading inside GPs. However, the sample contained anionic phosphate groups allowed for electrostatic binding to the surface of cationic PEI-GPs.

MSN was loaded with the chemotherapeutic doxorubicin (Dox), an anthracycline-type antitumor drug that exerts its antiproliferative activity via DNA intercalation and inhibition of DNA synthesis leading to cell death [40, 41]. Limitations in the use of Dox as an antitumor agent include chronic or acute cardiotoxicity. Dox has been studied using different nanoparticle delivery systems to enhance Dox delivery, minimize dosage, and reduce toxicity leading to the successful development of a liposomal Dox formulation (Doxil).

Dox was loaded into MSNs in DMSO at target concentrations ranging from 0 to 2 μmol Dox/mg MSN. Following MSN Dox loading, the Dox-MSN samples were washed to remove unbound Dox. The amount of Dox loaded into the MSN samples was quantified by measuring Dox fluorescence extracted in methanol, and the results showed that the binding of Dox to MSN was 0.06 μmol Dox/mg MSN, representing 3% of the input load. This binding is ∼5 times higher than Dox binding to a control MSN sample without phosphate groups. Other groups have reported similar Dox-binding capacities with phosphonate functionalized MSNs (6–8% w/w) and have shown higher binding to these functionalized MSNs compared to MSN controls [42]. The Dox-MSN samples were stable in PBS (pH 7) enabling the electrostatic binding of anionic Dox-MSN to the surface of cationic PEI-GPs. This binding reaction was monitored by a fluorescence-binding assay (Figure 7), zeta potential (Figure 8), and confirmed by fluorescent microscopy (Figure 8, inset). The fluorescence-binding assay showed efficient and selective binding of Dox-MSN to PEI-GP at low Dox-MSN concentrations. Higher concentrations showed a reduction in binding efficiency likely due to saturation of available PEI for binding of Dox-MSN. The level of background binding of Dox-MSN nanoparticles to

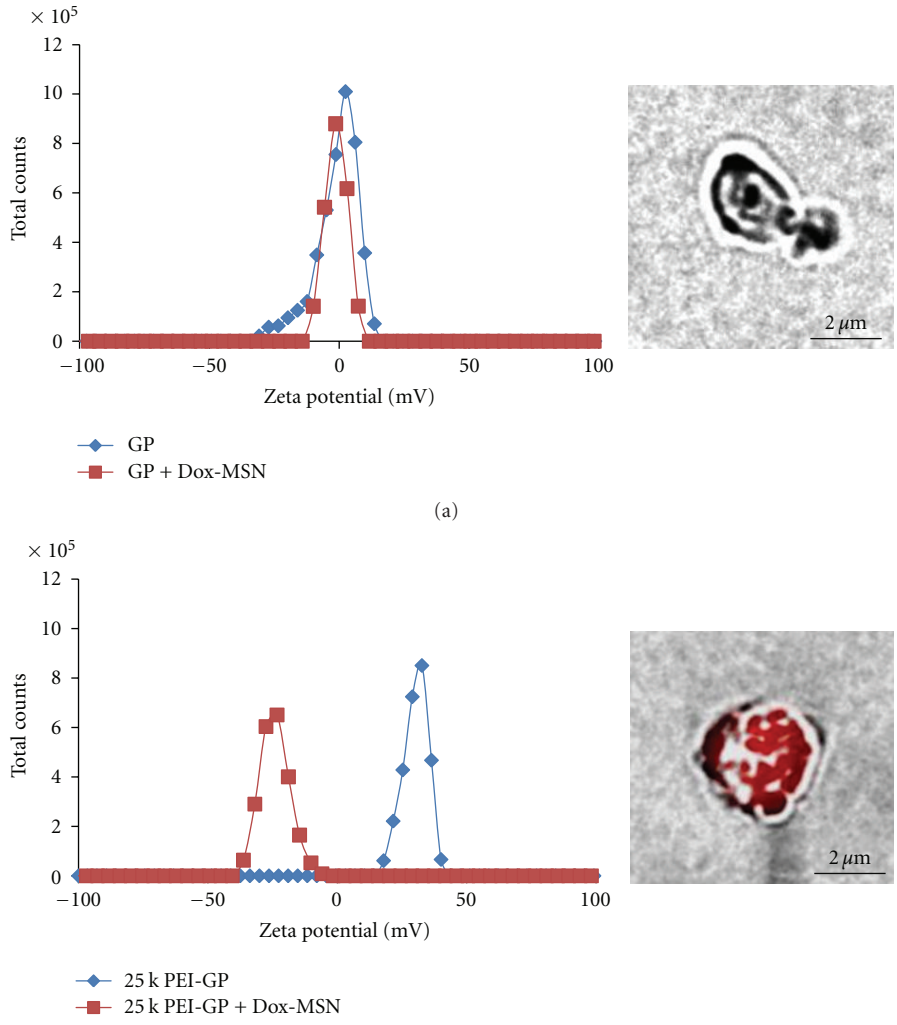

Figure 8: Zeta potential monitoring of Dox-MSN binding to (a) GP and (b) 25 k PEI-GP. Inset, fluorescent microscopic images of Dox-MSN bound to GP (a) and 25 k PEI-GP (b). Samples were prepared with 25 fg Dox-MSN/GP (~0.9 pg Dox/GP).

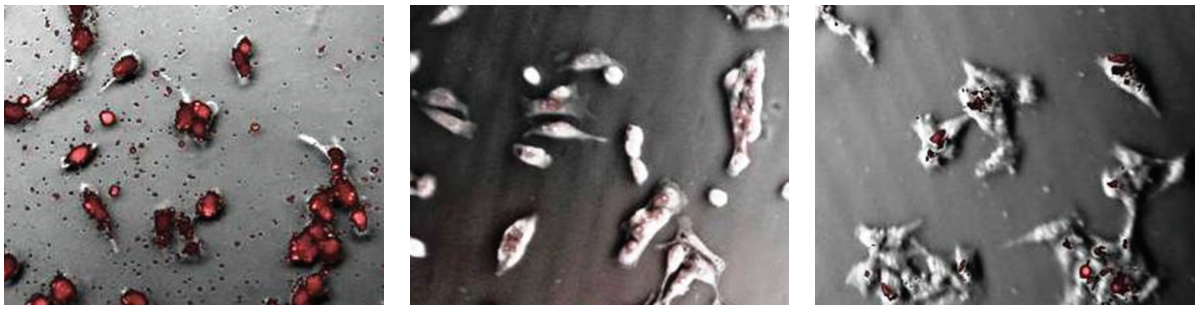

Dox-MSN + 25 k PEI-GP | Dox-MSN + GP | Dox-MSN

Figure 9: Efficient GP-mediated Dox delivery into NIH 3T3-D1 (pictures were taken at 40x magnification).

unmodified GPs corresponds to the fraction of nanoparticles that were not efficiently separated from the glucan particles. This is seen in Figure 7, both Dox-MSN alone and Dox-MSN with GP showed similar binding as a result of measuring the fluorescence of Dox-MSN-free nanoparticles in the pellet fraction. Dox-MSN-PEI-GP samples were incubated in 0.9% saline, PBS with 10% fetal bovine serum (FBS), and sodium acetate buffer (pH 5) at 37°C for 24 h and evaluated by fluorescence microscopy to confirm stability of Dox-MSN binding to PEI-GP.

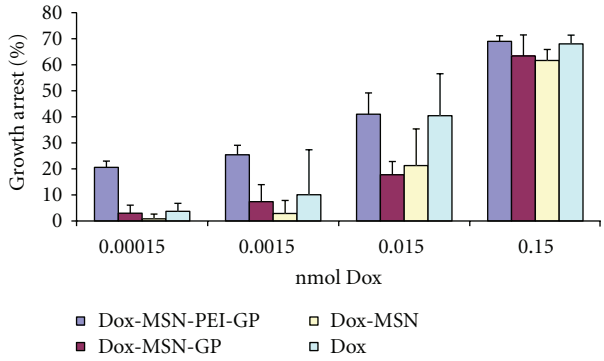

Figure 10: Growth arrest of NIH 3T3-D1 cells with Dox formulations (experimental results are the average of four samples).

Zeta potential measurements confirmed the selective binding of Dox-MSN to PEI-GP. Dox-MSN had a negative zeta potential corresponding to the outer phosphate groups of MSN. Binding of anionic Dox-MSN to cationic PEI-GP shifted the zeta potential of the PEI-GP sample from a positive to a negative value. In comparison, the zeta potential shift of the GP sample is minimal confirming that Dox-MSN does not bind to unmodified GPs. Fluorescent microscopy confirmed that Dox-MSN binds to cationic PEI-GP but not GPs.

The Dox-MSN-GP and Dox-MSN-PEI-GP samples were tested for intracellular Dox delivery, and antiproliferative and cytotoxic activities in the NIH 3T3-D1 cell line. This cell line has been genetically modified to express the Dectin-1 glucan receptor and efficiently phagocytoses GPs. Figure 9 shows that Dox-MSN-PEI-GP more effectively delivered Dox into NIH3T3-D1 cells than Dox-MSN-GP or Dox-MSN after 3-hour incubation.

Cells were incubated with varying concentrations of Dox-MSN-PEI-GP, Dox-MSN-GP, free Dox-MSN, or free Dox to assess antiproliferative and cytotoxic activities over 48 hours of incubation. Unincorporated materials were washed away after 3 hours of incubation, a sufficient period of time for efficient GP uptake by NIH 3T3-D1 cells, and the growth and viability of the cells were followed. High concentrations of free Dox or Dox-MSN (>2.5 μg Dox-MSN containing ~0.15 nmol Dox) inhibited cell growth (>60%). As seen in Figure 10 at a concentration of 0.015 nmol Dox the Dox-MSN-PEI-GP samples showed similar effect as free Dox, but free Dox-MSN or Dox-MSN-GP samples showed less growth inhibition. Below the minimum inhibitory concentration (MIC) of free Dox (0.0015 nmol Dox), there is still a significant growth inhibition (20–30%) by the Dox-MSN-PEI-GP formulation (Figure 10) showing the increased efficacy of GP-targeted delivery of Dox-MSN-PEI-GP. Other groups have reported the use of MSN for delivery of other chemotherapeutics (i.e., camptothecin) and showed a 10-fold reduction in the drug concentration compared to free drug to achieve 50% cell death [32, 33]. The use of PEI-GP for Dox-MSN delivery allows for a reduction in drug dosage compared to free Dox or Dox-MSN demonstrating the advantage of GP-targeted delivery. Future work will focus on optimization of Dox incorporation into nanoparticles and controlled release of Dox from MSN and other nanoparticles (i.e., gold nanoparticles) to improve cytotoxicity of Dox NP-GP formulations. These formulations will be evaluated in dividing tumor cells (i.e., NIH 3T3-D1) and nondividing primary macrophages, and in cocultivation macrophage-tumor cell assays to test the hypothesis that macrophages can act as cell-based carriers of GP-NP-Dox formulations into tumors. Optimal GP-Dox NP-GP formulations will be tested *in vivo* for targeted macrophage Dox delivery and accumulation in tumors.

4. Conclusions

We have developed two strategies for the targeted delivery of nanoparticles into phagocytic innate immune cells. Nanoparticles of less than 30 nm in diameter were encapsulated within the hollow cavity of GPs (~36,000 NPs/GP for 20 nm NPs). Larger anionic nanoparticles (>100 nm) were electrostatically bound to the surface of GPs derivatized with the cationic polymer PEI allowing for delivery of ~70 NPs/GP. Mesoporous silica nanoparticles (120 nm) containing doxorubicin were electrostatically bound to PEI-GPs providing for the targeted delivery of the Dox-MSN-PEI-GPs to cells capable of phagocytosing glucan particles. At Dox levels below an effective free-drug concentration, an equivalent amount of Dox-MSN-PEI-GPs efficiently delivered sufficient Dox to inhibit the growth of the GP-phagocytic cell line NIH 3T3-D1. These results demonstrate that the NP-GP delivery system offers the potential of GP-mediated macrophage-targeted delivery of multiple nanoparticles in a single uptake event providing for high efficiency intracellular drug delivery. The possibility that macrophages can serve as Trojan horses carrying and releasing the drug into solid tumors may further enhance the *in vivo* Dox-MSN-PEI-GP antitumor effect. We are currently studying a variety of drug loaded nanoparticulate formulations that may provide advantages of higher drug binding capacity and the possibility of controlled release. In addition, the use of certain types of nanoparticles (i.e., gold nanoparticles, magnetic iron oxide) may add theranostic properties to the NP-GP delivery system.

Acknowledgments

We appreciate the help of Shira Kahlon for the FACS analyses and the support from staff of the Core Flow Cytometry Lab. This work was supported by UMass Medical School and the Juvenile Diabetes Research Foundation [Grant no. 17-2009-546].

References

[1] S. S. Suri, H. Fenniri, and B. Singh, "Nanotechnology-based drug delivery systems," *Journal of Occupational Medicine and Toxicology*, vol. 2, no. 1, pp. 1–6, 2007.

[2] R. A. Petros and J. M. DeSimone, "Strategies in the design of nanoparticles for therapeutic applications," *Nature Reviews Drug Discovery*, vol. 9, no. 8, pp. 615–627, 2010.

[3] E. Brewer, J. Coleman, and A. Lowman, "Emerging technologies of polymeric nanoparticles in cancer drug delivery,"

Journal of Nanomaterials, vol. 2011, Article ID 408675, 10 pages, 2011.

[4] D. Sun, "Nanotheranostics: integration of imaging and targeted drug delivery," *Molecular Pharmaceutics*, vol. 7, no. 6, p. 1879, 2010.

[5] M. Ferrari, "Cancer nanotechnology: opportunities and challenges," *Nature Reviews Cancer*, vol. 5, no. 3, pp. 161–171, 2005.

[6] M. E. Davis, Z. Chen, and D. M. Shin, "Nanoparticle therapeutics: an emerging treatment modality for cancer," *Nature Reviews Drug Discovery*, vol. 7, no. 9, pp. 771–782, 2008.

[7] D. E. Owens III and N. A. Peppas, "Opsonization, biodistribution and pharmacokinetics of polymeric nanoparticles," *International Journal of Pharmaceutics*, vol. 307, no. 1, pp. 93–102, 2006.

[8] J. A. Champion, Y. K. Katare, and S. Mitragotri, "Particle shape: a new design parameter for micro and nanoscale drug delivery carriers," *Journal of Controlled Release*, vol. 121, no. 1-2, pp. 3–9, 2007.

[9] F. Alexis, E. Pridgen, L. K. Molnar, and O. C. Farokhzad, "Factors affecting the clearance and biodistribution of polymeric nanoparticles," *Molecular Pharmaceutics*, vol. 5, no. 4, pp. 505–515, 2008.

[10] S. V. Vinogradov, T. K. Bronich, and A. V. Kabanov, "Nanosized cationic hydrogels for drug delivery: preparation, properties and interactions with cells," *Advanced Drug Delivery Reviews*, vol. 54, no. 1, pp. 135–147, 2002.

[11] H. S. Choi, W. Liu, P. Misra et al., "Renal clearance of quantum dots," *Nature Biotechnology*, vol. 25, no. 10, pp. 1165–1170, 2007.

[12] M. D. Howard, M. Jay, T. D. Dziubla, and X. Lu, "PEGylation of nanocarrier drug delivery systems: state of the art," *Journal of Biomedical Nanotechnology*, vol. 4, no. 2, pp. 133–148, 2008.

[13] I. Hamad, A. C. Hunter, K. J. Rutt, Z. Liu, H. Dai, and S. M. Moghimi, "Complement activation by PEGylated single-walled carbon nanotubes is independent of C1q and alternative pathway turnover," *Molecular Immunology*, vol. 45, no. 14, pp. 3797–3803, 2008.

[14] X. Wang, J. Li, Y. Wang et al., "HFT-T, a targeting nanoparticle, enhances specific delivery of paclitaxel to folate receptor-positive tumors," *ACS Nano*, vol. 3, no. 10, pp. 3165–3174, 2009.

[15] P. S. Low, W. A. Henne, and D. D. Doorneweerd, "Discovery and development of folic acid based receptor targeting for imaging and therapy of cancer and inflammatory diseases," *Accounts of Chemical Research*, vol. 41, no. 1, pp. 120–129, 2008.

[16] C. H. J. Choi, C. A. Alabi, P. Webster, and M. E. Davis, "Mechanism of active targeting in solid tumors with transferrin-containing gold nanoparticles," *Proceedings of the National Academy of Sciences of the United States of America*, vol. 107, no. 3, pp. 1235–1240, 2010.

[17] M. B. Dowling, L. Li, J. Park et al., "Multiphoton-absorption-induced-luminescence (MAIL) imaging of tumor-targeted gold nanoparticles," *Bioconjugate Chemistry*, vol. 21, no. 11, pp. 1968–1977, 2010.

[18] L. Han, R. Huang, S. Liu, S. Huang, and C. Jiang, "Peptide-conjugated PAMAM for targeted doxorubicin delivery to transferrin receptor overexpressed tumors," *Molecular Pharmaceutics*, vol. 7, no. 6, pp. 2156–2165, 2010.

[19] A. K. Patri, A. Myc, J. Beals, T. P. Thomas, N. H. Bander, and J. R. Baker, "Synthesis and in vitro testing of J591 antibody-dendrimer conjugates for targeted prostate cancer therapy," *Bioconjugate Chemistry*, vol. 15, no. 6, pp. 1174–1181, 2004.

[20] C. Plank, K. Zatloukal, M. Cotten, K. Mechtler, and E. Wagner, "Gene transfer into hepatocytes using asialoglycoprotein receptor mediated endocytosis of DNA complexed with an artificial tetra-antennary galactose ligand," *Bioconjugate Chemistry*, vol. 3, no. 6, pp. 533–539, 1992.

[21] K. G. Neoh and E. T. Kang, "Functionalization of inorganic nanoparticles with polymers for stealth biomedical applications," *Polymer Chemistry*, vol. 2, no. 4, pp. 747–759, 2011.

[22] G. D. Brown and S. Gordon, "Immune recognition: a new receptor for β-glucans," *Nature*, vol. 413, no. 6851, pp. 36–37, 2001.

[23] H. Huang, G. R. Ostroff, C. K. Lee, J. P. Wang, C. A. Specht, and S. M. Levitz, "Distinct patterns of dendritic cell cytokine release stimulated by fungal beta-glucans and toll-like receptor agonists," *Infection and Immunity*, vol. 77, no. 5, pp. 1774–1781, 2009.

[24] E. R. Soto and G. R. Ostroff, "Characterization of multilayered nanoparticles inside yeast cell wall particles for DNA delivery," *Bioconjugate Chemistry*, vol. 19, no. 4, pp. 840–848, 2008.

[25] M. Aouadi, G. J. Tesz, S. M. Nicoloro et al., "Orally delivered siRNA targeting macrophage Map4k4 suppresses systemic inflammation," *Nature*, vol. 458, no. 7242, pp. 1180–1184, 2009.

[26] G. J. Tesz, M. Aouadi, M. Prot et al., "Glucan particles for selective delivery of siRNA to phagocytic cells in mice," *Biochemical Journal*, vol. 436, no. 2, pp. 351–362, 2011.

[27] E. Soto, Y. S. Kim, J. Lee, H. Kornfeld, and G. Ostroff, "Glucan particle encapsulated rifampicin for targeted delivery to macrophages," *Polymers*, vol. 2, no. 4, pp. 681–689, 2010.

[28] E. Soto and G. Ostroff, "Use of beta-1,3-D-glucans for drug delivery applications," in *Biology and Chemistry of Beta Glucan: Volume 1 Beta Glucans-Mechanisms of Action*, V. Vetvicka and M. Novak, Eds., p. 82, Bentham Press, 2011.

[29] C. T. Kresge, M. E. Leonowicz, W. J. Roth, J. C. Vartuli, and J. S. Beck, "Ordered mesoporous molecular sieves synthesized by a liquid crystal template mechanism," *Nature*, vol. 359, no. 6397, pp. 710–712, 1992.

[30] B. G. Trewyn, I. I. Slowing, S. Giri, G. T. Chen, and V. S. Lin, "Synthesis and functionalization of a mesoporous silica nanoparticle based on the sol-gel process and applications in controlled release," *Accounts of Chemical Research*, vol. 40, no. 9, pp. 846–853, 2007.

[31] M. Liong, J. Lu, M. Kovovich et al., "Multifunctional Inorganic Nanoparticles for Imaging, Targeting and Drug Delivery," *ACSNano*, vol. 2, no. 5, pp. 889–896, 2008.

[32] J. Lu, M. Liong, J. I. Zink, and F. Tamanoi, "Mesoporous silica nanoparticles as a delivery system for hydrophobic anticancer drugs," *Small*, vol. 3, no. 8, pp. 1341–1346, 2007.

[33] J. Lu, M. Liong, S. Sherman et al., "Mesoporous silica nanoparticles for cancer therapy: energy-dependent cellular uptake and delivery of paclitaxel to cancer cells," *Nanobiotechnology*, vol. 3, no. 2, pp. 89–95, 2007.

[34] H. Zhao and N. D. Heindel, "Determination of degree of substitution of formyl groups in polyaldehyde dextran by the hydroxylamine hydrochloride method," *Pharmaceutical Research*, vol. 8, no. 3, pp. 400–402, 1991.

[35] J. A. Willment, S. Gordon, and G. D. Brown, "Characterization of the human β-glucan receptor and its alternatively spliced isoforms," *Journal of Biological Chemistry*, vol. 276, no. 47, pp. 43818–43823, 2001.

[36] A. S. Marshall, J. A. Willmen, H. H. Lin, D. L. Williams, S. Gordon, and G. D. Brown, "Identification and characterization of a novel human myeloid inhibitory C-type lectin-like receptor (MICL) that is predominantly expressed on granulocytes and

monocytes," *Journal of Biological Chemistry*, vol. 279, no. 15, pp. 14792–14802, 2004.

[37] T. Azzam, H. Eliyahu, L. Shapira, M. Linial, Y. Barenholz, and A. J. Domb, "Polysaccharide-oligoamine based conjugates for gene delivery," *Journal of Medicinal Chemistry*, vol. 45, no. 9, pp. 1817–1824, 2002.

[38] F. Thielbeer, K. Donaldson, and M. Bradley, "Zeta potential mediated reaction monitoring on nano and microparticles," *Bioconjugate Chemistry*, vol. 22, no. 2, pp. 144–150, 2011.

[39] Y. Malam, E. J. Lim, and A. M. Seifalian, "Current trends in the application of nanoparticles in drug delivery," *Current Medicinal Chemistry*, vol. 18, no. 7, pp. 1067–1078, 2011.

[40] G. Bonadonna, S. Monfardini, M. De Lena, F. Fossati-Bellani, and G. Beretta, "Phase I and preliminary phase II evaluation of adriamycin (NSC 123127)," *Cancer Research*, vol. 30, no. 10, pp. 2572–2582, 1970.

[41] N. P. Niraula, S. H. Kim, J. K. Sohng, and E. S. Kim, "Biotechnological doxorubicin production: pathway and regulation engineering of strains for enhanced production," *Applied Microbiology and Biotechnology*, vol. 87, no. 4, pp. 1187–1194, 2010.

[42] H. Meng, M. Liong, T. Xia et al., "Engineered design of mesoporous silica nanoparticles to deliver doxorubicin and p-glycoprotein siRNA to overcome drug resistance in a cancer cell line," *ACS Nano*, vol. 4, no. 8, pp. 4539–4550, 2010.

Hindawi Publishing Corporation
Journal of Drug Delivery
Volume 2012, Article ID 751075, 12 pages
doi:10.1155/2012/751075

Review Article

Noble Metal Nanoparticles Applications in Cancer

João Conde,[1,2] Gonçalo Doria,[1] and Pedro Baptista[1]

[1] *CIGMH, Departamento de Ciências da Vida, Faculdade de Ciências e Tecnologia, Universidade Nova de Lisboa, Campus de Caparica, 2829-516 Caparica, Portugal*
[2] *Instituto de Nanociencia de Aragón, Universidad de Zaragoza, Pedro Cerbuna 12, 50009 Zaragoza, Spain*

Correspondence should be addressed to Pedro Baptista, pmvb@fct.unl.pt

Received 23 May 2011; Accepted 2 August 2011

Academic Editor: Paulo Cesar de Morais

Nanotechnology has prompted new and improved materials for biomedical applications with particular emphasis in therapy and diagnostics. Special interest has been directed at providing enhanced molecular therapeutics for cancer, where conventional approaches do not effectively differentiate between cancerous and normal cells; that is, they lack specificity. This normally causes systemic toxicity and severe and adverse side effects with concomitant loss of quality of life. Because of their small size, nanoparticles can readily interact with biomolecules both at surface and inside cells, yielding better signals and target specificity for diagnostics and therapeutics. This way, a variety of nanoparticles with the possibility of diversified modification with biomolecules have been investigated for biomedical applications including their use in highly sensitive imaging assays, thermal ablation, and radiotherapy enhancement as well as drug and gene delivery and silencing. Here, we review the available noble metal nanoparticles for cancer therapy, with particular focus on those already being translated into clinical settings.

1. Introduction

Cancer is one of the leading causes of mortality in the modern world, with more than 10 million new cases every year [1]. It is well established that cancer is a multifactorial disease caused by a complex mixture of genetic and environmental factors [2–4], where considerable advances have led to a more comprehensive understanding of cancer at the genetic, molecular, and cellular levels providing new targets and strategies for therapy [5]. Nevertheless, these advances have yet to be effectively translated into functioning diagnostics and therapy. For example, the effectiveness of many anticancer drugs is limited due to the inability to reach the target site in sufficient concentrations and efficiently exert the pharmacological effect without causing irreversible unwanted injury to healthy tissues and cells [6, 7].

The technological leap of controlling materials at nanoscale provides for a "big revolution" in medical and healthcare treatments and therapies [8, 9]. Nanotechnology offers a wealth of tools to diagnose and treat cancer—new imaging agents, multifunctional, targeted devices capable of bypassing biological barriers to deliver therapeutic agents directly to cells and tissues involved in cancer growth and metastasis, monitor predictive molecular changes allowing preventive action against precancerous cells, and minimizing costs and side effects [5, 10, 11]. Nanotechnology-based therapies for cancer with minimal side effects and high specificity are on the surge, where the main challenge is to develop a system for molecular therapy capable of circulating in the blood stream undetected by the immune system and recognize the desirable target, signaling it for effective drug delivery or gene silencing with minimum collateral cell damage—nanovectorization. As a result, personalized medicine could become a reality in cancer patient management.

Nanoparticles (NPs), and noble metal NPs in particular, are versatile agents with a variety of biomedical applications including their use in highly sensitive diagnostic assays [12, 13], thermal ablation, and radiotherapy enhancement [14–17], as well as drug and gene delivery [18–21]. Moreover, noble metal NPs have been proposed as nontoxic carriers for dru and gene-delivery applications [22–24]. Additionally, the nanoparticle-based systems can provide simultaneous diagnostic and therapy, that is, Theranostics, exploring their unique properties for better penetration of therapeutic

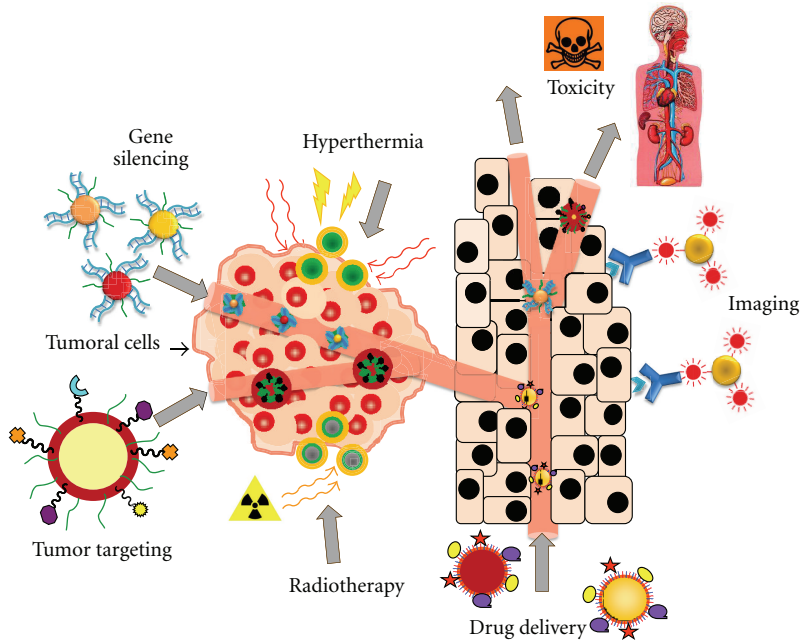

Figure 1: Noble metal NPs for cancer therapy. Once the tumor is directly connected to the main blood circulation system, NPs can exploit several characteristics of the newly formed vasculature and efficiently target tumors. Tumor cells are supplied by blood capillaries that perfuse the cells of the tissue where NPs can (i) passively accumulate or (ii) anchor through targeting moieties to biomarkers overexpress by tumor cells. NPs can act simultaneously as therapeutic agents, inducing hyperthermia, enhancing radiotherapy, silencing genes, and/or delivering drugs to induce tumor cell death, and as imaging enhancers or contrast agents, to help tracking the therapeutic effects in real time.

moieties and tracking within the body, allowing a more efficient therapy with a reduced risk in comparison to conventional therapies [25]—see Figure 1.

The unique characteristics of noble metal NPs, such as high surface-to-volume ratio, broad optical properties, ease of synthesis, and facile surface chemistry and functionalization hold pledge in the clinical field for cancer therapeutics [22, 26, 27]. Noble metal NPs (e.g., gold, silver, or a combination of both) present highly tunable optical properties, which can be easily tuned to desirable wavelengths according to their shape (e.g., nanoparticles, nanoshells, nanorods, etc.), size (e.g., 1 to 100 nm), and composition (e.g., core/shell or alloy noble metals), enabling their imaging and photothermal applications under native tissue [28, 29]. These NPs can also be easily functionalized with various moieties, such as antibodies, peptides, and/or DNA/RNA to specifically target different cells [30] and with biocompatible polymers (e.g., polyethylene glycol and PEG) to prolong their *in vivo* circulation for drug and gene delivery applications [23, 24]. Moreover, they can efficiently convert light or radiofrequencies into heat, thus enabling thermal ablation of targeted cancer cells [31, 32].

In this paper, we will focus on the application of noble metal NPs for cancer therapy with particular emphasis on their use *in vivo* and their potential to be translated into clinical settings.

2. Therapy

In medical terms, a therapeutic effect is a consequence of a medical treatment of any kind, the results of which are judged to be desirable and beneficial [33]. Conventional therapy methods in cancer involve the employment of agents that do not greatly differentiate between cancerous and normal cells, leading to systemic toxicity and adverse and severe side effects [34]. Efficient *in vivo* targeting to heterogeneous population of cancer cells and tissue still requires better selectivity and noncytotoxicity to surrounding healthy cells. However, universally targeting cells within a tumor is not always feasible, because some drugs cannot diffuse efficiently and the random nature of the approach makes it difficult to control the process and may induce multiple-drug resistance—a situation where chemotherapy treatments fail due to resistance of cancer cells towards one or more drugs [7]. Making use of their extraordinary properties, nanotechnology-based systems could offer a less-invasive alternative, enhancing the life expectancy and quality of life of the patient [35]. Among these, the potential therapeutic application of noble metal NPs represents an attractive platform for cancer therapy in a wide variety of targets and clinical settings [36, 37].

2.1. Tumor Targeting. It is expected that the greatest gains in therapeutic selectivity will be achieved by synergistic combinations of several multicomponent targeting strategies that is capable of simultaneously target and deliver multiple therapeutic agents while avoiding the organism's biological and biophysical barriers. NPs targeting strategies to cancerous tissues have focused on passive and active targeting. In passive targeting, because numerous tumors present defective vasculature and poor lymphatic drainage

due to the rapid growth of solid tumors, noble metal NPs can extravasate into the tumor stroma through the fenestrations of the angiogenic vasculature, demonstrating targeting by enhanced permeation and retention, thus accumulation at the tumor site [6, 8, 38]. Additionally, functionalization of the NP's surface with hydrophilic molecules, such as PEG, can also greatly increase their solubility, help evading macrophage-mediated uptake and, thus, avoid removal from the systemic circulation and protect their carriers from enzymatic degradation when used *in vivo* [30]. For active targeting, NPs can be easily functionalized with a wide variety of biological moieties, such as antibodies, peptides, and/or DNA/RNA to specifically target extracellular and intracellular receptors or pathways [30]. The use of NPs functionalized with multiple peptides or antibodies, such as monoclonal antibodies, have been described to successfully target specific cell surface proteins or receptors on cancer cells and further direct their antitumor action, leading to tumor cell death with minimal damage to collateral healthy cells [36, 39–41]. In nucleic-acid functionalized NPs, DNA and RNA macromolecules can be used to simultaneously target specific sequences and exert their genetic-based therapy [42, 43].

To help tracking noble metal NPs *in vivo* and enhance the imaging properties of such moieties, leading to more efficient control of their therapeutic properties, they can also be functionalized with chemical moieties, such as Raman [44, 45] or fluorescent [46, 47] reporters.

2.2. Gene Silencing. Antisense DNA [48, 49] and RNA interference (RNAi) via the use of small-interfering RNA [50–53] have emerged as a powerful and useful tools to block gene function and for sequence-specific posttranscriptional gene silencing, playing an important role in downregulation of specific gene expression in cancer cells.

Small interfering RNAs (siRNAs) can be transfected into mammalian cells by a variety of methods that influence the strength and duration of the silencing response, which in turn is affected by the amount of siRNA that is delivered and on the potential of each siRNA to suppress its target. Thus, one drawback of using naked siRNAs is that they show extremely short half-lives, weak protection against action by RNases, poor chemical stability, and common dissociation from vector [54]. In fact, the major obstacle to clinical application is the uncertainty about how to deliver therapeutic RNAs (e.g., miRNA and/or siRNA) with maximal therapeutic impact. Nanotechnology offers an unprecedented opportunity to overcome these problems, as nanoscale devices, due to their small size, can readily interact with biomolecules on both the surface of cells and inside of cells for longer periods of time [10]. Gold NPs (AuNPs) have shown potential as intracellular delivery vehicles for antisense oligonucleotides [55] and for therapeutic siRNA by providing protection against RNAses and ease of functionalization for selective targeting [42, 43]. For example, Mirkin and coworkers showed that AuNPs attached to single-stranded oligodeoxynucleotides can be used for gene therapy, providing a highly efficient gene regulator in terms of high loading of the antisense DNA with no toxicity at the concentrations studied [55]. They have also shown that polyvalent RNA-AuNP conjugates are readily taken up by cells and that the particle bound siRNA could effectively regulate genes in the context of RNA interference [42]. AuNPs modified with the hydrophilic PEG polymer, siRNAs and then coated with poly(β-aminoester)s have been shown to facilitate high levels of *in vitro* siRNA delivery and gene silencing in human cells [56]. Also, Braun et al. developed an Au-nanoshell functionalized with TAT-lipid layer for transfection and selective release of siRNA [57], where the TAT-lipid coating was used to efficiently mediate the cellular uptake of the nanoconjugates and the siRNA release was dependent on near-infrared (NIR) laser pulses. The authors demonstrated that this NIR strategy for siRNA release was proficient and time dependent.

Several other studies using engineered NPs modified with siRNA have demonstrated a cytoplasmic delivery system of siRNA and efficient gene silencing using AuNPs [42, 56, 58–60].

2.3. Hyperthermia. Hyperthermia is based on the effect increasing temperatures have on living cells, and it is commonly accepted that above 42°C cell viability is strongly reduced. In fact, hyperthermia effects can range from moderate denaturation of blood and extracellular proteins to induction of apoptosis and, above 50°C, to cell death and tissue ablation [61]. Hyperthermia therapy in cancer has been widely used either via direct irradiation or suitable temperature vectors, such as metal NPs [62]. In nanoparticle-mediated hyperthermia for cancer, NPs heat up cancerous cells beyond their temperature tolerance limits, which are lower than normal healthy tissue due to their poor blood supply, killing them selectively. This can be achieved by exposing the entire patient or the targeted area to an alternating current magnetic field, an intense light source or radiofrequencies which will cause the NPs to heat up and induce thermal ablation of the tumor. One of the most widespread examples of hyperthermia mediated by NPs, magnetic NPs have been introduced in the body through magnetic delivery systems or local injection to the affected area [63]. The first *in vivo* Phase II clinical trials of magnetic NP hyperthermia were undertaken in Germany in 2005 [64] by injecting the prostate of cancer patients with biocompatible magnetite NPs. Successful results were obtained using minimally invasive ablation of the tumor in an AC magnetic field after several sessions.

Noble metal NPs have thoroughly been used as photothermal agents for *in vivo* therapy as a less invasive experimental technique that holds great promise for the treatment of cancer [65]. It combines two key components: (i) light source, such as lasers with a spectral range of 650–900 nm [66] for deep tissue penetration and (ii) optical absorbing NPs which efficiently transforms the optical irradiation into heat on a picosecond time scale, thus inducing photothermal ablation [67, 68]. For example, Huang and coworkers demonstrated that Au-nanorods are effective photothermal agents due to their longitudinal absorption band in the NIR on account of their SPR oscillations [65, 66, 69]. Small diameter Au-nanorods are being used as photothermal converters of near infrared radiation (NIR) for *in vivo* applications due

to their high absorption cross-sections beyond the tissue absorption spectra. Since NIR light transmits readily through human skin and tissue, these nanorods can be used as ablation components for cancer [70, 71]. Other gold nanostructures such as Au-nanoshells [72–74], Au-nanocages [67, 75, 76], and spherical AuNPs [77] have also demonstrated effective photothermal destruction of cancer cells and tissue. PEG-modified Au-nanoshells (Silica/Au core/shell NPs) injected intravenously in tumor-bearing mice showed to passively accumulate in the tumor tissue due to the leakiness of the tumor vasculature. The rapid heating of Au-nanoshells upon NIR laser irradiation allowed for effective photothermal ablation of tumor in the mouse [78]. A similar approach was used by Terentyuk et al., where plasmonic silica/gold nanoshells were used to produce a controllable laser hyperthermia in tissues, thus enhancing the photothermal effect in cancer cells [79]. Sirotkina et al. described the use of AuNPs for skin tumor therapy based on local laser-inducing hyperthermia. After intravenous injection, the AuNPs accumulated in the skin tumor cells after 4-5 hours and induced apoptotic death of tumor cells, completely inhibiting the tumor growth after just five days of treatment [80].

The photothermal properties of AuNPs can also be used to generate transient vapor nanobubbles in order to produce a tunable nanoscale theranostic agent, described as plasmonic nanobubbles [81]. These nanobubbles are generated when the AuNPs are locally overheated with short laser pulses, due to the evaporation of a very thin volume of the surrounding medium, which in turn creates a vapor nanobubble that expands and collapses within nanoseconds. Plasmonic nanobubbles have been successfully applied as an *in vivo* tunable theranostic cellular agent in zebrafish hosting prostate cancer xenografts and in leukemia cells of human bone marrow specimens, presenting higher therapeutic selectivity when compared with AuNPs alone [82, 83]. The use of noninvasive radiowaves at 13.56 MHz have also been shown to induce heat in AuNPs and thermally destroy tumor tissue [84]. *In vivo* rat exposures to 35 Watts using direct AuNPs injections resulted in significant thermal injury at subcutaneous injection sites. Radio waves have the advantage of presenting significantly better penetration on tissue than NIR light, making them more efficient for deeper solid tumors [85]. Nonetheless, despite their greater depth of penetration, there is also greater energy attenuation by tissue.

Gold-silver-(AuAg-) nanorods labeled with molecular aptamers proved to require up to six orders of lower laser power irradiation to induce cell death when compared to Au-nanoshells or Au-nanorods [86]. These aptamer Scg8-AuAg-nanorods conjugates presented excellent hyperthermia efficiency and selectivity to CEM cells, exceeding the affinity of the original aptamer probes alone. Bimetallic AuAg-nanostructures with a dendrite morphology and hollow interior have also been developed as photothermal absorbers to destroy A549 lung cancer cells [87]. The photothermal performance of such dendrites required lower NP concentrations and laser power for efficient cancer cell damage when compared to Au-nanorods photothermal therapeutic agents. Likewise, Cheng and coworkers evaluated the photothermal efficiencies of three Au-based nanomaterials (silica@Au-nanoshells, hollow Au/Ag nanospheres and Au-nanorods) at killing three types of malignant cells (A549 lung cancer cells, HeLa cervix cancer cells, and TCC bladder cancer cells) using a CW NIR laser [88]. Silica@Au-nanoshells needed the lowest NP concentration for effective photo-ablation, whereas hollow Au/Ag nanospheres and Au-nanorods needed increasingly higher concentrations.

Gold has also been used together with magnetic or paramagnetic materials to enhance the photothermal effect and, thus, increase cancer cell death [89, 90].

2.4. Drug Delivery. The vast majority of clinically used drugs for cancer are low molecular-weight compounds that diffuse rapidly into healthy tissues being evenly distributed within the body, exhibit a short half-life in the blood stream and a high overall clearance rate. As a consequence, relatively small amounts of the drug reach the target site, and distribution into healthy tissues leads to severe side effects. Poor drug delivery and residence at the target site leads to significant complications, such as multidrug resistance [91]. As seen above, nanoparticles can be used as vectors for targeting cancer tissue/cells so as to optimize biodistribution of drugs. The NPs' performance as drug vectors depends on the size and surface functionalities of the particles, drug release rate, and particle disintegration. These systems show evidence of enhanced delivery of unstable drugs, more targeted distribution and capability to evade/bypass biological barriers.

AuNPs have already been used as vehicles for the delivery of anticancer drugs, such as paclitaxel- [92] or Platinum-(Pt-) based drugs (e.g., cisplatin, oxaliplatin, etc.) [93, 94]. Gibson et al. described the first example of 2 nm AuNPs covalently functionalized with the chemotherapeutic drug paclitaxel [92]. The administrations of hydrophobic drugs require molecular encapsulation, and it is found that nanosized particles are particularly efficient in evading the reticuloendothelial system [95]. Gold-gold sulfide nanoshells covered by a thermosensitive hydrogel matrix have been developed as a photothermal modulated drug-delivery system [96]. These nanoshell-composite hydrogels were designed to strongly absorb NIR light and release multiple bursts of any soluble material held within the hydrogel matrix in response to repeated NIR irradiation. More recently, Yavuz and coworkers developed a similar approach using 50-nm hollow Au-nanocubes (nanocages) with eight lopped-off porous corners covered by a thermosensitive polymer containing a preloaded effector that can be later released in a controllable fashion using an NIR laser [18].

2.5. Radiotherapy. Radiotherapy uses ionizing radiation for cancer treatment to control the proliferation of malignant cells. Nonetheless, the delivery of a lethal dose of radiation to a tumor while sparing nearby healthy tissues remains the greatest challenge in radiation therapy. Noble metal NPs can act as antennas, providing enhanced radiation targeting with lower radiation doses, consequently avoiding damage to healthy tissues. The irradiation may also be used to activate the NPs and set up the release of their cytotoxic action. AuNPs, upon X-ray irradiation, can act as dose enhancers and/or generate radicals that damage cancer cells and induce

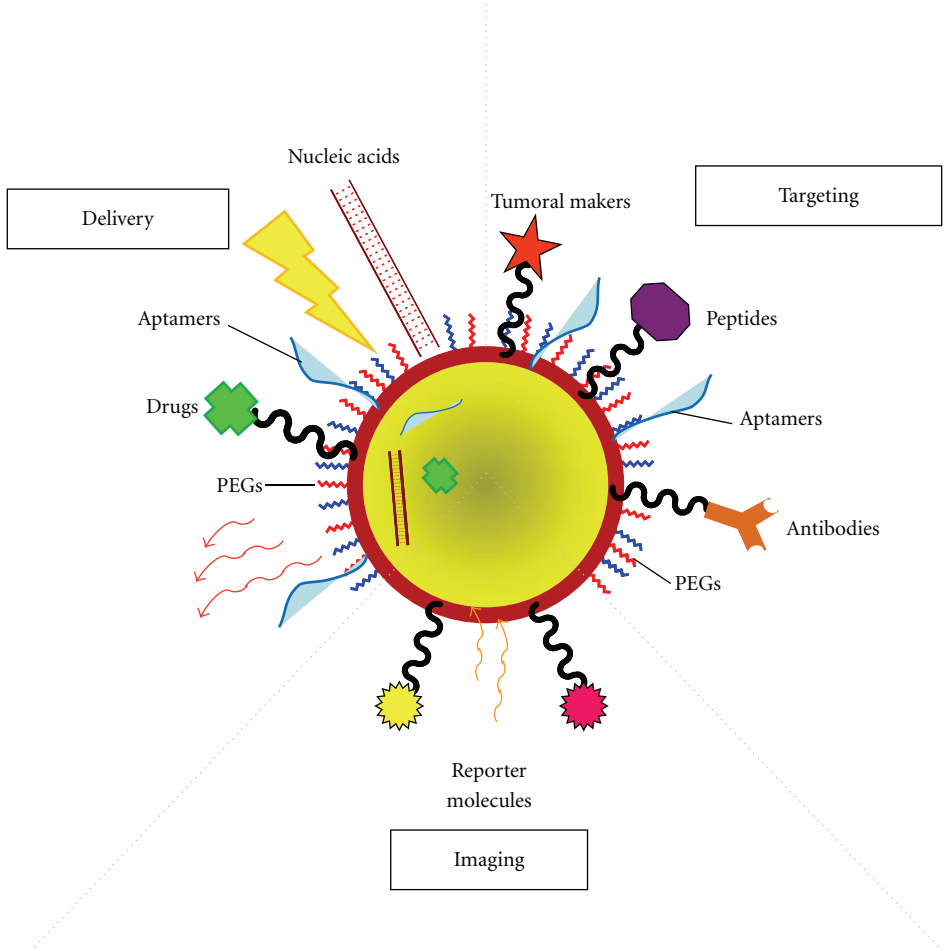

Figure 2: Multifunctional NP-based systems for tumor targeting, delivery and imaging. These innovative NPs comprise nucleic acids, aptamers and anticancer drug molecules for delivery to the target tissue. Depending on the targeting mechanism, they can be on the surface or inside the NPs. Responsive NPs/molecules can also trigger reaction upon external stimuli through the functionality of valuable tumor markers, peptides, polymers and antibodies that can used to improve NP circulation, effectiveness and selectivity. Multifunctional systems can carry reporter molecules tethered to the particle surface and employed as tracking and/or contrast agents.

cell apoptosis and have been proposed as potential radiosensitizers for X-ray cancer therapy [97]. The use of this strategy has led to improvement in the treatment on cancer cells with little or no increase in harm to normal surrounding tissues in mice models [15] and also in breast cancer [98]. More recently, Xu and coworkers studied the potential effects on radiation-induced killing of glioma cells mediated by 10, 20, and 40 nm AuNPs and 20, 50, and 100 nm silver nanoparticles (AgNPs), all modified with proteins from fetal bovine serum [99]. Treating glioma cells with AgNPs led to radiation dose-dependent cytotoxicity, with smaller size particles (20 and 50 nm) being the most cytotoxic at relatively harmless radiation doses. In this study, AuNPs showed little effect on cell survival across different doses of ionizing radiation, which contrasted with the results of previous studies performed with AuNPs coated with PEG or amino acids in mice colorectal adenocarcinoma and breast cancer cells [15, 98]. Hypothetically, the different coatings of the AuNPs used may be responsible for the different outcomes observed.

The use of platinum NPs (PtNPs) as prominent radiation sensitizers in radiotherapy cancer treatment showed strong enhancement of the biological efficiency of radiations, leading to amplified lethal damage in DNA from tumor cells, when compared to metal atoms [37].

3. Imaging

Along with their therapeutic capabilities, most noble metal NPs can be used for the simultaneous actuation and tracking *in vivo*—see Figure 2. Because light absorption from biologic tissue components is minimized at near infrared (NIR) wavelengths, most noble metal NPs for *in vivo* imaging and therapy have been designed to strongly absorb in the NIR so as to be used as effective contrast agents [100]. However, noble metal nanomaterials, such as NPs, nanoshells, nanoclusters, nanocages, and nanorods, have showed widespread application as contrast agents for *in vivo* cancer imaging: those presenting a significant absorbance and scattering in the NIR region [46, 101] or surface-enhanced Raman scattering (SERS) [102], or as contrast agents for computed

tomography (CT) [103], magnetic resonance imaging (MRI) [104], optical coherence tomography (OCT) [105–107], and photoacoustic imaging (PAI) [108]. Moreover, most noble metal nanomaterials are capable of combining multiple imaging modalities that can yield complementary information and offer synergistic advantages over any single imaging technique [109, 110].

Three-dimensional imaging can be achieved by computed tomography (CT), where a series of plane-cross-sectional images along an axis are interlinked by computer to create a 3D image. Typically, the cross-sectional images are acquired using X-ray radiation involving larger radiation doses than the conventional X-ray imaging procedures, which could lead to increased risk to public health [111]. The use of ~30 nm PEG-coated AuNPs for *in vivo* CT contrast agent was shown to increase image contrast, which allows to reduce the radiation dosage needed, allow to overcome the limitations of conventional contrast agents (e.g., iodine-based compounds), such as short imaging times due to rapid renal clearance, renal toxicity, and vascular permeation [103]. Hybrid NPs with a super-paramagnetic iron oxide/silica core and a gold nanoshell, with significant absorbance and scattering in the NIR region, have been used *in vivo* as dual contrast agents for CT and magnetic resonance imaging (MRI) presenting high CT attenuation and a good MR signal in hepatoma, compensating for the weakness of each modality [112].

Optical coherence tomography (OCT) is an imaging modality that provides cross-sectional subsurface imaging of biological tissue with micrometer scale resolution. The extra scattering achieved by using Au-nanoshells has been shown to provide an enhanced optical contrast and brightness for improved diagnostic imaging of tumors in mice due to the preferential accumulation of the nanoshells in the tumor. [78]. Tseng et al. developed nanorings with a localized surface plasmon resonance covering a spectral range of 1300 nm that produced both photothermal and image contrast enhancement effects in OCT when delivered into pig adipose samples [113]. Moreover, the image contrast enhancement effect could be isolated by continuously scanning the sample with a lower scan frequency, allowing to effectively control the therapeutic modality. Similarly, gold capped nanoroses have been used in photothermal OCT to detect macrophages in *ex vivo* rabbit arteries [114].

Photoacoustic imaging (PAI) and photoacoustic tomography (PAT) are noninvasive imaging techniques capable of resolving the optical absorption map of tissue at penetration depths akin with ultrasound imaging. Wang and coworkers have used this technique to image the distribution of Au-nanoshells circulating in the vasculature of a rat brain by achieving a gradual enhancement of the NIR optical absorption in the brain vessels [115]. These Au-nanocages enhanced the contrast between blood and the surrounding tissues by up to 81%, allowing a more detailed image of vascular structures at greater depths. Additionally, these nanocages were shown to be better suited for *in vivo* applications, specially due to their more compact size (<50 nm compared to >100 nm for Au-nanoshells) and larger optical absorption cross sections when compared to Au-nanoshells. Gold-nanorods show the maximum of the plasmon resonance tuned further into the NIR that allowed Motamedi et al. to develop a contrast agent for a laser optoacoustic imaging system for *in vivo* detection of gold nanorods and to enhance the diagnostic power of optoacoustic imaging [116]. Song et al. proposed a noninvasive *in vivo* spectroscopic photoacoustic sentinel lymph node mapping using gold nanorods as lymph node tracers in a rat model [117].

Also, noble metal NP probes can be used for *in situ* diagnostics of cancer. For example, NP-based NIR probes can overcome several limitations of conventional NIR organic dyes, such as poor hydrophilicity and photostability, low quantum yield and detection sensitivity, insufficient stability in biological systems, and weak multiplexing capability. Additionally, the high scattering properties of these NPs can enhance contrast of imaging systems based on microscopy, such as dark-field or dual-photon luminescence microscopy. Zhang et al. developed fluorescent metal nanoshells as molecular imaging agents to detect single microRNA (miRNA) molecules in lung cancer cells [47]. These metal nanoshells were composed of silica spheres with encapsulated $Ru(bpy)_3^{2+}$ complexes as core and thin silver layers as shell. The silver shell allowed to enhance emission intensity up to 6-fold and photostability by 2-fold, as well as to achieve longer lifetime emission signals that overcome cellular autofluorescence interference. Loo et al. demonstrated the use of NIR scattering Au-nanoshells as a contrast agent in dark-field microscopy to target antihuman epidermal growth factor receptor 2 (HER2), a clinically significant breast cancer molecular marker [72]. These Au-nanoshells were also used by Bickford et al. for imaging live HER2-overexpressing cancer cells using two-photon microscopy [118].

Surface-enhanced Raman scattering (SERS) using Au- or AgNPs with an attached reporter species with a Raman signature can be explored to highlight cellular structures and provide molecular structural information on the cellular environment in live cells [119, 120]. The use of such NPs allows for higher spectral specificity, multiplex capabilities, improved contrast and photostability to Raman-based imaging techniques. *In situ* monitoring of photothermal nanotherapy of LNCaP human prostate cancer cells by SERS was a significant enhancement of the Raman signal intensity by several orders of magnitude that have been observed [44].

4. Toxicity

Both *in vivo* and *in vitro*, nanoparticles have a tendency to accumulate within various types of cells with special affinity for macrophage-type cells (both histiocytes and blood phagocytic cells) and reticuloendothelial cells throughout the body. They also produce varying degrees of bioaccumulation in such tissues as lymph nodes, bone marrow, spleen, adrenals, liver, and kidneys [121–123]. The NPs size plays an important role in avoiding immune activation and renal clearance, thus enhancing their circulating time and availability for effective therapy. For example, hydrophilic NPs ranging in size between 10 and 100 nm are small enough to slow down activation of the mononuclear phagocyte

system but are big enough to avoid renal filtration [8]. Research shows that NPs can stimulate and/or suppress the immune responses and that their compatibility with the immune system is largely determined by their surface chemistry. In fact, the influence of size, solubility, and surface modification on the biocompatibility of NPs and their use in biological applications is well known [122]. In terms of acute toxic effects to cells, noble metal NPs have been shown to induce DNA damage and oxidative damage [124–126].

Generally, AuNPs are considered to be benign, but the size similarity to biological molecules could provide "camouflage" to cellular barriers, leading to undesired cellular entry which might be detrimental to normal cellular function [127]. A systematic investigation of the size-dependent cytotoxicity of AuNPs against four cell lines found that 1 to 2 nm AuNPs displayed cell-type-dependent cytotoxicity with high micromolar IC50s, whereas 15 nm AuNPs were nontoxic to cells at concentrations 60-fold higher than the IC50 of the smaller AuNPs [128]. These results seemed to confirm size-dependent toxicity of AuNPs, an inference that has hitherto been shown to be somewhat ambivalent [129–134]. In fact, Yen et al. showed that AuNPs, especially those of smaller sizes, dramatically led to a decrease in the population of the macrophages and upregulated the expressions of proinflammatory genes interlukin-1, interlukin-6, and tumor necrosis factor alpha [135]. Sun et al. studied the *in vivo* toxicity of AuNPs according to their shape in KM mice showing that rod-shaped AuNPs were the most toxic, followed by cube-shaped AuNPs, while sphere-shaped AuNPs displayed the best biocompatibility, revealing that toxicity is shape dependent. Moreover, this study revealed that all AuNPs accumulated preferentially in the liver and spleen organs [136]. Nonetheless, it is worth pointing out that CTAB (a cationic surfactant commonly used for Au-nanorods synthesis) was also recently pointed out as the source of Au-nanorods' cytotoxicity, which may explain their toxicity in the previous studies [137].

Silver NPs are generally considered more toxic than AuNPs, with several studies showing that cell exposure to AgNPs induced significant cytotoxicity [138–141]. Conversely, Yen et al. determined a lower cytotoxicity of AgNPs than that of the AuNPs and attributed this difference to the surface charges between NPs, which can explain the discrepancy with other studies related to AgNPs cytotoxicity [135].

As for platinum, the cytotoxicity of 5–8 nm PtNPs capped with polyvinyl alcohol (PVA) has been addressed in human cells, where PtNPs were shown to enter the cells through diffusion, leading to an increase in DNA damage, proliferating cell nuclear antigen-mediated growth arrest and apoptosis [126]. Asharani et al. performed a comparison between toxicity of 3–10 nm Pt-, 5–35 nm Ag-, and 15–35 nm AuNPs capped with PVA in developing zebrafish embryos, concluding that AgNPs were the most toxic, followed by PtNPs, while AuNPs presented no indication of toxicity [142].

Even though we have focused our attention on the toxicity aspects of the different noble metal nanoparticles based mainly on size and metal, attention should also be brought upon other properties of the nanoconjugates, such as surface chemistry, shape, and administration pathways. In fact, surface chemistry (e.g., functionalization with biomolecules, stabilizers, etc.) constitutes another interface of interaction with the organism's proteins and cells, which in term may be associated with unspecific adsorption or specific recognition by the immune system, thus contributing to the overall effects of the use of the nanoparticles. The interaction with the immune system contributes not only for the specificity of the targeting (passive and/or active), but also towards the toxicological effect of nanoconjugates (see [122] and references therein).

5. Conclusions

Nanotechnology has provided for novel and powerful systems that may be used treatment and diagnostic of cancer. *In vivo* demonstrations of noble metal NPs as theranostic agents are now emerging and serve as important milestones towards clinical application. Nonetheless, the majority of products, reagents and drugs being used for the development of these nanoscale theranostic agents have still to be approved by the main supervising agencies, such as the FDA and EMA. Thus far, there are some questions whose answers still provide no clear understanding about the design and application of NPs, such as pharmacokinetics, biodistribution and side effects of the nanotherapy, and safety profile of NPs before and after conjugation and toxicity [10]. Are noble metal NPs cytotoxic or biocompatible? And how can the NPs be design to avoid these effects? These seem to question more difficult to answer than previously believed. Most therapeutic and imaging approaches based on noble metal NPs rely on AuNPs, mostly due to their higher level of nontoxicity. Nonetheless, a more comprehensive application of core/shell or alloy noble metal NPs, that may allow combination of the benefits of each noble metal into a single carrier, is still to be thoroughly addressed. Even though there is not any general mechanism for making NPs universally "nontoxic" to all living cells and all organisms, there are important findings that can be applied for increasing nanoparticle biocompatibility and reducing cytotoxic interactions *in vivo* and *in vitro*. In general, using the lowest NP dose to get the desired response for the shortest period of time seems to promote biocompatibility. The coating/capping of a nanoparticle is also of the utmost relevance, since a noncontinuous covering, the presence of cracks, roughness, or interruptions could lead to complement or antibody attachment, or dissolution of the coating by cell digestion, decreasing bioavailability at target cell [143]. It is essential to test nanoparticle/biological interactions experimentally and modify the NPs for best biocompatibility with the cell in order to eliminate damage to healthy tissue, guarding against alterations in genetic/molecular function while killing the abnormal cells. When interpreting NPs interactions with biological cells and organisms, it is important to remember that living systems may appear normal and be capable of growth and function, but they may be genetically altered in subtle ways following NP exposure, which can produce serious consequences at some time in the distant future, such as cancer itself.

Noble metal nanoparticles have shown to be powerful tools against cancer though still in need of further optimization and characterization for full understanding of their whole potential. It is now time to start translating these promising platforms to the clinical settings towards widespread effective therapy strategies in the fight against cancer.

Acknowledgments

The authors acknowledge FCT/MCTES (Portugal) and CIGMH for financial support.

References

[1] A. Jemal, R. Siegel, J. Xu, and E. Ward, "Cancer statistics, 2010," *CA Cancer Journal for Clinicians*, vol. 60, no. 5, pp. 277–300, 2010.

[2] A. Balmain, J. Gray, and B. Ponder, "The genetics and genomics of cancer," *Nature Genetics*, vol. 33, pp. 238–244, 2003.

[3] D. Hanahan and R. A. Weinberg, "The hallmarks of cancer," *Cell*, vol. 100, no. 1, pp. 57–70, 2000.

[4] B. A. J. Ponder, "Cancer genetics," *Nature*, vol. 411, no. 6835, pp. 336–341, 2001.

[5] N. P. Praetorius and T. K. Mandal, "Engineered nanoparticles in cancer therapy," *Recent Patents on Drug Delivery & Formulation*, vol. 1, no. 1, pp. 37–51, 2007.

[6] M. Ferrari, "Cancer nanotechnology: opportunities and challenges," *Nature Reviews Cancer*, vol. 5, no. 3, pp. 161–171, 2005.

[7] D. Peer, J. M. Karp, S. Hong, O. C. Farokhzad, R. Margalit, and R. Langer, "Nanocarriers as an emerging platform for cancer therapy," *Nature Nanotechnology*, vol. 2, no. 12, pp. 751–760, 2007.

[8] P. R. Gil and W. J. Parak, "Composite nanoparticles take aim at cancer," *ACS Nano*, vol. 2, no. 11, pp. 2200–2205, 2008.

[9] N. Sanvicens and M. P. Marco, "Multifunctional nanoparticles—properties and prospects for their use in human medicine," *Trends in Biotechnology*, vol. 26, no. 8, pp. 425–433, 2008.

[10] P. V. Baptista, "Cancer nanotechnology—prospects for cancer diagnostics and therapy," *Current Cancer Therapy Reviews*, vol. 5, no. 2, pp. 80–88, 2009.

[11] J. R. Heath and M. E. Davis, "Nanotechnology and cancer," *Annual Review of Medicine*, vol. 59, pp. 251–265, 2008.

[12] S. T. Selvan, T. T. Y. Tan, D. K. Yi, and N. R. Jana, "Functional and multifunctional nanoparticles for bioimaging and biosensing," *Langmuir*, vol. 26, no. 14, pp. 11631–11641, 2010.

[13] P. Baptista, E. Pereira, P. Eaton et al., "Gold nanoparticles for the development of clinical diagnosis methods," *Analytical and Bioanalytical Chemistry*, vol. 391, no. 3, pp. 943–950, 2008.

[14] X. Huang, P. K. Jain, I. H. El-Sayed, and M. A. El-Sayed, "Gold nanoparticles: interesting optical properties and recent applications in cancer diagnostics and therapy," *Nanomedicine*, vol. 2, no. 5, pp. 681–693, 2007.

[15] J. F. Hainfeld, D. N. Slatkin, and H. M. Smilowitz, "The use of gold nanoparticles to enhance radiotherapy in mice," *Physics in Medicine and Biology*, vol. 49, no. 18, pp. N309–N315, 2004.

[16] J. F. Hainfeld, F. A. Dilmanian, D. N. Slatkin, and H. M. Smilowitz, "Radiotherapy enhancement with gold nanoparticles," *Journal of Pharmacy and Pharmacology*, vol. 60, no. 8, pp. 977–985, 2008.

[17] L. R. Hirsch, R. J. Stafford, J. A. Bankson et al., "Nanoshell-mediated near-infrared thermal therapy of tumors under magnetic resonance guidance," *Proceedings of the National Academy of Sciences of the United States of America*, vol. 100, no. 23, pp. 13549–13554, 2003.

[18] M. S. Yavuz, Y. Cheng, J. Chen et al., "Gold nanocages covered by smart polymers for controlled release with near-infrared light," *Nature Materials*, vol. 8, no. 12, pp. 935–939, 2009.

[19] G. Han, P. Ghosh, and V. M. Rotello, "Multi-functional gold nanoparticles for drug delivery," *Advances in Experimental Medicine and Biology*, vol. 620, pp. 48–56, 2007.

[20] M. Thomas and A. M. Klibanov, "Conjugation to gold nanoparticles enhances polyethylenimine's transfer of plasmid DNA into mammalian cells," *Proceedings of the National Academy of Sciences of the United States of America*, vol. 100, no. 16, pp. 9138–9143, 2003.

[21] M. R. Jones, J. E. Millstone, D. A. Giljohann, D. S. Seferos, K. L. Young, and C. A. Mirkin, "Plasmonically controlled nucleic acid dehybridization with gold nanoprisms," *ChemPhysChem*, vol. 10, no. 9-10, pp. 1461–1465, 2009.

[22] S. Bhattacharyya, R. A. Kudgus, R. Bhattacharya, and P. Mukherjee, "Inorganic nanoparticles in cancer therapy," *Pharmaceutical Research*, vol. 28, no. 2, pp. 237–259, 2011.

[23] P. Ghosh, G. Han, M. De, C. K. Kim, and V. M. Rotello, "Gold nanoparticles in delivery applications," *Advanced Drug Delivery Reviews*, vol. 60, no. 11, pp. 1307–1315, 2008.

[24] N. Nishiyama, "Nanomedicine: nanocarriers shape up for long life," *Nature Nanotechnology*, vol. 2, no. 4, pp. 203–204, 2007.

[25] J. Xie, S. Lee, and X. Chen, "Nanoparticle-based theranostic agents," *Advanced Drug Delivery Reviews*, vol. 62, no. 11, pp. 1064–1079, 2010.

[26] T. K. Sau, A. L. Rogach, F. Jäckel, T. A. Klar, and J. Feldmann, "Properties and applications of colloidal nonspherical noble metal nanoparticles," *Advanced Materials*, vol. 22, no. 16, pp. 1805–1825, 2010.

[27] R. A. Sperling, P. R. Gil, F. Zhang, M. Zanella, and W. J. Parak, "Biological applications of gold nanoparticles," *Chemical Society Reviews*, vol. 37, no. 9, pp. 1896–1908, 2008.

[28] P. K. Jain, X. Huang, I. H. El-Sayed, and M. A. El-Sayed, "Noble metals on the nanoscale: optical and photothermal properties and some applications in imaging, sensing, biology, and medicine," *Accounts of Chemical Research*, vol. 41, no. 12, pp. 1578–1586, 2008.

[29] K. S. Lee and M. A. El-Sayed, "Gold and silver nanoparticles in sensing and imaging: sensitivity of plasmon response to size, shape, and metal composition," *Journal of Physical Chemistry B*, vol. 110, no. 39, pp. 19220–19225, 2006.

[30] R. A. Sperling and W. J. Parak, "Surface modification, functionalization and bioconjugation of colloidal Inorganic nanoparticles," *Philosophical Transactions of the Royal Society A*, vol. 368, no. 1915, pp. 1333–1383, 2010.

[31] H. Chen, L. Shao, T. Ming et al., "Understanding the photothermal conversion efficiency of gold nanocrystals," *Small*, vol. 6, no. 20, pp. 2272–2280, 2010.

[32] E. S. Day, J. G. Morton, and J. L. West, "Nanoparticles for thermal cancer therapy," *Journal of Biomechanical Engineering*, vol. 131, no. 7, Article ID 740011, 2009.

[33] P. Chandra, D. Das, and A. A. Abdelwahab, "Gold nanoparticles in molecular diagnostics and therapeutics," *Digest Journal of Nanomaterials and Biostructures*, vol. 5, no. 2, pp. 363–367, 2010.

[34] Y. Liu, H. Miyoshi, and M. Nakamura, "Nanomedicine for drug delivery and imaging: a promising avenue for cancer therapy and diagnosis using targeted functional nanoparticles," *International Journal of Cancer*, vol. 120, no. 12, pp. 2527–2537, 2007.

[35] A. G. Cuenca, H. Jiang, S. N. Hochwald, M. Delano, W. G. Cance, and S. R. Grobmyer, "Emerging implications of nanotechnology on cancer diagnostics and therapeutics," *Cancer*, vol. 107, no. 3, pp. 459–466, 2006.

[36] A. C. Powell, G. F. Paciotti, and S. K. Libutti, "Colloidal gold: a novel nanoparticle for targeted cancer therapeutics," *Methods in Molecular Biology*, vol. 624, pp. 375–384, 2010.

[37] E. Porcel, S. Liehn, H. Remita et al., "Platinum nanoparticles: a promising material for future cancer therapy?" *Nanotechnology*, vol. 21, no. 8, p. 85103, 2010.

[38] C. Minelli, S. B. Lowe, and M. M. Stevens, "Engineering nanocomposite materials for cancer therapy," *Small*, vol. 6, no. 21, pp. 2336–2357, 2010.

[39] T. Stuchinskaya, M. Moreno, M. J. Cook, D. R. Edwards, and D. A. Russell, "Targeted photodynamic therapy of breast cancer cells using antibody-phthalocyanine-gold nanoparticle conjugates," *Photochemical and Photobiological Sciences*, vol. 10, no. 5, pp. 822–831, 2011.

[40] V. Raji, J. Kumar, C. S. Rejiya, M. Vibin, V. N. Shenoi, and A. Abraham, "Selective photothermal efficiency of citrate capped gold nanoparticles for destruction of cancer cells," *Experimental Cell Research*, vol. 317, no. 14, pp. 2052–2058, 2011.

[41] P. Mukherjee, R. Bhattacharya, N. Bone et al., "Potential therapeutic application of gold nanoparticles in B-chronic lymphocytic leukemia (BCLL): enhancing apoptosis," *Journal of Nanobiotechnology*, vol. 5, p. 4, 2007.

[42] D. A. Giljohann, D. S. Seferos, A. E. Prigodich, P. C. Patel, and C. A. Mirkin, "Gene regulation with polyvalent siRNA-nanoparticle conjugates," *Journal of the American Chemical Society*, vol. 131, no. 6, pp. 2072–2073, 2009.

[43] K. A. Whitehead, R. Langer, and D. G. Anderson, "Knocking down barriers: advances in siRNA delivery," *Nature Reviews Drug Discovery*, vol. 8, no. 2, pp. 129–138, 2009.

[44] W. Lu, A. K. Singh, S. A. Khan, D. Senapati, H. Yu, and P. C. Ray, "Gold nano-popcorn-based targeted diagnosis, nanotherapy treatment, and in situ monitoring of photothermal therapy response of prostate cancer cells using surface-enhanced raman spectroscopy," *Journal of the American Chemical Society*, vol. 132, no. 51, pp. 18103–18114, 2010.

[45] X. Qian, X. H. Peng, D. O. Ansari et al., "In vivo tumor targeting and spectroscopic detection with surface-enhanced Raman nanoparticle tags," *Nature Biotechnology*, vol. 26, no. 1, pp. 83–90, 2008.

[46] X. He, J. Gao, S. S. Gambhir, and Z. Cheng, "Near-infrared fluorescent nanoprobes for cancer molecular imaging: status and challenges," *Trends in Molecular Medicine*, vol. 16, no. 12, pp. 574–583, 2010.

[47] J. Zhang, Y. Fu, Y. Mei, F. Jiang, and J. R. Lakowicz, "Fluorescent metal nanoshell probe to detect single mirna in lung cancer cell," *Analytical Chemistry*, vol. 82, no. 11, pp. 4464–4471, 2010.

[48] Y. Fichou and C. Férec, "The potential of oligonucleotides for therapeutic applications," *Trends in Biotechnology*, vol. 24, no. 12, pp. 563–570, 2006.

[49] N. Toub, C. Malvy, E. Fattal, and P. Couvreur, "Innovative nanotechnologies for the delivery of oligonucleotides and siRNA," *Biomedicine and Pharmacotherapy*, vol. 60, no. 9, pp. 607–620, 2006.

[50] A. Fire, S. Xu, M. K. Montgomery, S. A. Kostas, S. E. Driver, and C. C. Mello, "Potent and specific genetic interference by double-stranded RNA in caenorhabditis elegans," *Nature*, vol. 391, no. 6669, pp. 806–811, 1998.

[51] M. Baker, "RNA interference: from tools to therapies," *Nature*, vol. 464, no. 7292, p. 1225, 2010.

[52] O. Milhavet, D. S. Gary, and M. P. Mattson, "RNA interference in biology and medicine," *Pharmacological Reviews*, vol. 55, no. 4, pp. 629–648, 2003.

[53] N. R. Wall and Y. Shi, "Small RNA: can RNA interference be exploited for therapy?" *The Lancet*, vol. 362, no. 9393, pp. 1401–1403, 2003.

[54] G. J. Hannon and J. J. Rossi, "Unlocking the potential of the human genome with RNA interference," *Nature*, vol. 431, no. 7006, pp. 371–378, 2004.

[55] N. L. Rosi, D. A. Giljohann, C. S. Thaxton, A. K. R. Lytton-Jean, M. S. Han, and C. A. Mirkin, "Oligonucleotide-modified gold nanoparticles for infracellular gene regulation," *Science*, vol. 312, no. 5776, pp. 1027–1030, 2006.

[56] J. S. Lee, J. J. Green, K. T. Love, J. Sunshine, R. Langer, and D. G. Anderson, "Gold, poly(β-amino ester) nanoparticles for small interfering RNA delivery," *Nano Letters*, vol. 9, no. 6, pp. 2402–2406, 2009.

[57] G. B. Braun, A. Pallaoro, G. Wu et al., "Laser-activated gene silencing via gold nanoshell-siRNA conjugates," *ACS Nano*, vol. 3, no. 7, pp. 2007–2015, 2009.

[58] S. Guo, Y. Huang, Q. Jiang et al., "Enhanced gene delivery and siRNA silencing by gold nanoparticles coated with charge-reversal polyelectrolyte," *ACS Nano*, vol. 4, no. 9, pp. 5505–5511, 2010.

[59] S. H. Lee, K. H. Bae, S. H. Kim, K. R. Lee, and T. G. Park, "Amine-functionalized gold nanoparticles as non-cytotoxic and efficient intracellular siRNA delivery carriers," *International Journal of Pharmaceutics*, vol. 364, no. 1, pp. 94–101, 2008.

[60] A. R. Wadhwani, W. L. Klein, and P. N. Lacor, "Efficient gene silencing in neural cells by functionalized gold nanoparticles," *Nanoscape*, vol. 7, no. 1, pp. 6–10, 2010.

[61] R. B. Roemer, "Engineering aspects of hyperthermia therapy," *Annual Review of Biomedical Engineering*, vol. 1, pp. 347–376, 1999.

[62] P. Cherukuri, E. S. Glazer, and S. A. Curley, "Targeted hyperthermia using metal nanoparticles," *Advanced Drug Delivery Reviews*, vol. 62, no. 3, pp. 339–345, 2010.

[63] D. P. O'Neal, L. R. Hirsch, N. J. Halas, J. D. Payne, and J. L. West, "Photo-thermal tumor ablation in mice using near infrared-absorbing nanoparticles," *Cancer Letters*, vol. 209, no. 2, pp. 171–176, 2004.

[64] M. Johannsen, U. Gneveckow, L. Eckelt et al., "Clinical hyperthermia of prostate cancer using magnetic nanoparticles: presentation of a new interstitial technique," *International Journal of Hyperthermia*, vol. 21, no. 7, pp. 637–647, 2005.

[65] X. Huang, P. K. Jain, I. H. El-Sayed, and M. A. El-Sayed, "Determination of the minimum temperature required for selective photothermal destruction of cancer cells with the use of immunotargeted gold nanoparticles," *Photochemistry and Photobiology*, vol. 82, no. 2, pp. 412–417, 2006.

[66] X. Huang, I. H. El-Sayed, W. Qian, and M. A. El-Sayed, "Cancer cell imaging and photothermal therapy in the near-infrared region by using gold nanorods," *Journal of the American Chemical Society*, vol. 128, no. 6, pp. 2115–2120, 2006.

[67] J. Chen, D. Wang, J. Xi et al., "Immuno gold nanocages with tailored optical properties for targeted photothermal

destruction of cancer cells," *Nano Letters*, vol. 7, no. 5, pp. 1318–1322, 2007.

[68] Y. Haba, C. Kojima, A. Harada, T. Ura, H. Horinaka, and K. Kono, "Preparation of poly(ethylene glycol)-modified poly(amido amine) dendrimers encapsulating gold nanoparticles and their heat-generating ability," *Langmuir*, vol. 23, no. 10, pp. 5243–5246, 2007.

[69] X. Huang, I. H. El-Sayed, and M. A. El-Sayed, "Applications of gold nanorods for cancer imaging and photothermal therapy," *Methods in Molecular Biology*, vol. 624, pp. 343–357, 2010.

[70] W. S. Kuo, C. N. Chang, Y. T. Chang et al., "Gold nanorods in photodynamic therapy, as hyperthermia agents, and in near-infrared optical imaging," *Angewandte Chemie—International Edition*, vol. 49, no. 15, pp. 2711–2715, 2010.

[71] L. Tong, Q. Wei, A. Wei, and J. X. Cheng, "Gold nanorods as contrast agents for biological imaging: optical properties, surface conjugation and photothermal effects," *Photochemistry and Photobiology*, vol. 85, no. 1, pp. 21–32, 2009.

[72] C. Loo, A. Lowery, N. Halas, J. West, and R. Drezek, "Immunotargeted nanoshells for integrated cancer imaging and therapy," *Nano Letters*, vol. 5, no. 4, pp. 709–711, 2005.

[73] C. Loo, L. Hirsch, M. H. Lee et al., "Gold nanoshell bioconjugates for molecular imaging in living cells," *Optics Letters*, vol. 30, no. 9, pp. 1012–1014, 2005.

[74] S. Lal, S. E. Clare, and N. J. Halas, "Nanoshell-enabled photothermal cancer therapy: impending clinical impact," *Accounts of Chemical Research*, vol. 41, no. 12, pp. 1842–1851, 2008.

[75] S. E. Skrabalak, L. Au, X. Lu, X. Li, and Y. Xia, "Gold nanocages for cancer detection and treatment," *Nanomedicine*, vol. 2, no. 5, pp. 657–668, 2008.

[76] Y. Xia, W. Li, C. M. Cobley et al., "Gold nanocages: from synthesis to theranostic applications," *Accounts of Chemical Research*. In press.

[77] X. Huang, P. K. Jain, I. H. El-Sayed, and M. A. El-Sayed, "Plasmonic photothermal therapy (PPTT) using gold nanoparticles," *Lasers in Medical Science*, vol. 23, no. 3, pp. 217–228, 2008.

[78] A. M. Gobin, M. H. Lee, N. J. Halas, W. D. James, R. A. Drezek, and J. L. West, "Near-infrared resonant nanoshells for combined optical imaging and photothermal cancer therapy," *Nano Letters*, vol. 7, no. 7, pp. 1929–1934, 2007.

[79] G. S. Terentyuk, G. N. Maslyakova, L. V. Suleymanova et al., "Laser-induced tissue hyperthermia mediated by gold nanoparticles: toward cancer phototherapy," *Journal of Biomedical Optics*, vol. 14, no. 2, Article ID 021016, 2009.

[80] M. A. Sirotkina, V. V. Elagin, M. V. Shirmanova et al., "OCT-guided laser hyperthermia with passively tumor-targeted gold nanoparticles," *Journal of Biophotonics*, vol. 3, no. 10-11, pp. 718–727, 2010.

[81] E. Y. Lukianova-Hleb, A. O. Oginsky, A. P. Samaniego et al., "Tunable plasmonic nanoprobes for theranostics of prostate cancer," *Theranostics*, vol. 1, pp. 3–17, 2011.

[82] D. S. Wagner, N. A. Delk, E. Y. Lukianova-Hleb, J. H. Hafner, M. C. Farach-Carson, and D. O. Lapotko, "The in vivo performance of plasmonic nanobubbles as cell theranostic agents in zebrafish hosting prostate cancer xenografts," *Biomaterials*, vol. 31, no. 29, pp. 7567–7574, 2010.

[83] D. O. Lapotko, E. Lukianova, and A. A. Oraevsky, "Selective laser nano-thermolysis of human leukemia cells with microbubbles generated around clusters of gold nanoparticles," *Lasers in Surgery and Medicine*, vol. 38, no. 6, pp. 631–642, 2006.

[84] J. Cardinal, J. R. Klune, E. Chory et al., "Noninvasive radiofrequency ablation of cancer targeted by gold nanoparticles," *Surgery*, vol. 144, no. 2, pp. 125–132, 2008.

[85] P. Bernardi, M. Cavagnaro, S. Pisa, and E. Piuzzi, "Specific absorption rate and temperature elevation in a subject exposed in the far-field of radio-frequency sources operating in the 10–900-MHz range," *IEEE Transactions on Biomedical Engineering*, vol. 50, no. 3, pp. 295–304, 2003.

[86] Y. F. Huang, K. Sefah, S. Bamrungsap, H. T. Chang, and W. Tan, "Selective photothermal therapy for mixed cancer cells using aptamer-conjugated nanorods," *Langmuir*, vol. 24, no. 20, pp. 11860–11865, 2008.

[87] K. W. Hu, C. C. Huang, J. R. Hwu, W. C. Su, D. B. Shieh, and C. S. Yeh, "A new photothermal therapeutic agent: core-free nanostructured Au x Ag1-x dendrites," *Chemistry*, vol. 14, no. 10, pp. 2956–2964, 2008.

[88] F. Y. Cheng, C. T. Chen, and C. S. Yeh, "Comparative efficiencies of photothermal destruction of malignant cells using antibody-coated silica@Au nanoshells, hollow Au/Ag nanospheres and Au nanorods," *Nanotechnology*, vol. 20, no. 42, p. 425104, 2009.

[89] F. Mohammad, G. Balaji, A. Weber, R. M. Uppu, and C. S. S. R. Kumar, "Influence of gold nanoshell on hyperthermia of superparamagnetic iron oxide nanoparticles," *Journal of Physical Chemistry C*, vol. 114, no. 45, pp. 19194–19201, 2010.

[90] D. H. Kim, E. A. Rozhkova, T. Rajh, S. D. Bader, and V. Novosad, "Synthesis of hybrid gold/iron oxide nanoparticles in block copolymer micelles for imaging, drug delivery, and magnetic hyperthermia," *IEEE Transactions on Magnetics*, vol. 45, no. 10, Article ID 5257027, pp. 4821–4824, 2009.

[91] B. Ehdaie, "Application of nanotechnology in cancer research: review of progress in the National Cancer Institute's alliance for nanotechnology," *International Journal of Biological Sciences*, vol. 3, no. 2, pp. 108–110, 2007.

[92] J. D. Gibson, B. P. Khanal, and E. R. Zubarev, "Paclitaxel-functionalized gold nanoparticles," *Journal of the American Chemical Society*, vol. 129, no. 37, pp. 11653–11661, 2007.

[93] S. Dhar, W. L. Daniel, D. A. Giljohann, C. A. Mirkin, and S. J. Lippard, "Polyvalent oligonucleotide gold nanoparticle conjugates as delivery vehicles for platinum(IV) warheads," *Journal of the American Chemical Society*, vol. 131, no. 41, pp. 14652–14653, 2009.

[94] S. D. Brown, P. Nativo, J. A. Smith et al., "Gold nanoparticles for the improved anticancer drug delivery of the active component of oxaliplatin," *Journal of the American Chemical Society*, vol. 132, no. 13, pp. 4678–4684, 2010.

[95] J. R. Hwu, Y. S. Lin, T. Josephrajan et al., "Targeted paclitaxel by conjugation to iron oxide and gold nanoparticles," *Journal of the American Chemical Society*, vol. 131, no. 1, pp. 66–68, 2009.

[96] S. R. Sershen, S. L. Westcott, N. J. Halas, and J. L. West, "Temperature-sensitive polymer-nanoshell composites for photothermally modulated drug delivery," *Journal of Biomedical Materials Research*, vol. 51, no. 3, pp. 293–298, 2000.

[97] H. C. Sang, "Estimation of tumour dose enhancement due to gold nanoparticles during typical radiation treatments: a preliminary Monte Carlo study," *Physics in Medicine and Biology*, vol. 50, no. 15, pp. N163–N173, 2005.

[98] T. Kong, J. Zeng, X. Wang et al., "Enhancement of radiation cytotoxicity in breast-cancer cells by localized attachment of gold nanoparticles," *Small*, vol. 4, no. 9, pp. 1537–1543, 2008.

[99] R. Xu, J. Ma, X. Sun et al., "Ag nanoparticles sensitize IR-induced killing of cancer cells," *Cell Research*, vol. 19, no. 8, pp. 1031–1034, 2009.

[100] J. H. Lee, Y. M. Huh, Y. W. Jun et al., "Artificially engineered magnetic nanoparticles for ultra-sensitive molecular imaging," *Nature Medicine*, vol. 13, no. 1, pp. 95–99, 2007.

[101] E. I. Altinoğlu and J. H. Adair, "Near infrared imaging with nanoparticles," *Wiley Interdisciplinary Reviews: Nanomedicine and Nanobiotechnology*, vol. 2, no. 5, pp. 461–477, 2010.

[102] J. Kneipp, H. Kneipp, B. Wittig, and K. Kneipp, "Novel optical nanosensors for probing and imaging live cells," *Nanomedicine: Nanotechnology, Biology, and Medicine*, vol. 6, no. 2, pp. 214–226, 2010.

[103] D. Kim, S. Park, H. L. Jae, Y. J. Yong, and S. Jon, "Antibiofouling polymer-coated gold nanoparticles as a contrast agent for in vivo X-ray computed tomography imaging," *Journal of the American Chemical Society*, vol. 129, no. 24, pp. 7661–7665, 2007.

[104] P. Vartholomeos, M. Fruchard, A. Ferreira, and C. Mavroidis, "MRI-guided nanorobotic systems for therapeutic and diagnostic applications," *Annual Review of Biomedical Engineering*, vol. 13, pp. 157–184, 2011.

[105] E. V. Zagaynova, M. V. Shirmanova, M. Y. Kirillin et al., "Contrasting properties of gold nanoparticles for optical coherence tomography: phantom, in vivo studies and Monte Carlo simulation," *Physics in Medicine and Biology*, vol. 53, no. 18, pp. 4995–5009, 2008.

[106] J. C. Kah, M. Olivo, T. H. Chow et al., "Control of optical contrast using gold nanoshells for optical coherence tomography imaging of mouse xenograft tumor model in vivo," *Journal of Biomedical Optics*, vol. 14, no. 5, p. 054015, 2009.

[107] A. L. Oldenburg, M. N. Hansen, T. S. Ralston, A. Wei, and S. A. Boppart, "Imaging gold nanorods in excised human breast carcinoma by spectroscopic optical coherence tomography," *Journal of Materials Chemistry*, vol. 19, no. 35, pp. 6407–6411, 2009.

[108] X. Yang, E. W. Stein, S. Ashkenazi, and L. V. Wang, "Nanoparticles for photoacoustic imaging," *Wiley Interdisciplinary Reviews. Nanomedicine and Nanobiotechnology*, vol. 1, no. 4, pp. 360–368, 2009.

[109] D. B. Chithrani, "Nanoparticles for improved therapeutics and imaging in cancer therapy," *Recent Patents on Nanotechnology*, vol. 4, no. 3, pp. 171–180, 2010.

[110] E. C. Cho, C. Glaus, J. Chen, M. J. Welch, and Y. Xia, "Inorganic nanoparticle-based contrast agents for molecular imaging," *Trends in Molecular Medicine*, vol. 16, no. 12, pp. 561–573, 2010.

[111] D. J. Brenner and E. J. Hall, "Computed tomography—an increasing source of radiation exposure," *The New England Journal of Medicine*, vol. 357, no. 22, pp. 2277–2284, 2007.

[112] D. Kim, M. K. Yu, T. S. Lee, J. J. Park, Y. Y. Jeong, and S. Jon, "Amphiphilic polymer-coated hybrid nanoparticles as CT/MRI dual contrast agents," *Nanotechnology*, vol. 22, no. 15, p. 155101, 2011.

[113] H. Y. Tseng, C. K. Lee, S. Y. Wu et al., "Au nanorings for enhancing absorption and backscattering monitored with optical coherence tomography," *Nanotechnology*, vol. 21, no. 29, p. 295102, 2010.

[114] A. S. Paranjape, R. Kuranov, S. Baranov et al., "Depth resolved photothermal OCT detection of macrophages in tissue using nanorose," *Biomedical Optics Express*, vol. 1, no. 1, pp. 2–16, 2010.

[115] Y. Wang, X. Xie, X. Wang et al., "Photoacoustic tomography of a nanoshell contrast agent in the in vivo rat brain," *Nano Letters*, vol. 4, no. 9, pp. 1689–1692, 2004.

[116] M. Eghtedari, A. Oraevsky, J. A. Copland, N. A. Kotov, A. Conjusteau, and M. Motamedi, "High sensitivity of in vivo detection of gold nanorods using a laser optoacoustic imaging system," *Nano Letters*, vol. 7, no. 7, pp. 1914–1918, 2007.

[117] K. H. Song, C. Kim, K. Maslov, and L. V. Wang, "Noninvasive in vivo spectroscopic nanorod-contrast photoacoustic mapping of sentinel lymph nodes," *European Journal of Radiology*, vol. 70, no. 2, pp. 227–231, 2009.

[118] L. Bickford, J. Sun, K. Fu et al., "Enhanced multi-spectral imaging of live breast cancer cells using immunotargeted gold nanoshells and two-photon excitation microscopy," *Nanotechnology*, vol. 19, no. 31, p. 315102, 2008.

[119] J. Kneipp, H. Kneipp, M. McLaughlin, D. Brown, and K. Kneipp, "In vivo molecular probing of cellular compartments with gold nanoparticles and nanoaggregates," *Nano Letters*, vol. 6, no. 10, pp. 2225–2231, 2006.

[120] A. Matschulat, D. Drescher, and J. Kneipp, "Surface-enhanced Raman scattering hybrid nanoprobe multiplexing and imaging in biological systems," *ACS Nano*, vol. 4, no. 6, pp. 3259–3269, 2010.

[121] Y. S. Chen, Y. C. Hung, I. Liau, and G. S. Huang, "Assessment of the in vivo toxicity of gold nanoparticles," *Nanoscale Research Letters*, vol. 4, no. 8, pp. 858–864, 2009.

[122] M. A. Dobrovolskaia and S. E. McNeil, "Immunological properties of engineered nanomaterials," *Nature Nanotechnology*, vol. 2, no. 8, pp. 469–478, 2007.

[123] C. Lasagna-Reeves, D. Gonzalez-Romero, M. A. Barria et al., "Bioaccumulation and toxicity of gold nanoparticles after repeated administration in mice," *Biochemical and Biophysical Research Communications*, vol. 393, no. 4, pp. 649–655, 2010.

[124] J. J. Li, D. Hartono, C. N. Ong, B. H. Bay, and L. Y. L. Yung, "Autophagy and oxidative stress associated with gold nanoparticles," *Biomaterials*, vol. 31, no. 23, pp. 5996–6003, 2010.

[125] S. Hackenberg, A. Scherzed, M. Kessler et al., "Silver nanoparticles: evaluation of DNA damage, toxicity and functional impairment in human mesenchymal stem cells," *Toxicology Letters*, vol. 201, no. 1, pp. 27–33, 2011.

[126] P. V. Asharani, N. Xinyi, M. P. Hande, and S. Valiyaveettil, "DNA damage and p53-mediated growth arrest in human cells treated with platinum nanoparticles," *Nanomedicine*, vol. 5, no. 1, pp. 51–64, 2010.

[127] E. E. Connor, J. Mwamuka, A. Gole, C. J. Murphy, and M. D. Wyatt, "Gold nanoparticles are taken up by human cells but do not cause acute cytotoxicity," *Small*, vol. 1, no. 3, pp. 325–327, 2005.

[128] Y. Pan, S. Neuss, A. Leifert et al., "Size-dependent cytotoxicity of gold nanoparticles," *Small*, vol. 3, no. 11, pp. 1941–1949, 2007.

[129] I. H. El-Sayed, X. Huang, and M. A. El-Sayed, "Surface plasmon resonance scattering and absorption of anti-EGFR antibody conjugated gold nanoparticles in cancer diagnostics: applications in oral cancer," *Nano Letters*, vol. 5, no. 5, pp. 829–834, 2005.

[130] M. E. H. El-Sayed, A. S. Hoffman, and P. S. Stayton, "Smart polymeric carriers for enhanced intracellular delivery of therapeutic macromolecules," *Expert Opinion on Biological Therapy*, vol. 5, no. 1, pp. 23–32, 2005.

[131] X. L. Huang, B. Zhang, L. Ren et al., "In vivo toxic studies and biodistribution of near infrared sensitive Au-Au2S nanoparticles as potential drug delivery carriers," *Journal of Materials Science: Materials in Medicine*, vol. 19, no. 7, pp. 2581–2588, 2008.

[132] C. K. Kim, P. Ghosh, C. Pagliuca, Z. J. Zhu, S. Menichetti, and V. M. Rotello, "Entrapment of hydrophobic drugs in nanoparticle monolayers with efficient release into cancer cells," *Journal of the American Chemical Society*, vol. 131, no. 4, pp. 1360–1361, 2009.

[133] G. F. Paciotti, L. Myer, D. Weinreich et al., "Colloidal gold: a novel nanoparticle vector for tumor directed drug delivery," *Drug Delivery*, vol. 11, no. 3, pp. 169–183, 2004.

[134] R. K. Visaria, R. J. Griffin, B. W. Williams et al., "Enhancement of tumor thermal therapy using gold nanoparticle-assisted tumor necrosis factor-α delivery," *Molecular Cancer Therapeutics*, vol. 5, no. 4, pp. 1014–1020, 2006.

[135] H. J. Yen, S. H. Hsu, and C. L. Tsai, "Cytotoxicity and immunological response of gold and silver nanoparticles of different sizes," *Small*, vol. 5, no. 13, pp. 1553–1561, 2009.

[136] Y. N. Sun, C. D. Wang, X. M. Zhang, L. Ren, and X. H. Tian, "Shape dependence of gold nanoparticles on in vivo acute toxicological effects and biodistribution," *Journal of Nanoscience and Nanotechnology*, vol. 11, no. 2, pp. 1210–1216, 2011.

[137] Y. Qiu, Y. Liu, L. Wang et al., "Surface chemistry and aspect ratio mediated cellular uptake of Au nanorods," *Biomaterials*, vol. 31, no. 30, pp. 7606–7619, 2010.

[138] L. Braydich-Stolle, S. Hussain, J. J. Schlager, and M. C. Hofmann, "In vitro cytotoxicity of nanoparticles in mammalian germline stem cells," *Toxicological Sciences*, vol. 88, no. 2, pp. 412–419, 2005.

[139] S. M. Hussain, K. L. Hess, J. M. Gearhart, K. T. Geiss, and J. J. Schlager, "In vitro toxicity of nanoparticles in BRL 3A rat liver cells," *Toxicology in Vitro*, vol. 19, no. 7, pp. 975–983, 2005.

[140] K. F. Soto, A. Carrasco, T. G. Powell, K. M. Garza, and L. E. Murr, "Comparative in vitro cytotoxicity assessment of some manufacture dnanoparticulate materials characterized by transmission electron microscopy," *Journal of Nanoparticle Research*, vol. 7, no. 2-3, pp. 145–169, 2005.

[141] R. Foldbjerg, D. A. Dang, and H. Autrup, "Cytotoxicity and genotoxicity of silver nanoparticles in the human lung cancer cell line, A549," *Archives of Toxicology*, vol. 85, no. 7, pp. 743–750, 2011.

[142] P. V. Asharani, Y. Lianwu, Z. Gong, and S. Valiyaveettil, "Comparison of the toxicity of silver, gold and platinum nanoparticles in developing zebrafish embryos," *Nanotoxicology*, vol. 5, no. 1, pp. 43–54, 2011.

[143] S. Bellucci, "Nanoparticles and nanodevices in biological applications," *Lecture Notes in Nanoscale Science and Technology*, vol. 4, pp. 1–198, 2009.

Hindawi Publishing Corporation
Journal of Drug Delivery
Volume 2012, Article ID 581363, 10 pages
doi:10.1155/2012/581363

Review Article

Lipoplatin Formulation Review Article

G. P. Stathopoulos[1] and T. Boulikas[2]

[1] *First Oncology Clinic, Errikos Dunant Hospital, Athens, Greece*
[2] *Regulon Inc. and Regulon AE, Afxentiou 7, Alimos, 17455 Athens, Greece*

Correspondence should be addressed to G. P. Stathopoulos, dr-gps@ath.forthnet.gr

Received 29 May 2011; Accepted 24 June 2011

Academic Editor: Rassoul Dinarvand

Patented platform technologies have been used for the liposomal encapsulation of cisplatin (Lipoplatin) into tumor-targeted 110 nm (in diameter) nanoparticles. The molecular mechanisms, preclinical and clinical data concerning lipoplatin, are reviewed here. Lipoplatin has been successfully administered in three randomized Phase II and III clinical trials. The clinical data mainly include non-small-cell lung cancer but also pancreatic, breast, and head and neck cancers. It is anticipated that lipoplatin will replace cisplatin as well as increase its potential applications. For the first time, a platinum drug has shown superiority to cisplatin, at least in non-squamous non-small-cell lung cancer as reported in a Phase III study which documented a simultaneous lowering of all of the side effects of cisplatin.

1. Introduction

Over the last twenty years, the effort to produce new, more effective, and less toxic cytotoxic agents has been intensive, in order to ameliorate the treatment of cancer patients. One of the most effective agents since the late 1970s has been cisplatin (CDDP) in patients with testicular cancer [1], ovarian cancer [2], head and neck [3], and lung cancer [4] as well as bladder cancer [5] and in other malignancies [6, 7]. Cisplatin was established as being quite effective and as one of the most important cytotoxic agents. It has mainly been administered in combination with other agents. The toxicity rendered by cisplatin has been its main drawback, particularly nephrotoxicity [8–10]. After 1990, new agents that did not cause nephrotoxicity were produced as a substitute for cisplatin. Agents such as carboplatin [11] paclitaxel, docetaxel, gemcitabine, vinorelbine, and irinotecan [12–15] were used either in combination or as substitutes for cisplatin [16, 17]. These agents succeeded in producing no nephrotoxicity but did produce other toxicities such as myelotoxicity, in comparison to cisplatin. The main example was carboplatin, an analogue of cisplatin, which showed no renal toxicity but produced higher myelotoxicity than cisplatin. Carboplatin has often been used as a substitute for CDDP [11, 12] in lung [15], head and neck, and ovarian cancers [11]. The effectiveness of carboplatin was more or less equal to that of CDDP but not better. For instance, CDDP was shown to be more effective than carboplatin in the most common lung cancer, adenocarcinoma [18]. The other agents, previously mentioned, are mainly administered in combination with CDDP than as a substitute for it. Over all of the last twenty years, cisplatin has been in regular usage since most oncologists still believe it has priority with regard to effectiveness. Liposomal agents comprise another direction which research is taking and several of these have become part of clinical practice as is the case of liposomal anthracycline. None of these agents has managed to become a substitute for cisplatin, and they are used as second-line treatment.

Our review article is related to a new formulation of cisplatin, that is, liposomal cisplatin (lipoplatin). The purpose of this agent is to become a substitute for the original cisplatin, and, thus, the two drugs must be compared with regard to toxicity and effectiveness.

There are preclinical data in cancer cell cultures and in animals as well as clinical data which involve Phase I studies, pharmacokinetics and Phase II and Phase III studies. The data in 16 published studies are related to patients with pancreatic cancer, non-small-cell lung cancer (NSCLC), head and neck, and breast cancers.

2. Lipoplatin: Formulation, Mechanisms, and Technology

Cisplatin was formulated into liposomes as depicted in Figure 1. The lipids of lipoplatin are composed of soy phosphatidyl choline (SPC-3), cholesterol, dipalmitoyl phosphatidyl glycerol (DPPG), and methoxy-polyethylene glycol-distearoyl phosphatidylethanolamine (mPEG 2000-DSPE). The formulation was achieved by the formation of reverse micelles between cisplatin and DPPG under special conditions of pH, ethanol, ionic strength, and other parameters, and the cisplatin-DPPG reverse micelles were subsequently converted into liposomes by interaction with neutral lipids. About 15 extrusions are performed to give to the nanoparticles their final size of 110 nm, using a thermobarrel, extruder and membranes of 0.2, 0.1, 0.08 and 0.05 μm pore sizes under ultra pure nitrogen pressure.

The nanoparticles, 110 nm in diameter, have the ability to target tumors and metastasis following intravenous administration using the compromised endothelium of the tumor vasculature sprouted during neoangiogenesis; this process, known as extravasation, takes advantage of the compromised endothelium of the vasculature of the tumors generated during neoangiogenesis. Lipoplatin has shown an amazing concentration in tumors and metastases at levels up to 200-fold higher compared to the adjacent normal tissue in surgical specimens from patients [19].

3. Molecular Mechanisms of Cisplatin and Lipoplatin

After infusion, cisplatin is rapidly excreted in the urine causing renal tubular damage. When it reaches normal and malignant cells, it uses the major copper influx transporter Ctr1 for entry inside the cytoplasm (Figure 2). Ctr1 has been convincingly demonstrated to transport cisplatin and its analogues, carboplatin, and oxaliplatin. Two copper efflux transporters, ATP7A and ATP7B, regulate the efflux of cisplatin [21].

The S-containing tripeptide glutathione is present in cells at mM concentrations, and the formation of complexes with cisplatin plays an important role in its detoxification and biological activities. The depletion of glutathione levels has been shown to increase the toxicity of cisplatin to kidney cells. Cancer cells that are resistant to cisplatin often have elevated glutathione levels. Glutathione could quench DNA-Pt monofunctional adducts before they can rearrange toxic bifunctional adducts on DNA. Human glutathione S-transferase P1 (GSTP1) contributes to chemoresistance and its suppression, decreasing the cisplatin-induced activation of ERK1/2 and might have synergistic therapeutic effects [22].

Cisplatin and other apoptotic stimuli trigger the release of cytochrome c from the mitochondrial intermembrane space to the cytosol, which induces the formation of the apoptosome and the activation of procaspase-9, leading to apoptosis. The apoptosome is an Apaf-1 cytochrome c complex that activates procaspase-9. Cisplatin can also activate the proapoptotic protein Bax, resulting in cytochrome c release, caspase activation, and apoptosis; Bax activation is implicated in the nephrotoxicity of cisplatin [23]. Bcl-2 plays an important role in the mitochondrial apoptotic pathway. Although the general role of Bcl-2 is antiapoptotic, Bcl-2 fragments resulting by caspase cleavage after cisplatin treatment of cells in culture could promote the apoptotic process [24]. Lipoplatin, releasing cisplatin molecules in the cytoplasm of the tumor cell, is also proposed to activate the mitochondrial apoptotic cascade.

During signal transduction, a cell senses both the external and internal environment and converts a stimulus into an ordered sequence of phosphorylation-dephosphorylation, protease degradation, gene regulation, or ion flux events, across the cell membrane. Receptor tyrosine kinases contribute to chemoresistance in tumors. A number of additional properties of cisplatin are now emerging including the activation of signal transduction pathways leading to apoptosis. The firing of such pathways may originate at the level of the cell membrane after damage of the receptor or lipid molecules by cisplatin, in the cytoplasm by modulation of proteins via the interaction of their thiol groups with cisplatin, (kinases, and other regulatory proteins and enzymes), or finally from DNA damage via the activation of the DNA repair pathways [25, 26].

Cisplatin induction of signaling is cell type, time and dose dependent. It induces oxidative stress and is an activator of stress-signaling pathways especially of the mitogen-activated protein (MAP) kinase cascades. The extracellular signal-regulated kinase (ERK) pathway is indeed activated by cisplatin. The acquisition of cisplatin resistance by ovarian carcinoma cells was associated with the loss of ERK activation in response to cisplatin [27]. ERK activation and DNA-damage induced apoptosis are tightly linked; p53 may act as one of the upstream regulators of ERK activation for the induction of apoptosis in carboplatin-treated cervical cancer cells [28]. The treatment of cells with high cisplatin concentrations (one order of magnitude higher than the IC_{50}) induces cellular superoxide formation and caspase activation independently of nuclear DNA damage. In contrast, cisplatin concentrations at IC_{50} doses, which do not induce acute apoptosis, are sufficient for the induction of DNA damage signaling [29].

The PI3K/Akt cascade has an important role in the resistance of ovarian cancer cells to cisplatin, and the inhibition of PI3K/Akt increases the efficacy of cisplatin [30]. The Akt-specific inhibitor LY294005 increased the efficacy of docetaxel, did not affect the efficacy of 6-thioguanine, and decreased the efficacy of cisplatin, lipoplatin, oxaliplatin, and lipoxal in human colorectal adenocarcinoma sublines, suggesting a novel property of Akt in aggravating drug sensitivity [31].

Cisplatin appears to exhibit synergistic effects with other potent inducers of apoptosis such as a synthetic isothiocyanate; the sequential administration of both agents led to increased intracellular platinum accumulation, glutathione depletion, poly (ADP-ribosyl) polymerase cleavage, stimulation of caspase-3 activity, upregulation of p53, FasL and Gadd45alpha, cyclin B1 downregulation, and an increase

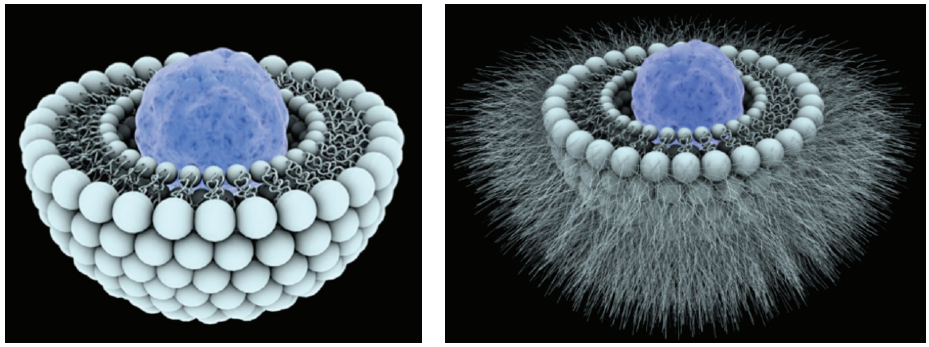

(a) (b)

Figure 1: Depiction of a lipoplatin nanoparticle (b). Cisplatin molecules are depicted as blue spheres surrounded by the lipid bilayer with the PEGylated lipid sticking out like hair from the outer surface. Thus, this toxic substance, cisplatin, is camouflaged by its lipid shell as a nutrient. This nanoparticle can pass undetected by macrophages after intravenous injection to human cancer patients because of its PEG coating thus escaping immune surveillance [20]. © CNRS Photothèque/SAGASCIENCE/CAILLAUD François.

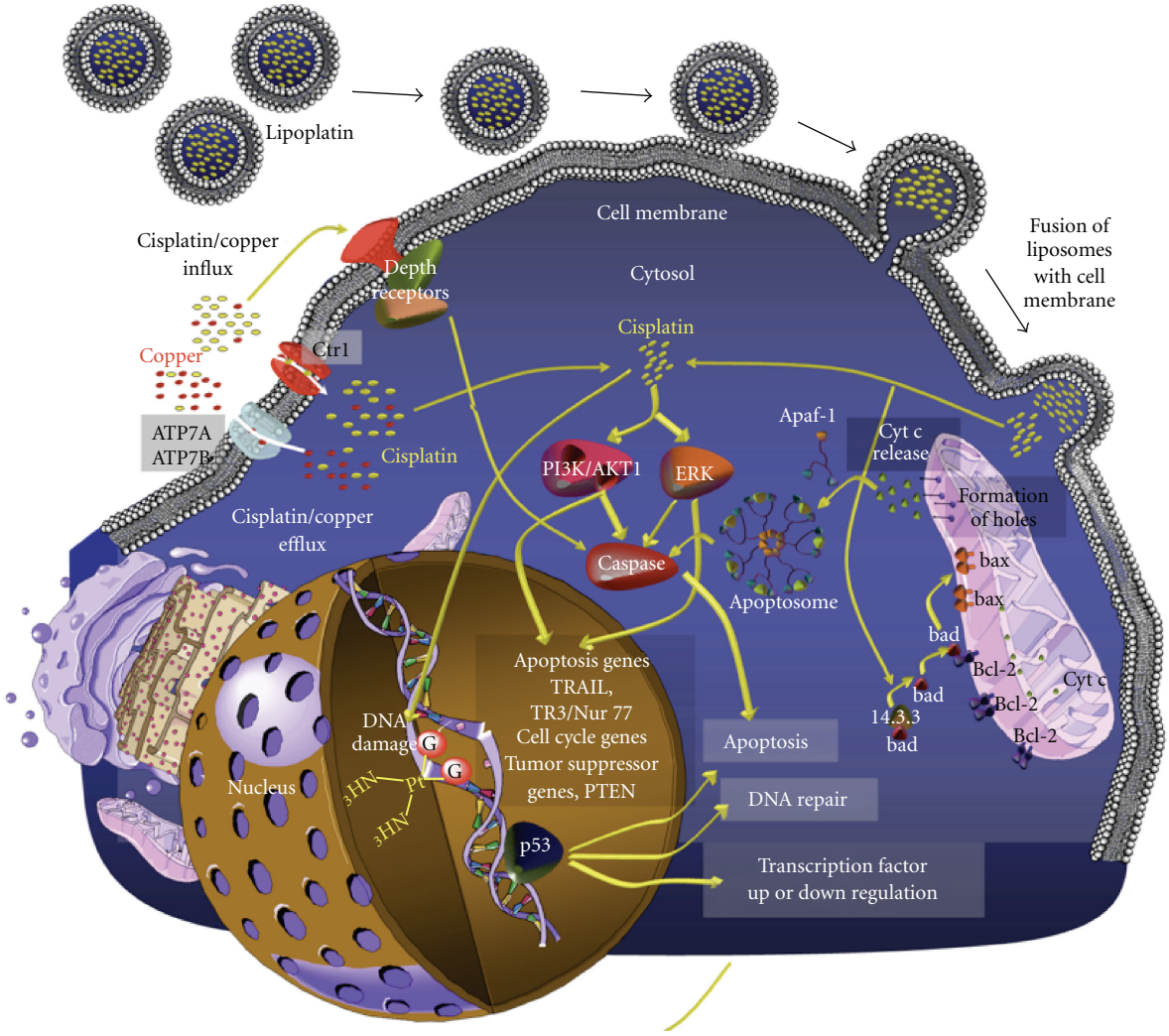

Figure 2: Penetration of lipoplatin nanoparticles through the cell membrane of tumor cells. lipoplatin nanoparticles once inside the tumor cell mass can fuse with the cell membrane because of the presence of the fusogenic lipid DPPG in their lipid bilayer; an alternative mechanism proposed is that lipoplatin is taken by *endocytosis* by tumor cells as shown from lipoplatin containing fluorescent lipids and imaging of the tumor cells in culture thus treated with fluorescent microscopy (see Figure 3). These processes occurring at the cell membrane level are promoted by the lipid shell of the nanoparticles (disguised as nutrients) [20].

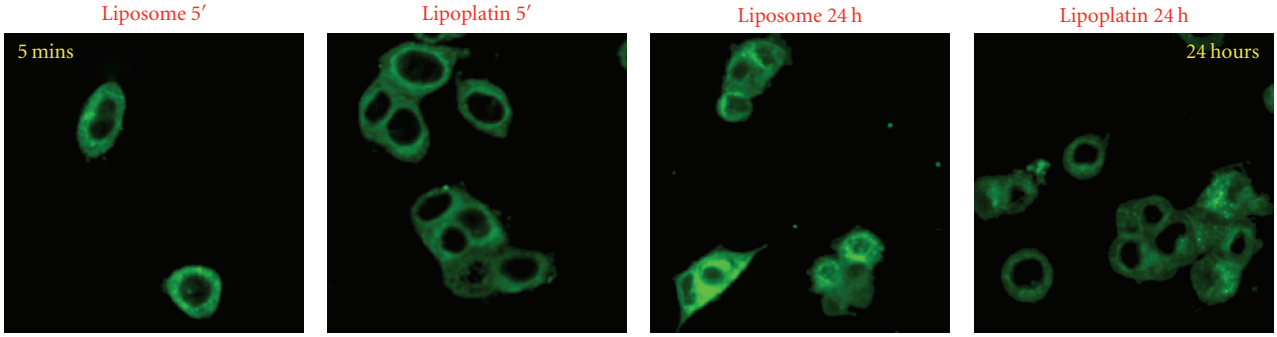

Figure 3: Lipoplatin or DPPG-liposomes with fluorescent lipids enter rapidly MCF-7 breast cancer cells in culture. Time-course processing of FITC-labeled DPPG-containing liposomes (a) and Lipoplatin (b) using confocal microscopy. At 5 min, the majority of the signal is localized in the membrane. Lipids are rapidly internalized and at 4–24 hours, a strong signal is observed in the cytoplasm and at the perinuclear area. These results demonstrate that *lipoplatin or DPPG-liposomes* nanoparticles are able to cross the cell membrane barrier [20].

in mitogen-activated protein kinases JNK, ERK, and p38 phosphorylation as well as PI3K level alterations [32].

4. Resistance of Tumor Cells to Cisplatin and a Role for Lipoplatin

The resistance of tumor cells to cisplatin is attributed to at least four different mechanisms: (i) decreased levels of cisplatin entrance to the cytoplasm or increased efflux through the cell membrane, (ii) increased levels of glutathione, (iii) modulation of signaling pathways, and (iv) enhanced levels of DNA repair.

However, additional pathways have been found for establishing the cisplatin resistant phenotype. For example, the selection of ovarian carcinoma cells in culture in the presence of cisplatin led to upregulated expression of the L1 adhesion molecule; this could constitute a mechanism for the establishment of chemoresistance and of a more malignant tumor phenotype [33].

The direct fusion of lipoplatin nanoparticles with the membrane of the tumor cell (Figure 2) suggests that lipoplatin can have applications after the failure of cisplatin front-line chemotherapy and the development of cisplatin resistance at the cell membrane level.

5. Preclinical Studies

A comparison of the cytotoxicity of lipoplatin and cisplatin in vitro in established cell lines (derived from NSCLC, renal cell carcinoma, and in normal hematopoietic cell precursors), as well as the identification of biological markers associated with sensitivity and resistance has rendered some interesting data. ERCC1 and LRP expression levels appeared to be valid predictors of sensitivity or resistance to both drugs. A superior cytotoxicity in all tumor cell models and a much lower toxicity in normal cells for lipoplatin compared with cisplatin were found, suggesting a higher therapeutic index for the liposomal compound [34].

Fedier et al. [35] investigated whether the cytotoxic effect of lipoplatin is dependent on the functional integrity of DNA mismatch repair (MMR). MMR is a postreplicative DNA repair mechanism implicated in cell cycle control and apoptosis. MMR function was found to be a relevant determinant accounting for the cytotoxicity of lipoplatin [35]. A possible relationship between MMR-mediated cisplatin DNA damage signaling, and the Akt signaling pathway was also found [31].

The fusion between liposomes and the cell membrane was suggested based on the fusogenic properties of DPPG and lipids integrated into the shell of lipoplatin (Figure 2). Subsequent cell culture studies where the lipids of the lipoplatin nanoparticle were labelled with fluorescein isothiocyanate (FITC) established the rapid uptake and internalization of the nanoparticles (Figure 3). In these studies the fluorescent nanoparticles were incubated with MCF-7 breast cancer cells in culture for various times ranging from 5 min to 24 h, and the cells were fixed and visualized by confocal microscopy (Figure 3). Liposomes containing DPPG without cisplatin were also used as a control. The study has provided proof that the lipids of lipoplatin labelled with FITC are transferred initially (in less than 5 min) to the cell membrane of MCF-7 cells in culture and are then (from 5 min to 24 h) docked to the interior of the cell. The membrane fusion is proposed to modulate signalling, an important process for cancer cell proliferation.

The lower nephrotoxicity of lipoplatin, compared to cisplatin, was shown in mice, rats, and SCID mice [36], whereas animals injected with cisplatin developed renal insufficiency with clear evidence of tubular damage, but those injected with the same dose of lipoplatin were almost completely free of kidney injury [36].

In order to explain the lower toxicity of lipoplatin compared to cisplatin, the levels of total platinum in rat tissue after cisplatin or lipoplatin injections were determined at different time intervals. The maximum levels of total platinum after cisplatin were found in the kidney followed by

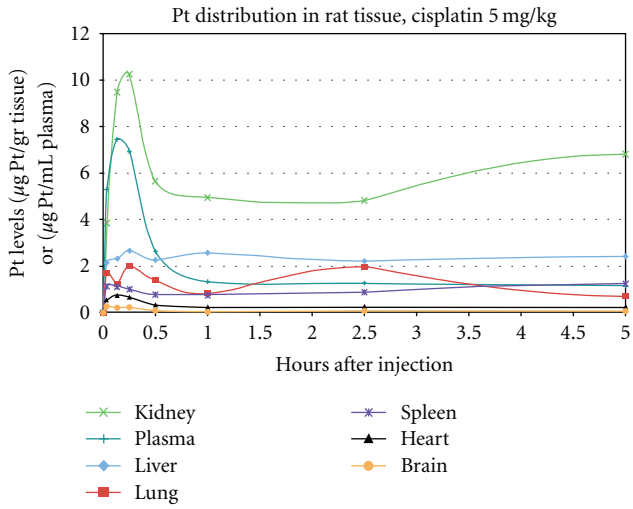

FIGURE 4: Kidney and other tissue accumulation of total platinum after *cisplatin* injection of rats (0–5h) [20].

the plasma, liver, lung, spleen, heart, and brain, in those tissues examined from 5 min to 5 h. At later times (up to 50 h), the order of the tissues with the highest levels of platinum was the kidney, liver spleen, plasma, lung, heart, and brain. A single treatment with 30 mg/kg lipoplatin in rats resulted in no toxicity, whereas 2 or 3 weekly administrations at 30 mg/kg in rats produced neutropenia but no nephrotoxicity. However, a single injection of 5 mg/kg cisplatin in rats resulted in severe nephrotoxicity. The levels of total platinum attained in animal kidneys after cisplatin administration are about the same as those after lipoplatin (Figure 4); however, at about 1 h and up to 5 days, the levels of total platinum are about 1 microgram after lipoplatin compared to 5 micrograms after cisplatin administration (Figure 4).

After cisplatin injection, the kidneys accumulate the highest levels of platinum among all of the animal tissues, followed by the liver and the lung. One hour after lipoplatin administration i.p., the kidney Pt levels drop from 13 to 3 μg/g tissue. The highest Pt levels among all of the animal tissues are in the liver and spleen after 4 h i.p. administration maintained for over 100 h.

The treatment of dogs with lipoplatin led to the conclusion that the drug can be safely administered to clinically normal dogs at dosages of up to 150 mg/m^2 without the need for concurrent hydration protocols. The maximum tolerated dose (MTD) of unencapsulated cisplatin in dogs has been established as 70 mg/m^2. Therefore, lipoplatin would allow the safe and repeated administration of doses higher than the MTD of unencapsulated cisplatin [37].

The intrapleural administration of lipoplatin in an animal model seems to offer a more effective therapeutic index while improving tolerability. Wistar rats were treated with doses of 10 mg/kg lipoplatin (intravenously) versus 10 or 20 mg/kg lipoplatin (intrapleurally) corresponding to 60 and 120 mg/m^2, respectively, in humans. The authors noted minor fibrotic changes in the pleura of rats injected intrapleurally, and mild kidney changes in rats injected intravenously, as expected [38].

6. Cellular Uptake and Cytoplasm/DNA Distribution of Cisplatin versus Lipoplatin

The antineoplastic or radio-sensitizing activity of platinum drugs is attributed to their binding to DNA. The time course of accumulation of cisplatin, lipoplatin, oxaliplatin, and lipoxal (liposomal oxaliplatin) in the human colorectal cancer HCT116 cell line and their distribution between the cytoplasm and DNA were measured by inductively coupled plasma mass spectrometry. The distribution of cytoplasm/DNA of free cisplatin and lipoplatin were similar. However, lipoxal displayed a higher accumulation in the cytoplasm compared to free oxaliplatin, consistent with its proposed mechanism of fusion with the cell membrane [39].

The cytotoxicity and synergic effect of platinum compounds with radiation were examined in F98 glioma cells. Lipoplatin improved the cell uptake of cisplatin by 3-fold, and its radiosensitizing potential was enhanced by 14-fold. Among the five platinum compounds tested, carboplatin and lipoplatin showed the best radiosensitizing effect. Lipoplatin seemed the most promising since it led to the best cellular incorporation and reduced all the toxicities of cisplatin [40].

7. Clinical Studies

7.1. Pharmacokinetics. In the administration of liposomal cisplatin to humans, the target was to determine the pharmacokinetics and adverse reactions. A Phase I study of 27 patients with different malignancies was performed. The drug was infused for 8 hrs every fourteen days at escalating doses. The drug levels started at 25 mg/m^2 and were increased by 25 mg/m^2 up to 125 mg/m^2. Three-5 patients were selected for each dosage. Blood was taken at certain time intervals in order to estimate the total platinum plasma levels. For pharmacokinetics, blood was drawn at 0, 3, 6, 8, 12, 24 hrs and 3, 5, 7 days, into tubes containing EDTA, and total platinum levels (i.e., free plus proteins bound plus liposomal) were analyzed by atomic absorption. Total platinum was also determined in the ultrafiltrate of less plasma. The maximum level attained in the plasma was 5.7 μg/mL at 8 hrs. The levels of platinum in the blood after lipoplatin infusion drop to normal on the fourth day at a dose of 100 mg/m^2, but at a dose of 125 mg/m^2 platinum can be detected in the blood for 7 days (Table 1) [41]. Renal function tests (blood urea, serum creatinine, and creatinine clearance) showed no change before and after treatment. The excretion of platinum in the urine in lipoplatin-treated patients attains a maximum within 8 hrs (infusion period) and declines thereafter. During the 3 following days (after infusion) 40.7% of the total platinum was excreted in the urine. Toxicity was very mild (grade 1 or 2 neutropenia and nausea/vomiting) at the 125 mg/m^2 dosage level. In another trial, the tumor uptake of lipoplatin was examined in comparison to normal tissue, in 4 patients with hepatocellular adenocarcinoma, gastric cancer, and colon cancer. Lipoplatin was administered to the patients 24 hours before the surgery [19]. This study showed liposomal cisplatin accumulation in tumors as compared to normal tissue after the intravenous infusion of lipoplatin.

Table 1: Pharmacokinetic parameters of total platinum in patients' sera at the different dose levels.

Dose mg/m^2	Pts (n)	AUC$_{0\varnothing A}$ (h μg/mL)	C_{max} (μg/mL)	Cl (L/m^2 h)	K_{el} (L/h)	$t_{1/2}$ (h)	V_{ss} (L/m^2)
25	5	139.63	2.48 ± 1.18	0.18	0.0114	60.79	15.71
50	3	119.19	2.87 ± 0.59	0.42	0.0001	N/A	N/A
100	5	172.89	3.74 ± 1.18	0.58	0.0059	117.46	98.03
125	4	256.09	5.65 ± 2.67	0.49	0.0085	81.53	57.42

N/A, not applicable.

Among the various surgical specimens examined, gastric tumors revealed the highest levels of total platinum (up to 262 μg cisplatin/gr tissue). The liver metastatic specimen displayed a total amount of 131.15 μg platinum/gr of tissue compared to 20.94 μg platinum/gr of normal liver tissue. Both specimens of gastric tumors appeared to accumulate the highest amounts of platinum among all specimens analyzed in this study: 262.62 and 66.38 μg/gr of tissue. The total platinum levels in the colon tumor specimens were 11.26 and 7.69 μg platinum/gr of tissue compared to 0.06 μg/gr normal colon tissue [19].

7.2. Dose-Limited Toxicity and Maximum Tolerated Doses. The human testing of this new agent primarily required the definition of toxicity by investigating the MTD as well as the dose-limited toxicity (DLT). Two Phase I and I-II studies examined these objectives. The first trial was in patients with advanced pancreatic cancer. The results showed that the dosages which began to produce side effects were 100 mg/m^2 and 125 mg/m^2. But these dosages did not later prove that this was the DLT since lipoplatin was combined with gemcitabine, the latter which may have been responsible for the toxicity [42]. The second study defined similar doses as the DLT and MTD. This trial also used two agents, lipoplatin and gemcitabine in pretreated patients with NSCLC. The two drugs were repeated on day 8. The small number of 13 patients was not efficacious enough to determine ample data concerning toxicity [43]. In both these aforementioned studies, there was also a defect in that all of the patients had undergone chemotherapy pretreatment when they were recruited and the efficacy of lipoplatin was tested. A proper third Phase I trial was eventually performed. The main objective of this study was to determine the DLT and MTD of lipoplatin tested as a single agent and in combination with a second cytotoxic agent. The selected second agent was paclitaxel. All of the patients had NSCLC. Adverse reactions, mainly myelotoxicity, renal toxicity and gastrointestinal toxicity (nausea, vomiting, diarrhea) were determined. Sixty-six patients were recruited and evaluated. Thirty-nine patients comprised the group that received lipoplatin monotherapy, and 27 patients were given lipoplatin in combination with paclitaxel. In the first group, the dosage of lipoplatin started at the level of 125 mg/m^2 and the drug-dose escalation increased to 350 mg/m^2. It was determined that 350 mg/m^2 was the DLT and 300 mg/m^2 the MDT. In the group that received combination therapy, the escalation of paclitaxel started at 100 mg/m^2 and went up to 175 mg/m^2 and of lipoplatin from 100 mg/m^2 to 250 mg/m^2. The results of the combined treatment evaluation determined the DLT as 250 mg/m^2 and the MTD, 200 mg/m^2. Nausea, vomiting, fatigue, and neutropenia were not higher than grade 1-2, and other adverse reactions in a small percentage of patients reached grade 3. In the combined modality, other side effects, such as neurotoxicity, were observed, and this was attributed to paclitaxel. Grade 1 nephrotoxicity was observed in a small percentage of patients, but this was only temporary (Table 2) [44].

Over the last five years, several Phase II and III trials have been performed in different institutions and countries. Lipoplatin has been tested in the following malignancies: pancreatic cancer, head and neck cancer, mesothelioma, breast and gastric cancer, and NSCLC. In pancreatic cancer, lipoplatin was administered as second-line treatment in combination with gemcitabine. The patients had initially undergone gemcitabine monotherapy as first-line treatment and were experiencing disease progression. The combination of lipoplatin with gemcitabine rendered a response rate of 8% [42].

A trial was done concerning a combination of lipoplatin 120 mg/m^2 plus 5-fluorouracil 400 mg/m^2 and leucovorin, both cytotoxic drugs administered weekly along with radiotherapy. The cytotoxic agents were given on day 1 and radiotherapy (dosage 3.5 Gy × 3, days 2, 3, 4) for four or five weeks. This treatment was given to patients with advanced gastric cancer. No serious toxicity was observed, and the therapy was well tolerated; 18.2% patients developed grade 1 renal toxicity and nausea and 25% showed fatigue. A good response to the combined treatment was observed [45].

It is too early to confirm that lipoplatin is effective in mesothelioma. There is a case report indicating the responsiveness of mesothelioma to lipoplatin given in combination with gemcitabine as second-line treatment on disease recurrence [46].

The testing of the toxicity and effectiveness of liposomal cisplatin was done in patients with squamous cell carcinoma of the head and neck. This was a randomized study comparing lipoplatin combined with 5-fluorouracil versus cisplatin combined with 5-fluorouracil. The toxicity was well tolerated. Grade 3 renal toxicity was much lower after lipoplatin administration than after cisplatin. Higher myelotoxicity was observed in the cisplatin arm (31.7% versus 12% in the lipoplatin arm). Mucositis and peripheral neuropathy were also much higher in the cisplatin group. The response rate was higher in the cisplatin arm, but

Table 2: Toxicity: lipoplatin monotherapy.

Dosage lipoplatin mg/m^2	Toxicity	Grade 1	2	3	4
		n	*n*	*n*	*n*
150–250	Nausea-vomiting	—	—	—	—
	Fatigue	—	—	—	—
	Diarrhea	—	—	—	—
	Nephrotoxicity	—	—	—	—
	Neutropenia	—	—	—	—
	Neurotoxicity	—	—	—	—
300	Nausea-vomiting	2/4	1/4	—	—
	Fatigue	2/4	1/4	—	—
	Neutropenia	1/4	—	—	—
	Nephrotoxicity	1/4	—	—	—
350	Nausea-vomiting	1/4	3/4	—	—
	Fatigue	1/4	3/4	—	—
	Neutropenia	2/4	1/4	1/4	—
	Nephrotoxicity	2/4	1/4	1/4	—

stable disease was higher in the lipoplatin arm. This low responsiveness of the lipoplatin arm may be due to the quite low dosage administered and its short duration. One should take into account that the MTD is 200 mg/m^2 and not 100 mg/m^2 [47].

A Phase II trial combining lipoplatin with vinorelbine in first-line treatment of HER2/neu-negative metastatic breast cancer was done. The investigators administered the above agents on the basis of the rationale that the frequent use of anthracyclines and taxanes in the adjuvant setting of breast cancer has led to drug resistance and cardiac toxicity. This raised the need for new agents in the metastatic setting. Another reason for testing the aforementioned combination was that the use of cisplatin-vinorelbine showed interesting results with an overall response rate of 64%. The administered dose of lipoplatin was 120 mg/m^2 and of vinorelbine 30 mg/m^2. The objective response rate of the latter combination was 50% (one complete response). Stable disease was 45.5%. Toxicity was well tolerated [48].

One Phase II and two Phase III trials have been recently integrated and published. In these studies, lipoplatin was combined with a second agent in comparison with cisplatin also combined with the same second agent, and the objectives were to determine the side effects and efficacy. In the Phase II randomized study, lipoplatin (dosage 120 mg/m^2 given on days 1, 8, 15) combined with gemcitabine (1000 mg/m^2 given on days 1, 8) was compared with cisplatin (100 mg/m^2 day 1) combined with gemcitabine (1000 mg/m^2 given on days 1, 8). With respect to efficacy, the overall response rate of the lipoplatin arm was 31.7%, and the cisplatin arm 25.6%. Although the efficacy of lipoplatin was not statistically higher than that of cisplatin, a better response rate was achieved with lipoplatin, particularly in cases of adenocarcinoma. The more important finding was the toxicity outcome which was shown to be much lower in patients treated with lipoplatin versus in patients treated with cisplatin. Very low nephrotoxicity was observed in the patients who received lipoplatin. Although the aforementioned study [49] included a rather limited number of patients (88 in total), the results were confirmed by another study which was done in parallel to the above trial.

These results with respect to the study done in parallel, mentioned above, are as follows: this Phase III trial included 229 evaluable patients. The differences between this study and the previous one were, the number of patients, the dosage of the drugs, the repetition of the courses, and the second agent which was combined with lipoplatin and cisplatin. The dose of lipoplatin was 200 mg/m^2, which is the proper MTD combined with paclitaxel 135 mg/m^2 repeated every 2 weeks for a planned 9 courses. The control arm received cisplatin 75 mg/m^2 also combined with paclitaxel 135 mg/m^2, repeated every 2 weeks. The planned number of courses was 9. The treatment of both agents and arms was on day 1. The main objectives of this trial were to determine the toxicity and median survival. The results were quite impressive; nephrotoxicity, in particular, leukopenia, nausea/vomiting, and asthenia were statistically significantly lower after lipoplatin treatment ($P \leq 0.001$, 0.017, 0.042, 0.019, resp.) (Table 3). The comparison of efficacy was also important; the response rate was 59.7% for the lipoplatin arm, and 47% for the cisplatin arm (no statistically significant difference, $P = 0.073$) (Table 4). The median and overall survival for both arms was the same [50].

The data documented in the last two trials indicate that the cisplatin formulation (lipoplatin) could be considered as the best substitute for cisplatin, at least in NSCLC, with regard to efficacy and toxicity.

The next Phase III trial was based on certain indications from the previous trials, and this was the possibility that NSCLC subtypes may have a different response rate with the

Table 3: Toxicity/statistical differences.

Toxicity grade 1–4	Arm A *n* (%)	Arm B *n* (%)	*P* value*
Anemia	50 (43.9)	62 (54.9)	0.112
Leucopenia (neutropenia)	38 (33.3)	52 (45.2)	0.017
Thrombocytopenia	2 (1.8)	3 (2.6)	1.000†
Nephrotoxicity (renal)	7 (6.1)	46 (40.0)	<0.001
Neurotoxicity	52 (45.6)	63 (54.8)	0.145
GI toxic nausea/vomiting	37 (32.5)	52 (45.2)	0.042
GI diarrhea	2 (1.8)	3 (2.6)	1.000†
Asthenia	65 (57.0)	82 (71.3)	0.019
Alopecia	96 (84.2)	87 (75.7)	0.134

GI, gastrointestinal.
*Pearson's chi-square test.
†Fisher's exact test.

Table 4: Response rate/survival time (months), Log-rank test *P* value: 0.577.

		ARM			
Response rate		A	B	Total	*P* value*
CR					
n		1	0	1	—
% within ARM		0.9	0.0	0.4	—
PR					
n		67	54	121	
% within ARM		58.8	47.0	52.8	0.073
SD					
n		42	50	92	
% within ARM		36.8	43.5	40.2	0.306
PD					
n		4	11	15	
% within ARM		3.5	9.6	6.6	0.064
Total	*n*	114	115	229	
Survival time	*n*	Median		95% CI	
Arm A	114	9.0		6.2–11.8	
Arm B	115	10.0		6.8–13.2	
Total sample	229	10.0		8.3–11.7	

CR: complete response; PR: partial response; SD: stable disease; PD: progressive disease.
*Pearson's chi-square test.

Table 5: Response rate.

	Arm A ($n = 103$)	Arm B ($n = 99$)	*P* value
Partial response	61 (59.22%)	42 (42.42%)	0.036
Stable disease	35 (33.98%)	43 (43.43%)	0.220
Progressive disease	7 (6.80%)	14 (14.14%)	0.110

administration of lipoplatin or cisplatin. This study recruited patients with nonsquamous cell lung cancer, mainly adenocarcinomas, and they were treated with lipoplatin combined with paclitaxel versus cisplatin combined with paclitaxel. The dosage and administration of these two combined treatments was the same as in the previous study. It was found in 202 patients randomized into two groups, that the response rate was superior in the lipoplatin group. The difference was statistically significant ($P = 0.036$) (Table 5). The median survival for the lipoplatin group was 10 months and for

cisplatin group 8 months, approaching statistical significance ($P = 0.1551$) [51].

There are data examining the possibility of using lipoplatin in cancer patients with renal failure. The preliminary data show that patients with serum creatinine ranging from 1.6–3.5 mg/dL tolerate lipoplatin without increasing renal failure and without side effects such as neutropenia, nausea/vomiting, and fatigue.

8. Conclusion

The efforts over the last 20 years to produce a substitute for cisplatin, a very important and effective anticancer agent, with a similarly effective and less toxic agent, have not properly succeeded. The current data in a number of preclinical and clinical trials shed new light on the previous efforts to produce a substitute for cisplatin. Liposomal cisplatin (lipoplatin), is a new formulation of cisplatin and one would expect at least to achieve equal effectiveness. Phase I, II, and III trials have shown lipoplatin to produce similar efficacy to that of cisplatin in pancreatic, head and neck, breast cancers, and NSCLC (the latter has been more broadly tested). In a new substitute for cisplatin, what is more important, apart from effectiveness, is significant toxicity reduction. The reduction of toxicity, mainly nephrotoxicity, has been shown and confirmed in published trials. It will be important to use this new cisplatin formulation in future trials and to test it in malignancies such as ovarian and bladder cancers.

References

[1] L. H. Einhorn, S. D. Williams, P. J. Loehrer et al., "Evaluation of optimal duration of chemotherapy in favorable-prognosis disseminated germ cell tumors: a Southeastern Cancer Study Group protocol," *Journal of Clinical Oncology*, vol. 7, no. 3, pp. 387–391, 1989.

[2] K. Aabo, M. Adams, P. Adnitt et al., "Chemotherapy in advanced ovarian cancer: four systematic meta-analyses of individual patient data from 37 randomized trials," *British Journal of Cancer*, vol. 78, no. 11, pp. 1479–1487, 1998.

[3] J. P. Pignon, J. Bourhis, C. Domenge, and L. Designe, "Chemotherapy added to locoregional treatment for head and neck squamous-cell carcinoma: three meta-analyses of updated individual data," *The Lancet*, vol. 355, no. 9208, pp. 949–955, 2000.

[4] Non-small Cell Lung Cancer Collaborative Group, "Chemotherapy in non-small cell lung cancer, a meta-analysis using updated data on individual patients from 52 randomized clinical trials," *British Medical Journal*, vol. 311, no. 7010, pp. 899–909, 1995.

[5] D. Kaufman, D. Raghavan, M. Carducci et al., "Phase II trial of gemcitabine plus cisplatin in patients with metastatic urothelial cancer," *Journal of Clinical Oncology*, vol. 18, no. 9, pp. 1921–1927, 2000.

[6] B. Rosenberg, "Platinum complexes for the treatment of cancer: why the research goes on," in *Cisplatin: Chemistry of a Leading Anticancer Drug*, B. Lippert, Ed., pp. 3–12, Verlag Helvetica Chemica Acta, Zurich, Switzerland, 1999.

[7] D. M. Hayes, E. Cvitkovic, R. B. Golbey, E. Scheiner, L. Helson, and I. H. Krakoff, "High dose cis-platinum diamminedichloride: amelioration of renal toxicity by mannitol diuresis," *Cancer*, vol. 39, pp. 1372–1378, 1977.

[8] C. M. Sorenson and A. Eastman, "Mechanism of cis-diamminedichloroplatinum(II)-induced cytotoxicity: role of G2 arrest and DNA double-strand breaks," *Cancer Research*, vol. 48, no. 16, pp. 4484–4488, 1988.

[9] D. R. Gandara, N. A. Nahhas, M. D. Adelson et al., "Randomized placebo-controlled multicenter evaluation of diethyldithiocarbamate for chemoprotection against cisplatinum-induced toxicities," *Journal of Clinical Oncology*, vol. 13, no. 3, pp. 490–496, 1995.

[10] I. Arany and R. L. Safirstein, "Cisplatin nephrotoxicity," *Seminars in Nephrology*, vol. 23, no. 5, pp. 460–464, 2003.

[11] A. E. Taylor, E. Wiltshaw, M. E. Gore, I. Fryatt, and C. Fisher, "Long-term follow-up of the first randomized study of cisplatin versus carboplatin for advanced epithelial ovarian cancer," *Journal of Clinical Oncology*, vol. 12, no. 10, pp. 2066–2070, 1994.

[12] A. Tognoni, F. Pensa, F. Vaira et al., "A dose finding study of carboplatin and gemcitabine in advanced non-small cell lung cancer," *Journal of Chemotherapy*, vol. 14, no. 3, pp. 296–300, 2002.

[13] B. E. Johnson, "Integration of new agents into the treatment of advanced non-small cell lung cancer," in *American Society of Clinical Oncology Educational Book*, pp. 345–356, Lipincott Williams and Wilkins, Baltimore, Md, USA, 2000.

[14] F. A. Shepherd, J. Dancey, A. Arnold et al., "Phase II study of pemetrexed disodium, a multitargeted antifolate and cisplatin as first-line therapy in patients with advanced non-small cell lung cancer," *Cancer*, vol. 92, no. 3, pp. 595–600, 2001.

[15] F. Barlesi and J. L. Pujal, "Combination of chemotherapy without platinum compounds in the treatment of advanced non-small cell lung cancer: a systemic review of phase III trials," *Lung Cancer*, vol. 49, no. 3, pp. 289–298, 2005.

[16] G. P. Stathopoulos, M. Veslemes, N. Georgatou et al., "Paclitaxel and vinorelbine combination in advanced inoperable adenocarcinoma of the lung: a phase II study," *Anticancer Research*, vol. 23, no. 4, pp. 3479–3484, 2003.

[17] G. P. Stathopoulos, J. Dimitroulis, D. Antoniou et al., "Front-line paclitaxel and irinotecan combination chemotherapy in advanced non-small-cell lung cancer: a phase I-II trial," *British Journal of Cancer*, vol. 93, no. 10, pp. 1106–1111, 2005.

[18] A. Ardizzoni, L. Boni, M. Tiseo et al., "Cisplatin- versus carboplatin-based chemotherapy in first-line treatment of advanced non-small-cell lung cancer: an individual patient data meta-analysis," *Journal of the National Cancer Institute*, vol. 99, no. 11, pp. 847–857, 2007.

[19] T. Boulikas, G. P. Stathopoulos, N. Volakakis, and M. Vougiouka, "Systemic lipoplatin infusion results in preferential tumor uptake in human studies," *Anticancer Research*, vol. 25, no. 4, pp. 3031–3040, 2005.

[20] Boulikas Teni, "Lipoplatin: a successful cisplatin formulation," *Cancer Therapy*. In press.

[21] M. T. Kuo, H. H. W. Chen, I. S. Song, N. Savaraj, and T. Ishikawa, "The roles of copper transporters in cisplatin resistance," *Cancer and Metastasis Reviews*, vol. 26, no. 1, pp. 71–83, 2007.

[22] G. Huang, L. Mills, and L. L. Worth, "Expression of human glutathione S-transferase P1 mediates the chemosensitivity of osteosarcoma cells," *Molecular Cancer Therapeutics*, vol. 6, no. 5, pp. 1610–1619, 2007.

[23] Q. Wei, G. Dong, J. Franklin, and Z. Dong, "The pathological role of Bax in cisplatin nephrotoxicity," *Kidney International*, vol. 72, no. 1, pp. 53–62, 2007.

[24] J. Zhu, Y. Yang, and J. Wu, "Bcl-2 cleavages at two adjacent sites by different caspases promote cisplatin-induced apoptosis," *Cell Research*, vol. 17, no. 5, pp. 441–448, 2007.

[25] T. Boulikas and M. Vougiouka, "Cisplatin and platinum drugs at the molecular level. (Review)," *Oncology Reports*, vol. 10, no. 6, pp. 1663–1682, 2003.

[26] D. Wang and S. J. Lippard, "Cellular processing of platinum anticancer drugs," *Nature Reviews Drug Discovery*, vol. 4, no. 4, pp. 307–320, 2005.

[27] M. Villedieu, M. Briand, M. Duval, J. F. Heron, P. Gauduchon, and L. Poulain, "Anticancer and chemosensitizing effects of 2,3-DCPE in ovarian carcinoma cell lines: link with ERK activation and modulation of p21(WAF1/CIP1), Bcl-2 and Bcl-x(L) expression," *Gynecologic Oncology*, vol. 105, no. 2, pp. 373–384, 2007.

[28] M. Singh, H. Sharma, and N. Singh, "Hydrogen peroxide induces apoptosis in HeLa cells through mitochondrial pathway," *Mitochondrion*, vol. 7, no. 6, pp. 367–373, 2007.

[29] M. Berndtsson, M. Hägg, T. Panaretakis, A. M. Havelka, M. C. Shoshan, and S. Linder, "Acute apoptosis by cisplatin requires induction of reactive oxygen species but is not associated with damage to nuclear DNA," *International Journal of Cancer*, vol. 120, no. 1, pp. 175–180, 2007.

[30] T. Ohta, M. Ohmichi, T. Hayasaka et al., "Inhibition of phosphatidylinositol 3-kinase increases efficacy of cisplatin in in vivo ovarian cancer models," *Endocrinology*, vol. 147, no. 4, pp. 1761–1769, 2006.

[31] A. Fedier, R. Erdmann, T. Boulikas, and D. Fink, "Potential of the Akt inhibitor LY294005 to antagonize the efficacy of cisplatin against HCT116 tumor cells in a DNA mismatch repair-dependent manner," *International Journal of Oncology*, vol. 29, no. 5, pp. 1303–1310, 2006.

[32] J. Bodo, L. Hunakova, P. Kvasnicka et al., "Sensitisation for cisplatin-induced apoptosis by isothiocyanate E-4IB leads to signalling pathways alterations," *British Journal of Cancer*, vol. 95, no. 10, pp. 1348–1353, 2006.

[33] A. Stoeck, D. Gast, M. P. Sanderson, Y. Issa, P. Gutwein, and P. Altevogt, "L1-CAM in a membrane-bound or soluble form augments protection from apoptosis in ovarian carcinoma cells," *Gynecologic Oncology*, vol. 104, no. 2, pp. 461–469, 2007.

[34] C. Arienti, A. Tesei, A. Ravaioli et al., "Activity of lipoplatin in tumor and in normal cells in vitro," *Anticancer Drugs*, vol. 19, no. 10, pp. 983–990, 2008.

[35] A. Fedier, C. Poyet, D. Perucchini, T. Boulikas, and D. Fink, "MLH1-deficient tumor cells are resistant to lipoplatin, but retain sensitivity to lipoxal," *Anticancer Drugs*, vol. 17, no. 3, pp. 315–323, 2006.

[36] P. Devarajan, R. Tarabishi, J. Mishra et al., "Low renal toxicity of lipoplatin compared to cisplatin in animals," *Anticancer Research*, vol. 24, no. 4, pp. 2193–2200, 2004.

[37] A. K. Marr, I. D. Kurzman, and D. M. Vail, "Preclinical evaluation of a liposome-encapsulated formulation of cisplatin in clinically normal dogs," *American Journal of Veterinary Research*, vol. 65, no. 11, pp. 1474–1478, 2004.

[38] M. E. Froudarakis, L. Greillier, S. Monjanel-Mouterde et al., "Intrapleural administration of lipoplatin in an animal model," *Lung Cancer*, vol. 72, no. 1, pp. 78–83, 2010.

[39] T. Tippayamontri, R. Kotb, B. Paquette, and L. Sanche, "Cellular uptake and cytoplasm/DNA distribution of cisplatin and oxaliplatin and their liposomal formulation in human colorectal cancer cell HCT116," *Investigational New Drugs*. In press.

[40] G. Charest, B. Paquette, D. Fortin, D. Mathieu, and L. Sanche, "Concomitant treatment of F98 glioma cells with new liposomal platinum compounds and ionizing radiation," *Journal of Neuro-Oncology*, vol. 97, no. 2, pp. 187–193, 2010.

[41] G. P. Stathopoulos, T. Boulikas, M. Vougiouka et al., "Pharmacokinetics and adverse reactions of a new liposomal cisplatin (lipoplatin): phase I study," *Oncology Reports*, vol. 13, no. 4, pp. 589–595, 2005.

[42] G. P. Stathopoulos, T. Boulikas, M. Vougiouka, S. K. Rigatos, and J. G. Stathopoulos, "Liposomal cisplatin combined with gemcitabine in pretreated advanced pancreatic cancer patients: a phase I-II study," *Oncology Reports*, vol. 15, no. 5, pp. 1201–1204, 2006.

[43] M. E. Froudarakis, A. Pataka, P. Pappas et al., "Phase 1 trial of lipoplatin and gemcitabine as a second-line chemotherapy in patients with nonsmall cell lung carcinoma," *Cancer*, vol. 113, no. 10, pp. 2752–2760, 2008.

[44] G. P. Stathopoulos, S. K. Rigatos, and J. Stathopoulos, "Liposomal cisplatin dose escalation for determining the maximum tolerated dose and dose-limiting toxicity: a phase I study," *Anticancer Research*, vol. 30, no. 4, pp. 1317–1321, 2010.

[45] M. I. Koukourakis, A. Giatromanolaki, M. Pitakoudis et al., "Concurrent liposomal cisplatin (lipoplatin), 5-fluorouracil and radiotherapy for the treatment of locally advanced gastric cancer: a phase I-II study," *International Journal of Radiation Oncology Biology Physics*, vol. 78, no. 1, pp. 150–155, 2009.

[46] G. Karpathiou, E. Argiana, A. Koutsopoulos, and M. E. Froudarakis, "Response of a patient with pleural and peritoneal mesothelioma after second-line chemotherapy with lipoplatin and gemcitabine," *Oncology*, vol. 73, no. 5-6, pp. 426–429, 2008.

[47] C. F. Jehn, T. Boulikas, A. Kourvetaris, K. Possinger, and D. Luftner, "Pharmacokinetics of liposomal cisplatin (lipoplatin) in combination with 5-FU in patients with advanced head and neck cancer: first results of a phase III study," *Anticancer Research*, vol. 27, no. 1, pp. 471–476, 2007.

[48] F. S. Farhat, K. Ibrahim, J. Kattan et al., "Preliminary results of phase II study of liposomal cisplatin—vinorelbine combination as first-line treatment in HER2/neu negative metastatic breast cancer (MBC)," in *Proceedings of the ASCO Annual Meeting*, 2009.

[49] N. Mylonakis, A. Athanasiou, N. Ziras et al., "Phase II study of liposomal cisplatin (lipoplatin) plus gemcitabine versus cisplatin plus gemcitabine as first line treatment in inoperable (stage IIIB/IV) non-small cell lung cancer," *Lung Cancer*, vol. 68, no. 2, pp. 240–247, 2010.

[50] G. P. Stathopoulos, D. Antoniou, J. Dimitroulis et al., "Liposomal cisplatin combined with paclitaxel versus cisplatin and paclitaxel in non-small-cell lung cancer: a randomized phase III multicenter trial," *Annals of Oncology*, vol. 21, no. 11, pp. 2227–2232, 2010.

[51] G. P. Stathopoulos, D. Antoniou, J. Dimitroulis, J. Stathopoulos, K. Marosis, and P. Michalopoulou, "Comparison of lipo-somal cisplatin versus cisplatin in non-squamous cell non-small cell lung cancer," *Cancer Chemotherapy and Pharmacology*. In press.